TUM School of Engineering and Design

Simulation of stationary lithium-ion battery energy storage systems in urban distribution grids

Daniel Kucevic, M.Sc.

Vollständiger Abdruck der von der TUM School of Engineering and Design der Technischen Universität München zur Erlangung des akademischen Grades eines

Doktors der Ingenieurwissenschaften (Dr.-Ing.)

genehmigten Dissertation.

Vorsitz:		Prof. Dr.-Ing. Rolf Witzmann
Prüfer*innen der Dissertation:	1.	Prof. Dr.-Ing. Andreas Jossen
	2.	Prof. Dr. Andreas Sumper

Die Dissertation wurde am 16.12.2021 bei der Technischen Universität München eingereicht und durch die TUM School of Engineering and Design am 14.03.2022 angenommen.

Zusammenfassung

Der stetig steigende Strombedarf und die anstehende Integration von Lademöglichkeiten für Elektrofahrzeuge stellen vor allem städtische Stromnetze vor neue Herausforderungen. Als Beispiel kann hier die Überlastung einzelner Stromkabel genannt werden. Bei kontinuierlich sinkenden Kosten für Lithium-Ionen-Batterien stellen Speichersysteme eine Alternative zum konventionellen Netzausbau dar. Diese Arbeit schlägt verschiedene Energiemanagementstrategien für Batteriespeichersysteme vor, um Verbesserungen innerhalb eines Verteilnetzes zu erreichen. Ziel ist es, die Spitzenleistung am Kopplungspunkt zum Hochspannungsnetz durch Anpassung der Steuerung von autarken sowie gekoppelten Batteriespeichersystemen zu reduzieren. Im Rahmen dieser Arbeit wurden Open-Source Simulationstools entwickelt und adaptiert, welche zur realitätsnahen Simulation von Energiespeichern mit verschiedenen Betriebsmodi in Verteilnetzen verwendet werden. Abschließend wird eine wirtschaftliche Analyse durchgeführt, um Speichersysteme als Alternative zur konventionellen Netzverstärkung ökonomisch zu bewerten. Die Ergebnisse der Arbeit zeigen, dass Batteriespeichersysteme bereits heute eine technische Alternative und in Zukunft verstärkt auch eine wirtschaftliche Alternative zum konventionellen Netzausbau sein können.

Abstract

The growing global electricity demand and the upcoming integration of charging options for electric vehicles are creating challenges for urban power grids, such as line overloading. With continuously falling costs for lithium-ion batteries, storage systems represent an alternative to conventional grid reinforcement. This thesis proposes various energy management strategies for battery energy storage systems to achieve an improvement in a distribution grid. The objective is to reduce the peak power at the point of common coupling by adapting the control of stand-alone as well as coupled battery energy storage systems located at various nodes in the distribution grid. Open-source simulation tools, which enable a realistic simulation of the effects of storage systems in different operating modes on the distribution grid, have been developed and adapted as part of this work. Consequently, an economic analysis is conducted to evaluate storage systems as an alternative to conventional grid reinforcement. Results show that battery energy storage systems can already be a technical and, in some cases, also an economic alternative to conventional grid reinforcement.

Acknowledgment

This thesis originates from my time as a research associate at the Chair for Electrical Energy Storage Technology (EES) at the Technical University of Munich. The achieved results have only been possible thanks to the support of various individuals, collaborations, and institutions. First of all, I would like to thank Prof. Dr.-Ing. Andreas Jossen for giving me the opportunity to carry out my research in the field of stationary storage. I really appreciated the opportunity to work at the chair and the freedom we all had to shape the interdisciplinary cooperation of all teams.

Furthermore, I thank the team for stationary energy systems for the support I have gained during my research. On the one hand, all the colleagues who initially introduced me to the world of science, especially Holger Hesse, Michael Schimpe, Nam Truong, and Maik Naumann. And on the other hand, I hope I was able to support all new colleagues, particularly Anupam Parlikar, Nils Collath, and Martin Cornejo in their initial phase. I thank Benedikt (Bene) Tepe for the collaboration in the open_BEA project and for the enjoyable time in the office despite the cultural differences. Also, a big thank you to Marc Möller for the many hours of developing SimSES together and preaching the coding guidelines to me. Also thank you to Stefan Englberger for the help at the final stage of this thesis and for helping to represent Austria at the EES.

To all the colleagues at the chair: It was a pleasure to work with all of you and I am very grateful for the numerous friendships that developed from this. In addition, I would like to thank (or apologize) the EES rapid for the many hours that you spent on training to win the campus run several times with me. Another big thank you goes out to my hosts at the National University of Singapore that I visited during my time as a researcher: Anurag Sharma, Anupam Trivedi and Dipti Srinivasan. I also want to thank my students, in particular Leo Semmelmann and Rebecca Meißner, whose work contributed to this thesis. This thesis would not have been possible without the support of the project partners in open_BEA: Petra Dotzauer from the ZAE and all the people from the RLI, especially Birgit Schachler.

I am also very grateful to my family and friends for their support during this journey. Last but not least, my biggest thanks go to my girlfriend Daniela. Thank you so much for your never-ending love and support during all the ups and downs of this dissertation. Also, for the countless hours you have spent reviewing my publications and listening to my lectures and presentations. To all of you I dedicate this thesis.

List of Publications

Peer-Reviewed Journal Paper Contributions (Lead Author)

I Kucevic, D.; Tepe, B.; Englberger, S.; Parlikar, A.; Mühlbauer, M.; Bohlen, O.; Jossen, A.; Hesse, H.: Standard battery energy storage system profiles: Analysis of various applications for stationary energy storage systems using a holistic simulation framework, in: Journal of Energy Storage 28, p. 101077, 2020 [1]

II Kucevic, D.; Englberger, S.; Sharma, A.; Trivedi, A.; Tepe, B.; Schachler, B.; Hesse, H.; Srinivasan, D.; Jossen, A.: Reducing grid peak load through the coordinated control of battery energy storage systems located at electric vehicle charging parks, in: Applied Energy 295, p. 116936, 2021 [2]

III Kucevic, D.; Semmelmann, L.; Collath, N.; Jossen, A.; Hesse, C: Peak Shaving with Battery Energy Storage Systems in Distribution Grids: A Novel Approach to Reduce Local and Global Peak Loads, in: Electricity 2(4), p. 573-589, 2021 [3]

Peer-Reviewed Conference Paper Contributions (Lead Author)

I Kucevic, D.; Truong, C.N.; Jossen, A.; Hesse, H.: Lithium-Ion Battery Storage Design for Buffering Fast Charging Stations for Battery Electric Vehicles and Electric Buses, in: Schulz, D. (ed.): NEIS 2018, VDE VERLAG GMBH, Berlin, 2019 [4]

II Kucevic, D.; Göschl, S.; Röpcke, T.; Hesse, H.; Jossen, A.: Reducing grid peak load through smart charging strategies and battery energy storage systems: 5th E-Mobility Power System Integration, Berlin, 2021 [5]

III Kucevic, D.; Meißner, R.; Jossen, A.; Hesse, H: Battery Energy Storage Systems as an Alternative to Conventional Grid Reinforcement (unpublished work): International Conference on Applied Energy 2021, Bangkok (virtual), 2021 [6]

Self-written sections of peer-reviewed lead author journal/conference paper contributions are partially contained in this doctoral thesis without further reference in the text. Figures are continuously referenced.

Peer-Reviewed Journal Paper Contributions (Co-Author)

I Hesse, H.; Schimpe, M.; Kucevic, D.; Jossen, A.: Lithium-Ion Battery Storage for the Grid — A Review of Stationary Battery Storage System Design Tailored for Applications in Modern Power Grids, in: Energies 10 (12), p. 2107, 2017 [7]

II Englberger, S.; Hesse, H.; Kucevic, D.; Jossen, A.: A Techno-Economic Analysis of Vehicle-to-Building: Battery Degradation and Efficiency Analysis in the Context of Coordinated Electric Vehicle Charging, in: Energies 12 (5), p. 955, 2019 [8]

III Möller, M.; Kucevic, D.; Collath, N.; Parlikar, A; Dotzauer, P; Tepe, B.; Englberger, S.; Jossen, A.; Hesse, H: SimSES: A holistic simulation framework for modeling and analyzing stationary energy storage systems, in: Journal of Energy Storage 49, p. 103743, 2022 [9]

Peer-Reviewed Conference Contributions (Co-Author)

I Naumann, M.; Truong, C.N.; Schimpe, M.; Kucevic, D.; Jossen, A.; Hesse, H.C.: SimSES: Software for techno-economic Simulation of Stationary Energy Storage Systems, in: Proceedings of the International ETG Congress 2017, Bonn, 2017 [10]

Selection of Conference Presentations

I Kucevic, D.; Pietsch, M.; Schimpe, M.; Hesse, H.; Jossen, A.: Bewertung der energetischen Performance von stationären Batteriespeichersystemen, at: Design & Elektronik, Munich, 2018

II Kucevic, D.; Truong, C.N.; Jossen, A.; Hesse, H.: Lithium-Ion Battery Storage Design for Buffering Fast Charging Stations for Battery Electric Vehicles and Electric Buses, at: NEIS - Conference on Sustainable Energy Supply and Energy Storage Systems, Hamburg, 2018

III Kucevic, D.; Hesse, H.; Jossen, A.: Battery Requirements for the Electrification of Urban Public Transport. 7. Conference on Future Automotive Technology: Focus E-mobility, Munich, 2018

IV Kucevic, D.; Dotzauer, P.; Zhao, Y.; Rzepka, M.; Hesse, H.; Jossen, A.: Open Battery Models for Electrical Grid Applications, at: Batterieforum Deutschland, Berlin, 2019

V Kucevic, D.; Hesse, H.; Jossen, A.: Modellierung und Simulation von stationären Batteriespeichern, at: BVES Fachforum Batteriespeicher, virtual, 2020

VI Kucevic, D.; Göschl, S.; Röpcke, T.; Hesse, H.; Jossen, A.: Reducing grid peak load through smart charging strategies and battery energy storage systems, at: 5th E-Mobility Power System Integration, Berlin, 2021

VII Kucevic, D.; Meißner, R.; Jossen, A.; Hesse, H: Battery Energy Storage Systems as an Alternative to Conventional Grid Reinforcement, at: International Conference on Applied Energy, Bangkok (virtual), 2021

Contents

Abbreviations

AC . . . . . alternating current

BESS . . . . . battery energy storage system

BMS . . . . . battery management system

C . . . . . carbon/graphite

DC . . . . . direct current

DOC . . . . . depth of cycle

DOF . . . . . degrees of freedom

eDisGo . . . . . software for electric distribution grid optimization

EMS . . . . . energy management system

EV . . . . . electric vehicle

FCR . . . . . frequency containment reserve

FEC . . . . . full equivalent cycle

LFP . . . . . lithium-iron-phosphate

LIB . . . . . lithium-ion battery

lp_opt . . . . . linear programming optimization tool for energy storage systems

LV . . . . . low voltage

MV . . . . . medium voltage

OCV . . . . . open circuit voltage

open_BEA . . . open battery models for electrical grid applications

PCC . . . . . point of common coupling

SimSES . . . . . simulation of stationary energy storage systems

SOE . . . . . state of energy

Sets & indices

B	total number of nodes b in the distribution grid
H	time vector for the simulation period (time horizon)
T	time horizon
N	vector for all industrial consumers in the distribution grid
b	nodes in the distribution grid
b_j	specific node b at location j in the distribution grid
b_k	specific node b at location k in the distribution grid
t	specific time step

Parameters & variables

E_t^{actual} . . . . . actual energy content of a battery energy storage system for a specific time step t

E_t^{charge} . . . . . charged energy of a battery energy storage system for a specific time step t

$E_t^{\text{discharge}}$ . . . . . discharged energy of a battery energy storage system for a specific time step t

$E_{\text{T}}^{\text{neg}}$ . . . . . negative energy throughput of a battery energy storage system for a time horizon T

E^{nominal} . . . . . nominal energy content of a battery energy storage system

$E_{\text{T}}^{\text{pos}}$ . . . . . positive energy throughput of a battery energy storage system for a time horizon T

P^{Load} . . . . . power of residual consumer

P^{PQ} . . . . . prequalified power of a battery energy storage system providing frequency containment reserve

P^{PV} . . . . . generated power by a photovoltaic system

P^{charge} . . . . . charging power of a battery energy storage system

$P^{\text{discharge}}$ . . . . . discharging power of a battery energy storage system

P^{rated} . . . . . rated power of the power electronics

$\text{I}_t^{\text{b}_j \to \text{b}_k}$ . . . . . line current between two specific nodes b (b_j and b_k) for a specific time step t

$\text{P}_{\text{BESS,0}}^{\text{invest}}$ . . . . . discounted battery energy storage system investment costs

$\text{P}_{\text{Grid,0}}^{\text{invest}}$ . . . . . discounted grid reinforcement costs

R_i . . . . . internal resistance

SOE^{max} . . . . . state of energy upper limit

SOE^{min} . . . . . state of energy lower limit

S_t^{b} . . . . . apparent power at a specific node b for a specific time step t

U_T . . . . . terminal voltage

σ_b . . . . . scaling factor: peak power at the point of common coupling in relation to the peak load at a specific node b

$\mathbf{I}^{\text{b}_j \to \text{b}_k}$ . . . . . vector for the line current between two specific nodes b (b_j and b_k) for each time step t

$\mathbf{S}^{\text{b}}$ . . . . . vector for the apparent power at a specific node b for each time step t

$\mathbf{S}$ . . . . . matrix for the apparent power at each node b for each time step t

e^{rate} . . . . . energy rate of the battery energy storage system

l_{GR} . . . . . length of the grid reinforcement required

p_{BESS}^{invest} . . . . . battery energy storage system investment costs per kWh

p_{Grid}^{invest} . . . . . grid reinforcement costs per km

r . . . . . discount rate

t^{re} . . . . . predicted remaining time, until the load is higher than the solar generation

t_{proj} . . . . . project operation / depreciation period in years

η_{BESS} . . . . . efficiency of a battery energy storage system

η_{PE} . . . . . efficiency of the power electronics

1 Introduction and motivation

Renewable energy sources and electric vehicles (EVs) are seen as future key drivers for the substantial decrease in carbon emissions in both the transportation and power generation sectors [11]. However, this transformation poses new challenges to the power grid and in particular to the alternating current (AC) distribution grid [12]. On the one hand, in rural areas the increased share of renewable energy sources, such as photovoltaic generation units or wind energy and the resulting over-voltage are the main cause of grid reinforcement [13]. On the other hand, in urban distribution grids it is forecasted that over-loading caused by an increasing number of charging possibilities will be the main driver for grid reinforcement [14].

A report of the European Federation for Transport and Environment predicted that the number of public chargers in the EU will increase from 185 000 in 2020 to 1.3 million in 2025 and 2.9 million in 2030 [14]. This is motivated by the increasing prioritization of shared cars or electric taxis in these urban areas. They recommend introducing charging parks at easily accessible locations, with dedicated parking spots for electric taxis and shared EVs, notably in cities. It is estimated that the number of direct current (DC) fast charging stations in Germany will quadruple from about 2000 in 2018 to about 8000 in 2030 [15]. Both studies as well as additional published papers [16, 17] identified that the existing distribution grid infrastructure is not capable to include the additional power of these charging stations.

In the past, research mainly focused on over-voltage issues in distribution grids caused by the upcoming integration of renewable energy sources. This thesis focuses more on the difficulties that arise in the distribution grid due to increased energy demand. Nevertheless, research has already been conducted in both areas. The most important aspects for the scope of this thesis are discussed in detail in the following sections. The main research questions and the novelties of this work are explained in Section 1.2.

1.1 Literature review

With the shift towards more generation of electricity from renewable energy sources, the requirements for the energy supply grid have also changed [18, 19]. Examples for technical issues related to a high local wind or photovoltaic integration are local over-voltages and equipment over-loading [20]. Sinsel et al. summarized possible solutions for these challenges in their review [21]. Examples to solve these issues include grid reinforcement, energy storage system integration or distributed demand response. In the following paragraphs, the focus will lie in the integration and simulation of battery energy storage systems (BESSs) in distribution grids.

In the work of Müller et al., a BESS was installed in an exemplary low voltage (LV) grid [22, 23]. They observed major voltage limit violations if no BESS is installed. With an installed BESS and additional connection of two lines to a ring line, significant improvements in voltage can be seen. They concluded

that the positive effect of distributed storage systems is comparable to central storage units connected to the higher grid level. And in addition to the transformer relief, a significant reduction in grid losses can be achieved with increasing BESS distribution radius. However, the work deals with increasing photovoltaic penetration in rural distribution grid and not with an increasing EV-share in urban areas and the associated problems.

One further approach to face the difficulties with over-voltage was suggested in the work of Resch [24]. In the PhD thesis as well as an additional published paper, the author and his co-authors tried to find and combine profitable business cases with reactive power control for large scale BESS in distribution grids [13]. Another focus is the techno-economic comparison of these profitable grid supportive business cases supported by a field test with a redox-flow battery. It is concluded that a traditional planning method in distribution grids with a high share of renewable energy sources will lead to over-capacity in the grid. Including energy storage system is an alternative approach, but detailed simulations are necessary.

To face the challenges of possible future over-loading in an existing grid infrastructure, various approaches exist in the literature. Conventional grid reinforcement or transformer upgrading, as investigated by Brinkel et al., is one possible solution for covering the increasing demand or for enabling the integration of more EVs in the future [25]. However, with falling costs of lithium-ion batteries (LIBs), stationary BESSs are becoming increasingly attractive as an alternative method to reduce peak loads [26, 27].

Additionally, several vehicle-to-grid approaches exist aiming to reduce the peak power in distribution grids. A detailed overview of the concept and possible services is presented in the publications of both Kempton et al. [28] and Tan et al. [29]. However, various social dimensions, such as the behavior and acceptance of EV users, are often neglected in these approaches. Another disadvantage is the impact on vehicle battery lifetime due to a higher stress to the LIB, caused by these vehicle-to-grid applications [30, 31].

Besides bidirectional charging approaches, a number of researchers, such as Hanemann et al. [32, 33] are examining the effect of using various smart charging strategies on the distribution grid. It is concluded that the curtailment of renewable energy sources can be reduced by smart charging strategies, but they focus on the effects on spot markets and CO_2 prices rather than on over-loading issues in the urban distribution grid. The studies by Mehta et al. deal with a grid optimal placement of EV charging stations [34, 35]. They focus on achieving both economic benefits in terms of daily costs for the EV users and technical benefits in terms of peak load reduction and optimized active and reactive power flows. As with the bidirectional charging strategies, however, it must also be assumed here that EV users will provide their EVs for those smart charging strategies and therefore may expect longer charging time.

An approach more related to storage systems for reducing grid peak load was introduced in the work of Danish et al. [36]. Aiming to find the optimal size, location, and control strategy for a BESS in a distribution grid an optimization method was applied. The work was conducted using commercial software and is based on a 20 kV distribution grid with 22 nodes in Kabul. It is shown that the power losses in the grid can be reduced up to 20.62 %. The authors conclude that an optimally placed BESS with a peak shaving operation strategy can significantly improve the system performance, but the storage system was only implemented as a black box model and the potential losses of the BESS were not included.

The work of Wilkening shows a stimulative approach for a techno-economic evaluation of grid related BESSs [37]. The focus was on black-start capability of decentralized BESSs and on providing system related services, such as frequency containment reserve (FCR). The techno-economic simulation was conducted using MATLAB® and it is concluded that BESS is often not profitable for a single grid related service. However, in this work the focus was not on a detailed co-simulation of distribution grids and BESSs. Furthermore, it was not investigated how storage system can be used to avoid grid reinforcement.

Another work of techno-economic analysis is shown in the PhD thesis of Naumann [38]. The objective of the work was on the examination of aging mechanisms and the development of an aging model for a LIB. The simulation of two stand-alone application (providing FCR and residential self-consumption increase) for stationary BESSs was conducted using MATLAB®. It is concluded that if the battery aging is neglected, the total return would be about 21.3% with the investigated LIB in the application of residential self-consummation increase. Besides the detailed cell model, additional components, such as power electronic models, were included in the simulations of the storage systems. Hence, the simulation of BESS was very detailed, but the effects on the distribution grid were neglected and thus not discussed.

One more grid related approach analyzing storage systems in detail was done by the work of Zeh [39]. In the PhD thesis as well as an additional published paper, the author and his co-authors showed various operation strategies for BESS for common applications and discussed the effects on the distribution grid [40, 41]. The focus was again on storage systems proving FCR and residential BESSs to increase the self-consumption. Simulations indicated that storage systems' positive effect related to the stress on various grid equipment can be achieved in the medium voltage (MV) grid. However, the focus in this work was more on distribution grid with a high share of renewable energy sources than on over-loading issues caused by a high share of EV charging stations.

Summarizing the literature, there seems to be a consensus that a high EV-share requires an increased number of charging parks and this will require adaptations or new solutions in the power grid, especially in urban distribution grid. While in the past the focus was on dealing with over-voltage issues in rural areas, the focus in this thesis is on over-loading issues caused by the mentioned higher EV-share. None of the authors mentioned above have conducted a detailed co-simulation of BESSs and distribution grids.

The possibility of using stand-alone or coupled BESSs to reduce the peak power at the point of common coupling (PCC) in existing distribution grids has not yet been adequately investigated. This would consequently avoid or decelerate grid reinforcement requirements caused by over-loading. Furthermore, no detailed comparison of grid reinforcement costs and storage system costs currently exists in the literature.

1.2 Scope of this work

Different research questions are crucial for the formation of this thesis. Based on these research questions, novel approaches are developed and the answers to these questions are shown in the various chapters. After describing the basics of stationary BESSs for the grid in Chapter 2, Chapter 3 focuses on modeling various components of an BESS for an accurate simulation of different use-cases. Defining reference profiles and identifying essential applications for grid integration is the aim of Chapter 4.

Chapter 5 focuses on how stationary BESSs with established use-cases can be considered in grid planning and which adaptions are necessary. Is a multi-storage approach suitable for grid planning? And how should the battery control be coordinated? These are the two main research questions of Chapter 6. Chapter 7 summarizes this thesis with the question: Are BESSs an economical alternative to conventional grid reinforcement? Table 1.1 sums up the main research questions of this thesis and their affiliation to the topics BESSs and grid reinforcement.

Table 1.1: Main research questions of this thesis and their affiliation to the two core topics as well as the individual chapters.

Research question	**Scope**	**Affiliation**
What are the requirements for modeling the various components for an accurate simulation of stationary energy storage systems?	BESS	Chapter 3
Which applications are essential for storage systems for grid integration? And which pattern do reference profiles have for these applications?	BESS	Chapter 4
Can existing stationary BESSs reduce the need for grid reinforcement through central coordination?	BESS & grid reinforcement	Chapter 5
Is a multi-storage approach suitable for grid planning? And how should the battery control be coordinated?	BESS & grid reinforcement	Chapter 6
Are BESSs an economical alternative to conventional grid reinforcement?	BESS & grid reinforcement	Chapter 7

1.3 Thesis outline

The remainder of this thesis is described in this section. The fundamentals of BESSs, distribution grids and the simulation of those are described in Chapter 2. Common applications for BESSs are discussed and conventional distribution grid reinforcement is described. Based on this state-of-the-art description, the novelty and the methods of this thesis are also discussed there.

Chapter 3 (*SimSES: A holistic simulation framework for modeling and analyzing stationary energy storage systems*) describes the open-source simulation tool for stationary energy storage systems SimSES. Here, the modeling of the individual components of a BESS is discussed in detail and the basic functionalities are demonstrated using two use-cases. The functionality and some key technical performance indicators for simulation of stationary energy storage systems (SimSES) are used to analyze various stand-alone operation strategies in detail in Chapter 4 (*Standard battery energy storage system profiles: Analysis of various applications for stationary energy storage systems using a holistic simulation framework*). The peak shaving algorithm in particular can be seen as a basis for the following work of this thesis.

Chapter 5 (*Peak Shaving with Battery Energy Storage Systems in Distribution Grids: A Novel Approach to Reduce Local and Global Peak Loads*) and Chapter 6 (*Reducing grid peak load through the coordinated control of battery energy storage systems located at electric vehicle charging parks*) form the core of this work. A method to reduce the peak power at a specific node as well as at the transformer or PCC in

distribution grids using stand-alone BESSs is presented in Chapter 5. An enhancement is described in Chapter 6, by coupling and coordinating the energy management system (EMS) of several storage units.

To complete the story of this PhD thesis an economic analysis is conducted in Chapter 7 (*Battery Energy Storage Systems as an Alternative to Conventional Grid Reinforcement*). Present as well as predicted costs for BESSs are compared with the costs for cable replacement in the MV-grid to evaluate the possibility of storage operation for grid operators. Finally, Chapter 8 concludes the thesis with an outlook of possible future research tasks. The outline of this thesis including all chapter captions is shown schematically in Figure 1.1

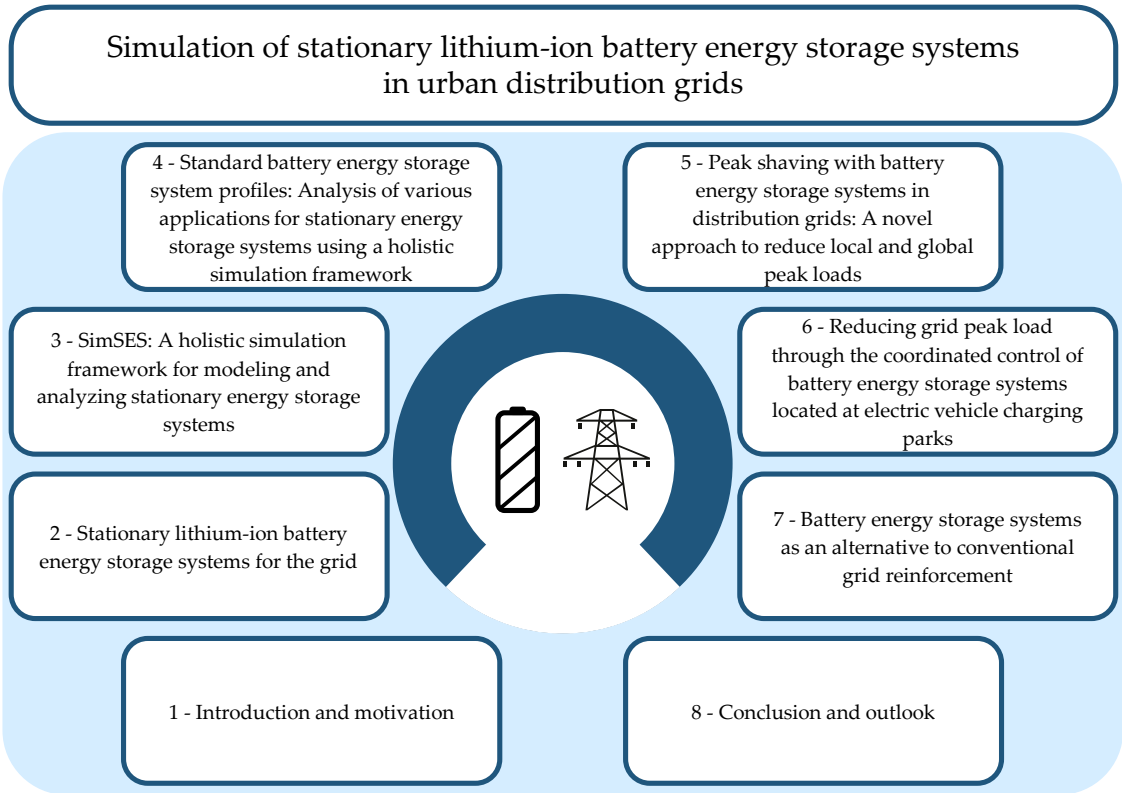

Figure 1.1: Schematic representation of the remainder of this thesis. The individual chapter headings are indicated in the boxes.

2 Stationary lithium-ion battery energy storage systems for the grid

A physical description of a stationary storage system and the distribution grid is essential for an understanding of the simulation models used in this thesis. This chapter forms the basis for the methods and developed EMSs of this PhD Thesis.

First, in Section 2.1, the fundamentals of stationary BESSs based on LIBs are described. Beside the basic composition of a BESS including the most relevant components, the functionality of LIBs is shown. However, the focus is on modeling of stationary BESSs. The models described there form the basis for the simulation tool SimSES, which is developed, used, and adapted in the individual publications.

Section 2.2 describes the most common use-cases for BESSs. The focus is on the state-of-the-art peak shaving strategy aiming to reduce the peak load of individual consumers. This strategy is used as a reference to compare the novel EMSs developed in this work. Furthermore, in this section the evaluation of storage systems regarding to the different applications are described with key characteristics. The six key characteristics are used and discussed in the further progress of this thesis to evaluate the stress on the BESSs operated with the developed EMSs.

Finally, Section 2.3 deals with the fundamentals of distribution grids. In this section mainly the simulation and the modeling used for this work is described and the basics of the software eDisGo, which is used for the power-flow analysis are shown. In addition, the current approach of grid operators for conventional grid reinforcement is discussed.

2.1 Fundamentals of stationary battery energy storage systems

Figure 2.1 shows a schematic overview of a LIB based stationary storage system including the connection to the electric grid. The major components of a BESS are typically the battery itself including a battery management system (BMS), a power electronics part as well as an EMS control. The power electronics part or AC/DC link may consist of single or multiple inverter units, depending on the application and storage size. Depending on the grid connection a transformer coupling element is necessary for integration to higher grid voltage levels. [42]

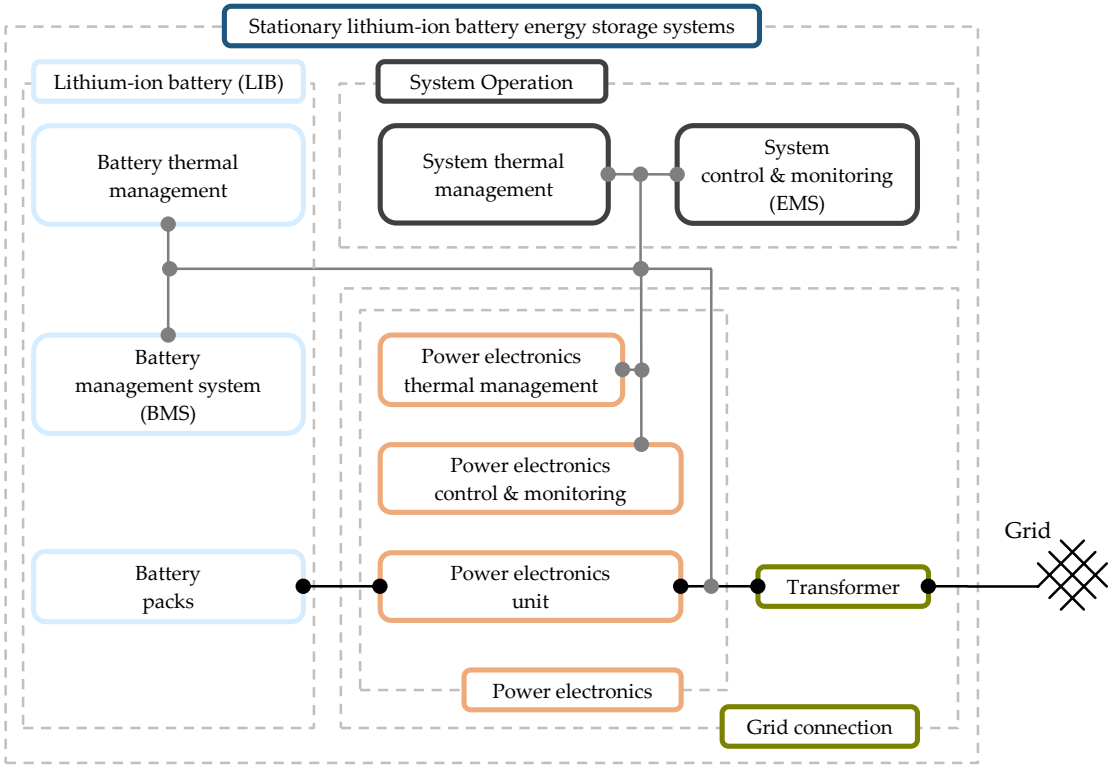

Figure 2.1: Schematic drawing of a stationary lithium-ion battery energy storage system including the grid connection. The figure is based on [7].

While the description of the LIB technology is shown in detail in the next subsection, here the battery pack is the starting point. Interconnection of individual LIB cells to battery modules and packs is a necessary step for developing stationary BESSs. On the one side a serial connection of cells sums up the voltage of the individual LIBs to the desired module or pack voltage and on the other side parallel connection of cells increases the usable capacity [43]. The BMS, linked to the system operation components, plays an important role in monitoring, calculating, reporting and controlling the states of LIBs, such as: voltage, temperature, cooling or heating demand, and current [44].

In addition, the LIB technology, the power electronics components are crucial in terms of system efficiency [45]. The power electronics unit may contribute significantly to the overall system efficiency, depending on topology and application [42]. Common topologies for power electronics units are the dedicated installation to each battery pack or the battery packs are connected in parallel to a common DC-bus [46]. If the BESS is connected to a higher grid level (i.e. MV-grid), a transformer unit is essential. Usually the transformer is a single-unit three phase transformer or consist of three separate

single-phase transformers [47].

The system operation components are required for reliable operation of the overall BESS. The EMS contains the hardware as well as the software to control the power flow and enable execution of operational strategies [48]. A supervisory control and data acquisition (SCADA) system is needed to monitor all system relevant states, to have centralized access, and to control the operation scheduling of the EMS [49]. Finally, the system thermal management controls all functions related to the heating, ventilation, and air conditioning of the BESS. The system thermal management is usually linked to the thermal management of the LIBs and the thermal management of the power electronics [50].

Appropriate sizing of the storage system components including the batteries capacity and nominal power of the power electronics part is an important criterion for system optimization, as for a maximizing the stakeholders' revenue not only attainable profits but also the investment costs and potential replacement costs have to be taken into account [51]. For this purpose, the method of linear optimization is often used in the literature [52, 53]. The relevant basics, which are necessary for this thesis, of this method will be described in Section 2.2.

2.1.1 Lithium-ion battery technology

The LIB cell forms the core of a BESS and is essential for an understanding of the electrical and thermal characteristics of an entire system [7]. In brief a LIB cell consists of two composite electrodes including current collectors and a separator in-between [54]. The battery cells are filled with an electrolyte, which typically contains an organic solvent, a conducting salt, as well as additives. [55]. Typical materials used for the negative electrode (anode) are carbon/graphite (C), lithium titanate oxide-based or silicon-based materials [56]. The positive electrode (cathode) typically consists of oxides such as lithium cobalt oxide, lithium nickel cobalt manganese oxide, lithium nickel cobalt aluminum oxide or other materials such as lithium-iron-phosphate (LFP) [57].

State-of-art lithium-ion cells exist in various cell formats, being prismatic, cylindrical, and pouch format [58]. During the charging process under an applied voltage, deintercalation of some lithium-ions from the cathode into electrolyte occurs and simultaneously an intercalation of an equivalent number of lithium-ions from the electrolyte into the anode, while the charge compensation takes place through the external circuit. During a discharge process, the reverse reaction occurs [54].

While discussing about LIBs degradation must be considered. These various cell-internal side reactions can have significant impact on the economics of an BESS project [7]. During lifetime and operation of a BESS, aging may result in significant changes of capacity and resistance and therefore it should be taken into account in system design as well as operation strategies [38]. The various aging effects are mainly caused by external environmental factors such as temperature and internal factors such as the generation of a solid electrolyte interface layer [59]. All these degradation effects and the link to various material compositions are discussed in detail in numerous papers and books such as the publications of Barré et al. [60], Wang et al. [61], Smith et al. [62], and Vetter et al. [63].

2.1.2 Modeling of stationary battery energy storage systems

In-depth models of the components of a BESS allow the simulation of energy storage systems. Each of these components require specific implementations regarding their physics and behavior. The focus

in the following is on modeling the LIB as well as the power electronics unit in SimSES. Thermal models are neglected in this dissertation, while the temperature is set to a constant of 25°C. And the various EMSs will be explained in Section 2.2. Figure 2.2 shows all in-depth models with the structure mainly used in this thesis for a stationary BESS including four main components: A AC/DC converter, a BMS, a LIB modeled as an equivalent circuit model, and an aging model with a coupled cycle detector.

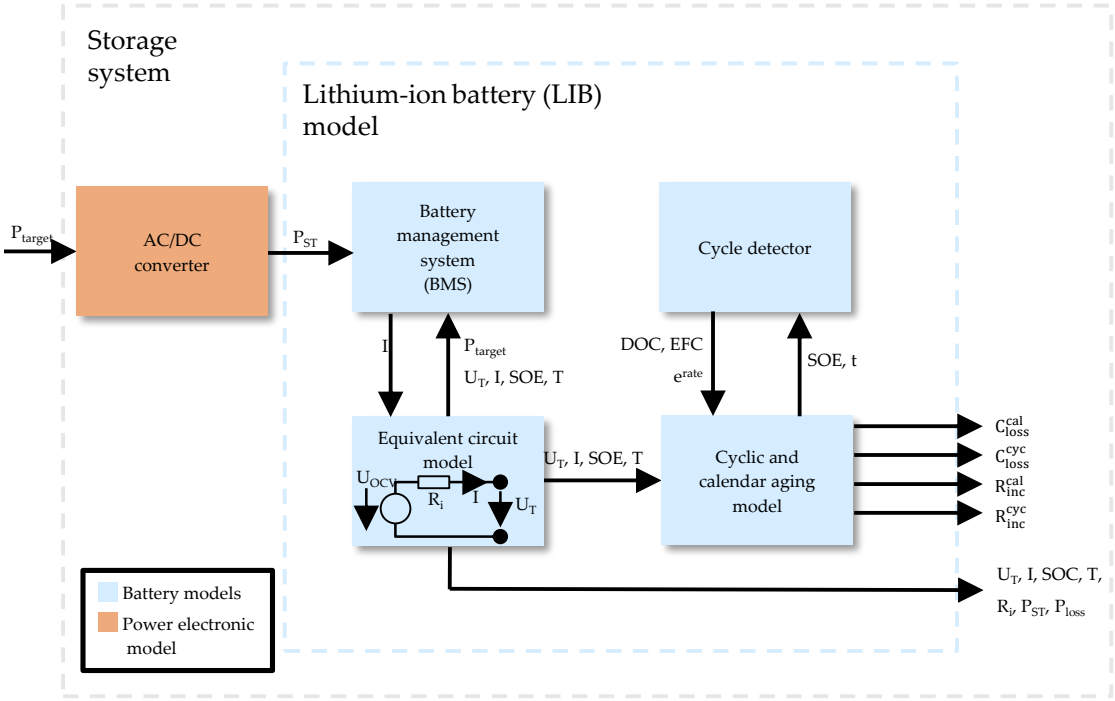

Figure 2.2: Overview of all in-depth models used in this thesis for a stationary lithium-ion battery energy storage system. The figure is based on [9].

Models of power electronics units are represented by power and voltage-dependent efficiency curves. In brief, the efficiency η_{PE} of a power electronics module is represented by a given storage power (P^{charge} or $P^{\mathrm{discharge}}$) and the rated power (P^{rated}) of the power electronics component as shown in Equation (2.1) for a charging event. Equation (2.2) shows the model mainly used in this dissertation, which is based on the work of Notton et al. [64]. In this thesis the following exemplary values are used: For the load dependent part $k = 0.0345$ and for the load independent part $p_0 = 0.0072$. This model of an AC/DC converter achieves a high efficiency above 10 % of the rated power P^{rated}. The efficiency η_{PE} is independent of the direction of the power flow and there is no hysteresis. Maximum efficiency is attained at $0.46 \cdot P^{\mathrm{rated}}$ with an efficiency of $\eta_{\mathrm{PE}} = 96.9\,\%$. Fixed efficiency values, linearized models or other functions, for example based on datasheets or own measurements, can be modeled in SimSES as well.

$$\eta_{\mathrm{PE}} = \mathrm{f}\left(\mathrm{P}^{\mathrm{charge}}, \mathrm{P}^{\mathrm{rated}}\right) \tag{2.1}$$

$$\eta_{\mathrm{PE}} = \frac{\frac{P_t^{\mathrm{charge,b}}}{P^{\mathrm{rated}}}}{\frac{P_t^{\mathrm{charge,b}}}{P^{\mathrm{rated}}} + \mathrm{p_0} + \mathrm{k} \cdot \left(\frac{P_t^{\mathrm{charge,b}}}{P^{\mathrm{rated}}}\right)^2} \tag{2.2}$$

The BMS is linked to the LIB model and is responsible for monitoring critical cell parameters. The BMS is modeled as a control unit to avoid that cell specific parameters, such as state of energy (SOE), voltage, current, and temperature, are beyond permissible ranges. According to these parameters, the BMS checks the input parameters and if limit violations occur, the current is restricted and returned to the LIB model. The other parameters are recalculated accordingly.

In the simulation tools used in this thesis, the LIB is represented as an equivalent circuit model including an open circuit voltage (OCV) and an internal resistance $\mathrm{R_i}$, due to an acceptable modeling accuracy with ease of parametrization [65, 66]. However, with an improved understanding of the cell-internal behavior, an increasing number of non-empirical physicochemical models have gained increasing interest in cell modeling [67–69]. These physicochemical models are giving a more detailed insight to cell internal states and loss mechanisms. But it remains challenging to find a valid parameter set for these cells of such models and to scale these models to the level of a full BESS with an acceptable computing time [70, 71].

In the used equivalent circuit model, the OCV is only dependent on the SOE but in future implementations in SimSES, the OCVs could be extended with further parameters like temperature or state of health. To improve performance, the interpolation of the OCV data was replaced by a fitted mathematical function. The internal resistance $\mathrm{R_i}$ takes the cell temperature, current, and the SOE into consideration. The required data is based on literature models and stored as look-up tables in SimSES and in between the available data points are linearized. Equation (2.3) shows the mathematical description of a LIB used in this thesis.

$$\mathrm{U_T} = \mathrm{U_{OCV}} - \Delta\mathrm{U} = \mathrm{U_{OCV}}\left(\mathrm{SOC}\right) - \mathrm{I} \cdot \mathrm{R_i}\left(\mathrm{SOC}, \mathrm{I}, \mathrm{T_{LIB}}\right) \tag{2.3}$$

As the current and the terminal voltage $\mathrm{U_T}$ are interdependent, differential equations are necessary for calculating these values in the discrete time domain as seen in Equation (2.3). To enhance the performance of the simulations the differential equations are replaced by an iteration loop. Using numerical approximation, the current and terminal voltage $\mathrm{U_T}$ are iteratively derived and the loop terminates after a predefined maximum number of iterations or as soon as the change of these values falls below a preset limit. As the battery values have to be checked in every iteration, this loop interacts between the equivalent circuit model and the BMS.

The main LIB used in this thesis is a LFP:C cell [72]. This type of cell is particularly suitable for stationary applications due to its higher cycle durability [38, 73]. The single cell capacity is 2850 mAh, the nominal cell voltage is 3.2 V, and the OCV is in the range of 2.0 - 3.6 V. The maximum $\mathrm{e^{rate}}$ according to the datasheet is 6.6 $\frac{1}{\mathrm{h}}$ in discharging direction and 1.0 $\frac{1}{\mathrm{h}}$ in charging direction. The internal resistance $\mathrm{R_i}$ of a new cell is 44.8 mΩ for a SOE of 50 %, a temperature of 25°C, and a charging event.

The modeling of aging characteristics of LIBs plays a crucial role in the simulative evaluation of BESSs, as degradation can have significant impact on the economics of a BESS project [74, 75]. In this dissertation the degradation is modeled following a semi-empirical superposition approach of

cyclic and calendar aging based on investigations by Naumann et al. for the used cell type as shown in Equation (2.4) and Equation (2.5) [10, 73]. In SimSES additional degradation models are implemented, such as two models for a LIB with a C anode and a lithium nickel cobalt manganese oxide cathode based on the work of Schmalstieg et al. [76] and Schuster et al.[77].

$$C_{\text{loss}}^{\text{total}} = C_{\text{loss}}^{\text{cal}} + C_{\text{loss}}^{\text{cyc}} \tag{2.4}$$

$$R_{\text{inc}}^{\text{total}} = R_{\text{inc}}^{\text{cal}} + R_{\text{inc}}^{\text{cyc}} \tag{2.5}$$

According to the used aging model, calendar aging is computed once every simulation step and takes the following cell parameters into account for both, the capacity loss ($C_{\text{loss}}^{\text{cal}}$) as well as the resistance increase ($R_{\text{inc}}^{\text{cal}}$): the actual time t, the SOE, and the cell temperature. The capacity loss and resistance increase regarding the cyclic aging is only calculated following the detection of a half cycle by the cycle detector.

A half cycle is detected if the SOE is at predefined limits for the maximum (SOE^{max}) or minimum (SOE^{min}) energy content or if there is a change from charging to discharging or discharging to charging respectively. The usage of such a cycle detector decreases the calculation time and allows determining required states for the cyclic aging model. Required parameters for both, the capacity loss ($C_{\text{loss}}^{\text{cyc}}$) as well as the resistance increase ($R_{\text{inc}}^{\text{cyc}}$) are the total number of full equivalent cycles (FECs), the e^{rate} as well as the depth of cycle (DOC) for this event. The total number of FECs is calculated by summing up the detected half cycles. For example, two half cycles from 0 % to 100 % SOE or 100 % to 0 % SOE result in one FEC.

2.2 Grid-connected battery energy storage system

It is essential for the description of the developed EMSs in this dissertation, to discuss state-of-the-art applications for LIB based stationary storage systems. This section describes a selection of distribution grid applications for BESSs with a focus on the peak shaving strategy. As mentioned earlier, this strategy is used as a reference to compare the novel EMSs developed in this work. Similar to the modeling approach of all relevant storage components as shown in Section 2.1, this section shows the method of conducting the simulations of various use-cases. Finally, the technical key characteristics used for the evaluation of BESSs are described herein.

2.2.1 Distribution grid level applications of stationary battery energy storage systems

In Figure 2.3 an overview of common distribution grid level applications for stationary BESSs is given. The focus herein is on BESSs, based on the LIB technology. Additional applications and grid level affiliation of non-LIB based storage technologies, such as redox flow batteries or compressed air energy storage systems, are described in various other publications [78–80]. It should be taken into account, that this figure is only a schematic representation and the affiliation to the LV grid or MV grid is not fixed.

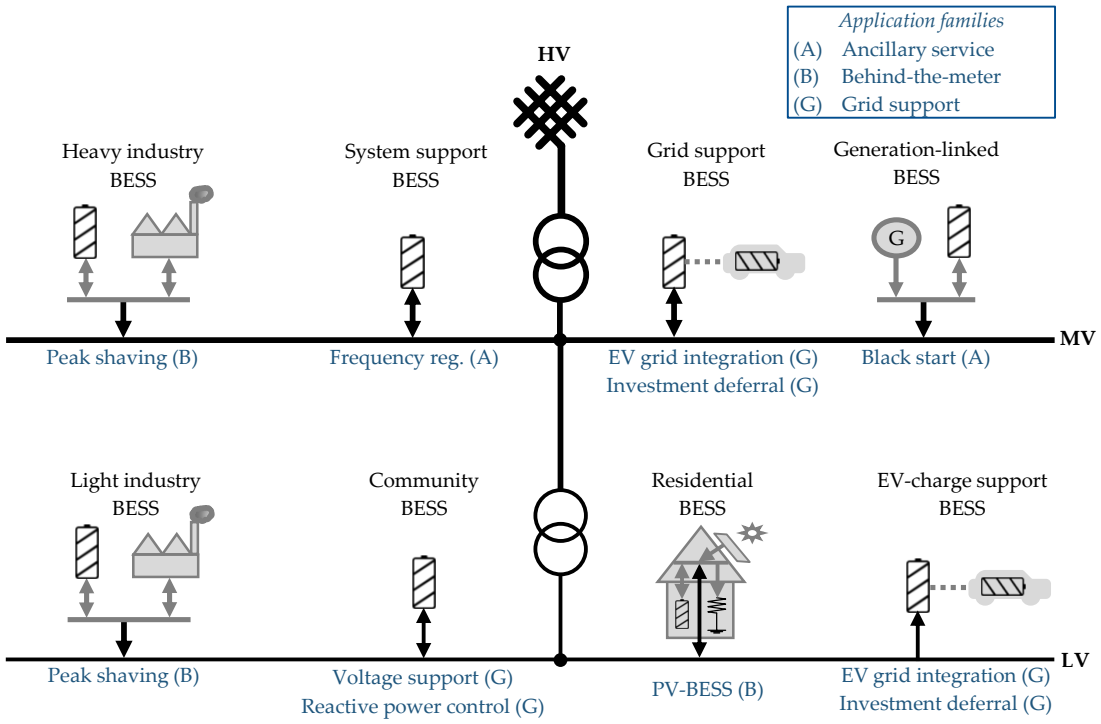

Figure 2.3: Overview of common applications for stationary battery energy storage systems based on lithium-ion batteries in medium voltage (MV) grids as well as low voltage (LV) grids. The figure is based on [7].

As the focus in this thesis is on LIB based storage systems, the applications are classified to three categories: Ancillary service, behind-the-meter, and investment deferral or local grid support. It should be considered that this classification is suitable for analysis of all BESS applications relevant for this dissertation and may not match well for other types of storage systems or types of applications. Energy trading to use alternating price signals at the energy spot markets is an example, which is gaining increasing interest for BESSs [81–83]. However, this kind of application focuses on maximizing the revenue of a BESS project, while in the following also technical benefits are discussed.

In the application family of ancillary services, the use cases are mainly located at a MV level. One application task for BESSs in this classification is linked to generation units. The black start capability of a generation unit describes the characteristics to restart the generation of electricity without the support of an external power [84, 85]. In case of supply failure, such as technical defects or cyber attacks, parts, or the entire generation unit may collapse [86]. A LIB based BESS is well-suited for this application, due to its high nominal power and high availability [87].

This AC grid in Germany is part of the European Network of Transmission System Operators for Electricity (ENTSO-E) and is characterized by a nominal frequency of 50 Hz [88]. Due to constantly fluctuating generation and power demand, the grid frequency alternates around these 50 Hz. A drop in frequency indicates that the current generation is below the power demand. To keep the balance between consumption and feed-in and consequently achieving a frequency of 50 Hz again, different market systems with different time horizons exist [89]. BESSs are most suitable for providing FCR, as this is currently the first product, and it must be activated at full power within 30 seconds [90, 91].

In-depth, providing FCR with a BESS underlies an established market according to a regulatory framework overseen by the transmission system operators [92, 93]. As FCR is a symmetric product, a BESS must provide its prequalified power ($\geq$ 1 MW) in both directions. Additionally, an energy reserve at the lower and at the upper end of its SOE is necessary. To fulfil these requirements for FCR provision, energy is sold or bought at the spot market to keep the SOE in the valid range.[94]. While the focus in this thesis is on stand-alone storage systems, there are approaches to use aggregated BESSs [95, 96] or EVs [97, 98] to achieve the minimum required power of 1 MW. The implementation of the EMS in SimSES will be explained in the following subsection.

In contrast to ancillary services, BESS can also serve various applications within the behind-the-meter classification. The combination of a local generation, such as photovoltaic units, with a BESS for residential households is gaining a high level of interest in the last few years [99, 100]. In brief, whenever a solar surplus occurs, the BESS is charged and vice versa. The end user expects with this use-case to increase its self-consumption and to save energy costs [101]. LIB based storage systems are well-suited for this application due to acceptable lifetime, a high level of safety, and high energy as well as high power densities [102, 103].

Adapting this simple (greedy) control strategy for these BESSs to reduce the maximum power fed into the grid may allow achieving additional grid reliving effects [104]. As these kind of storage systems are mainly located at the LV grid, this strategy may prevent over-voltage issues but is not suitable for avoiding over-loading problems caused by a high share of EVs [40]. However, various techno-economic calculations showed that self-consumption increase via BESS integration is in most cases not an economically viable option at present, when taking into account LIB storage investment and degradation costs [105, 106]. Such a storage system could only be an economical option for regions with low feed-in tariffs for photovoltaic systems and high costs for energy consumed [107].

In contrast, to the residential consumers, the tariff system for industrial consumers (annual energy consumption $\geq$ 100 MWh) consists of costs for the consumed energy and a demand charge for the highest peak power of an industrial consumer [108]. The aim for a BESS with a state-of-the-art peak shaving strategy is to minimize power peak value within a defined billing period [109, 110]. With continuously falling costs for LIBs, it is expected that the market for peak shaving storage system will grow dramatically in the next years [111].

In brief, the peak shaving algorithm operates with a comparison of the consumer power and a predefined peak shaving threshold [36, 112]. If the demand is above the threshold, the BESS starts to discharge until the consumer power falls below the threshold again [27]. The expected benefit for the grid operator of this tariff scheme is to avoid cable overloading and lower peak loads on the transformer, which consequently would avoid cost intensive grid reinforcement [113]. Using the state-of-the-art peak shaving algorithm, the BESS is recharged as soon as the demand is below the threshold [114]. However, this operation strategy is independent of the power at the PCC and therefore it is not reliable in order to reduce the peak power in the associated distribution grid.

In the application family of grid supportive storage systems, BESSs may act as support unit for reactive power control or in local voltage regulation processes [115]. Due to increasing integration of renewable energy sources, reactive power management has become a major planning and operation issue in modern distribution grids [116]. As the voltage at PCC might increase beyond the maximum limit in certain time periods, reactive power control is necessary to keep the grid stable [117, 118]. Integration and appropriate control of BESS for voltage support can help to reduce such voltage fluctuations via coordinated active and reactive power [11, 23]. However, there is currently no standardized market that financially compensates the storage stakeholders [13].

As the reactive power control is mainly a task for storage systems in rural areas, grid supportive BESSs in urban areas are used for active power control [119]. This is due to the fact, that over-loading caused by an increasing number of charging possibilities will be a main issue in the future [14]. As an alternative to grid infrastructure updates, it is proposed that EV charging stations should be supported via BESS serving as power boost [120]. LIBs are seen as a well-suited solution due to their high power density and slow degradation compared to other types of batteries [121, 122]. Summarizing this grid supportive use-case for BESS, it can be derived, that co-simulation of BESSs and distribution grids are necessary to investigate the effects on the distribution grid of such storage systems in detail.

2.2.2 Simulation of battery energy storage systems and evaluation metrics

Independent of the application of the choice, technical and economical parameters, such as efficiency or return on investment, for BESSs are crucial to the success of a storage project [123]. To address this challenge, holistic simulation tools are essential before investing in energy storage systems [124]. SimSES is developed, adapted, and used in this thesis to predict internal states of a storage system such as the SOE or the storage internal losses. Based on the modeling of the components of a BESS shown in Section 2.1, the methodology for developing a EMS is discussed in the following paragraphs. In particular, the state-of-the-art EMS for a BESS with a peak shaving strategy, including the storage sizing, is shown. This strategy is the reference for the novel developed EMSs in Chapter 5 and Chapter 6. In order to gain a deeper understanding of development EMSs, the strategies for providing FCR and self-consumption increase are briefly presented. To analyze various EMS, six key characteristics are derived and described in detail at the end of this subsection.

In this dissertation, a pre-processing linear optimization algorithm is used to find a valid peak shaving threshold $\mathrm{PS}^{\mathrm{threshold}}$ within a defined time horizon T for a load profile of an industrial consumer at a specific node b in the grid. The load profile $\mathrm{S}_t^{\mathrm{b}}$ for each time step t is described as a vector $\mathbf{S}^{\mathrm{b}}$ as shown in Equation 2.6. As the focus in this dissertation, is on detailed co-simulations of BESSs and distribution grids, perfect foresight is assumed for the load profile of an industrial consumer. However, in the field of uncertainties in forecasting load profiles, various approaches exist [125, 126].

$$\mathbf{S}^{\mathrm{b}} = \left[\mathrm{S}_1^{\mathrm{b}}, \cdots, \mathrm{S}_t^{\mathrm{b}}, \cdots, \mathrm{S}_{\mathrm{T}}^{\mathrm{b}}\right] \tag{2.6}$$

To find a valid peak shaving threshold $\mathrm{PS}^{\mathrm{threshold}}$ through a linear programming optimization tool for energy storage systems (lp_opt) is used. After defining the problem mathematically, including an objective function and constraints, the algorithm is usually able to find the solution relatively fast and therefore well-suited this BESS related problem [8]. The objective is to minimize the peak load at the industrial consumers connection point to the distribution grid for the time horizon T. Therefore, the objective function for a fixed storage capacity E^{nominal} is defined in Equation 2.7.

$$\text{minimize} : \left\{\mathrm{PS}^{\mathrm{threshold}}\right\} \tag{2.7}$$

If the capacity of a BESS (E^{nominal}) is also to be determined, a cost function must be taken into account. This enhanced objective function (cf. Equation 2.8) allows finding a profit optimal compromise between electricity costs as well as BESS investment costs ($\mathrm{p}_{\mathrm{BESS}}^{\mathrm{invest}}$). In this equation t_{proj} indicates the project operation/depreciation period.

$$\text{minimize} : \left\{\mathrm{PS}^{\mathrm{threshold}} \cdot \mathrm{p}_{\mathrm{peak}} \cdot \mathrm{t}_{\mathrm{proj}} + E^{\mathrm{nominal}} \cdot \mathrm{p}_{\mathrm{BESS}}^{\mathrm{invest}}\right\} \tag{2.8}$$

In addition, the BESS is also subject to a number of boundary conditions, independent of the optimization function chosen. First of all, the SOE must remain within the given bounds $\mathrm{SOE}^{\mathrm{min}}$ and $\mathrm{SOE}^{\mathrm{max}}$. Equation 2.9 shows this constraint, while the actual energy content for a specific time step t of a BESS is denoted as E_t^{actual}.

$$\mathrm{SOE}^{\mathrm{min}} \cdot E^{\mathrm{nominal}} \leq E_t^{\mathrm{actual}} \leq \mathrm{SOE}^{\mathrm{max}} \cdot E^{\mathrm{nominal}} \tag{2.9}$$

The charging power (P^{charge}) as well as the discharging power ($P^{\mathrm{discharge}}$) has to be lower than the respective maximum energy rate ($\mathrm{e}^{\mathrm{rate}}$) of the BESS (cf. Equation 2.10 and Equation 2.11). As the $\mathrm{e}^{\mathrm{rate}}$ can be different depending on the power flow direction, the maximum $\mathrm{e}^{\mathrm{rate}}$ is denoted as $\mathrm{e}_{rate}^{\mathrm{charge}}$ and in discharging direction as $\mathrm{e}_{rate}^{\mathrm{discharge}}$. The charging and discharging powers are also limited by the rated power P^{rated} of the power electronics as shown in Equation 2.12 and Equation 2.13. These constraints must be sufficient for each time step t.

$$P_t^{\mathrm{charge}} \leq \mathrm{e}_{rate}^{\mathrm{charge}} \cdot E^{\mathrm{nominal}} \quad \forall\, \mathrm{t} \tag{2.10}$$

$$P_t^{\mathrm{discharge}} \leq \mathrm{e}_{rate}^{\mathrm{discharge}} \cdot E^{\mathrm{nominal}} \quad \forall\, \mathrm{t} \tag{2.11}$$

$$P_t^{\text{charge}} \leq P^{\text{rated}} \quad \forall\, \text{t} \tag{2.12}$$

$$P_t^{\text{discharge}} \leq P^{\text{rated}} \quad \forall\, \text{t} \tag{2.13}$$

Finally, the energy conservation of a BESS is defined in Equation 2.14 and again this constraint must be sufficient for each time step t. The actual energy content E_t^{actual} of a BESS depends on the energy content of the previous time step, the charged energy E_t^{charge} and the discharged energy $E_t^{\text{discharge}}$. An estimated efficiency η_{BESS} of 90 % is considered for both, E_t^{charge} and $E_t^{\text{discharge}}$.

$$E_t^{\text{actual}} = E_{t-1}^{\text{actual}} + E_t^{\text{charge}} \cdot \eta_{\text{BESS}} - \frac{E_t^{\text{discharge}}}{\eta_{\text{BESS}}} \tag{2.14}$$

The resulting peak shaving threshold $\text{PS}^{\text{threshold}}$ is used as an input parameter for the operation strategy within SimSES. This operation strategy works as follows: as soon as the power S_t^{b} is above the specified threshold, the additionally required power is provided by the BESS, as illustrated in Figure 2.4. In this example a fixed storage capacity of 100 kWh was assumed. The peak shaving threshold $\text{PS}^{\text{threshold}}$ (dashed red line) was determined in accordance with Equation 2.7. Furthermore, it can be seen that the BESS recharges as soon as the power S_t^{b} is below the peak shaving threshold $\text{PS}^{\text{threshold}}$. This ensures that the charging of the storage system does not cause the exceedance of the threshold. It must be noticed that this strategy only takes the local profile into consideration. To use the BESS also to reduce the peak load at the PCC, the shown state-of-the-art peak shaving strategy must be adapted.

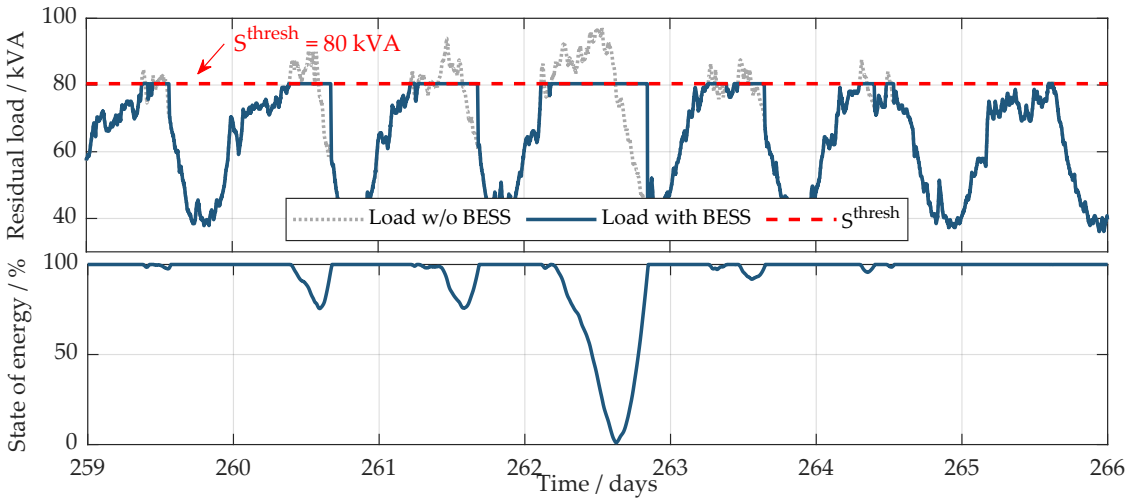

Figure 2.4: Exemplary load profile and the behavior of a battery energy storage system (BESS) operating with a state-of-the-art peak shaving strategy. The power above the threshold is provided by a stationary BESS and the associated state of energy is illustrated at the subplot at the bottom. The figure is reproduced from [1].

The EMS for providing FCR in SimSES was developed according to the German regulatory framework [92, 93] and due to the legal interpretation at the time of developing this EMS (May 9, 2019) [127]. However, it can be easily adapted, in future releases of SimSES. A BESS providing FCR has to always ensure that the full prequalified power P^{PQ} can be provided for 15 min as long as the frequency is in normal progression. The requested charging P^{charge} and discharging power $P^{\mathrm{discharge}}$ is proportional to the frequency deviation $\Delta \mathrm{f}$ and is dependent on the prequalified power P^{PQ}, which has a minimum of 1 MW. Below 49.8 Hz or above 50.2 Hz the storage power is set to $\pm P^{\mathrm{PQ}}$. Equation 2.15 shows the behavior of a storage system in this application.

$$\begin{aligned}
P^{\mathrm{charge}} &= P^{\mathrm{PQ}} \cdot \frac{\Delta \mathrm{f}\,(\mathrm{t})}{0.2\,\mathrm{Hz}} && \text{for} && 0\,\mathrm{Hz} \leq \Delta \mathrm{f} \leq 0.2\,\mathrm{Hz} \\
P^{\mathrm{charge}} &= P^{\mathrm{PQ}} && \text{for} && \Delta \mathrm{f} > +0.2\,\mathrm{Hz} \\
P^{\mathrm{discharge}} &= -P^{\mathrm{PQ}} \cdot \frac{\Delta \mathrm{f}\,(\mathrm{t})}{0.2\,\mathrm{Hz}} && \text{for} && 0\,\mathrm{Hz} \geq \Delta \mathrm{f} \geq -0.2\,\mathrm{Hz} \\
P^{\mathrm{discharge}} &= -P^{\mathrm{PQ}} && \text{for} && \Delta \mathrm{f} < -0.2\,\mathrm{Hz}
\end{aligned} \tag{2.15}$$

If the SOE falls below a predefined lower limit or it exceeds an upper limit the BESS in these simulations charges or discharges by trading energy on the electricity market, in particular the intra-day market [41]. The SOE limits are depending on the prequalified power P^{PQ} and the storage capacity E^{nominal} as shown in Equation 2.16 and Equation 2.17. To reach these limits as infrequently as possible, the efficiency must be considered and therefore the SOE set-point is above 50 %. The efficiency is depending on the system configuration and is estimated at the beginning of the simulation.

$$\mathrm{SOE}^{\mathrm{min}} = \frac{0.25\,\mathrm{h} \cdot P^{\mathrm{PQ}}}{E^{\mathrm{nominal}}} \tag{2.16}$$

$$\mathrm{SOE}^{\mathrm{max}} = \frac{E^{\mathrm{nominal}} - 0.25\,\mathrm{h} \cdot P^{\mathrm{PQ}}}{E^{\mathrm{nominal}}} \tag{2.17}$$

Additionally, to this SOE set-point shift, the regulatory framework in Germany allows different degrees of freedoms (DOFs) [128]. In SimSES the following DOFs are only used, if this can delay market participation in the intraday market.

- **Frequency dead band:** In the frequency range between 49.99 Hz and 50.01 Hz, the output power of the BESS can be set to 0 MW and must not follow the frequency derivation according to Equation 2.15.
- **Overfulfillment:** In both cases, charging and discharging, it is allowed to exceed the requested power as shown in Equation 2.15) by 20 %.

Another DOF is slope of the requested FCR power. The charging power P^{charge} or discharging power $P^{\mathrm{discharge}}$ as calculated in Equation 2.15 must be provided within 30 s or earlier. Therefore, the slope of the provided FCR power can be adjusted within the time interval of 30 s allowing to control the charging or discharging rate. However, this DOF is neglected in this thesis, as the response time of a BESS is very fast [129, 130]. The market FCR was initially launched in 2007 and started with monthly delivery periods, but this period has shortened steadily to weekly, daily, and to the currently applicable 4 hours [128].

In this thesis two different operation strategies for the self-consumption increase of residential consumers with a BESS are discussed: A greedy strategy and an extension of the deed-in damping EMS based on Zeh and Witzmann [40]. The EMS for the greedy algorithm works with a simple comparison between the generation of the photovoltaics unit P^{PV} and the consumption by the household P^{Load} at each timestep t. Whenever a solar surplus occurs, the BESS is charged and vice versa as shown in Equation 2.18) and Equation 2.19). At sunny summer days, the BESS is fully charged at around 12PM with this conventional strategy. This causes a rapid rise of the power fed into the grid. Another disadvantage of this strategy is the high charging power, which may lead to a faster decrease of the LIB capacity as described in [131].

$$P^{\mathrm{charge}} = P^{\mathrm{PV}} - P^{\mathrm{Load}} \qquad \text{for} \qquad P^{\mathrm{PV}} > P^{\mathrm{Load}} \tag{2.18}$$

$$P^{\mathrm{discharge}} = P^{\mathrm{Load}} - P^{\mathrm{PV}} \qquad \text{for} \qquad P^{\mathrm{Load}} > P^{\mathrm{PV}} \tag{2.19}$$

In order to reduce the maximum power fed into the grid, a nearly constant BESS charging power P^{charge} during the whole daytime is calculated by the EMS. Reducing the maximum feed-in power allows for a higher self-consumption rate, if the maximum feed-in power is limited by the distribution grid operator as described in [107]. If a surplus ($P^{\mathrm{PV}} > P^{\mathrm{Load}}$) occurs, the charging power P^{charge} is calculated by dividing the actual battery capacity E_t^{actual} by a predicted time t^{re} and an estimated mean efficiency η_{BESS} of the BESS. This predicted time t^{re} indicates the time span until the load P^{Load} is higher than the solar generation P^{PV}. The calculation of the charging power P^{charge} is shown in Equation 2.20. As soon as the consumption by the household P^{Load} is higher than the output power of the photovoltaics unit P^{PV}, the discharging power $P^{\mathrm{discharge}}$ is calculated according to the greedy algorithm (cf. Equation 2.19).

$$P^{\mathrm{charge}} = \frac{E_t^{\mathrm{actual}}}{t^{\mathrm{re}} \cdot \eta_{\mathrm{BESS}}} \quad \text{for} \quad P^{\mathrm{PV}} > P^{\mathrm{Load}} \tag{2.20}$$

For EMSs for other applications, the reader is referred to further literature. For example, in the field of energy trading a EMS is presented in the work of Bui et al. [132]. A comprehensive review of EMSs can be found in the publication of Li and Wang [48]. However, when discussing about beneficial effects on the distribution grid through storage systems, one should also consider the stress of a BESS. Hence, six technical characteristics are defined aim to discuss the differences within the storage applications. These characteristics will be used in the following chapters of this thesis to compare the novel developed EMSs with the state-of-the-art peak shaving strategy. The technical performance indicators are implemented in the analysis of SimSES and described in the following paragraphs in detail.

1. Number of full equivalent cycles

The total number of full equivalent cycle (FEC) within a time horizon T is calculated by dividing the positive energy throughput $E_{\mathrm{T}}^{\mathrm{pos}}$ by the storage capacity E^{nominal} as shown in Equation 2.21. Other terms such as equivalent full cycles (EFC) or full cycle equivalents (FCE) are also used in the literature. The FEC varies between the applications and is crucial for the degradation of a LIB [131, 133]. For example, a BESS providing FCR comes along with more than 240 FECs per year, while a storage

system in the peak shaving application reaches around 20 FECs annually.

$$\mathrm{FEC} = \frac{E_{\mathrm{T}}^{\mathrm{pos}}}{E^{\mathrm{nominal}}} \tag{2.21}$$

2. Efficiency

The efficiency of a storage system η_{BESS} is calculated by counting the energy that is extracted from the storage system $E_{\mathrm{T}}^{\mathrm{neg}}$ divided by the energy that is stored in the storage system $E_{\mathrm{T}}^{\mathrm{pos}}$. The SOE at the beginning of an analyzed time horizon T and at the end of this analyzed time horizon T is taken into account as well. Equation 2.22 shows this calculation as implemented in SimSES. This characteristic allows to determine losses in the various components of a BESS while operating in a specific application. Losses in power electronic units are usually far higher than the losses in the LIB [42, 134]. Depending on the application of choice, the simulations in this dissertation derive storage system efficiencies (η_{BESS}) between 70 % and 90 %. Through improved power flow distribution strategies, a higher efficiency for the power electronic unit and consequently the overall storage system can be reached [135].

$$\eta_{\mathrm{BEES}} = \frac{|E_{\mathrm{T}}^{\mathrm{neg}}|}{E_{\mathrm{T}}^{\mathrm{pos}} - (\mathrm{SOE}_{\mathrm{end}} - \mathrm{SOE}_{\mathrm{start}}) \cdot E^{\mathrm{nominal}}} \tag{2.22}$$

3. Cycle depth in discharge direction

The DOC in discharge direction is calculated by using the differences in SOE, whenever a cycle is detected. As described earlier, in SimSES a half-cycle detector is implemented. A half cycle is detected, if there is a change from charging to discharging or discharging to charging. Furthermore, if the SOE is at predefined limits for the maximum ($\mathrm{SOE}^{\mathrm{max}}$) or minimum ($\mathrm{SOE}^{\mathrm{min}}$) energy content. For example, if the full energy of a BESS can be used, these limits are $\mathrm{SOE}^{\mathrm{max}} = 100\,\%$ and $\mathrm{SOE}^{\mathrm{min}} = 0\,\%$. Then the DOC is calculated by subtracting the SOE at the beginning and the SOE at the end of the half-cycle as indicated in Equation 2.23.

This characteristic describes how deep the storage system is discharged before recharging it. Higher DOCs may lead to a higher cyclic aging of the LIB [76, 77]. To enable a comparison between the applications and consequently varying storage capacities the DOC is stated in percentage of the total nominal energy E^{nominal}. If, for example, a discharge event occurs with 20 kW for one hour, the DOC is 0.2 for a 100 kWh storage system and 0.1 for a 200 kWh BESS.

$$\mathrm{DOC}_{\mathrm{dis}} = \mathrm{SOE}_{\mathrm{cycle,start}} - \mathrm{SOE}_{\mathrm{cycle,end}} \tag{2.23}$$

4. Number of changes of sign

Depending on the storage application, the resulting storage profile might change from charging to discharging and vice versa very often or just a few times per day. Those changes of signs activate the power electronics. Beside switching losses, a high number of sign changes may also lead to a reduced lifetime of the power electronics unit [136]. On the one hand a storage system used for providing FCR follows the grid frequency a high number of about 600 sign changes occur each day. On the other hand, a BESS operating in the peak shaving application is only stressed with 0.1 to 5 sign changes per day.

5. Length of resting periods

Regardless of the application of choice, a storage system will not be used consistently over time. Hence, the length of resting periods represents another characteristic, which indicates times, the BESS

is neither charged nor discharged ($P^{\text{charge}} = P^{\text{discharge}} = 0$). In this thesis, the average value of resting period length is indicated in minutes. Depending on the application the length of those resting periods may vary significantly. On the one side this characteristic is chosen because auxiliary users can be turned off during long resting periods. On the other hand, BESSs with a high average value of resting period length are underutilized and it should be considered to use these for stacking multiple applications [137, 138].

6. Energy between changes of sign

Another chosen characteristic is the energy that is charged or discharged between changes of signs. The amount of the energy is normalized to the nominal capacity E^{nominal}, which is necessary to compare BESSs with different capacities.

Beside the technical comparison of storage systems, it is also necessary to evaluate BESSs. With the focus to an economic comparison of the BESS and conventional grid reinforcement in Chapter 7, the data research only includes investment costs. Issuances for operation and maintenance are neglected. In this thesis it is assumed that the storage system is only used as to avoid grid upgrade and therefore does not generate any income. To enable a comparison, the depreciation period t_{proj} and the discount rate r must be taken into account. The total investment costs are calculated by multiplying the specific costs $\text{p}_{\text{BESS}}^{\text{invest}}$ with the nominal energy E^{nominal}. Equation 2.24 shows the calculation of the discounted total costs for a BESS $\text{P}_{\text{BESS},0}^{\text{invest}}$.

$$\text{P}_{\text{BESS},0}^{\text{invest}} = \frac{\text{p}_{\text{BESS}}^{\text{invest}} \cdot E^{\text{nominal}}}{(1+\text{r})^{t_{\text{proj}}}} \tag{2.24}$$

2.3 Fundamentals of distribution grids

Besides the simulation of BESS, it is necessary to model and simulate a distribution grid to analyze the effects on the grid of various EMSs. This section describes the distribution grid mathematically, which is necessary to calculate the line flows in a grid [139]. Based on this model the simulation tool for the power flow analysis is described. Furthermore, the used load profiles in this study are shown. Based on these descriptions, the effects of storage systems in a synthetic distribution grid are analyzed in this thesis. Finally, the fundamentals of conventional distribution grid upgrade are shown in this section. This allows to evaluate storage systems operated as an alternative to this distribution grid reinforcement.

2.3.1 Simulation of distribution grids

Figure 2.5 shows a graphical representation for a medium-voltage grid including all denotations for a mathematical description. Besides an industrial consumer and a BESS, a charging park is included. This allows the description of the included load profiles for the studies in this thesis. It should be noticed that the BESS is operated in an active power mode only. The load profiles for the industrial as well as residential consumers are shown as well in this subsection. The following equations, definitions, and load profiles are used to perform a power flow analysis to evaluate the states of a distribution grid both with and without storage systems.

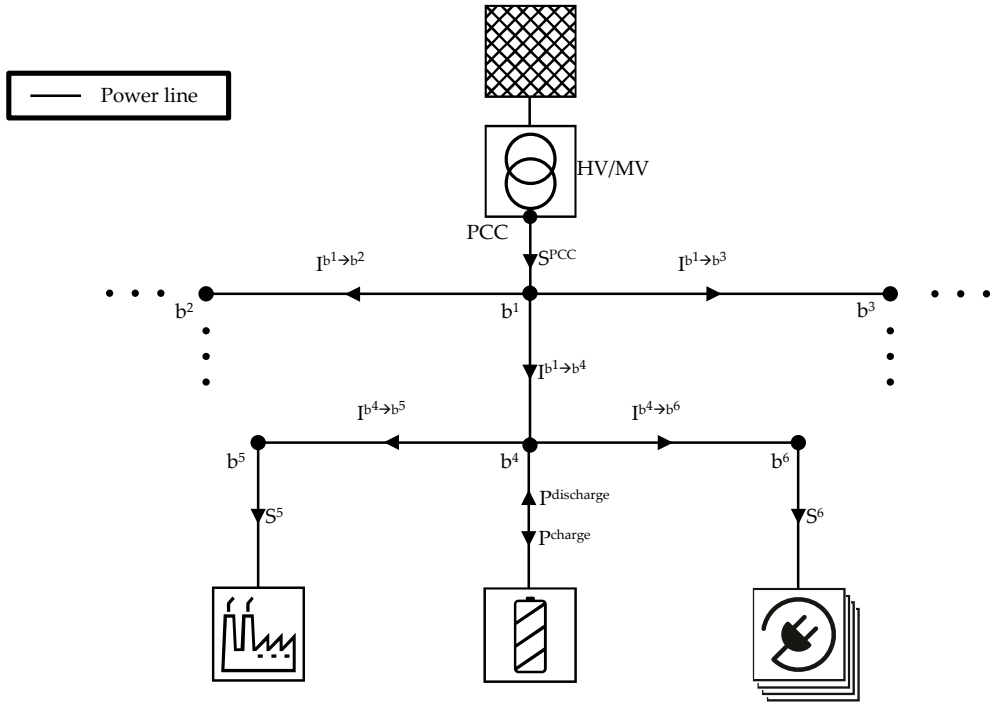

Figure 2.5: Graphical representation of a medium-voltage grid including all denotations for a mathematical description. The figure is based on [2].

In Equation 2.25 the vector **N** for all nodes b within a distribution grid is described. The total number of nodes is denoted as B in this thesis.

$$\mathbf{N} = [1, \cdots, \mathrm{b}, \cdots, \mathrm{B}]^{\mathrm{T}} \tag{2.25}$$

The time step t within a defined time horizon T is indicated by a vector H as shown in Equation 2.26. The results shown in the Chapters 5, 6, and 7 are based on a simulation duration of six months (T = 6 months), which represents a tradeoff between seasonal fluctuation and computation time. The simulation step size t in these studies is set to 15 minutes. The 15-minute time discretization is due to the fact that the power tariff scheme in Germany is based on 15-minute time step demand averages [108].

$$\mathbf{H} = [1, \cdots, t, \cdots, \mathrm{T}] \tag{2.26}$$

The apparent power $\mathrm{S}_t^{\mathrm{b}}$ at each node b for each time step t before is defined by a matrix **S**. This load matrix, shown in Equation 2.27, is beside the structure of the distribution grid crucial for the power flow analysis.

$$\mathbf{S} = \begin{pmatrix} \mathrm{S}_1^1 & \cdots & \mathrm{S}_t^1 & \cdots & \mathrm{S}_{\mathrm{T}}^1 \\ \vdots & \ddots & \vdots & \ddots & \vdots \\ \mathrm{S}_1^{\mathrm{b}} & \cdots & \mathrm{S}_t^{\mathrm{b}} & \cdots & \mathrm{S}_{\mathrm{T}}^{\mathrm{b}} \\ \vdots & \ddots & \vdots & \ddots & \vdots \\ \mathrm{S}_1^{\mathrm{B}} & \cdots & \mathrm{S}_t^{\mathrm{B}} & \cdots & \mathrm{S}_{\mathrm{T}}^{\mathrm{B}} \end{pmatrix} \tag{2.27}$$

In order to apply and test the EMSs introduced in this dissertation, a synthetic test grid is selected consisting of a MV grid and 146 underlying LV grids [140]. The simulations in this dissertation are based different load profiles for residential and industrial consumers at the various nodes b in the selected grid. The household loads used were created and published by HTW Berlin [141]. The industrial profiles are provided by industry partners of the Technical University of Munich. The load profiles of the EV charging stations have been examined by using *SimBEV* [142]. This tool was developed by researchers of the Reiner Lemoine Institute in Berlin. All profiles differ in time, frequency, and peak load duration.

Power flow analysis, or load flow analysis, is widely used to calculate the voltages at different buses as well as line flows in the grid [143, 144]. The input variables of a power system are built using the relevant grid data, loads, and generation data. Since the equations to calculate the outputs are nonlinear, iterative methods such as the Newton-Raphson algorithm or the Gauss-Seidel algorithm are commonly used to solve this problem numerically [145]. To calculate the line flows and the grid reinforcement demand a software for electric distribution grid optimization (eDisGo) is used.

The purpose of the eDisGo software is to perform a power flow analysis for a certain time period. Within eDisGo the grid settings are linked with the load profiles, while the single step non-linear power flow calculation is conducted using the open-source *PyPSA* software [146]. The eDisGo tool is implemented in Python and has been previously used in various studies [147, 148]. Apart from this thesis, this tool enables to assess the potential of flexibility options as a further alternative to conventional grid reinforcement [140].

One important output of a power flow analysis is the current $\mathrm{I}_t^{\mathrm{b}_j \to \mathrm{b}_k}$ for a specific line between two specific nodes b_k and b_j at each time step t. The line current is defined by a vector $\mathbf{I}^{\mathrm{b}_j \to \mathrm{b}_k}$ as shown in Equation 2.28 and this vector is essential for checking if grid reinforcement is necessary. If two nodes are not linked to each other, this value in the matrix remains 0.

$$\mathbf{I}^{\mathrm{b}_j \to \mathrm{b}_k} = \left[\mathrm{I}_1^{\mathrm{b}_j \to \mathrm{b}_k}, \cdots, \mathrm{I}_t^{\mathrm{b}_j \to \mathrm{b}_k}, \cdots, \mathrm{I}_\mathrm{T}^{\mathrm{b}_j \to \mathrm{b}_k}\right] \quad \forall\, \mathrm{b}_j \in \mathbf{N},\, \mathrm{b}_k \in \mathbf{N},\, \mathrm{b}_j \neq \mathrm{b}_k \tag{2.28}$$

2.3.2 Conventional distribution grid reinforcement

The procedure and the framework in distribution grid planning are based on various regulations at national and international level, but no standardized process has been implemented yet. One reason for this is, for example, the regional differences among the individual distribution grid structures. In this thesis the focus is on required grid reinforcement in MV grids, caused by a high penetration of EVs, as this will be the main driver in urban areas [14]. A MV grid, which is connected to the high-voltage level via a transformer at a single substation (PCC) and operated as an open loop is assumed in the following chapters of this dissertation. This structure reflects the most common topology encountered in Germany [140].

The most important aspects of grid stability in urban areas with a high share of EVs is the thermal capacity of cables, which is linked to the current (cf. Equation 2.28) [149]. In Germany, MV grids must be able to withstand the outage of any single component, such as a cable or a transformer unit (n-1 criterion) [150]. According to German law, grid operators are obliged to operate, maintain and expand a safe, reliable, and efficient energy supply network [150]. So far, various approaches have been considered to keep the quality of energy supply in the future. One possibility that network operators are considering avoiding or delay grid reinforcement is the introduction of a time of use tariff [151]. A lower price at off-peak times is offered to the consumers, so they can better manage demand, and consumers can lower their bills [152–154]. A highly discussed topic is also planning the charging of electric drive vehicles including electricity grid constraints [155, 156]. However, none of these approaches seem to be gaining acceptance among grid operators at the moment [14].

The constant change in the energy system leads to necessary adaptions in the regulatory framework. Due to current interpretation of German law, grid operators are now allowed to use BESSs as an option to avoid grid reinforcement, if they are only used for a safe and reliable grid operation [157]. However, for an economic comparison of storage systems with grid reinforcement, it is necessary to consider the various methods conventional distribution grid reinforcement in medium voltage grids. Table 2.1 presents an overview of these methods. As the simulation in this thesis showed, that in most cases single cables are overloaded, the focus at the economic comparison is on the grid reinforcement method of adding parallel cables.

Table 2.1: Overview of methods for conventional distribution grid reinforcement in medium voltage grids.

Grid reinforcement method	**Source**
Additional primary or secondary substation	[13, 150]
Rerouting of MV rings	[158, 159]
Additional parallel cable	[13, 160]

As shown in the section before for storage systems, it is also necessary to evaluate grid reinforcement costs. With the focus to an economic comparison of the BESS and conventional grid reinforcement in Chapter 7, the data research only includes investment costs. Issuances for operation and maintenance are neglected. To enable a comparison, the depreciation period t_{proj} and the discount rate r must be taken into account. It must be noticed that the depreciation period of BESSs (cf. Equation 2.24) and grid reinforcement can differ. The total investment costs are calculated by multiplying the specific costs $\mathrm{p}_{\mathrm{Grid}}^{\mathrm{invest}}$ with the length of the required grid reinforcement l_{GR}. Equation 2.29 shows the calculation of the discounted total costs for grid reinforcement $\mathrm{P}_{\mathrm{Grid},0}^{\mathrm{invest}}$.

$$\mathrm{P}_{\mathrm{Grid},0}^{\mathrm{invest}} = \frac{\mathrm{p}_{\mathrm{Grid}}^{\mathrm{invest}} \cdot \mathrm{l}_{\mathrm{GR}}}{(1+\mathrm{r})^{t_{\mathrm{proj}}}} \tag{2.29}$$

3 SimSES: A holistic simulation framework for modeling and analyzing stationary energy storage systems

Main research question: *What are the requirements for modeling the various components for an accurate simulation of stationary energy storage systems?*

Stationary BESS are seen as an alternative to conventional grid reinforcement to face the challenges of an increasing energy demand. The prediction of technical and economical behavior is essential before investing in energy storage systems. Holistic simulation tools are needed in order to determine key performance indicators such as lifetime, efficiency, and monetary returns. This publication shows the functionality of such a holistic simulation framework. SimSES is specialized in evaluating various energy storage technologies, technically and economically.

The modular approach of SimSES allows to combine various topologies, system components, and storage technologies embedded in an energy storage application. Energy storage models including their aging characteristics represent the core of SimSES. At the time of writing this manuscript, three detailed models of three storage technologies had been implemented: LIB, redox-flow battery, and a hydrogen energy chain. However, due to the modular approach of SimSES, further technologies or additional models for existing technologies can be implemented in future work.

An included analysis illustrated by key performance indicator allows to evaluate a storage system technical and economically. An extensive plotting functionality presents the results graphically. The main functionalities are demonstrated within this publication with two use-cases: A BESS providing FCR and a peak shaving application. In the following the highlights of this publication are summarized:

- A unique open-source holistic simulation framework for stationary energy storage systems based on Python code is presented.
- SimSES provides detailed analysis opportunities for simple and complex energy storage systems configurations.
- Different storage technologies and other components of a storage system, such as power electronic models, are covered within the simulation framework for a detailed evaluation of efficiency and aging behavior.
- SimSES offers interfaces for an easy integration into other simulation tools, such as tools for power-flow analysis.
- The simulation framework offers various EMS for common applications, such as an EMS for providing FCR or an EMS for a residential storage system. However, individual stand-alone or coupled strategies are easy to implement.

Within this thesis, SimSES is used to determine the technical and economical behavior of BESS used as an alternative of conventional grid reinforcement to face the challenges of an increasing energy

demand. Technical key performance indicators of a BESS for common applications are determined in Chapter 4. In the following Chapters 5, 6, and 7 various stand-alone as well as coupled EMS are simulated with SimSES to validate their functionality. This leads to the ability to evaluate storage systems economically to the costs of grid reinforcement.

Author contribution Marc Möller was the principal author tasked with coordinating and writing the paper and developing SimSES. Daniel Kucevic led the parts for EMS and LIB technology. Nils Collath implemented the economic evaluation and contributed to the thermal model as well as EMS. Anupam Parlikar was mainly responsible for the thermal model. Petra Dotzauer contributed to redox flow battery technology. Benedikt Tepe implemented and wrote the technical evaluation as well as contributed to the case studies. Stefan Englberger helped with execution and writing of the case studies. Andreas Jossen contributed via fruitful scientific discussions and reviewed the manuscript. Holger Hesse wrote the introduction and was giving valuable input throughout the manuscript preparation. All authors contributed with constructive feedback, reviews, and programming.

SimSES: A holistic simulation framework for modeling and analyzing stationary energy storage systems

Marc Möller, Daniel Kucevic, Nils Collath, Anupam Parlikar, Petra Dotzauer, Benedikt Tepe, Stefan Englberger, Andreas Jossen, Holger Hesse

Journal of Energy Storage, Volume 49, 2022

Permanent weblink:
https://doi.org/10.1016/j.est.2021.103743

Journal of Energy Storage 49 (2022) 103743

Contents lists available at ScienceDirect

Journal of Energy Storage

journal homepage: www.elsevier.com/locate/est

Research papers

SimSES: A holistic simulation framework for modeling and analyzing stationary energy storage systems

Marc Möller [a,*], Daniel Kucevic [a], Nils Collath [a], Anupam Parlikar [a], Petra Dotzauer [b], Benedikt Tepe [a], Stefan Englberger [a], Andreas Jossen [a], Holger Hesse [a]

[a] Institute for Electrical Energy Storage Technology, Technical University of Munich (TUM), Arcisstr. 21, 80333 Munich, Germany
[b] Bavarian Center for Applied Energy Research (ZAE Bayern), Department of Energy Storage, Walther-Meiner-Str. 6, 85748 Garching, Germany

ARTICLE INFO

Keywords:
Energy storage system simulation
Lithium-ion battery
Redox flow battery
Hydrogen technology
Storage system design
Stationary application

ABSTRACT

The increasing feed-in of intermittent renewable energy sources into the electricity grids worldwide is currently leading to technical challenges. Stationary energy storage systems provide a cost-effective and efficient solution in order to facilitate the growing penetration of renewable energy sources. Major technical and economical challenges for energy storage systems are related to lifetime, efficiency, and monetary returns. Holistic simulation tools are needed in order to address these challenges before investing in energy storage systems. One of these tools is SimSES, a holistic simulation framework specialized in evaluating energy storage technologies technically and economically. With a modular approach, SimSES covers various topologies, system components, and storage technologies embedded in an energy storage application. This contribution shows the capabilities and benefits of SimSES by providing in-depth knowledge of the implementations and models. Selected functionalities are demonstrated, with two use cases showing the easy-to-use simulation framework while providing detailed technical analysis for expert users. Hybrid energy storage systems consisting of lithium-ion and redox-flow batteries are investigated in a peak shaving application, while various system topologies are analyzed in a frequency containment reserve application. The results for the peak shaving case study show a benefit in favor of the hybrid system in terms of overall cost and degradation behavior in applications that have a comparatively low energy throughput during lifetime. In terms of system topology, a cascaded converter approach shows significant improvements in efficiency for the frequency containment reserve application.

1. Introduction

In former decades, the worldwide energy transition was predominantly driven by introducing more Renewable Energy Sources (RES) capacity to existing power networks, a process strongly supported by both globally declining cost for wind and solar power generation as well as through local legislation support, including subsidy schemes [1,2]. Following these early stage developments, the energy transition in various regions has now started to face new constraints and technical challenges, which demand other and often more site-specific solution approaches. Coupling of the power grid to both heating and electrified transport is certainly a key strategy to increase RES penetration on a global and nationwide level within the power system itself. At the same time, increasing the intermittence of supply that relies more on variable sources like solar and wind generation brings incorporation of grid-tied energy storage into discussion as a technically mature and potentially cost-competitive measure addressing volatility issues [3].

In order to categorize storage integration in power grids we may distinguish among Front-The-Meter (FTM) and Behind-the-Meter (BTM) applications [4]. FTM includes applications such as storage-assisted renewable energy time shift [5], wholesale energy arbitrage [6,7], and Frequency Containment Reserve (FCR) provision [8]. A more distributed and locally coordinated power supply is discussed in the context of BTM applications, e.g., Peak Shaving (PS) for industrial sites or at electric vehicle charging stations [9], or bill-saving at residential sites through Self-Consumption Increase (SCI) with local photovoltaic generation (residential battery storage) [10]. However, before taking a solid investment decision, it is crucial to analyze and optimize the technical parameters, storage dispatch control, as well as cost/revenue streams over the course of the entire project lifetime. Simulation and modeling tools in conjunction with sensitivity analyzes and optimization routines are commonly used to support these crucial steps in the planning and operational phase of grid-integrated storage projects.

* Corresponding author.
E-mail address: marc.moeller@tum.de (M. Möller).

https://doi.org/10.1016/j.est.2021.103743
Received 10 March 2021; Received in revised form 30 August 2021; Accepted 2 December 2021
Available online 24 February 2022

The Simulation Tool for Stationary Energy Storage Systems (**SimSES**) was developed to assist through the aforementioned tasks of storage system planning and operation. Through combining user-defined inputs with pre-parameterized component building blocks, as well as calculation methods and result analysis functions, a reserve is built for research, industry, and policy makers in equal measure to support deployment and enrollment of storage integration to the grid. The approach of **SimSES** is presented within this contribution.

In Section 2, comparable existing tools are reviewed and evaluated before the structure of **SimSES** is elaborated further in Section 3 as well as its detail models for storage technologies (Section 4) and its periphery (Section 5). Afterwards, in Section 6 two case studies are presented to show the capabilities of **SimSES** and concludes with a summary and outlook of further investigations in Section 7.

2. Literature review

Various authors have analyzed sizing and (economically) optimal operation of a specifically chosen storage system in a dedicated application setting, e.g., the usage of redox flow battery (RFB) for industrial PS applications [9] or the usage of lithium-ion battery (LIB) for SCI [11, 12]. Fewer studies exist comparing the suitability of different storage options for a given use case, e.g., refer to Toledo et al. [13] for a suitability comparison of different storage types for conducting residential self-consumption increase. Also, the profitability attainable across different applications was analyzed with a given technology to start off with, e.g., LIB in a wide range of application settings [14]. There is consensus that no uniform ideal candidate to meet all application-specific requirements exists within the storage technologies available to date [15]. In order to predict internal states of a storage system such as the State of Health (SOH) or the storage internal losses, it may become necessary to parameterize and simulate an adequately complex model of a storage system. Furthermore, simulations need to be fed with an operational concept that complies with the application constrains, and may deliver the compatibility of a given configuration as well as provide state predictions for the storage system. From an investor's perspective and ultimately for the most cost-effective integration of storage system to power grids with a high share of Variable Renewable Energy Sources (vRES), it is detrimental to conduct in-depth sensitivity and optimization studies relying on a full spectrum techno-economic model before subsequent tasks of project acquisition, realization, operation, and ultimately disposal are to be considered.

In the following, an overview of a selection of depicted tools for the techno-economic modeling of stationary storage in grid applications is provided. While Table 1 summarizes some of the main characteristics of these tools, it should be noted that this paper does not claim to provide a complete overview of all tools that may be relevant in the context matter.

GridLab-D,[1] developed and distributed via Pacific Northwest National Laboratory (*PNNL*), is a universal tool that allows modeling and analyzing multi-component power system networks. Its strength lies in the ability to simulate physical properties of various components through setting up and solving multiple differential equations, describing all sub-components in the modeling region. While the tool is certainly strong in modeling an entire micro-grid with its numerous grid states, it lacks detailed performance models for energy storage systems as well as application-specific parameterization and is therefore not applicable for detailed techno-economic analysis and optimization of storage project as it is focused in this work.

Other tools like **NAS Battery Simulator**,[2] **PNNL Flow Battery Calculator**,[3] and **H2FAST**,[4] are tools dedicated to specific storage types being sodium sulfur battery (NaS) redox flow, and electrolysis/hydrogen storage, respectively. These tools are developed for conducting rapid cost-revenue calculations for the specific technology of choice and offer limited user-specific input in terms of system parameterization and choice of application use case. Nevertheless, the aforementioned tools are confined to a dedicated storage system technology, rendering them less suitable for cross-technology comparisons. Furthermore, most tools of this kind are distributed as a proprietary code, matching only a dedicated commercial product well, and are not suitable for conducting sensitivity analyzes and adaption to envisioned new storage system control and operation.

More tailored simulations can be conducted using the tool **PerModAC** developed at htw Berlin [16]. Using this open-source software tool, performance and efficiency modeling of PV-coupled residential battery storage systems can be conducted. While the tool is extraordinarily strong in conducting battery storage product-specific performance and efficiency modeling, the model lacks the capabilities to analyze battery degradation. More importantly, the current version of this open-source tool is strictly confined to a specific residential BTM use case and cannot be used directly for cross-application assessments, as is desired for an investor's decision support.

Homer Pro and **Homer Grid** are more versatile modeling tools when it comes to comparing and optimizing the techno-economic performance of storage systems in (micro-)grids. The tools support various storage specific libraries and application-specific modeling capabilities, e.g., storage-supported renewable energy time shift in island grids as well as peak-shaving and solar-plus storage calculations in the current professional versions, and has been used in various scientific publications [17,18]. The software was developed by National Renewable Energy Laboratory (*NREL*), but the license for these tools are distributed solely via *Homerenergy* as a commercial product and cannot be extended/adapted according to the users' desire to address new application scenarios, specific personal needs, or local regulation frameworks. E.g., applications like the provision of frequency containment reserve and arbitrage marketing scenarios are not covered in the current version of the software tools.

Two other tools developed by *NREL* and Sandia National Laboratories (*SNL*) are worth looking at in more detail: **BLAST**[5] (Battery Lifetime Analysis and Simulation Tool) is a powerful software suite programmed using MATLAB® and it is distributed for both vehicle and stationary BTM applications. BLAST-BTM-Lite has powerful modeling capabilities for battery performance and lifetime calculations in stationary BTM applications and it includes both optimization and basic economic calculations. While it is highly recommended that this tool to be looked at closer by users interested in PV self-consumption and PS application, applications (only BTM) and storage systems to be analyzed (only conventional electro-chemical batteries) are clearly limited and confined. Furthermore, its original code structure lies hidden behind a graphical user interface and a proprietary executable file, making it unfeasible for the end-user to adapt parameters, e.g., sample time for peak shaving control.

The System Advisor Model[6] (**SAM**) tool builds up on a PV modeling framework originally set up by *SNL* and is now distributed via *NREL*. In its current version it allows coupling of battery storage with PV systems and incorporates financial models, e.g., for Power Purchase Agreement (PPA) calculations. More importantly, the user interface has been re-factored and is now distributed as an open-source software development kit for the Python programming language, allowing others to contribute with their individual extensions and developments. Nevertheless, on the technology side of its current version only batteries are supported and implemented (no other storage media).

[1] https://www.gridlabd.org/
[2] https://www.ngk-insulators.com/en/product/nas/simulator/
[3] https://github.com/PNNL-OE-Redox-Flow-Battery-Cost-Tool/PNNL-OE-Redox-Flow-Battery-Cost-Tool
[4] https://www.nrel.gov/hydrogen/h2fast.html
[5] https://www.nrel.gov/transportation/blast-btm-lite.html
[6] https://sam.nrel.gov/about-sam.html

Table 1
Overview of technical and economic modeling tools for energy storage in stationary applications.

Tool name	License type	Developer (primary)	Focus
GridLab-D	BSD open license	PNNL	Multi-domain state modeling for power distribution system simulation
NAS Battery Simulator	commercial	NGK-insulators	NGK product-tailored NaS battery simulation in peak shaving application
Flow Battery Calculator	open source	PNNL	Estimation tool of cost for redox flow batteries
H2FAST	open source (Excel sheet)	NREL	Economic assessment of hydrogen fuel stations
PerModAC	open source	htw	Performance and efficiency modeling of PV coupled residential battery storage systems
Homer Pro	commercial	Homerenergy (UL.com)	Residential/Microgrid modeling—multiple storage systems, multiple application scenarios
BLAST-BTM-Lite	commercial freeware (lite version)	NREL	Analysis and modeling of battery degradation
StorageVET	open source	EPRI	Optimization of size and financial evaluation of energy storage
SAM — System Advisor Model	BSD-3-clause	NREL	Modeling and analysis software for renewable energy projects
SimSES	BSD-3-clause	TUM	Physically motivated energy storage component, system and application behavior model

The storage value estimation tool[7] (**StorageVET**) developed mainly by the Electric Power Research Institute (*EPRI*) comes with a documentation, tutorial videos, and a user feedback forum. Since the release of version 2.0 the tool has been available as a Python package and most functional parts are licensed as 3-clause BSD open source. The tools allow conducting cost–benefit analysis and includes various application services like voltage support, retail demand charge reduction, frequency regulation, and even value stacking via aggregating multiple services to be served by one storage system. While the interface to the generation and storage technologies allows multiple options, at present only a very limited number of choices is available (PV/Internal Combustion Engine (ICE) and Battery/Compressed Air Energy Storage (CAES)). Furthermore, performance and degradation modeling is very limited, as it is based on an energy bucket model rather than analyzing the voltage and current specific phenomena of real world electro-chemical devices. Also, there is no thermal model included in the calculations, limiting the value of simulations for temperature sensible parameters like storage system efficiency (including Heating Ventilation Air Conditioning (HVAC) consumption) and storage aging.

Unlike the aforementioned tools, **SimSES** aims to bring together the model precision of tools like **SAM** and **PermodAC** and combine it with an interface to various applications and energy market scenarios. To do so, the model is distributed as open-source code on Gitlab[8] and Python Package Index[9] and builds up on a object-oriented approach programmed in Python language. Several modules are interlinked and interchangeable, and configuration files are used to select the setting of choice for typical time-series evaluations. The program as a whole, or parts of it, can also be integrated into simulation toolchains and modeling environments, making it feasible to be used in sensitivity and optimization studies and at the interface to a super-ordinate multi-instance controlling unit, as is further described in one of the case scenarios (Section 6.1). In order to allow the Energy Storage Systems (ESS) to react directly to states in a distribution grid, **SimSES** can be coupled to grid models, thus making it possible to have a power flow analysis and a detailed simulation of an ESS at the same time. **SimSES** stands out against above-mentionded tools, e.g., **Homer Pro** or **SAM**, by providing various detailed energy storage systems including validated and literature-based degradation models. Furthermore, a plethora of predefined storage-specific application Energy Management System (EMS) like ancillary services and energy trading are implemented and combined with suitable economic parameters, so that end-users are able to test a system of choice for a selected application use case. At the same time, the existent code framework is open-source accessible and open for future contributions from other developers worldwide.

[7] https://www.storagevet.com/
[8] https://gitlab.lrz.de/open-ees-ses/simses
[9] https://pypi.org/project/simses/

3. Simulation framework for stationary energy storage systems

Stationary ESS may become a key component for future energy systems and incorporating various FTM and BTM applications supporting the electricity grid. Simulation tools are needed in order to provide advice for investment decisions and to analyze the impact of a stationary ESS. These tools should be able to model impact of applications on the health status of the ESS and its implications for prospective revenues.

While SimSES aims to allow for techno-economic cross-application and cross-technology comparisons, the tool is designed in a modular fashion and incorporates all technical components necessary for the grid connection of energy storage. Hence, **SimSES** does not only model various technologies, but also their thermal behavior, the corresponding power electronics, as well as the impact of different operating strategies. An integration into other energy simulation frameworks can be easily applied, as shown in project *openBEA*.[10]

The main task of **SimSES** is to determine the effects of the target power provided by the EMS regarding efficiency, temperature, and degradation of the ESS when applied to the storage system. Each implemented component is responsible for modeling its relevant principles. **SimSES** is divided into a simulation part for modeling the physical representation of the ESS and an evaluation part that provides technical and economic results as shown in Fig. 1. The figure also shows the basic working principle of **SimSES**: the time-series based simulation allocates an AC power target provided by the selected EMS to the storage system. After updating all models of the storage system, the current state regarding important variables such as SOC, temperature, SOH, and delivered power is transferred back to the operating strategy on which a new target power is calculated for the next time step.

In order to represent a storage system as a whole, various components need to be taken into account for a storage simulation. Besides the storage technology, power electronics is an important element. For instance, a simple Battery Energy Storage System (BESS) configuration consists of an Alternating Current to Direct Current (ACDC) converter connected to the grid and a battery. Additionally, stationary ESS are usually covered by a housing. These housings need to be thermally controlled in order to keep the ESS within its safety ranges. **SimSES** covers these possibilities with various configurable components and topologies.

More complex topologies can also include Direct Current to Direct Current (DCDC) converter or parallel connected ACDC converters, each connected to an ESS. Various ESS topologies are built with an AC connection to the grid or site location by connecting an ACDC converter to the storage system. However, in recent years Direct Current (DC)-coupled ESS has gained importance, especially in the residential

[10] https://openbeaproject.wordpress.com/

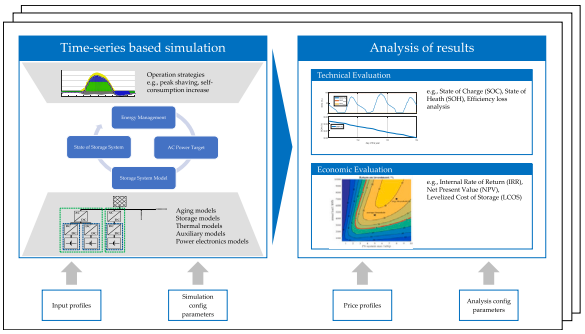

Fig. 1. Graphical overview of **SimSES** showing its simulation and analysis models, including the Energy Management System (EMS), storage system setup, technical and economical evaluation, and its necessary inputs. The state of a storage system includes the most important variables of the storage models, e.g., State of Charge (SOC), temperature, and State of Health (SOH).

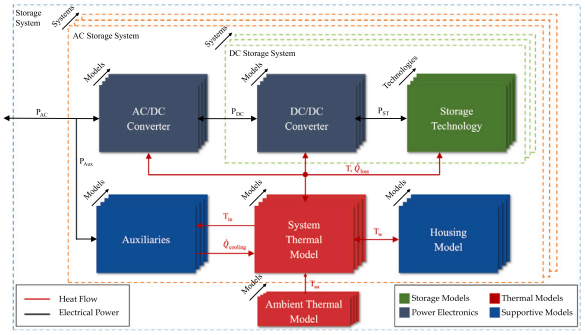

Fig. 2. Main component classes in **SimSES**: Interconnection of electrical and thermal models for ESS including the abstract AC and DC storage systems. Multiple model implementations exist for each component. Possible parallel connections of various AC and DC storage systems are indicated.

sector [19]. Hence, a state-of-the-art storage simulation framework needs to take varying topologies into account. **SimSES** considers these topologies by defining two abstract systems: AC and DC storage systems, which can also be combined in order to meet versatile topology configurations. Every AC storage system consists at least of an ACDC converter and a DC storage system. On the one hand, this allows the connection of several storage systems to the grid in parallel; on the other hand, this allows multiple DC-connected ESS within one storage system. Furthermore, the main ESS model is located inside the DC storage system behind a DCDC converter. These models are depicted in Fig. 2.

In the following sections, each of the **SimSES** packages as well as the underlying models and implementations are described in detail and shown in Fig. 3. *Storage Technology* and *System* provides models to represent physical models of storage system components while *Analysis* focuses on examining the simulation results regarding the technical and economical behavior of the simulated storage systems. All control algorithms and power flow management are handled within the *Logic* package.

Additional packages like *Commons*, *Simulation*, and *Data* deliver supportive functions for **SimSES**. *Config* is tasked to deliver functionality for the mentioned modular configuration of the ESS. In this package, software design patterns like the factory pattern are used to provide a wide range of configurable components [20]. Additionally, the structure allows the use of sensitivity analysis, e.g., by varying either different components or their dimensions. *Simulation* is another package that supports sensitivity analysis by allowing running multiple

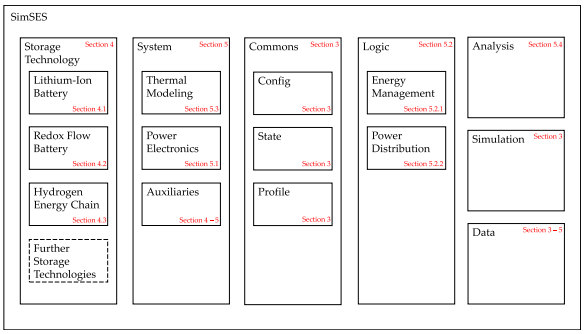

Fig. 3. Structure of **SimSES**: Packages are divided into *Storage Technology*, *System*, *Commons*, *Logic*, *Analysis*, *Simulation*, and *Data*. Within *Storage Technology*, the physical representation of each technology, namely LIB, RFB, and Hydrogen, is located. The *Commons* package delivers general functions for configuration and common features. The periphery is handled in the *System* package. Control algorithm and management is dealt with in the *Logic* package. *Analysis* focuses on the technical and economical evaluation of the simulation results. *Simulation* provides functions for simultaneous simulations, whereas *Data* stores all necessary information.

SimSES instances in parallel, therefore increasing simulation speed. For this purpose, Python's multiprocessing library is used. Further time series functions are implemented, like handling of profiles for power or price time series. These functions are used throughout **SimSES**, for example, by providing power profiles for the EMS. These supportive functions are covered within *Commons*, providing general functionality for time-series based simulations.

4. Storage technology models

Energy storage models represent the core of **SimSES**. In-depth models of various storage technologies are implemented, namely for LIB, RFB, and a hydrogen energy chain represented by electrolyzer, fuel cell and hydrogen storage. Each of these storage technologies have specific implementations regarding their physics and behavior. Due to the modularity of **SimSES**, further technologies can be implemented in future work.

4.1. Lithium-ion battery

ESSs based on LIB have evolved rapidly with a wide range of cell technologies and falling costs in recent years [11,21]. In **SimSES** LIBs are implemented as a distinct storage technology. The target power for this technology P_{st} depends on the storage structure and the power distributor as described in Section 5.

Four subcomponents are implemented in **SimSES** for behavior modeling of LIB. The **Equivalent Circuit Model (ECM)** is used to describe the electrical behavior of a specific cell type providing terminal voltage according to operational input data. The **Battery Management System (BMS)** monitors the cell operation conditions and updates values for the current. The electrical characteristics of LIBs in **SimSES** differ with chemistry and composition of constituent materials and may be fed with predefined manufacturer-specific datasets. Furthermore, various cell-specific degradation models can be selected in **SimSES**. The **aging** calculation is based on the cycle detector selected (e.g., half-cycle detector). These four main components are schematically illustrated in Fig. 4, and explained in detail in the following subsections.

4.1.1. Equivalent circuit model

To describe the electrical behavior, in **SimSES** the battery is implemented as a single-cell ECM. The currently implemented model includes an Open Circuit Voltage (OCV) and an internal resistance R_i, which is depicted in Fig. 4. According to Eq. (1), the terminal voltage

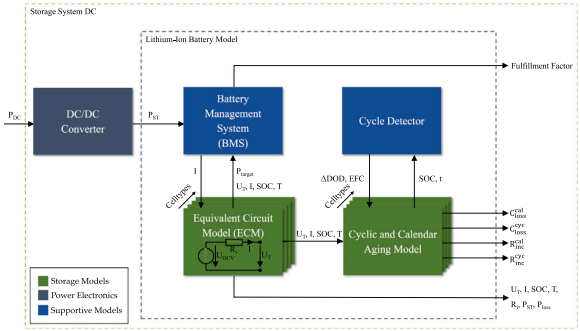

Fig. 4. Package structure of a lithium-ion battery. The battery package in **SimSES** includes four main components: a battery management system, a cell type including a equivalent circuit model, a degradation model, and a cycle detector.

U_T of each cell is calculated from the OCV and the voltage drop ΔU across R_i, due to the cell current I.

The OCVs of all currently implemented cell types are only dependent on the SOC but could be extended with further parameters like temperature and SOH. The internal resistance R_i of all currently implemented cell types takes the cell temperature T_{cell}, I, and the SOC into consideration. For both the SOC as well as R_i, the required data for different cell types are stored as look-up tables in **SimSES**. In between the available data points a linear interpolation is executed. Hence, the result quality relies on the number of data points. To improve performance, the interpolation of the SOC data was replaced by a fitted mathematical function, which is explained in Appendix A.

$$U_T = U_{OCV} - \Delta U = U_{OCV}(SOC) - I \cdot R_i\left(SOC, I, T_{cell}\right) \quad (1)$$

4.1.2. Battery management system

The BMS is linked to the ECM and is responsible for maintaining critical cell parameters within their permissible ranges. In addition to the target power P_{target}, voltage U_T, temperature T_{cell}, SOC, and current I are further input parameter for the BMS. According to the cell-specific parameters (e.g., maximum temperature), the BMS checks the input parameters and indicates whether they are within their limits. If limit violations occur, the current is restricted and returned to the ECM. The other parameters are recalculated accordingly and passed on to the aging models. The fulfillment factor indicates the share of the output power to the target power and will become sub-unity for simulations with boundary violations.

As seen in Eq. (1), the current I and the terminal voltage U_T are interdependent. Differential equations are necessary for calculating these values in the discrete time domain. To avoid these computationally intensive differential equations, an iteration loop is integrated in **SimSES**: the updated current I and terminal voltage U_T are iteratively derived through repetitive numerical approximation. This loop terminates after a predefined maximum number of iterations or as soon as the change in the current I or the terminal voltage U_T falls below a preset limit.

4.1.3. Lithium-ion battery cell types

The LIB cell forms the core of the BESS, and is essential for understanding the electrical and thermal characteristics of an entire system. For a more detailed discussion the reader is referred to [22,23] and for a description of current and future materials for LIBs as well as beyond lithium-based anode materials the reader is referred to [24]. In **SimSES**, three state-of-the-art technologies based on a Carbon-Graphite (C) anode and various cathode materials are currently implemented: two cells with a Nickel-Manganese-Cobalt-Oxide (NMC) cathode and one cell, each with a Lithium-Iron-Phosphate (LFP) and Nickel-Cobalt-Aluminum-Oxide (NCA) cathode, respectively. In addition, a generic cell with linear OCV is implemented in order to run simulations independent of the cell chemistry. Table 2 gives an overview of these cells, including their electrical attributes. The thermal parameters are summarized in Appendix B.

4.1.4. Lithium-ion battery degradation models

LIBs are subject to degradation due to multiple cell-internal aging processes, which can have significant impact on the economics of a BESS project [30]. In **SimSES**, degradation is modeled following a semi-empirical superposition approach of cyclic and calendar aging, as shown in Eqs. (2) and (3).

$$C_{loss}^{total} = C_{loss}^{cal} + C_{loss}^{cyc} \quad (2)$$

$$R_{inc}^{total} = R_{inc}^{cal} + R_{inc}^{cyc} \quad (3)$$

The resulting capacity loss C_{loss}^{total} and resistance increase R_{inc}^{total} are calculated through the addition of the respective calendar aging (C_{loss}^{cal}, R_{inc}^{cal}) and cyclic-aging components (C_{loss}^{cyc}, R_{inc}^{cyc}). Table 3 provides an overview of the primary LIB degradation models that are available in **SimSES** and their dependencies, as well as the sources on which these models are based. Here, t, SOC, T_{cell}, and U_T refer to the simulation time, state of charge, cell terminal voltage, and cell temperature, respectively. ΔDOD, EFC, Q, and $\overline{U_T}$ refer to the delta in depth of discharge for a cycle, the number of equivalent full cycles, the charge throughput, and the average cell terminal voltage over one equivalent cycle. The delta in depth of discharge (ΔDOD), as it is implemented here, is also referenced as depth of cycle or cycle depth in literature by some authors.

While calendar aging is computed once every simulation step, the model routine to calculate increase in cyclic aging is only triggered following the detection of half an equivalent cycle of charge throughput. This decreases the calculation time and allows determining the C-rate as well as DOC for that half equivalent cycle.

4.2. Redox flow battery

Large-scale storage systems are purportedly to be of rising concern in order to ease the growing penetration of RES. Hence, RFBs are of particular interest for multiple hour- and large-scale stationary ESSs because they can be easily and efficiently scaled according to the needs and become cost competitive at an energy range of multiple MWh [31]. To analyze their potential in different applications from small-scale (e.g., residential storage) to large-scale applications (e.g., industrial storage), they are integrated into **SimSES** as an additional storage technology. In an RFB, the liquid storage medium (electrolyte) is stored in external tanks. To charge and discharge the RFB, the electrolyte is pumped through a stack where the electrochemical reactions take place. The electrolyte divided in anolyte and catholyte solutions are separated by an ion-exchange membrane through which the charge carriers are transported. There are several known possible electrolyte combinations, e.g., all-vanadium or vanadium/bromine solutions [32]. As the energy conversion unit and the energy storage medium are decoupled, the power and energy of an RFB can be scaled separately [31,32].

Fig. 5 shows the structure of the main components modeled in **SimSES** to describe an RFB. The electrochemical model calculates the electrical operating parameters of a specific stack module dependent on the chemical composition of the selected electrolyte system. The control system checks whether the target parameters are within safe operating limits and returns the actual usable values. Different pumps and pump control algorithms can be configured. In the following, the model components are described in more detail.

Table 2
Lithium-ion battery cells currently implemented in **SimSES**, including their electrical parameters.

Manufacturer Model	Acronym in **SimSES**	Anode Cathode	Nom. voltage (V) Voltage range (V)	Capacity (Ah)	C_{rate} Ch. (1/h) C_{rate} Dch. (1/h)	Source
Sony[a] US26650FTC1	SonyLFP	Graphite $LiFePo_4$	3.2 2.0–3.6	3.0	1.0 6.6	[25,26]
Panasonic NCR18650PD	Panasonic-NCA	Graphite $LiNiCoAlO_2$	3.6 2.5–4.2	2.73	0.5 3.5	[27]
E-One Moli Energy IHR18650A	MolicelNMC	Graphite $LiNiCoMnO_2$	3.7 3.0–4.25	1.9	1.05 2.1	[28]
Sanyo UR18650E	SanyoNMC	Graphite $LiNiCoMnO_2$	3.6 2.5–4.2	2.05	1.0 3.0	[27,29]
Generic cell model	GenericCell	–	3.5 3.0–4.0	2.5	2.0 2.0	–

[a]Murata Manufacturing Co. acquired the Sony battery division in 2017.

Table 3
LIB-specific degradation models along with corresponding variable dependencies and literature sources.

Cell acronym	Calendar aging		Cyclic aging		Model based on
	C_{loss}^{cal}	R_{inc}^{cal}	C_{loss}^{cyc}	R_{inc}^{cyc}	
SonyLFP	t, SOC, T_{cell}	t, SOC, T_{cell}	EFC, ΔDOD, C-rate	EFC, ΔDOD, C-rate	[25,26]
PanasonicNCA	t, U_T, T_{cell}	t, SOC, T_{cell}	EFC, U_T, C-rate	EFC, U_T, C-rate	[27]
MolicelNMC	t, SOC, T_{cell}	t, SOC, T_{cell}	Q, ΔDOD, C-rate	Q, ΔDOD, C-rate	[28]
SanyoNMC	t, U_T, T_{cell}	t, U_T, T_{cell}	Q, ΔDOD, $\overline{U_T}$	Q, ΔDOD, $\overline{U_T}$	[29]
GenericCell	t	–	EFC	–	–

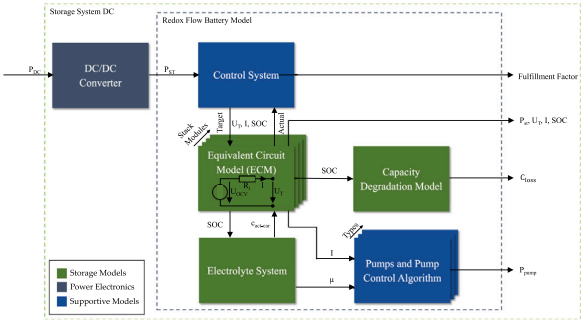

Fig. 5. Package structure for a redox flow battery (RFB). It contains an electrochemical model (equivalent circuit model) with specific parameters for different stack modules, an implemented control system, an electrolyte system, a degradation model, and pumps, with interchangeable control algorithms.

4.2.1. Electrochemical model

As with LIB, the currently implemented electrochemical model of an RFB is based on an equivalent circuit model (cf. Fig. 5). The terminal voltage U_T is directly calculated from the power applied to the RFB. Eq. (4) can be derived from Eq. (1) by using the relation between storage power P_{st}, terminal voltage U_T, and current I ($P_{st} = U_T \cdot I$). U_T is therefore calculated by P_{st}, the OCV, and the internal resistance R_i. Both OCV and R_i are dependent on the SOC and the electrolyte temperature in the stack module T_{stack}.

$$\begin{aligned} U_T &= 0.5 \cdot \left(U_{OCV} + \sqrt{U_{OCV}^2 + 4 \cdot R_i \cdot P_{st}} \right) \\ U_{OCV} &= f\left(SOC, T_{stack}\right) \\ R_i &= f\left(SOC, T_{stack}\right) \end{aligned} \tag{4}$$

Charge effects are taken into account by implementing a current for the charging losses $I_{char\text{-}loss}$ when calculating the change of the system SOC (SOC_{system}) via Eq. (5), considering the simulation time step Δt, the nominal voltage at the stack module U_{nom}, and the total energy of the electrolyte E_{total}. $I_{char\text{-}loss}$ includes coulombic losses due to self-discharge through the transport of reactants over the membrane and shunt currents. Shunt currents occur due to a connection of cells in the stack through an ionic conductive electrolyte distribution system. This creates a bypass current forced by the electric field due to the electrical series connection of the cells [33].

$$\Delta SOC_{system} = \frac{\left(I - I_{char\text{-}loss}\right) \cdot \Delta t \cdot U_{nom}}{E_{total}} \tag{5}$$

A control system is integrated in the electrochemical model, which checks whether U_T, I, and SOC are within safe operating limits. If the values are out of range, they will be adapted and the other parameters are recalculated accordingly.

Additionally, a capacity degradation model including the capacity losses C_{loss} due to hydrogen evolution is implemented in the RFB model. Further research is required to estimate a realistic hydrogen evolution current for industrial-sized stacks to predict the capacity reduction realistically over time. A current approach using experimental data of a laboratory cell from Schweiss et al. [34] overestimates the resulting capacity losses. Whitehead et al. [35] stated a capacity loss of less than 1% per year due to hydrogen evolution. Therefore, a hydrogen current of $5 \cdot 10^{-8}$ $\frac{mA}{cm^2}$ is assumed, resulting in a capacity loss of about 1% per year for a system with an Energy-to-Power Ratio (EPR) of 1. As the EPR increases, the loss decreases accordingly.

4.2.2. Stack module and electrolyte system

The calculations in the electrochemical model are based on electrical and geometrical data for a stack. A stack consists of a fixed number of cells electrically connected in series. The data to consider the voltage, charge, and hydraulic losses of a stack can be obtained either from experimental data or from the literature values and models. Stacks can be electrically connected in parallel or in series to a stack module to increase power and voltage of the RFB system. In this configuration the electrolyte flows in parallel through all cells and stacks. The performance parameters of the stack are directly connected to the used electrolyte system. The currently in **SimSES** examined and implemented electrolyte is an all-Vanadium system, consisting of 1.6 mol/l Vanadium solved in an aqueous sulfuric acid (2 mol/l H_2SO_4) from GfE (Gesellschaft für Elektrometallurgie mbH). To reduce side reaction due to high potentials and to prevent performance penalties the electrolyte needs to operate in a limited SOC range. A typical usable SOC range for a RFB lies between 20 and 80% [36]. Based on this SOC

Table 4
Redox-flow battery stack types in **SimSES**.

Acronym in SimSES	Cell number	Cell area (cm^2)	Based on experimental data of	Model based on
CellDataStack5500W	40	2160	Appendix C	[37–39]
DummyStack3000W	20	1000	N/A	N/A
IndustrialStack1500W	18	551	Voltstorage GmbH	[37,38]

range the nominal power of a stack is calculated. An overview of the in **SimSES** implemented stacks is listed in Table 4. The name of the stack includes its nominal power. In addition, some modifications of the described stacks are included, which are up-scaled or simplified versions that are not included in the list.

4.2.3. Pumps and pump control algorithm

The pump control algorithm used to control the flow rate or pressure drop in the system is an important performance-determining factor that affects the operating losses. Two different algorithms to choose from are currently integrated: the constant and the stoichiometric flow rate. It is assumed that the pumps always stop during stand-by to reduce the operating losses. If flow rate $\dot{V}$ or pressure drop Δp is given, the other value is calculated via Eq. (6) from the specific hydraulic, viscosity-corrected resistance $R_{hydraulic,specific}$ and the viscosity μ of the anolyte or catholyte.

$$\Delta p = \dot{V} \cdot R_{hydraulic,specific} \cdot \mu \tag{6}$$

If the pump is operating with a constant flow rate, it must be ensured that the volume flow is sufficiently high so that the stack module is supplied with enough reactants at any time of operation (depending on SOC and I). This is checked by the control system integrated in the electrochemical model.

For the stoichiometric flow rate algorithm $\dot{V}$ is calculated according to Eq. (7) via the stoichiometric factor ν, the total concentration of the active charge carriers in the electrolyte $c_{act\text{-}car}$ (for the implemented Vanadium electrolyte it is 1.6 mol/l), the Faraday constant F, and the still available concentration of reactants in the electrolyte, which is described through the SOC for discharging and (SOC − 1) for charging. If, for example, the RFB is charging at SOC 70%, reactants that can be maximal charged in the Stack are 30% of the total concentration, therefore value is 0.3.

$$\begin{aligned} \dot{V} &= \frac{\nu \cdot I}{F \cdot c_{act\text{-}car} \cdot (SOC - 1)} \quad \text{for} \quad P >= 0 \\ \dot{V} &= \frac{\nu \cdot I}{F \cdot c_{act\text{-}car} \cdot SOC} \quad \text{for} \quad P < 0 \end{aligned} \tag{7}$$

The pump losses P_{pump} can be calculated with Δp, $\dot{V}$, and the pump efficiency η_{pump} of a specific pump that can be selected in **SimSES** via Eq. (8) [40].

$$P_{pump} = \frac{\dot{V} \cdot \Delta p}{\eta_{pump}} \tag{8}$$

4.3. Hydrogen energy chain: Electrolyzer, storage, and fuel cell

Hydrogen as an energy carrier is supposed to be one of the major contributors impacting future energy provision, storage, and distribution [41]. The abundance of chemically-bound hydrogen in the form of water as well as its very high-energy density is compelling for its deployment as an energy carrier for large-scale energy storage. However, the efficiency of splitting water into its separate components via electrochemical electrolysis and reverting the process through fuel cells or combustion power plants is comparatively low, in striking contrast to electrochemical storage like LIB [14,42]. As such, hydrogen is thought to complement rather than to compete with LIB and RFB. In order to understand the effects of a hydrogen-based energy chain on a system level including its periphery, models for *electrolyzers*, *fuel cells*, *hydrogen storage*, and its auxiliary components like pumps and compressors are integrated as models within **SimSES**. Within this section, implementations of the respective models are explained in detail.

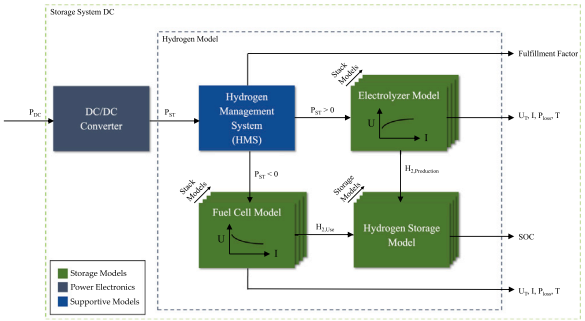

Fig. 6. Package structure for hydrogen in **SimSES** includes four main components: a *hydrogen management system*, an *electrolyzer*, a *fuel cell*, and a *storage model*.

The hydrogen package structure is displayed in Fig. 6, consisting of a *Hydrogen Management System (HMS)*, an *electrolyzer*, a *fuel cell*, and a H_2 *storage model*. The *HMS* supervises the whole hydrogen chain for valid ranges of temperature and SOC and reduces applied power if necessary. The storage model could be a gas pipe with an assumed infinite capacity or a hydrogen pressure tank with a predefined energy capacity. Depending on the pressure of the gas within the storage tank, the gas needs to be compressed to the desired pressure level. The *electrolyzer* and *fuel cell* models are explained in detail in the following sections. It is worth to mention that **SimSES** also allows a single-direction hydrogen energy chain by neglecting either the *electrolyzer* or the *fuel cell* component with special implementations. A summary of all currently implemented models is given in Table 5. Due to the modular structure of **SimSES**, additional models can be implemented in a future release accordingly.

4.3.1. Electrolyzer

A water electrolyzer splits water with the use of electricity into hydrogen and oxygen by passing ions through an electrolyte from one electrode to the other. The pressure and temperature-dependent polarization curve is based on the general equation of Nernst voltage U_{nernst} as well as overpotentials represented by ohmic η_{ohm}, activation η_{act}, and diffusion losses η_{diff} as shown in Eq. (9) [50]. In some implementations mass transport and membrane permeation are also considered.

$$U_{T,EL} = U_{nernst} + \eta_{ohm} + \eta_{act} + \eta_{diff} \tag{9}$$

Depending on the stack technology, e.g., alkaline or polymer electrolyte membranes (PEM), the *electrolyzer* is operated at different pressure and temperature levels, which is taken into consideration by varying polarization curves for each technology [50]. As shown in Fig. 7, the *electrolyzer* model is divided into its stack and corresponding degradation models, pressure and thermal models as well as necessary auxiliaries like a pump, water heater, and gas dryer. The electrical auxiliary power is calculated according to the hydrogen and oxygen generation pressures for the anode and cathode, as well as the stack temperature. A water pump regulates the humidification of the *electrolyzer*, whereas the generated hydrogen gas needs to be dried. These auxiliary models calculate the necessary electrical power in order to provide a temperature and mass equilibrium.

Table 5
Overview of implemented *electrolyzer*, *fuel cell* and *hydrogen storage* models in **SimSES**.

Technology	Acronym in SimSES	Type	Degradation effects	Based on experimental data of	Model based on
Electrolyzer	PemElectrolyzerMultiDimAnalytic	PEM	Resistance increase, Decrease of exchange current	Forschungszentrum Jülich	[43–45]
	PemElectrolyzer	PEM	N/A	N/A	[46]
	AlkalineElectrolyzer	Alkaline	N/A	Hydrogen Research Institute	[47,48]
Fuel Cell	PemFuelCell	PEM	N/A	N/A	[49]
	JupiterFuelCell	PEM	N/A	SFC Energy AG	–
Hydrogen Storage	PressureTank	Pressure Tank	N/A	N/A	–
	SimplePipeline	Pipeline	N/A	N/A	–

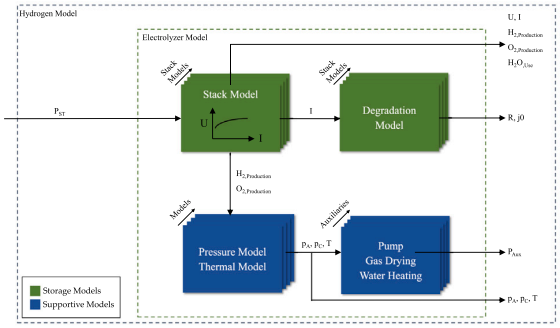

Fig. 7. Package structure for *electrolyzer* in **SimSES** includes a stack, pressure, thermal and degradation model as well as a pump and gas dryer.

Electrolyzer degradation is a field of ongoing research with controversy over underlying mechanisms and influencing factors [51,52]. However, active operation time and applied current density seem to be major impact factors for electrolyzer degradation. For instance, the implemented degradation for the Polymer Electrolyte Membrane (PEM) electrolyzer acquired from the work of Tjarks [43] is based on the findings of Rakousky et al. [44,45] considering a resistance increase and a decrease of the exchange current. Other implementations of electrolyzers are a PEM variant without degradation effects based on the work of Marangio et al. [46] and an alkaline version based on the work of Hammoudi et al. [47] and Henao et al. [48].

4.3.2. Fuel cell

As an opposite to *electrolyzers*, *fuel cells* combine hydrogen and oxygen to water while releasing usable energy in the form of electricity [42]. The terminal voltage is calculated by the Nernst voltage subtracted by the voltages due to ohmic, activation, and diffusion losses shown in Eq. (10).

$$U_{T,FC} = U_{nernst} - \eta_{ohm} - \eta_{akt} - \eta_{diff} \tag{10}$$

The *fuel cell* package has a structure that is similar to the *electrolyzer* package, with a stack, pressure, and thermal model. During operation, the water handling especially for PEM fuel cells is crucial and handled by water pumps. An implementation of a PEM fuel cell based on Feroldi et al. [49] as well as a model for the Jupiter PEM fuel cell of SFC Energy AG[11] including a thermal model is available in **SimSES**. However, the implementation of adequate degradation models within SimSES is a task for future action.

5. System periphery, management, and evaluation

Energy storage systems not only consist of the underlying storage technology but also the periphery like power electronic components and thermal behavior as well as an EMS. These elements are crucial for evaluating energy storage systems as a whole. In order to provide insights into the overall system behavior, **SimSES** not only models the periphery and the EMS, it also provides in-depth technical and economical analysis of the investigated ESS.

5.1. Power electronics

Besides the storage technology, the power electronic components play a crucial role in terms of system efficiency. Depending on topology and application, power electronics may contribute significantly to the overall system losses [53]. Hence, **SimSES** has to consider these electronic components for an accurate simulation of a storage system like ACDC and DCDC converters. An overview of the implemented models in **SimSES** is given in Table 6. Models of these converters are represented by power and voltage-dependent efficiency curves. In principle, the efficiency of a power electronics module is represented by a given storage power $P_{Storage}$ and the rated power of the power electronics component P_{Rated} as displayed in Eq. (11).

$$\eta_{PE} = f\left(P_{Storage}, P_{Rated}\right) \tag{11}$$

The power applied to the power electronic components is crucial for simulating the efficiency. When considering storage systems, it is possible that these systems do not fully deliver the requested power. These situations occur, for example, if the storage is outside of its temperature limits or the SOC is at its lower or upper limits. Hence, the power is adjusted compared to the target power of the EMS, which leads not only to non-fulfillment, but also to an altered efficiency.

5.2. Power control

Every power flow in an ESS has to be monitored and controlled. The power flow is dependent on the application and system topology. In **SimSES**, these two dependencies are handled separately with an EMS, respectively, Power Distribution Strategies (PDS). The EMS defines the target power for the ESS as a function of the application while the PDS allocates the target power to the configured subsystems. These control mechanisms are explained in detail in the following sections.

5.2.1. Energy management system

The EMS in an ESS is a system consisting of both hardware and software that allows the user to monitor and control the energy flows within an ESS. In **SimSES**, the function of the EMS is to calculate and supply a target power value for each simulation timestep (Δt) based on the selected operation strategy. This target power value can be dependent or independent of previous system states as well as interfere with various input profiles. In **SimSES** both stand-alone and stacked operation strategies can be simulated. Stacked operation strategies are sorted according to their user-associated priority level. Consequently, the individual stand-alone operating strategies are executed one after another depending on their priority. Additionally, time-discrete serial stacking is already available within **SimSES**. More complex multi-use strategies can be integrated as stand-alone strategies. At present, a handful of

[11] https://www.efoy-pro.com/efoy-pro/efoy-jupiter-2-5/

Table 6
Overview of implemented ACDC and DCDC converter models in **SimSES**.

Converter type	Acronym in SimSES	Based on experimental data of	Model based on
AC/DC	FixEfficiencyAcDcConverter	N/A	N/A
	NottonAcDcConverter	N/A	[54]
	Sinamics120AcDcConverter	Sinamics S120	[55]
	BonfiglioliAcDcConverter	Bonfiglioli RPS TL-4Q	Datasheet[a]
	SungrowAcDcConverter	Sungrow SC 1000 TL	Datasheet[b]
	M2bAcDcConverter	Stable Energy GmbH	[56]
DC/DC	FixEfficiencyDcDcConverter	N/A	N/A

[a] https://www.docsbonfiglioli.com.
[b] https://en.sungrowpower.com.

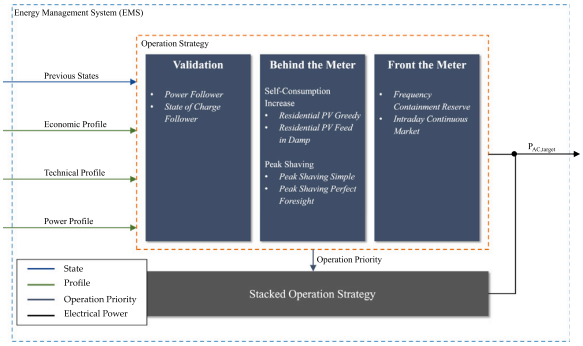

Fig. 8. Structure of the energy management system and overview of available operation strategies and their categorization in **SimSES**.

operation strategies are implemented in **SimSES**. An overview of these operation strategies and their categorization is depicted in Fig. 8.

The *power follower* strategy is a basic operation strategy which aims to get the storage system operation to replicate a given power profile. Similar to the aforementioned strategy, the *SOC follower* converts a given SOC profile to a power profile and attempts to make the storage system fulfill this calculated demand power at each timestep.

Based on the work of Zeh and Witzmann [57], two operation strategies for residential SCI in combination with Photovoltaic (PV) generation units have been implemented. The *residential PV greedy* operation strategy charges the ESS as fast as possible without consideration of the grid by meeting the residual load at all times. To reduce the maximum grid load the *residential PV feed in damp* operation strategy schedules the charging of the ESS according to a PV prediction. It attempts to provide a constant charging power and aims for a fully charged ESS at sundown.

Two strategies have currently been implemented for industrial consumers. The simple *Peak Shaving (PS)* strategy works as follows. As long as the target power is above a specified threshold, the additionally required power is provided by the ESS. In addition, the ESS will recharge itself if the power value is below the PS threshold [58] (used in the case study in Section 6.1). In order to reduce calendar aging for a lithium-ion based ESS, the *PS perfect foresight* strategy operates under the assumption of perfect foresight for the load profile. The ESS will only charge up to the energy that is required for the next load peak, right before the occurrence of that load peak [59].

The EMS strategy for providing *FCR* implemented in **SimSES** is based on the German regulatory framework [60,61]. The requested charging and discharging power is proportional to the frequency deviation. Below 49.8 Hz or above 50.2 Hz the output power is set to the prequalified power. Within the frequency dead band around 50 Hz with +/-10 mHz the output power is set to 0 W. The degree of freedom to exceed the output power by 20% is used, aiming to bring the SOC back to a predefined SOC set-point. The *IDM* operation strategy charges or discharges the ESS by trading energy on the electricity market, in particular on the IDM, if the SOC falls below a predefined lower limit or it exceeds an upper limit [62]. An example for a *FCR* and a *IDM* stacked operation strategy is provided in Section 6.2.

5.2.2. Power distribution strategies

For complex storage system topologies, the power needs to be distributed between the different subsystems of an ESS [63,64]. For this purpose, several power distribution logics are implemented in **SimSES**. These logics distribute the power to the corresponding storage systems, for instance, based on the respective SOH or SOC. In **SimSES**, the ESS is differentiated between an AC and DC storage system (see Section 3). For each node of parallel connected AC systems as well as DC systems, a power flow decision has to be made similar to Bauer [64]. Mühlbauer et al. [63] as well as Bauer [64] define PDS as a simple problem of a distribution factor α as shown in Eq. (12).

$$P_i = P_{target} \cdot \alpha_i, \tag{12}$$

where P_{target} is the target power provided by the EMS, α_i the power distribution factor for system i, and P_i the corresponding power of system i on condition that the sum of all α_i equals one. In an optimal case the PDS takes the current limitations of the underlying storage technology for P_i into consideration in order to be able to fulfill the requested power, e.g., temperature limitations could lead to lower deliverable power. For each node, a PDS can be configured.

Mühlbauer et al. distinguish between static and dynamic categories for PDS while Bauer has more subtle definitions for a dynamical PDS approach with a fixed and variable sequence [63,64]. Bauer also mentions a PDS as an optimization problem currently not considered in **SimSES**. In the following, PDS implemented in **SimSES** are presented.

The most straightforward implementation of a PDS is an equal distribution of the power to all storage systems. This is a static PDS approach with a fixed power distribution factor. Other static PDS-like distribution based on the ESS capacity can be easily added to the PDS set of **SimSES**. In addition, a dynamic PDS is implemented by differentiating between charge and discharge distribution factors depending on the SOC of each system based on [63].

Due to the modularity of **SimSES**, multiple ESSs with different storage technologies can be combined with a hybrid ESS, e.g., a LIB and a RFB system. For this purpose, a novel PDS is introduced prioritizing configured storage technologies by base and peak loads, respectively. While the prioritized system stays within a defined SOC range, e.g., between 25 % and 75 %, it tries to fulfill the target power within its power limits. If either the SOC or the power limit is exceeded, the next highest prioritized system takes over. If the power target is not completely allocated, a second loop distributes the power independent from the defined SOC range. In addition, the logic balances the SOC of the configured ESS if one or more systems are outside of the defined SOC range while other systems are within those ranges. The algorithm also allows a two or one way balancing, e.g., if only the peak load system should be balanced by the base load system (used in the case studies in Section 6).

5.3. Thermal modeling

Performance, efficiency, and aging of all aforementioned storage processes depend not only on charge and discharge currents, but are also highly sensitive to thermal conditions. While for some small-scale storage realizations (e.g., residential battery storage) modeling electricity flows in a fixed temperature setting might be a solution of choice with sufficient accuracy for techno-economic simulations [65], larger storage systems along with investigations about storage efficiency particularly require detailed thermal models [53]. Utility-scale LIB stationary ESS are often designed as free-standing systems, which are installed outdoors and exposed to the environment. The use of standard shipping containers to install entire energy storage systems is the preferred option in the industry today to shield sensitive electric components from adverse environmental conditions. The benefits of such a configuration include modularity, scalability, ease of logistics, conformance with road-transport regulations, and the ability to plan and optimize land usage. Such containers are also specially fitted out with insulation to limit heat flow to/from the environment, and to present a stable operation temperature to the components inside.

Heat is generated in LIBs due to internal resistance to the passage of current during operation. Lithium-ion cell technology is particularly vulnerable to adverse changes in cell temperatures, and degrade faster when operated outside of their optimal temperature ranges. In particular, degradation may result from accelerated kinetics for unwanted side reactions at elevated temperatures resulting in a loss of capacity and an increase in the internal resistance. If the generated heat is not rejected to the environment at a rate greater than the rate of heat generation, overheating and—in extreme cases—a *thermal runaway* may occur. In contrast, for applications with relatively lower current rates (alike most stationary storage use cases), air cooling systems are deemed adequate to aid the heat rejection process to maintain the cell temperatures within the stipulated ranges. It is worth to mention in this context, that in the absence of cooling systems, the capabilities of the cells are severely limited, and under-utilized [66].

In summary, thermal modeling of energy storage systems is a crucial step of the system design process, especially due to the following factors:

- temperature-dependence of the energy conversion efficiency of LIB (dependent on the internal resistance) [67] and other storage technologies,
- temperature-dependence of the degradation mechanisms [68,69],
- dependence of the round-trip efficiency on the energy consumption of auxiliary components, such as the HVAC system [55] and
- operational hazards under extreme temperatures which are too low, or too high [70].

Thermal modeling in **SimSES** follows a zero-dimensional lumped-capacity approach, and consists of a number of component packages which run in tandem to emulate the thermal behavior of a system under the specified operating conditions. Zero-dimensional lumped-capacity approaches are widely used in the reviewed literature and found to be suitable for system models [55,71]. Each of these packages and their core features are presented in this section, along with how they fit into the larger picture within **SimSES** and its architecture. The thermal model and its associated components function at the AC storage system level in **SimSES**. **SimSES** currently supports a container-based housing solution with an air cooling system for LIB stationary ESS. An overview of these packages and their interplay is seen in Fig. 9.

5.3.1. Ambient thermal model

The primary function of the ambient thermal model is to account for the predominant environmental effects that play a role in the thermal behavior of the ESS. The ambient thermal model currently consists of an ambient temperature which supplies a value of ambient air temperature T_{aa} for each simulation timestep Δt at time t. The ambient temperature is available in two variants: a constant temperature model, which supplies a user-specified T_{aa} for each timestep, and a location-specific model, which, depending on the time of day and year, supplies a value of T_{aa} based on recorded temperature time-series data. The ambient temperature datasets currently present in SimSES have been generated with the help of the publicly available simulation tool *greenius*, developed by the German Aerospace Center (DLR) [72]. A solar irradiation model is also envisioned for a future release of SimSES as an extension of the ambient thermal model in order to be able to supply values of incident solar irradiation at a given location at time t to allow for better estimation of the heat load on an ESS. The ambient thermal model is understandably applicable to all AC storage system instances present in a given BESS configuration.

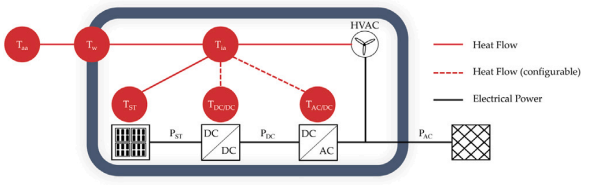

Fig. 9. SimSES is thermally interconnected with the thermal nodes of ambient air T_{aa}, wall T_w, inner air T_{ia}, and storage technology T_{ST}. The temperature conjunction of T_{ACDC} and T_{DCDC} can be switched off. The HVAC system controls T_{ia} of the storage system.

5.3.2. Housing model

The housing model emulates the physical attributes of the specified housing type. **SimSES** currently supports system simulations with a standard 20 foot shipping container as the housing. The walls are modeled with three layers of materials, including an insulating layer of Polyurethane (PU) between the outer and inner metal layers. The geometrical dimensions and physical and thermal properties of the walls of the shipping container can be adapted to suit any desired variant. The modular and extendable structure of **SimSES** ensures that the choice is not limited to the presently implemented model, but rather allows for other housing types or installation conditions to be modeled and included in simulations.

5.3.3. Heating, ventilation and air conditioning model

As the temperature inside the housing is to be maintained within a stipulated range to ensure safe and optimal operating conditions, a HVAC unit is necessary to correct temperature deviations. **SimSES** also supports inclusion and modeling of HVAC systems. Two basic HVAC models are currently implemented: one, which uses the internal air temperature T_{ia} deviation from its user-specified set-point to roughly estimate the amount of thermal power required to counter this deviation, and the other, which employs a Proportional-Integral-Derivative (PID) controller logic to arrive at a value of thermal power to counteract the deviation in T_{ia} from its set-point. The corresponding electrical power consumption $P_{electrical}$ of the HVAC, which is related to the thermal power P_{hvac} by the Coefficient of Performance (COP) (see Eq. (13)), is logged in the state of the AC storage system, and influences the round-trip efficiency of the ESS.

$$P_{electrical} = \frac{P_{hvac}}{COP} \tag{13}$$

5.3.4. System thermal model

The system thermal model is central to the thermal modeling process in **SimSES**, in that it emulates the physical phenomenon of heat transfer among the components of the ESS and its environment, as well as integrates the functioning of all aforementioned components. The

system thermal model estimates the temperatures of all components of interest after each simulation timestep Δt, based on the various heat loads—both external and internal—that the ESS is subjected to. Each instance of AC storage system has its own system thermal model, and captures the thermal behavior of all components present in each AC storage system. The analysis applies the zero-dimensional lumped capacity approach, and the central assumption is that all the components are treated as lumped isotropic homogeneous objects with heat capacities and heat transfer coefficients. The internal air in the container is assumed to possess a uniform temperature throughout its volume, and flows are not considered. The temperatures of the storage technologies influence important parameters such as efficiency and voltage, as well as the rate at which they degrade. The component models used in **SimSES**, which are explained in the subsequent sections, take these temperature variations into account.

The system thermal model solves a system of first-order coupled differential equations to obtain the temperatures of the storage technologies, the internal air, and components such as the ACDC converter, if they are present within the same housing. This list of components, whose temperatures are of interest, can be expanded as required owing to the modular structure of the system thermal model. As the temperatures at the start of each timestep Δt are known, and the temperatures at the end of each timestep are of interest, an initial value problem can be formulated.

Within each DC storage system, for each instance of storage technology *i* with a mass m_{st} and specific heat c_p^{st}, a differential equation capturing the variation in its temperature T_{ST} under the combined effects of natural convection with the internal air (ia) P_{conv}^{st-ia} and the heat generation within itself on account of energy conversion losses P_{loss}^{st} can be formulated (see Fig. 9). For an AC storage system with a total of *n* storage technology instances within its DC storage systems, a total of *n* differential equations based on Eq. (14) can be formulated.

$$m_{st,i} \cdot c_p^{st,i} \cdot \frac{dT_{st,i}}{dt} = P_{loss}^{st,i} - P_{conv}^{st,i-ia} \tag{14}$$

Similarly, a heat balance equation with a form similar to Eq. (14) can be formulated for other components such as the ACDC converter, which also introduce heat into the housing due to the energy conversion losses (see Fig. 9).

For the internal air with a mass m_{ia} and specific heat c_p^{ia}, a heat balance can also be formulated to determine the variation in its temperature T_{ia}. The heat balance outlines its interaction via natural convection with each storage technology P_{conv}^{st-ia}, other components such as the ACDC converter (if present) $P_{conv}^{acdc-ia}$, and the innermost layer (il) of the housing walls P_{conv}^{il-ia}. The thermal power of the HVAC P_{hvac} is also accounted for in this balance (see Eq. (15)).

$$m_{ia} \cdot c_{p,ia} \cdot \frac{dT_{ia}}{dt} = \Sigma P_{conv}^{st,i-ia} + P_{conv}^{acdc-ia} - P_{hvac} - P_{conv}^{ia-il} \tag{15}$$

The innermost layer of the housing walls, in addition to the convective heat transfer with the internal air, also exchanges heat with the insulation layer adjacent to it via heat conduction, and a heat balance equation can be written.

The insulation layer interacts with both the innermost and outer layers via heat conduction, and a corresponding heat balance equation can be drafted as well. The outer layer exchanges heat with the adjacent insulation layer via conduction, and interacts with the ambient air via natural convection. The outer layer is also subjected to a heat load due to the direct and diffuse solar irradiation incident on its surfaces. A heat balance for the outer layer can be applied by taking into account the heat loads due to the incident solar irradiation, the conduction through the layers, and the natural convection with the ambient air.

Depending on the chosen simulation timestep Δt, the heat balance equations for all considered components are then solved simultaneously at least once, or in the case of very large Δt, the system of equations is solved multiple times in an attempt to obtain a greater degree of accuracy. The solution of this system of equations yields the values of the temperatures at the end of each simulation timestep, which influence the component models.

In case simpler simulations are to be conducted, the thermal model can also be disabled, in which case the storage technologies experience a constant (user-defined) ambient temperature, and the temperatures of the storage technologies and other components are also set to remain at this value and are not updated. **SimSES** currently only offers modeling of thermal behavior for LIB. Augmentation of these capabilities for other storage technologies is planned for future releases.

5.4. Analysis

Following the simulation of ESSs, an analysis of the simulation results is conducted automatically by **SimSES** providing Key Performance Indicators (KPIs) and plots that allow the user to gain insights of the configured ESS. Furthermore, the analysis can be used to compare simulation results of different scenarios quantitatively and qualitatively. While the *Data* subpackage provides relevant parsers and utility functions for processing the time series of simulation results, the *Evaluation* subpackage includes the actual methods for deriving the KPIs and creating plots. Which evaluations should be performed, as well as relevant input data (e.g., electricity prices and storage cost) can be specified by the user. In the following, the technical evaluation and economic evaluation will be explained in more detail.

5.4.1. Technical evaluation

Within the *Technical Evaluation* part of **SimSES**, technical KPIs are determined on the system and storage technology level. Depending on the storage technology used, the respective KPIs are exported at the end of the analysis. Automatically generated plots give the user an impression of the usage and performance of the simulated ESS like time variance of AC and DC power, SOC and capacity. More advanced users can also use the simulation results to calculate characteristic values beyond the displayed KPIs. The technical evaluation's KPIs on system, lithium-ion, redox flow and hydrogen level are summarized in Table 7. As an example, the calculation of two KPIs is shown below.

The Round-Trip Efficiency (RTE) is calculated on the system level using Eq. (17) deviated from Eq. (16). To calculate the RTE, the discharged energy (E_{out}) is divided by the charged energy (E_{in}), from which the change of energy by SOC rise or decrease (ΔE) is subtracted. For simulations over a longer period of time, the efficiency influence on the SOC change can be neglected because charged and discharged energy are substantially larger than the change in energy between the start and end SOC of the simulation. For shorter simulation periods, the influence of efficiency on the SOC change must be considered. For this purpose, the SOC change is divided by the root of the efficiency, since, for example, the additionally charged energy at SOC increase has already passed through the power electronics in one direction and was thus influenced by the efficiency. A symmetrical efficiency for charge and discharge is assumed here.

$$\eta_{RTE} = \frac{E_{out}}{E_{in} - \frac{\Delta E}{\sqrt{\eta_{RTE}}}} \tag{16}$$

with $\Delta E = SOC_{last} \cdot E_{last} - SOC_{initial} \cdot E_{initial}$. Solving Eq. (16) for η_{RTE} leads to:

$$\eta_{RTE} = \frac{E_{out}}{E_{in}} + \frac{\Delta E^2 + \Delta E\sqrt{4E_{out}E_{in} + \Delta E^2}}{2E_{in}^2} \tag{17}$$

Another KPI calculated in the technical analysis is the remaining energy content (e_{rem}) as a percentage of the initial energy (Eq. (18)). For this, the current energy (E_{act}) is divided by the initial energy (E_{nom}).

$$e_{rem} = \frac{E_{act}}{E_{nom}} \tag{18}$$

Table 7
Key Performance Indicators (KPIs) for technical evaluation and the level at which they are calculated. Crosses indicate for which level the respective KPI is calculated.

Selected key performance indicators (KPI)	System	Lithium-ion	Redox flow	Hydrogen
Round-trip efficiency (%)	x	x	x	x
Mean state of charge (%)	x	x	x	x
Number of changes of signs per day (#)	x	x	x	x
Avg. length of resting times (min)	x	x	x	x
Pos. energy between changes of sign (% of capacity)	x	x	x	x
Avg. fulfillment factor (%)	x	x	x	x
Remaining capacity (%)	x	x	x	x
Energy throughput (kWh)	x	x	x	x
Mean power electronics efficiency (%)	x			
Equivalent full cycles (#)		x	x	
Depth of discharges (%)		x	x	
Coulomb efficiency (%)			x	
State of health (%)				x
Energy for heating of water (kWh)				x
Energy for compression of hydrogen produced (kWh)				x
Total mass of hydrogen (kg)				x

5.4.2. Economic evaluation

The economic evaluation of **SimSES** allows assessing the overall profitability of an energy storage project through economic KPIs. These KPIs include the net present value (NPV), internal rate of return, profitability index, return on investment, and levelized cost of storage. Eq. (19) shows the calculation of the NPV as it is performed in **SimSES**.

$$\mathrm{NPV} = -\mathrm{I}_0 + \sum_{\mathrm{n}=1}^{\mathrm{N}} \frac{\mathrm{CF}_\mathrm{n}}{(1+\mathrm{i})^\mathrm{n}} \tag{19}$$

I_0 denotes the initial investment cost, i the discount rate, CF the cashflow, and n and N the current and total number of project years, respectively. All parameters apart from the cashflow are derived from the settings in the Configuration File. The cashflow itself is calculated from the time series of logged simulation results. Depending on the selected operation strategy, the cashflows of multiple revenue streams ($\mathrm{CF}_{\mathrm{n,r}}$) may be added to obtain the cashflow for a single project year (CF_n), as shown in Eq. (20).

$$\mathrm{CF}_\mathrm{n} = -\mathrm{OM}_\mathrm{n} + \sum_{\mathrm{r}\in\mathrm{R}} \mathrm{CF}_{\mathrm{n,r}} \tag{20}$$

Here, R denotes the set of applicable revenues streams r for the selected operation strategy and OM the operation and maintenance cost. Table 8 shows the matching of revenue streams and operation strategies, while the following list provides brief descriptions for all currently implemented revenue streams. For stacked operation strategies, such as *FCR* paired with *IDM*, all respective revenue streams will be considered in Eq. (20).

- *Energy Cost Reduction (ECR)*: Reduction of energy-based electricity costs, caused, for example, by increased self-consumption of PV-generated electricity. This is calculated based on the total site load for both with and without the BESS, the electricity purchase price, and the electricity sales price or feed-in tariff.
- *Demand Charge Reduction (DCR)*: Savings generated by a reduction in demand charges, calculated based on the maximum site load with and without the BESS, the applicable billing period, and the demand charge price per unit of power.
- *Frequency Containment Reserve (FCR)*: Revenue that is generated by participating in the FCR market, calculated based on the system's nominal power, the FCR price, and the power allocated to the FCR market.
- *Spot Market Trading (SMT)*: Revenue that is generated through spot market trading, based on the amount of energy traded and the specified time series of prices.

6. Case studies

The following section will focus on **SimSES** from a user perspective. Compared to other solutions and tools in the field of energy system simulation, **SimSES** provides detailed modeling of ESS and applications on a system level during the full investment period. Both the technical properties of different storage technologies and the economic modeling of the components and systems are mapped in detail.

In order to clarify the implementation and adaptability of the tool, two applications are discussed. First, Peak Shaving (PS) for an industrial application comparing a different set of storage technologies—LIB, RFB, and a hybrid system of both technologies. Second, Frequency Containment Reserve (FCR) including an Intraday Continuous Market (IDM) by considering various system topologies are discussed. The underlying system costs are discussed in Appendix D. These case studies can be downloaded and executed as described in Appendix E.

6.1. Case study 1: Peak shaving application

A commonly used application for ESS is Peak Shaving (PS). The tariff model with separate energy- and power-related prices plays an important role here. The PS application aims to cut high power demands from the distribution grid. Since the highest power peak per billing period (usually monthly or annually) is multiplied by the power-related price, it can be economical favorable to cap high demand peaks by using an ESS to provide the necessary power and energy [9].

In this case study, three different storage systems are simulated: a LIB system with 150 kWh, a RFB system with 200 kWh, and a hybrid system with 10 kWh LIB capacity and 180 kWh RFB capacity. More detail on the system configuration chosen for this case study is given in Fig. 10. When investing in a system the user may be interested in deciding upfront which of the three configurations will provide the best economic solution. All systems are dimensioned to provide the peak shaving power even after 20 years, including capacity degradation. In addition, the restriction of a usable SOC range of RFB systems from 20% to 80% is considered [36]. The power electronics is dimensioned with 40 kW rated power. The Sony LFP cell technology for LIB and a scaled *CellDataStack5550W* model (cf. Table 4) as an all-Vanadium RFB system is considered. The assumed system costs for the economic evaluation are provided in Table D.11. As a revenue for reducing the power peak a fixed price of 100 EUR/kW in a yearly billing period is assumed. As an input power profile for the PS application, the Cluster 1 PS power profile from Kucevic et al. [73] is used and scaled to an annual load of 347.55 MWh from which the peak power is reduced to 63.5 kW.

After the simulation has been executed, the analysis and evaluation include both detailed technical and economic evaluations. An extract of the evaluations and results can be seen in the following illustrations:

Table 8
Matching of revenue streams and operation strategies for the cashflow calculation within the economic evaluation.

	ECR	DCR	FCR	SMT
Residential PV Greedy	x			
Residential PV Feed in Damp	x			
Peak Shaving	x	x		
Peak Shaving Perfect Foresight	x	x		
Frequency Containment Reserve			x	
Intraday Continuous Market				x

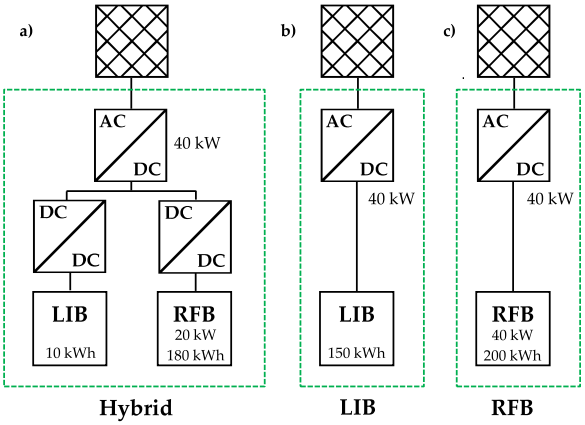

Fig. 10. Three different Energy Storage Systems (ESS) are investigated in the Peak Shaving (PS) case study: **(a)** A hybrid ESS consisting of a DC-coupled LIB and RFB system as well as single storage systems of **(b)** LIB and **(c)** RFB. All systems are dimensioned for providing the PS power even after 20 years of operation. A maximum Depth of Discharge (DOD) for RFB systems of 0.6 is considered. The Power Distribution Strategies (PDS) for the hybrid system performs according to the technology prioritization as described in Section 5.2.2. The DCDC converter is assumed with a fixed efficiency of 98%.

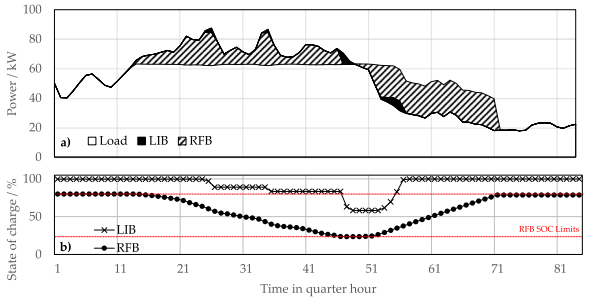

Fig. 11. Peak Shaving (PS) application on a hybrid Energy Storage System (ESS). **(a)** Residual load with and without the PS application with the delivered AC power of the installed ESS as well as the power distribution between the two DC-coupled storage systems. **(b)** State of Charge (SOC) development of the hybrid ESS. LIB systems takes over if target power exceed RFB stack power or if the RFB system hits its SOC limits.

Fig. 11 shows the characteristic curve of the power during the PS application for the hybrid storage system. The residual power can be seen with and without energy storage. It can be seen that the power drawn from the grid does not exceed the value of the PS threshold as was dictated by the operation strategy. Power demand values above the PS threshold are provided by the respective storage unit. This comes in line with charging and discharging power from the ESS and a simultaneous change in the storage-lumped SOC. According to the conditions set, recharging of the storage systems is executed only at times such that the PS threshold is never exceeded. In addition, the power distribution to the corresponding storage technologies of the hybrid system can be seen. The RFB system is prioritized to provide the bulk energy of the PS event while the LIB system covers high power peaks, especially if the RFB systems power capabilities are exhausted.

The remaining capacity (SOH) of the ESS can be seen in Fig. 12. The LIB capacity decreases to 70% during the 20-year simulation, while for the hybrid system as well as for the RFB system the capacity remains higher at 97% and 96%, respectively. Although the integrated degradation models consider both the calendar and the cycle degradation, it is noteworthy that the calendar degradation takes up the largest share in this operation of PS application [59].

In Fig. 12 the difference of the system round-trip efficiency can be observed. The LIB system demonstrates the highest efficiency with 88%, followed by the hybrid system with 68% and the RFB system with 62%. The energy losses of the RFB storage compartments are higher compared to LIB, attributed to a comparably low Coulomb efficiency and additional energy needed for electrolyte pumps.

In addition to the technical evaluation, **SimSES** also provides a comprehensive economic analysis of the simulated time series. In order to show a metric for overall costs, an alternative NPV considering capacity degradation as well is shown in Eq. (21), where c_{ST} represents energy-specific costs of the storage technology and C_{deg} the capacity degradation.

$$NPV_{CD} = NPV - c_{ST} \cdot C_{deg} \tag{21}$$

Fig. 12 shows the overall costs of the ESS operated with baseline cost set to 100% of the LIB system. For the evaluation of the system, not only real tariff models but also the investment costs for the ESS are integrated in the tool resulting in the NPV. In addition, the cost of capacity degradation is added to the NPV in order to take not only the system efficiency into account but also the capacity loss over 20 years (see Eq. (21)). It can be seen that the hybrid system is 5% more cost effective while the RFB system has 81% higher overall costs. The primary reason for these values are the cost of capacity degradation, which is 51% of the overall costs for the LIB system although the NPV for the LIB systems is lowest compared to the other systems. In conclusion, a hybrid system can deliver an overall better solution compared to single storage systems although only a small peak LIB ESS is added to an RFB system, combining the benefits of both techniques, i.e., a higher NPV compared to a single RFB system and a lower capacity degradation compared to a single LIB system. However, with the input parameters chosen herein, none of the three negative storage solutions were able to justify an investment as all resulted in negative NPV_{CD} values. The overall economics of this case study could potentially be improved if the ESS value generation was increased, e.g., by applying multi-use operation and dispatching storage in PS idle times [4,74]. Additionally, results with hybrid storage systems could be improved with optimization and machine learning techniques instead of applying a rule-based algorithm [75,76].

6.2. Case study 2: Frequency containment reserve application

A widely used application of utility-scale ESS is participation in the market for FCR. In this application, the ESS compensate for fluctuations

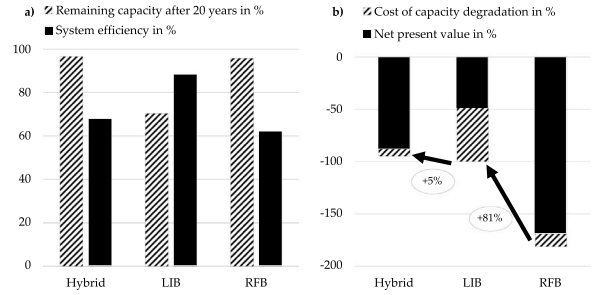

Fig. 12. Economic analysis of the three different Energy Storage Systems (ESS) serving the Peak Shaving (PS) application. **(a)** Comparison of remaining capacity and system efficiency of all simulated ESS after 20 years. **(b)** Overall costs consisting of the NPV and cost of capacity degradation using the LIB system as the baseline. The hybrid system could decrease overall cost by 5%, whereas the RFB system increased the cost by 81%.

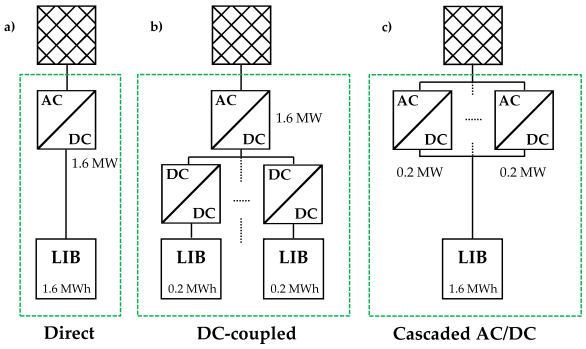

Fig. 13. Three different ESS topologies are investigated in the FCR case study, all with a LIB system of 1.6 MWh and an ACDC connection to the grid of 1.6 MW. The ACDC converter model is the *NottonAcDcConverter* (cf. Table 6). **(a)** A direct-coupled ESS with one ACDC converter. **(b)** Eight parallel DC-coupled systems with an assumed fixed DCDC efficiency of 98%. **(c)** Eight parallel connected ACDC converter with a cascaded activation: The first ACDC converter drives to its nominal power of 0.2 MW before the second ACDC converter is activated.

between consumption and generation in the power grid by reacting accordingly to changes in the grid frequency. The regulations and degrees of freedom for FCR application complying to German regulation criteria are taken into account and are described in detail in [4,8,62,73]. In this operation strategy of **SimSES** the SOC stabilization of the ESS is achieved by support of IDM. FCR and IDM are each basic operation strategies running in a stacked operation. For the simulation a grid frequency profile of 2014 is used to account for the provided stabilizing power [77]. It is assumed that the provided power of 1 MW does not affect the integrated network frequency.

In this case study, three different ESS topologies are simulated (cf. Fig. 13), each with a Sony LFP cell technology providing a capacity of 1.6 MWh and a grid-connection power of 1.6 MW. First, a simple direct approach of connecting a LIB to a grid-connected ACDC converter is investigated. Second, eight parallel DC-coupled systems with a LIB capacity of 0.2 MWh each are simulated. Third, eight parallel connected ACDC converters with a nominal power of 0.2 MW each are activated in a cascaded approach promising a higher efficiency [78]. The assumed system costs for the economic evaluation are provided in Table D.12. The revenue of FCR[12] is taken as a fixed price of 0.2 EUR per kW and day and the IDM[13] price is fixed to 0.04 EUR/kWh, corresponding to a price level of 2020.

The results of the 20-year simulations are displayed in Fig. 14. The cascaded ACDC converter approach shows the best efficiency with 92% compared to the direct approach with 78% and the least efficient topology with DC-coupled systems of 63%. FCR is an application with a high partial-load frequency below 30% of nominal power [55]. Hence, the cascaded ACDC converter are either under a high load compared to their nominal power or deactivated, leading to a higher overall efficiency compared to the direct system. The DC-coupled system shows an overproportional efficiency decrease compared to the direct system. The systems of the DC-coupled ESS are activated similar to the cascade of ACDC converter: one system is ramped up to full power before the second system is activated. Due to relatively high currents in addition to the losses of the DCDC converter, the DC-coupled system shows a comparatively low efficiency. This result suggests that the chosen PDS is inappropriate in terms of efficiency for a FCR application with the given system for the DC-coupled system. Comparing the remaining capacity of the three investigated systems, no large difference can be observed, with a remaining capacity of each system after 20 years of around 80%. One target of the chosen PDS for the DC-coupled system was to reduce the capacity degradation by cycling a few systems more often than other systems in order to get an overall better degradation behavior. However, it can be observed that the chosen strategy shows no improvement in terms of the degradation behavior for this application compared to the other systems.

Analyzing the economics, the high efficiency advantage of the cascaded system could be transferred to a slight monetary improvement compared to the other systems. The cascaded system shows a 4% increase of the NPV compared to the direct system. The DC-coupled system falls behind with a lower NPV of 5% in comparison to the direct system (cf. Fig. 14). This could be explained with IDM recharging cost over the simulation time period since the FCR revenue is the same for all investigated systems (cf. Table 9).

First, the IDM transaction costs are comparatively low: The direct system accounts for 36 kEUR, the DC-coupled system for 64 kEUR and the cascaded system for 14 kEUR, accumulated after 20 years of operation. In comparison, the FCR revenue compensates for around 1,218 kEUR. Second, the low efficiency of the DC-coupled system results in 231 MWh energy sold on the IDM whereas the direct system and the cascaded system could sell 347 MWh and 494 MWh, respectively. This is also reflected in the numbers of bought energy: the DC-coupled system had to buy most energy with 1,829 MWh while the cascaded system had to buy 851 MWh. Although large differences in terms of efficiency exist compared to the direct system (+14% for the cascaded system and -15% for the DC-coupled system) this could only be translated into a 4% increase of the NPV, respectively to a 5% decrease. The economic result of more efficient ESS could be improved by reducing the storage capacity and improving the IDM operation strategy. In conclusion, all three systems have a positive NPV, likely leading to a positive investment decision.

With these case studies a high variety of topologies as well as technology combinations could be investigated. Parameter variations, e.g., for the investment costs or sizing of individual components can easily be made by the user when adapting according initialization files of the case studies available as presented in Appendix E.

7. Conclusion and outlook

Within this work, the simulation and analysis tool for energy storage systems **SimSES** is presented. **SimSES** provides a library of state-of-the-art energy storage models by combining modularity of multiple topologies as well as the periphery of an ESS. This paper summarizes the structure as well as the capabilities of **SimSES**. Storage technology

[12] Prices for the German FCR market can be found at https://www.regelleistung.net.

[13] Prices for the European spot market can be found at https://www.epexspot.com.

Table 9
Overview of the IDM transaction costs for all three investigated ESS.

System	IDM transaction costs/EUR	Energy bought/MWh	Energy sold/MWh
Direct	35,772	1242	347
DC-coupled	63,894	1829	231
Cascaded	14,280	851	494

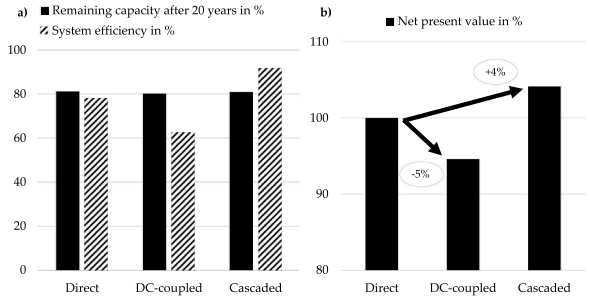

Fig. 14. Technical and economical analysis of the three different Energy Storage Systems (ESS) serving the Frequency Containment Reserve (FCR) application. **(a)** Comparison of remaining capacity after 20 years and system efficiency of all simulated ESSs. **(b)** Economic value consisting of the NPV using the direct system as baseline.

models based on current research for lithium-ion batteries, redox flow batteries, as well as hydrogen storage-based electrolysis and fuel cell are presented in detail. In addition, thermal models and their corresponding HVAC systems, housing, and ambient models are depicted. Power electronics are represented with ACDC and DCDC converters mapping the main losses of power electronics within a storage system. Additionally, auxiliary components like pumps, compressors, and HVAC are considered. Standard use cases like peak shaving, residential storage, and control reserve power provisions through dispatch of storage are discussed in this work, with the possibility to stack these applications in a multi-use scenario. The analysis is provided by technical and economic evaluations illustrated by KPIs.

SimSES' capabilities are demonstrated through the discussion of two case studies mapped to the applications of peak shaving and frequency containment reserve, respectively. It is demonstrated how different energy storage system topologies as well as various performance indicators can be investigated and analyzed with **SimSES**. For the specific cases discussed, the results underline that hybrid storage systems can lead in terms of overall cost and degradation behavior to a beneficial economic results. Special ESS topologies like the cascaded ACDC converter approach can lead to a substantial increase in system efficiency for the FCR application, although the economic benefits are comparatively low.

In the future, more detailed performance and aging models for all types of storage systems will be implemented. This will allow a more detailed cross-technology comparison. For instance, models for bidirectional thermal storage system could be implemented in future versions. Further operating strategies matching internationally renowned and national derivatives of application scenarios could also be investigated. This may allow assessing the value of storage deployment across different regions and convince internationally active investors to reveal best investment scenarios worldwide. **SimSES** has interfaces that can be easily integrated into physically derived and more accurate storage models as well as grid modeling and system analysis tools. While selected validation experiments have already been executed, the authors encourage others in the research community to conduct hardware validation experiments at their sites and contribute to the presented tool. The authors envision interlinking **SimSES** to the vast selection of open-source tools in order to expand on the value chain that storage simulations are capable of covering, e.g., **SimSES** is already a part of the *openMOD*[14] initiative. **SimSES** is open-source available, and the authors encourage users and developers to join in and assist in its further development.

CRediT authorship contribution statement

Marc Möller: Conceptualization, Methodology, Writing - original draft, Writing - review & editing, Software, Project administration, Visualization, Investigation. **Daniel Kucevic:** Writing - original draft, Writing - review & editing, Validation, Software, Methodology. **Nils Collath:** Writing - original draft, Writing - review & editing, Software, Methodology. **Anupam Parlikar:** Writing - original draft, Writing - review & editing, Software, Methodology. **Petra Dotzauer:** Writing - original draft, Writing - review & editing, Software, Methodology. **Benedikt Tepe:** Investigation, Validation, Writing - original draft, Writing - review & editing, Software. **Stefan Englberger:** Investigation, Validation, Writing - original draft, Writing - review & editing. **Andreas Jossen:** Writing - review & editing, Funding acquisition. **Holger Hesse:** Writing - original draft, Writing - review & editing, Supervision.

Declaration of competing interest

The authors declare that they have no known competing financial interests or personal relationships that could have appeared to influence the work reported in this paper.

Acknowledgments

This work was financially supported by the Federal Ministry for Economic Affairs and Energy within the open_BEA project (Grant No. 03ET4072) and the EffSkalBatt project (Grant No. 03ET6148). Both projects are supported by Project Management Juelich. The responsibility for this publication rests with the authors.

We thank Jacob Klinkenberg, Kareem Abo Gamra, and Benedikt Wiesend for their contribution with simulating and implementing models in the hydrogen package, Timo Sandner and Felix Müller for their implementations of ACDC converters, Dang The Phong for his work on the model for a RFB stack as well as Ni Chuanqin and Yuhui Geng for their implementations of two LIB degradation models.

Appendix A. Open circuit voltage curve fitting

The OCV for LIBs (see Section 4.1) is dependent on the cell type. The OCV data for all currently implemented cell types have been measured at the Institute for Electrical Energy Storage Technology at the Technical University of Munich. To improve the performance, the look-up tables of the voltage values are replaced with a mathematical function. These curve-fitting functions are based on the work of Weng et al. [79]. The parameters of this function for the OCV are estimated using the MATLAB® global optimization toolbox. Fig. A.15 shows the OCV in V for the measured data as well as the curve-fitted data and the difference between those in mV.

[14] https://openmod-initiative.org/

Table B.10
Physical parameters for modeling of thermal behavior of lithium-ion batteries (LIBs).

Manufacturer model	Mass (g)	Dimensions (mm)	Specific heat ($Jkg^{-1}K^{-1}$)	Convection coefficient ($Wm^{-2}K^{-1}$)	Source
Sony US26650FTC1	70	dia: 26 len: 65	1001	15	[55,80–89]
Panasonic NCR18650PD	44	dia: 18 len: 65	1048	15	[88–90]
E-One Moli Energy IHR18650A	45	dia: 18 len: 65	965	15	[83,86,89,91–94]
Sanyo UR18650E	46	dia: 18 len: 65	965	15	[83,86,89,92–95]

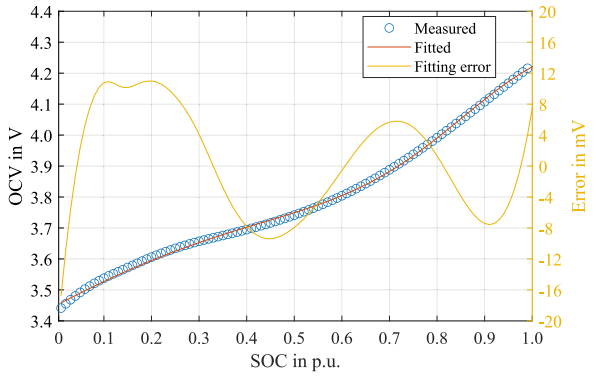

Fig. A.15. Open Circuit Voltage (OCV) curve fitting for the MolicelNMC lithium-ion battery (LIB). The figure shows the OCV in V for the measured data as well as the curve-fitted data and the difference between those in mV.

Appendix B. Thermal parameters

The geometrical and thermal parameters used for modeling the thermal behavior of LIBs are presented in Table B.10. Geometrical parameters such as the dimensions and the weight are obtained from datasheets of the cells. The thermal properties, such as the specific heat capacity for each cell type, are determined from the literature for each cell chemistry, and averaged over several values found in the literature. The value of the convection coefficient is known with the least accuracy, and a value of 15 $Wm^{-2}K^{-1}$ is selected as a "reasonable" value lying between typical values for purely natural convection and forced convection. This is assumed to emulate slow intermittent motion of air around the cells. It is expected that availability of better data in the future will increase the accuracy of the modeling process.

Appendix C. Stack data for a redox flow battery

The parameters are based on single-cell measurements carried out at ZAE Bayern of a cell with a technical representative cell area of 2160 cm^2. To obtain parameters for a stack, the measured values were scaled up with a number of 40 cells. Fig. C.16 shows the data of the internal resistance of the 40-cell stack for charge and discharge. The internal resistance is determined by applying a constant current and measuring the resulting change of voltage. The cell was operating in Vanadium electrolyte (1.6 mol/l V solved in 2 mol/l H_2SO_4) from GfE (Gesellschaft für Elektrometallurgie mbH). Temperature and flow rate were controlled during the procedure. The SOC was determined with an OCV-cell. Due to the relatively high ohmic resistance of the cell and the low possible operation current density (up to approx. 50 mA/cm^2), the cell resistance shows no significant current dependency. The cell

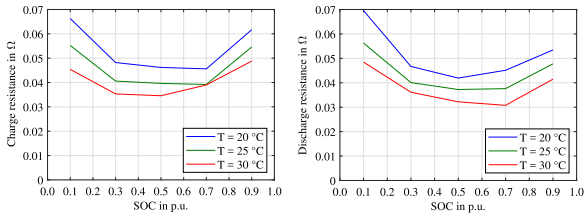

Fig. C.16. Charge and discharge resistance of a stack for a redox flow battery (cell area = 2160 cm^2) dependent on State of Charge (SOC) and temperature (T). The single-cell measurements were scaled up to a stack resistance with a cell number of 40.

resistance R_{cell} was scaled up with the number of cells n_{cell} to receive the stack resistance R_{stack} ($R_{stack} = n_{cell} \cdot R_{cell}$).

Appendix D. Economics for case studies

Assumptions for economical analysis of the case studies are based on Tsiropoulos et al. Minke et al. Figgener et al. and Mongird et al. [96–99]. Challenges for determining energy-specific costs for ESS occur due to a wide range of technology costs as well as various system sizes and designs. In order to distinguish between power and energy system design, Tsiropoulos et al. takes the EPR as an indicator: If EPR is above one, the authors talk about an energy-driven design, otherwise about power-driven design [96]. In addition, it is not always clearly stated which costs for a system design are included, e.g., power electronics, housing, and grid connection [96,98]. For instance, utility scale system costs for LIB in 2017 ranged between 300 EUR/kWh and 1200 EUR/kWh with an average around 570 EUR/kWh [96]. Figgener et al. depicted a similar range for 2018 [98] as well as one reported system for 2019 with an EPR of 1 h and system costs of around 900 EUR/kWh. However, LIB systems with an EPR of 0.125 h show lowest cost with 300 EUR/kWh and costs increase with rising EPR [96]. Mongird et al. have presented system costs for LIB system with an EPR larger than 1 h with falling costs [99]. Interestingly, the system costs of [99] show a lower average system cost price than those of [96,98] representing European costs' levels (a USD to EUR conversion of 0.82 is assumed). In contrast, a broad cost database does not exist for RFB systems. However, Minke et al. investigated various RFB projects from 2004 to 2017 by determining system prices for different EPR, similar to Tsiropoulos et al. [97]. The authors also found an even broader range of system costs for RFB from 155 EUR/kWh to 1738 EUR/kWh, especially due to different electrolytes, stack modules, sizing, and system definition. RFB system costs decrease with a rising EPR with average system costs of 717 EUR/kWh for an EPR of 2 h and 166 EUR/kWh for a ratio of 15 h. These findings are also in agreement with the results of Mongird et al. [99].

For the following case studies, system cost curves depending on EPR are assumed for LIB and RFB systems with the prices and ratios

Table D.11
Economics for Case Study 1.

Storage technology	Power/kW	Capacity/kWh	EPR/h	Specific system cost/EUR kWh^{-1}	System cost/EUR	Overall system cost/EUR
LIB	40	10	0.25	584	5,839	
RFB	20	180	9.00	329	59,216	65,055
LIB only	40	150	3.75	367	55,089	55,089
RFB only	40	200	5.00	451	90,247	90,247

Table D.12
Economics for Case Study 2.

Storage technology	Power/kW	Capacity/kWh	EPR/h	Specific system cost/EUR kWh^{-1}	System cost/EUR
LIB	1,600	1,600	1	473	756,800

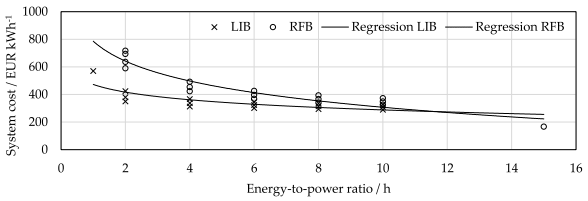

Fig. D.17. System costs curves depending on EPR for LIB and RFB systems based on [96,97,99].

given represented by regression curves in Eqs. (D.1) and (D.2). From an EPR of 1 h up to 15 h, this cost curve has a realistic cost range with decreasing cost over EPR. The system costs, however, have a high uncertainty attached, as shown in the previous analysis. The used price curves are shown in Fig. D.17. It is worth mentioning that the cost assumptions for RFB systems are based on a usable SOC range of 20% and 80%, which reduces the gross capacity configured by 40% [97].

$$c_{LIB} = -80 \cdot \ln(EPR) + 473 \quad \text{and} \tag{D.1}$$

$$c_{RFB} = -208 \cdot \ln(EPR) + 786, \tag{D.2}$$

where c represents the energy specific costs of LIB, respectively RFB.

Using Eqs. (D.1) and (D.2) the system costs for the two case studies discussed in Section 6 are calculated as provided in Tables D.11 and D.12.

Appendix E. Availability of SimSES

SimSES is available as open source[15] and is part of the open-source simulation and optimization toolchain of the Institute for Electrical Energy Storage Technology at the Technical University of Munich.[16] A *readme.md* helps with the first steps in order to get **SimSES** running. An installed Python environment is mandatory as well as the required packages installed automatically if you run *setup.py*. With executing *main.py*, a default configured simulation could be started directly. This file offers also all necessary interfaces in order to connect it to other simulation programs. The case studies presented within this paper are conducted with the open-source release version 1.0.4.

For configuring a simulation, there are two important configuration files: *simulation.ini* and *analysis.ini*. These configuration files are documented and offer all possible settings for setting up a simulation and the consequent evaluation. These config files follow a pattern for a *default* and *local* configuration. The *default* configuration inherits all possible settings, in the *local* file: only the changed settings are necessary. This allows a quick exchange of configuration settings between users.

The *Simulation* package allows multiple simultaneous simulations, which are also used for the presented case studies. In here, the configurations and code could be found with the case study configs in *case_studies*. In order to execute the case studies, the configuration needs to be copied to the config location and renamed to *simulation.local.ini*.

[15] https://gitlab.lrz.de/open-ees-ses/simses
[16] http://www.simses.org

References

[1] V. Lauber, S. Jacobsson, The politics and economics of constructing, contesting and restricting socio-political space for renewables – the German renewable energy act, Environ. Innov. Soc. Transitions 18 (2016) 147–163, http://dx.doi.org/10.1016/j.eist.2015.06.005.
[2] H.E. Murdock, D. Gibb, T. André, F. Appavou, A. Brown, B. Epp, B. Kondev, A. McCrone, E. Musolino, L. Ranalder, Renewables 2019 global status report, REN21, https://www.ren21.net/wp-content/uploads/2019/05/gsr_2019_full_report_en.pdf.
[3] P. Denholm, E. Ela, B. Kirby, M. Milligan, The Role of Energy Storage with Renewable Electricity Generation, Technical Report NREL (2010), 2010, http://dx.doi.org/10.2172/972169.
[4] S. Englberger, A. Jossen, H. Hesse, Unlocking the potential of battery storage with the dynamic stacking of multiple applications, Cell Rep. Phys. Sci. 1 (11) (2020) http://dx.doi.org/10.1016/j.xcrp.2020.100238.
[5] A. Evans, V. Strezov, T.J. Evans, Assessment of utility energy storage options for increased renewable energy penetration, Renew. Sustain. Energy Rev. 16 (6) (2012) 4141–4147, http://dx.doi.org/10.1016/j.rser.2012.03.048.
[6] D. Zafirakis, K.J. Chalvatzis, G. Baiocchi, G. Daskalakis, The value of arbitrage for energy storage: Evidence from European electricity markets, Appl. Energy 184 (2016) 971–986, http://dx.doi.org/10.1016/j.apenergy.2016.05.047.
[7] R.H. Byrne, R.J. Concepcion, C.A. Silva-Monroy, Estimating potential revenue from electrical energy storage in PJM, in: IEEE Power and Energy Society General Meeting (2016), 2016, http://dx.doi.org/10.1109/PESGM.2016.7741915.
[8] T. Thien, D. Schweer, D. vom Stein, A. Moser, D.U. Sauer, Real-world operating strategy and sensitivity analysis of frequency containment reserve provision with battery energy storage systems in the german market, J. Energy Storage 13 (2017) 143–163, http://dx.doi.org/10.1016/j.est.2017.06.012.
[9] A. Oudalov, R. Cherkaoui, Sizing and optimal operation of battery energy storage system for peak shaving application: Lausanne, Switzerland, 1 - 5 july 2007, IEEE Lausanne Power Tech. (2007) http://dx.doi.org/10.1109/PCT.2007.4538388.
[10] J. Hoppmann, J. Volland, T.S. Schmidt, V.H. Hoffmann, The economic viability of battery storage for residential solar photovoltaic systems – A review and a simulation model, Renew. Sustain. Energy Rev. 39 (2014) 1101–1118, http://dx.doi.org/10.1016/j.rser.2014.07.068.
[11] H. Hesse, R. Martins, P. Musilek, M. Naumann, C. Truong, A. Jossen, Economic optimization of component sizing for residential battery storage systems, Energies 10 (7) (2017) 835, http://dx.doi.org/10.3390/en10070835.
[12] S. Englberger, H. Hesse, D. Kucevic, A. Jossen, A techno-economic analysis of vehicle-to-building: Battery degradation and efficiency analysis in the context of coordinated electric vehicle charging, Energies 12 (5) (2019) 955, http://dx.doi.org/10.3390/en12050955.
[13] O.M. Toledo, D. Oliveira Filho, A.S.A.C. Diniz, Distributed photovoltaic generation and energy storage systems: A review, Renew. Sustain. Energy Rev. 14 (1) (2010) 506–511, http://dx.doi.org/10.1016/j.rser.2009.08.007.
[14] H. Hesse, M. Schimpe, D. Kucevic, A. Jossen, Lithium-ion battery storage for the grid—A review of stationary battery storage system design tailored for applications in modern power grids, Energies 10 (12) (2017) 2107, http://dx.doi.org/10.3390/en10122107.
[15] B. Dunn, H. Kamath, J.-M. Tarascon, Electrical energy storage for the grid: A battery of choices, Science 334 (2011) http://dx.doi.org/10.1126/science.1212741.

[16] J. Weniger, T. Tjaden, Performance-Simulationsmodell für AC-gekoppelte PV-Batteriesysteme (PerModAC): Dokumentation | Version 1.0, Hochschule für Technik und Wirtschaft H.T.W. Berlin, Berlin, 2017, URL https://pvspeicher.htw-berlin.de/wp-content/uploads/2017/03/PerModAC_doku.pdf.

[17] N.-K.C. Nair, N. Garimella, Battery energy storage systems: Assessment for small-scale renewable energy integration, Energy Build. 42 (11) (2010) 2124–2130, http://dx.doi.org/10.1016/j.enbuild.2010.07.002.

[18] U. Sureshkumar, P.S. Manoharan, A.P.S. Ramalakshmi, Economic cost analysis of hybrid renewable energy system using HOMER, in: IEEE-International Conference on Advances in Engineering, Science and Management, ICAESM -2012, 2012, pp. 94–99.

[19] J. Figgener, P. Stenzel, K.-P. Kairies, J. Linßen, D. Haberschusz, O. Wessels, G. Angenendt, M. Robinius, D. Stolten, D.U. Sauer, The development of stationary battery storage systems in Germany – A market review, J. Energy Storage 29 (2020) http://dx.doi.org/10.1016/j.est.2019.101153.

[20] E. Gamma, R. Helm, R. Johnson, J.M. Vlissides, Design Patterns: Elements of Reusable Object-Oriented Software, first ed., Addison-Wesley Professional, 1994.

[21] B. Nykvist, M. Nilsson, Rapidly falling costs of battery packs for electric vehicles, Nature Clim. Change 5 (4) (2015) 329–332, http://dx.doi.org/10.1038/nclimate2564.

[22] G. Zubi, R. Dufo-López, M. Carvalho, G. Pasaoglu, The lithium-ion battery: State of the art and future perspectives, Renew. Sustain. Energy Rev. 89 (2018) 292–308, http://dx.doi.org/10.1016/j.rser.2018.03.002.

[23] M. Yoshio, R.J. Brodd, A. Kozawa, Lithium-Ion Batteries, Springer New York, New York, NY, 2009, http://dx.doi.org/10.1007/978-0-387-34445-4.

[24] A.M. Divakaran, M. Minakshi, P.A. Bahri, S. Paul, P. Kumari, A.M. Divakaran, K.N. Manjunatha, Rational design on materials for developing next generation lithium-ion secondary battery, Prog. Solid State Chem. 62 (2021) 100298, http://dx.doi.org/10.1016/j.progsolidstchem.2020.100298.

[25] M. Naumann, F.B. Spingler, A. Jossen, Analysis and modeling of cycle aging of a commercial LiFePO4/graphite cell, J. Power Sources 451 (2020) 227666, http://dx.doi.org/10.1016/j.jpowsour.2019.227666.

[26] M. Naumann, M. Schimpe, P. Keil, H.C. Hesse, A. Jossen, Analysis and modeling of calendar aging of a commercial LiFePO4/graphite cell, J. Energy Storage 17 (2018) 153–169, http://dx.doi.org/10.1016/j.est.2018.01.019.

[27] P. Keil, S.F. Schuster, J. Wilhelm, J. Travi, A. Hauser, R.C. Karl, A. Jossen, Calendar aging of lithium-ion batteries, J. Electrochem. Soc. 163 (9) (2016) A1872–A1880, http://dx.doi.org/10.1149/2.0411609jes.

[28] S.F. Schuster, T. Bach, E. Fleder, J. Müller, M. Brand, G. Sextl, A. Jossen, Nonlinear aging characteristics of lithium-ion cells under different operational conditions, J. Energy Storage 1 (2015) 44–53, http://dx.doi.org/10.1016/j.est.2015.05.003.

[29] J. Schmalstieg, S. Käbitz, M. Ecker, D.U. Sauer, A holistic aging model for li(NiMnCo)o2 based 18650 lithium-ion batteries, J. Power Sources 257 (2014) 325–334, http://dx.doi.org/10.1016/j.jpowsour.2014.02.012.

[30] M.M. Rahman, A.O. Oni, E. Gemechu, A. Kumar, Assessment of energy storage technologies: A review, Energy Convers. Manage. 223 (2020) 113295, http://dx.doi.org/10.1016/j.enconman.2020.113295.

[31] G. Kear, A.A. Shah, F.C. Walsh, Development of the all-vanadium redox flow battery for energy storage: a review of technological, financial and policy aspects, Int. J. Energy Res. 36 (11) (2012) 1105–1120, http://dx.doi.org/10.1002/er.1863.

[32] A.Z. Weber, M.M. Mench, J.P. Meyers, P.N. Ross, J.T. Gostick, Q. Liu, Redox flow batteries: a review, J. Appl. Electrochem. 41 (10) (2011) 1137–1164, http://dx.doi.org/10.1007/s10800-011-0348-2.

[33] N. Hagedorn, M.A. Hoberecht, L.H. Thaller, NASA redox cell stack shunt current, pumping power, and cell performance tradeoffs, U.S. Department of Energy / NASA Technical Memorandum, 1982, URL https://ntrs.nasa.gov/citations/19820011459.

[34] R. Schweiss, A. Pritzl, C. Meiser, Parasitic hydrogen evolution at different carbon fiber electrodes in vanadium redox flow batteries, J. Electrochem. Soc. 163 (9) (2016) A2089–A2094, http://dx.doi.org/10.1149/2.1281609jes.

[35] A.H. Whitehead, M. Harrer, Investigation of a method to hinder charge imbalance in the vanadium redox flow battery, J. Power Sources 230 (2013) 271–276, http://dx.doi.org/10.1016/j.jpowsour.2012.11.148.

[36] M. Skyllas-Kazacos, L. Cao, M. Kazacos, N. Kausar, A. Mousa, Vanadium electrolyte studies for the vanadium redox battery-a review, ChemSusChem 9 (13) (2016) 1521–1543, http://dx.doi.org/10.1002/cssc.201600102.

[37] A. Tang, J. Bao, M. Skyllas-Kazacos, Studies on pressure losses and flow rate optimization in vanadium redox flow battery, J. Power Sources 248 (2014) 154–162, http://dx.doi.org/10.1016/j.jpowsour.2013.09.071.

[38] E.A. Kaminski, R.F. Savinell, A technique for calculating shunt leakage and cell currents in bipolar stacks having divided or undivided cells, J. Electrochem. Soc. 130 (5) (1983) 1103–1107.

[39] fumatech, in: fumatech (Ed.), Redox-Flow-Batteries: data sheet: fumasep® membrane types, URL https://www.fumatech.com/NR/rdonlyres/6E4FA7B9-0AAA-42B9-98E4-BF756C23F981/0/FUMATECH_BWT_GmbHRedoxFlowBatteries.pdf.

[40] C. Blanc, R. Alfred, Understanding the vanadium redox flow batteries, in: InTech (Ed.), Paths to Sustainable Energy, InTechOpen, 2010, pp. 333–358.

[41] M. Robinius, P. Markewitz, P. Lopion, D. Stolten, Cost-efficient and climate-friendly transformation strategies for the german energy system up to 2050, in: Forschungszentrum JÜLich: Energy & Environment, 499, 2019.

[42] R.P. O'Hayre, S.-W. Cha, W.G. Colella, F.B. Prinz, Fuel cell fundamentals, third ed., John Wiley & Sons Inc, Hoboken New Jersey, 2016.

[43] G. Tjarks, PEM-electrolysis-systems for the integration in power-to-gas applications, (Ph.D. thesis), Lehrstuhl für Brennstoffzellen, RWTH Aachen, Aachen, 2017, http://dx.doi.org/10.18154/RWTH-2017-04470.

[44] C. Rakousky, U. Reimer, K. Wippermann, M. Carmo, W. Lueke, D. Stolten, An analysis of degradation phenomena in polymer electrolyte membrane water electrolysis, J. Power Sources 326 (2016) 120–128, http://dx.doi.org/10.1016/j.jpowsour.2016.06.082.

[45] C. Rakousky, U. Reimer, K. Wippermann, S. Kuhri, M. Carmo, W. Lueke, D. Stolten, Polymer electrolyte membrane water electrolysis: Restraining degradation in the presence of fluctuating power, J. Power Sources 342 (2017) 38–47, http://dx.doi.org/10.1016/j.jpowsour.2016.11.118.

[46] F. Marangio, M. Santarelli, M. Cali, Theoretical model and experimental analysis of a high pressure pem water electrolyser for hydrogen production, Int. J. Hydrogen Energy 34 (3) (2009) 1143–1158, http://dx.doi.org/10.1016/j.ijhydene.2008.11.083.

[47] M. Hammoudi, C. Henao, K. Agbossou, Y. Dubé, M.L. Doumbia, New multi-physics approach for modelling and design of alkaline electrolyzers, Int. J. Hydrogen Energy 37 (19) (2012) 13895–13913, http://dx.doi.org/10.1016/j.ijhydene.2012.07.015.

[48] C. Henao, K. Agbossou, M. Hammoudi, Y. Dubé, A. Cardenas, Simulation tool based on a physics model and an electrical analogy for an alkaline electrolyser, J. Power Sources 250 (2014) 58–67, http://dx.doi.org/10.1016/j.jpowsour.2013.10.086.

[49] D. Feroldi, M.S. Basualdo, Description of PEM Fuel Cells Systems, Springer, London and New York, 2012, http://dx.doi.org/10.1007/978-1-84996-184-4_2.

[50] A. Buttler, H. Spliethoff, Current status of water electrolysis for energy storage, grid balancing and sector coupling via power-to-gas and power-to-liquids: A review, Renew. Sustain. Energy Rev. 82 (2018) 2440–2454, http://dx.doi.org/10.1016/j.rser.2017.09.003.

[51] Q. Feng, X.-Z. Yuan, G. Liu, B. Wei, Z. Zhang, H. Li, H. Wang, A review of proton exchange membrane water electrolysis on degradation mechanisms and mitigation strategies, J. Power Sources 366 (2017) 33–55, http://dx.doi.org/10.1016/j.jpowsour.2017.09.006.

[52] A. Ursúa, E.L. Barrios, J. Pascual, I. San Martín, P. Sanchis, Integration of commercial alkaline water electrolysers with renewable energies: Limitations and improvements, Int. J. Hydrogen Energy 41 (30) (2016) 12852–12861, http://dx.doi.org/10.1016/j.ijhydene.2016.06.071.

[53] M. Schimpe, N. Becker, T. Lahlou, H.C. Hesse, H.-G. Herzog, A. Jossen, Energy efficiency evaluation of grid connection scenarios for stationary battery energy storage systems, Energy Procedia 155 (2018) 77–101, http://dx.doi.org/10.1016/j.egypro.2018.11.065.

[54] G. Notton, V. Lazarov, L. Stoyanov, Optimal sizing of a grid-connected PV system for various PV module technologies and inclinations, inverter efficiency characteristics and locations, Renew. Energy 35 (2) (2010) 541–554, http://dx.doi.org/10.1016/j.renene.2009.07.013.

[55] M. Schimpe, M. Naumann, N. Truong, H.C. Hesse, S. Santhanagopalan, A. Saxon, A. Jossen, Energy efficiency evaluation of a stationary lithium-ion battery container storage system via electro-thermal modeling and detailed component analysis, Appl. Energy 210 (2018) 211–229, http://dx.doi.org/10.1016/j.apenergy.2017.10.129.

[56] M. Förstl, N. Truon, M. Möller, H. Hesse, A. Singer, T. Weyh, The efficiency and profitability of the modular multilevel battery for frequency containment reserve, Atlantis Highlights Eng. 6 (2020) 80–85, http://dx.doi.org/10.2991/ahe.k.210202.012.

[57] A. Zeh, R. Witzmann, Operational strategies for battery storage systems in low-voltage distribution grids to limit the feed-in power of roof-mounted solar power systems, Energy Procedia 46 (2014) 114–123, http://dx.doi.org/10.1016/j.egypro.2014.01.164.

[58] D. Kucevic, C.N. Truong, A. Jossen, H.C. Hesse, Lithium-ion battery storage design for buffering fast charging stations for battery electric vehicles and electric buses, in: D. Schulz (Ed.), NEIS 2018, VDE VERLAG GMBH, Berlin, 2019, pp. 1–6, URL http://ieeexplore.ieee.org/stamp/stamp.jsp?tp=&arnumber=8669466&isnumber=8669446.

[59] N. Collath, S. Englberger, A. Jossen, H. Hesse, Reduction of battery energy storage degradation in peak shaving operation through load forecast dependent energy management, in: D. Schulz (Ed.), NEIS 2020, VDE VERLAG GMBH, 2020, pp. 250–254, URL https://ieeexplore.ieee.org/stamp/stamp.jsp?tp=&arnumber=9273426.

[60] D. Übertragungsnetzbetreiber, Eckpunkte und Freiheitsgrade bei Erbringung von Primaerregelleistung (in German): Leitfaden für Anbieter von Primaerregelleistung, Berlin, Germany, 50Hertz Transmission GmbH and Amprion GmbH and TenneT TSO GmbH and TransnetBW GmbH, https://www.regelleistung.net/ext/download/eckpunktePRL.

[61] D. Übertragungsnetzbetreiber, Anforderungen an die Speicherkapazitaet bei Batterien für die Primaerregelleistung (in German), Berlin, Germany, 50Hertz Transmission GmbH and Amprion GmbH and TenneT TSO GmbH and TransnetBW GmbH, https://www.bves.de/wp-content/uploads/2015/08/2015_08_26_Anforderungen_Speicherkapazitaet_Batterien_PRL.pdf.
[62] A. Zeh, M. Müller, M. Naumann, H. Hesse, A. Jossen, R. Witzmann, Fundamentals of using battery energy storage systems to provide primary control reserves in Germany, Batteries 2 (3) (2016) 29, http://dx.doi.org/10.3390/batteries2030029.
[63] M. Mühlbauer, O. Bohlen, M.A. Danzer, Analysis of power flow control strategies in heterogeneous battery energy storage systems, J. Energy Storage 30 (2020) 101415, http://dx.doi.org/10.1016/j.est.2020.101415.
[64] M. Bauer, System Design and Power Flow of Stationary Energy Storage Systems, (Ph.D. thesis), ETH Zurich, 2019, http://dx.doi.org/10.3929/ETHZ-B-000374736.
[65] C.N. Truong, M. Naumann, R.C. Karl, M. Müller, A. Jossen, H.C. Hesse, Economics of residential photovoltaic battery systems in Germany: The case of teslas powerwall, Batteries 2 (2) (2016) 14, http://dx.doi.org/10.3390/batteries2020014.
[66] A.M. Divakaran, D. Hamilton, K.N. Manjunatha, M. Minakshi, Design, development and thermal analysis of reusable li-ion battery module for future mobile and stationary applications, Energies 13 (6) (2020) 1477, http://dx.doi.org/10.3390/en13061477.
[67] D. Wang, Y. Bao, J. Shi, Online lithium-ion battery internal resistance measurement application in state-of-charge estimation using the extended Kalman filter, Energies 10 (9) (2017) 1284, http://dx.doi.org/10.3390/en10091284.
[68] C.R. Birkl, M.R. Roberts, E. McTurk, P.G. Bruce, D.A. Howey, Degradation diagnostics for lithium ion cells, J. Power Sources 341 (2017) 373–386, http://dx.doi.org/10.1016/j.jpowsour.2016.12.011.
[69] T. Waldmann, M. Wilka, M. Kasper, M. Fleischhammer, M. Wohlfahrt-Mehrens, Temperature dependent ageing mechanisms in lithium-ion batteries – a post-mortem study, J. Power Sources 262 (2014) 129–135, http://dx.doi.org/10.1016/j.jpowsour.2014.03.112.
[70] S. Ma, M. Jiang, P. Tao, C. Song, J. Wu, J. Wang, T. Deng, W. Shang, Temperature effect and thermal impact in lithium-ion batteries: A review, Prog. Nat. Sci. Mater. Int. 28 (6) (2018) 653–666, http://dx.doi.org/10.1016/j.pnsc.2018.11.002.
[71] B. Shabani, M. Biju, Theoretical modelling methods for thermal management of batteries, Energies 8 (9) (2015) 10153–10177, http://dx.doi.org/10.3390/en80910153.
[72] Deutsches Zentrum für Luft- und Raumfahrt (DLR) / German Aerospace Centre, greenius: Green Energy System Analysis, Deutsches Zentrum für Luft- und Raumfahrt (DLR) / German Aerospace Centre, Köln, Germany, 2018, URL https://www.dlr.de/sf/en/desktopdefault.aspx/tabid-11688/20442_read-44865/.
[73] D. Kucevic, B. Tepe, S. Englberger, A. Parlikar, M. Mühlbauer, O. Bohlen, A. Jossen, H. Hesse, Standard battery energy storage system profiles: Analysis of various applications for stationary energy storage systems using a holistic simulation framework, J. Energy Storage 28 (2020) 101077, http://dx.doi.org/10.1016/j.est.2019.101077.
[74] S. Englberger, H. Hesse, N. Hanselmann, A. Jossen, SimSES multi-use: A simulation tool for multiple storage system applications, in: 2019 16th International Conference on the European Energy Market, EEM, 2019, pp. 1–5, http://dx.doi.org/10.1109/EEM.2019.8916568, URL https://ieeexplore.ieee.org/abstract/document/8916568/.
[75] L. Gerlach, T. Bocklisch, Experts versus algorithms? Optimized fuzzy logic energy management of autonomous PV hybrid systems with battery and H2 storage, Energies 14 (6) (2021) 1777, http://dx.doi.org/10.3390/en14061777.
[76] L. Desportes, I. Fijalkow, P. Andry, Deep reinforcement learning for hybrid energy storage systems: Balancing lead and hydrogen storage, Energies 14 (15) (2021) 4706, http://dx.doi.org/10.3390/en14154706.
[77] 50Hertz Transmission GmbH, Archive of mains frequency of ENTSO-e, 2021, URL https://www.50hertz.com/de/Transparenz/Kennzahlen/Regelenergie/ArchivNetzfrequenz.
[78] A. Parlikar, H. Hesse, A. Jossen, Topology and efficiency analysis of utility-scale battery energy storage systems, Atlantis Highlights Eng. 4 (2019) 119–131, http://dx.doi.org/10.2991/ires-19.2019.15.
[79] C. Weng, J. Sun, H. Peng, A unified open-circuit-voltage model of lithium-ion batteries for state-of-charge estimation and state-of-health monitoring, J. Power Sources 258 (2014) 228–237, http://dx.doi.org/10.1016/j.jpowsour.2014.02.026.
[80] Akkuplus.de, Panasonic - UR18650e - 3,7 volt 2150mah Li-Ion - EOL, 2020, URL https://akkuplus.de/Panasonic-UR18650E-37-Volt-2150mAh-Li-Ion-EOL.
[81] N. Damay, C. Forgez, M.-P. Bichat, G. Friedrich, Thermal modeling of large prismatic LiFePO 4 /graphite battery. Coupled thermal and heat generation models for characterization and simulation, J. Power Sources 283 (2015) 37–45, http://dx.doi.org/10.1016/j.jpowsour.2015.02.091.
[82] C. Forgez, D. Vinh Do, G. Friedrich, M. Morcrette, C. Delacourt, Thermal modeling of a cylindrical LiFePO4/graphite lithium-ion battery, J. Power Sources 195 (9) (2010) 2961–2968, http://dx.doi.org/10.1016/j.jpowsour.2009.10.105.
[83] B. Lei, W. Zhao, C. Ziebert, N. Uhlmann, M. Rohde, H. Seifert, Experimental analysis of thermal runaway in 18650 cylindrical li-ion cells using an accelerating rate calorimeter, Batteries 3 (4) (2017) 14, http://dx.doi.org/10.3390/batteries3020014.
[84] M.S. Rad, D.L. Danilov, M. Baghalha, M. Kazemeini, P.H.L. Notten, Thermal modeling of cylindrical LiFePO4 batteries, J. Mod. Phys. 04 (07) (2013) 1–7, http://dx.doi.org/10.4236/jmp.2013.47A2001.
[85] L.H. Saw, K. Somasundaram, Y. Ye, A. Tay, Electro-thermal analysis of lithium iron phosphate battery for electric vehicles, J. Power Sources 249 (2014) 231–238, http://dx.doi.org/10.1016/j.jpowsour.2013.10.052.
[86] A. Lidbeck, K.R. Syed, Experimental Characterization of Li-ion Battery cells for Thermal Management in Heavy Duty Hybrid Applications, (Ph.D. thesis), Department of Energy and Environment - Division of Electric Power Engineering, Chalmers University of Technology, 2017, URL http://publications.lib.chalmers.se/records/fulltext/252994/252994.pdf.
[87] K.K. Parsons, Design and Simulation of Passive Thermal Management System for Lithium-Ion Battery Packs on an Unmanned Ground Vehicle, (Ph.D. thesis), Faculty of California Polytechnic State University, 2012, URL https://digitalcommons.calpoly.edu/cgi/viewcontent.cgi?article=1961&context=theses.
[88] M.W. Tahir, Thermal characterization, multi-scale thermal modeling and experimental validation of lithium-ion batteries for automobile application, (Ph.D. thesis), University of Stuttgart, 2016, http://dx.doi.org/10.18419/OPUS-8775.
[89] A. Greco, Numerical and Analytical Modelling of Battery Thermal Management using Passive Cooling Systems, (Ph.D. thesis), Faculty of Science and Technology, Lancaster University, 2015, URL https://eprints.lancs.ac.uk/id/eprint/78600/1/2016AngeloGrecophd.pdf.
[90] akkuteile.de, Panasonic NCR18650 3,6v 2900mah (flat top) ungeschützt, 2020, URL https://www.akkuteile.de/lithium-ionen-akkus/18650/panasonic/panasonic-ncr18650_100605_1206.
[91] E-One Moli Energy, Molicel IHR18650c, 2020, URL https://www.custompower.com/documents/MOLICELIHR18650CDataSheetV1.0LC.pdf.
[92] A. Awarke, M. Jaeger, O. Oezdemir, S. Pischinger, Thermal analysis of a li-ion battery module under realistic EV operating conditions, Int. J. Energy Res. 37 (6) (2013) 617–630, http://dx.doi.org/10.1002/er.2884.
[93] A. Hales, L.B. Diaz, M.W. Marzook, Y. Zhao, Y. Patel, G. Offer, The cell cooling coefficient: A standard to define heat rejection from lithium-ion batteries, J. Electrochem. Soc. 166 (12) (2019) A2383–A2395, http://dx.doi.org/10.1149/2.0191912jes.
[94] P.E. Roth, Thermal Abuse Performance of MOLI, Panasonic and Sanyo 18650 Li-Ion Cells, Sandia National Laboratories, https://prod-ng.sandia.gov/techlib-noauth/access-control.cgi/2004/046721.pdf.
[95] Akkuplus.de, Sony - US26650FTC1 - 3,2 Volt 3000mah LiFePO4, 2020, URL https://akkuplus.de/Sony-US26650FTC1-32-Volt-3000mAh-LiFePO4.
[96] I. Tsiropoulos, D. Tarvydas., N. Lebedeva, Li-ion batteries for mobility and stationary storage applications - Scenarios for costs and market growth, JRC Science for Policy Report, 2018, http://dx.doi.org/10.2760/87175.
[97] C. Minke, T. Turek, Materials, system designs and modelling approaches in techno-economic assessment of all-vanadium redox flow batteries – A review, J. Power Sources 376 (2018) 66–81, http://dx.doi.org/10.1016/j.jpowsour.2017.11.058.
[98] J. Figgener, P. Stenzel, K.-P. Kairies, J. Linßen, D. Haberschusz, O. Wessels, M. Robinius, D. Stolten, D.U. Sauer, The development of stationary battery storage systems in Germany – status 2020, J. Energy Storage 33 (2021) 101982, http://dx.doi.org/10.1016/j.est.2020.101982.
[99] K. Mongird, V. Viswanathan, J. Alam, C. Vartanian, V. Sprenkle, Energy Storage Grand Challenge Cost and Performance Assessment 2020, U.S. Department of Energy / Pacific Northwest National Laboratory, 2020, DOE/PA-0204, URL https://www.pnnl.gov/sites/default/files/media/file/Final20-20ESGC20Cost20Performance20Report2012-11-2020.pdf.

4 Standard battery energy storage system profiles: Analysis of various applications for stationary energy storage systems using a holistic simulation framework

Main research questions: *Which applications are essential for storage systems for grid integration? And which pattern do reference profiles have for these applications?*

While in the automotive industry standard profiles are an established standard to compare the performance and efficiency of competing vehicles, a similar comparative metric has not been proposed for stationary BESSs. Missing standard profiles leads to difficulties in comparing the evaluation of different applications for storage systems with respect to efficiency, long-term behavior, and profitability. This publication presents a method to create these standard profiles. The results are available as open-data for download and used in the further publications of this thesis.

Storage profiles including storage power and SOE are developed by using input profiles including frequency data for several years, industry load profiles, and residential load profiles. Therefore, the holistic simulation framework SimSES described in Chapter 3 is used. Various degrees of freedom for the design of a BESS as well as the EMS are implemented, and the results are post-processed with a profile analyzer tool in order to identify six key characteristics: FEC, efficiency, depth of cycles, resting periods, number of changes of sign and energy throughput between changes of sign.

The three different applications, which are analyzed in detailed are implemented as follows: The EMS for providing FCR in SimSES is developed according to the German regulatory framework and various degrees of freedom. Two algorithms are implemented for a residential BESS in order to increase the resident's self-consumption. A two-step approach with a linear programming algorithm and SimSES is applied for an industrial peak shaving BESS to minimize the maximum power peak value. This publication can be summarized with three highlights:

- Standard BESSs profiles are determined and published as open-source data for the applications self-consumption increase, industrial peak shaving, and FCR.
- Open-source simulation framework SimSES (cf. Chapter 3) is used to derive storage profiles from input profiles and various system topologies.
- The six characteristics, which differ greatly depending on the BESS application, are essential for evaluating various EMS for storage systems.

In the following chapters of this thesis, the six key characteristics developed in this publication are used for comparison with self-developed EMSs. In particular the numbers for the peak shaving algorithm are used to evaluate the EMSs for BESSs with the aim of avoiding grid reinforcement in Chapter 5 and 6. This allows the novel approaches to be compared with a state-of-the-art peak shaving strategy and the stress on the storage system can be discussed using the six key characteristics.

Author contribution Daniel Kucevic was the principal author tasked with coordinating and writing the paper and developing SimSES. Benedikt Tepe programmed the profile analyzer tool and wrote contents within the data preparation, analysis and results. Both Daniel Kucevic and Benedikt Tepe contributed equally to this work. Stefan Englberger helped with programming and writing the peak shaving algorithm. Anupam Parlikar helped with gathering data and the selection of the characteristics. Markus Mühlbauer was co-responsible for the dynamization of the input data and helped with the selection of the characteristics. Both Oliver Bohlen and Andreas Jossen contributed via fruitful scientific discussions and reviewed the manuscript. Holger Hesse reviewed the manuscript and gave valuable input throughout the manuscript preparation. All authors discussed the data and commented on the results.

Standard battery energy storage system profiles: Analysis of various applications for stationary energy storage systems using a holistic simulation framework

Daniel Kucevic, Benedikt Tepe, Stefan Englberger, Anupam Parlikar, Markus Mühlbauer, Oliver Bohlen, Andreas Jossen, Holger Hesse

Journal of Energy Storage, Volume 28, 2020

Permanent weblink:
https://doi.org/10.1016/j.est.2019.101077

Journal of Energy Storage 28 (2020) 101077

Contents lists available at ScienceDirect

Journal of Energy Storage

journal homepage: www.elsevier.com/locate/est

Standard battery energy storage system profiles: Analysis of various applications for stationary energy storage systems using a holistic simulation framework

Daniel Kucevic[a,1,*], Benedikt Tepe[1,a], Stefan Englberger[a], Anupam Parlikar[a], Markus Mühlbauer[b], Oliver Bohlen[b], Andreas Jossen[a], Holger Hesse[a]

[a] Institute for Electrical Energy Storage Technology, Technical University of Munich (TUM), Arcisstr. 21, Munich 80333, Germany
[b] Department for Electrical Engineering and Information Technology, Munich University of Applied Sciences (HM), Lothstr. 64, Munich 80335, Germany

ARTICLE INFO

Keywords:
Battery energy storage system
Lithium ion
Storage system design
Stationary application
Operation strategy
Standard profiles

ABSTRACT

Lithium-ion batteries are used for both stationary and mobile applications. While in the automotive industry standard profiles are used to compare the performance and efficiency of competing vehicles, a similar comparative metric has not been proposed for stationary battery energy storage systems. Because standard profiles are missing, the comparable evaluation of different applications with respect to efficiency, long-term behavior and profitability is very difficult or not possible at all. This work presents a method to create these standard profiles and the results are available as open data for download. Input profiles including frequency data, industry load profiles and household load profiles are transformed into storage profiles including storage power and state of charge using a holistic simulation framework. Various degrees of freedom for the energy management system as well as for the storage design are implemented and the results are post-processed with a profile analyzer tool in order to identify six key characteristics, these being: full-equivalent cycles, efficiency, depth of cycles, resting periods, number of changes of sign and energy throughput between changes of sign. All applications examined in this paper show unique characteristics which are essential for the design of the storage system. E.g., the numbers for annual full-equivalent cycles vary from 19 to 282 and the efficiency lies between 83% and 93%. With aid of this work in conjunction with the *open data* results, users can test and compare their own cell types, operation strategies and system topologies with those of the paper. Furthermore, the storage power profiles and state of charge data can be used as a reference for lifetime and profitability studies for stationary storage systems.

1. Introduction

A high share of renewable energies poses new challenges to the power grid. Due to decreasing costs of Lithium-Ion Battery (LIB), stationary Battery Energy Storage Systems (BESSs) are discussed as a viable building block in this context. In Germany, the installed storage power with batteries increased from 126 MW in 2015 to over 700 MW in 2018 [1]. Many use cases seem to be of interest for BESSs, as summarized in a report by Eyer and Corey [2]. In particular, the provision of Frequency Containment Reserve (FCR), Peak Shaving (PS) in the industry sector and Self-consumption Increase (SCI) in the private sector are seen as the most prominent applications for BESSs [3,4]. There seems to be consensus, that these applications are the main drivers for the stationary battery storage market. However, if it comes to quantitative analyses of profitability, efficiency and aging of storage systems in a singular use case or even across applications, striking differences in numbers become apparent. In order to make single applications easier to compare, open-source available reference profiles for stationary BESS, similar to the widely used Worldwide Harmonized Light Vehicles Test Procedure (WLTP) for electric vehicles applications, are suggested herein and may help to assess the performance of BESSs.

1.1. Literature review

The state of the art of LIB based stationary BESSs is reviewed e.g. by Diouf et al. [5] and Hesse et al. [3]. Both conclude that LIB based stationary BESSs have advantages in different stationary applications compared to alternative technologies. A more general overview of

* Corresponding author.
E-mail address: daniel.kucevic@tum.de (D. Kucevic).
[1] These authors contributed equally to this work.

https://doi.org/10.1016/j.est.2019.101077
Received 19 August 2019; Received in revised form 8 October 2019; Accepted 13 November 2019
Available online 28 January 2020

List of Abbreviation

AC	Alternating Current
BESS	Battery Energy Storage System
C	Carbon-Graphite
DC	Direct Current
DOC	Depth of Cycle
DOF	Degrees of Freedom
E-rate	Energy Rate
ECM	Equivalent Circuit Model
EMS	Energy Management System
FCR	Frequency Containment Reserve
FEC	Full Equivalent Cycles
IDM	Intra-Day Market
IP	Input Profile
LFP	Lithium-Iron-Phosphate
LIB	Lithium-Ion Battery
NMC	Nickel-Manganese-Cobalt-Oxide
OCV	Open Circuit Voltage
PE	Power Electronics
PER	Power to energy ratio
PS	Peak Shaving
PV	Photovoltaic
SCI	Self-consumption Increase
SimSES	Simulation Tool for Stationary Energy Storage Systems
SP	Storage Profile

stationary storage systems, including other storage technologies, is given by Palizban and Kauhaniemi [6], Resch et al. [4] and Dunn et al. [7]. All authors highlight the high efficiency of LIB-based BESSs, but the numbers, due to different definitions, vary from less than 90% up to 94%. A systematic review of Energy Management System (EMS) for BESS was published by Weitzel and Glock [8]. The placement in distribution grids of stationary BESS is summarized in the review of Das et al. [9]. An example for optimized placement using simultaneous perturbation stochastic approximation method was published by Carpinelli et al. [10].

Regarding the provision of FCR with BESS, a number of papers have been published in the past. Specifically for several techno-economic evaluations different approaches exist [11–15]. Münderlein et al. [16] analyzed a large scale 5 MW and 5 MWh BESS in the FCR market. Apart from the fact that the focus of the individual authors is different, it is noticeable that many different numbers exist. For example the authors in [16] determined 147 Full Equivalent Cycles (FEC) per year, while the numbers of FECs in [13] varies from 207 to 254 per year.

In the case of SCI, many publications with various objectives exist. The publications can be split into economic analyses [17–20] and sizing of the system [21–23]. All authors conclude that a BESS for SCI can be economically viable, if the Photovoltaic (PV) unit and the storage capacity are dimensioned correctly. However, a wide variety of input data and parameters for the storage system (e.g. the efficiency for the LIB varies from 95% in [21] to 98% in [20]) are used in the publications, which makes comparability difficult.

For industry PS BESSs with LIB, fewer publications are available, in contrast to SCI BESSs. Martins et al. [24] present an approach for an

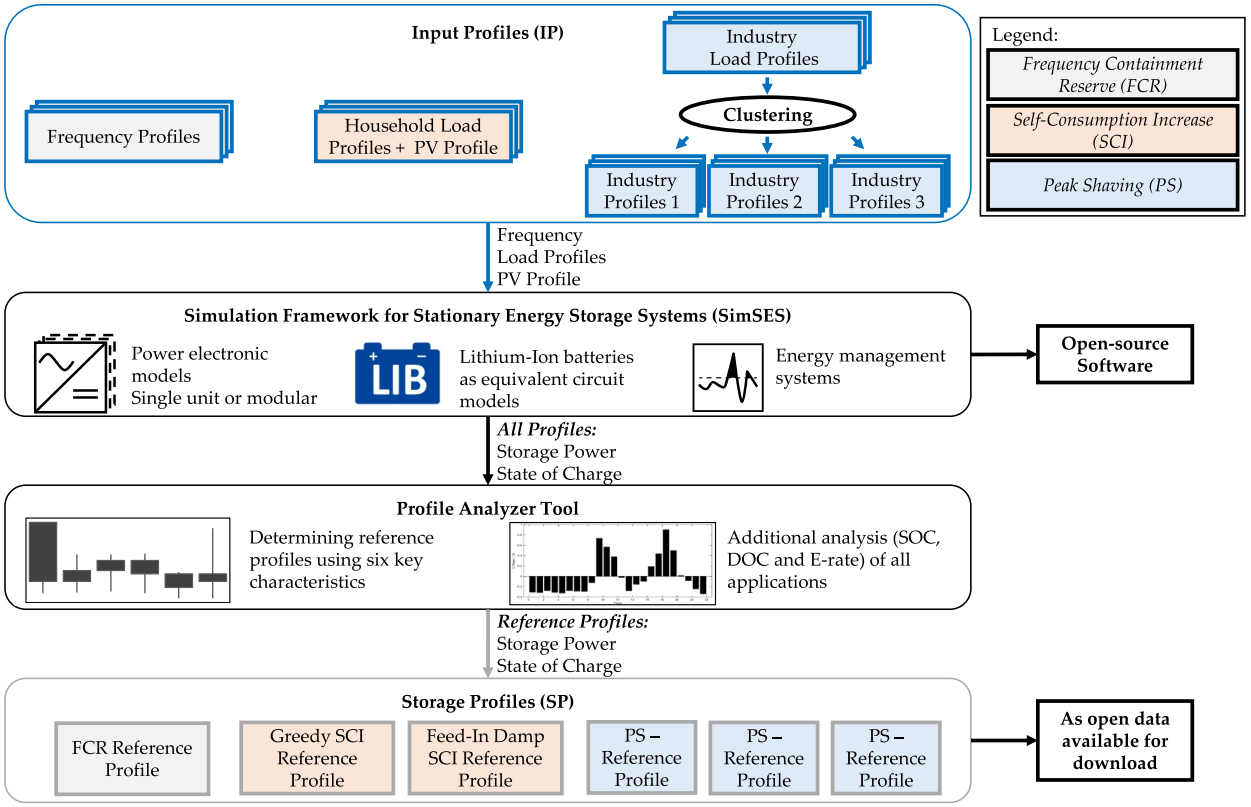

Fig. 1. Graphical overview of this work. The input profiles including frequency data, industry load profiles and household load profiles are transformed into storage profiles including storage power and state of charge using the simulation framework SimSES. The selection of suitable reference profiles is done with a profile analyzer tool developed as part of this publication.

Table 1
Storage applications, the data basis, the required data and the data resulution used in this work.

Application:	FCR	SCI	PS
Database	5 years of Frequency Data	74 yearly load profiles & one PV generation profile	36 yearly industry load profiles
Data resolution (raw data)	1 s	1 s	15 min
Data resolution (simulation)	1 s	1 s	1 s

optimal component sizing and the authors also performed an economic analysis. They showed in a case study that the number of FEC varies between 1 and 51 per year. Dagdougui et al. [25] show an EMS for a real world example. They optimized the size of a PS BESS for a university campus. It has been found that in this example the economically optimal storage capacity is 436 kWh. Telaretti and Dusonchet [26] concucted an economic analysis and compared the use of LIB in PS applications with three other electrochemical technologies: Lead-acid, flow based batteries and sodium-sulphur.

Although each author makes different assumptions and sets the focus differently, the results, some of which are very diverse, indicate that *open data* available standards for stationary BESS are desired.

1.2. Scope of this work

This work presents a method to create standard Storage Profile (SP) including the storage power and the SOC from Input Profile (IP) including frequency data, industry load profiles and household load profiles. The IPs are transformed into SPs by using the holistic simulation framework Simulation Tool for Stationary Energy Storage Systems (SimSES). Various Degrees of Freedom (DOF) for the EMS and the system configuration are implemented in SimSES and the results are post-processed with a newly developed profile analyzer tool in order to identify some key characteristics, such as efficiency, FEC or Depth of Cycle (DOC).

Fig. 1 shows the scope of this paper in detail. The simulation framework, as well as the results, including SPs and the SOCs, are made available as open-source. The results are available in one second resolution and may facilitate the comparison of the same applications among each other in the future. As an example, own system configurations or developed EMS can be compared with the numbers of this paper. Furthermore, the open-source available data can be used as a reference for lifetime and profitability studies for LIBs.

1.3. Paper structure

Section 2 gives an overview of the origin of the IPs and the preprocessing of the raw data sets. Section 3 describes the simulation tool SimSES with various DOFs and the developed EMS. In the remaining part of the paper, the SPs are analyzed (Section 4) and the choice of the reference profiles (Section 5) is described. Section 6 gives an outlook to future work and concludes this paper.

2. Profile data and preparation

In this chapter, the database of household load profiles, industry load profiles and frequency data is explained (Section 2.1). Herein, the data sources and time frames are described. The processing of this data is covered in Section 2.2. Subsequently, the normalization of the profiles is illustrated, which is required for comparison of data (Section 2.3). Finally, Section 2.4 covers the clustering of profiles.

2.1. Data basis

The creation of reference load and storage profiles demands a database that is sufficiently detailed to represent the specific type of profile. As described in Section 1, this paper considers three different applications of storage systems: SCI in the private sector, PS in the industry sector and the provision of FCR. These three applications require specific data with specific resolution which is displayed in Table 1.

Firstly, high resolution frequency data is required to investigate the storage application of FCR [27]. This one second resolution data for the years 2013 until 2017, that can be measured at every socket within the synchronous grid of Continental Europe, is provided by the transmission system operator *50hertz Transmission GmbH* [27]. Exemplary data of the year 2017 is shown in Fig. A.12.

The analysis of the performance of SCI requires household load profiles and photovoltaic generation profiles. Therefore, 74 load profiles published by the *HTW Berlin* are used [28]. Moreover, one photovoltaic profile measured at *TU Munich* which was already published in several previous papers [17,19,29] was used. These profiles also have a resolution of one second. To perform PS with a storage system, industry load profiles are needed. Therefore, 36 annual industry profiles with a resolution of 15 min are gathered within the *EffSkalBatt* project[2]Frequency data, household load profiles and industry load profiles work as IPs for SimSES (see Fig. 1) which will be explained in Section 3.

2.2. Data processing

The gathered data of frequency, load and photovoltaic profiles is processed before using them within the simulations. The frequency data for performing FCR with a BESS contains some doubtful values ($<$ 49 Hz or $>$ 51 Hz). All such values were replaced by linear interpolation of frequencies before and after. As the raw industry load profiles used for PS have a resolution of 15 min, this data is transformed into profiles with a resolution of one second. For this reason, the following procedure is applied to create second-based profiles: First, the 15-min points are interpolated linearly to create points based on minutes. Then random numbers are build, which replace each interpolated value. Each random number lies within the coefficient of variation of 0.25 of the normal distribution with a mean of the interpolated value. Afterwards, the minute-based values are interpolated linearly again to reach a second-based load profile.

This procedure only estimates the high-resolution load profile. Possible load peaks that just appear for a few seconds are not taken into account. Those short peaks are crucial when regarding battery lifetime and safety [30,31]. Within the application of PS the presented procedure to reach second-based load profiles is sufficient, as the storage system only has to provide the required energy when peaks appear as long as the storage's power is sufficient. The required energy can also be extracted from the 15-min load profile. Moreover, the yearly industry load profiles are chopped to match a Monday to Sunday pattern.

2.3. Normalization

After the aforementioned data pre-processing, the industry profiles are normalized, which is necessary for a comparison of profiles. The industry profiles are normalized to their maximum value within the year. Thus, the maximal value of each profile is one and the minimal

[2] EffSkalBatt Project: Efficient scalable system technology for stationary storage systems. Research project funded by the Federal Ministry for Economic Affairs and Energy (BMWi) with grant number 03ET6148 (http://www.ees.ei.tum.de/en/research/effskalbatt/).

value is zero. This normalization method on each highest peak might differentiate profiles that are similar except for their highest peaks. If only those load profiles were compared, this method would not be appropriate. However, regarding the application of peak shaving, which concentrates on the highest peaks, those profiles are very different. With this method of normalization users can compare their own profiles with the published ones and add their profiles to the simulation. The raw data of household load profiles is already normalized to each maximal value.

2.4. Clustering

Prior to the creation of reference profiles from the pre-processed data, a clustering of the different groups of profiles is considered. This is due to the fact that, for example, the industry profiles do not all have homogeneous curves. Thus, similar profiles are clustered into groups. The clustering is performed using the simulation platform MATLAB® and the clustering algorithm k-means with euclidean distances as measure of dissimilarity [32]. The k-means algorithm was chosen, as it appears to be the most prominent one when comparing electric load profiles [33–35]. Other possible clustering methods would have been the hierarchical clustering or self-organizing maps, as published in [36] and [37].

When comparing the household load profiles to each other, they appear very homogeneous. The average value of each yearly household load varies between 0.6% and 4.4% of its yearly maximum value. In addition, the mean absolute deviations of the profiles' offsets lie between 0.8 and 3.6 percentage points. In contrast to that, the industry load profiles show bigger variations. The mean load of each profile lies between 30% and 75% of the profile's yearly maximum. Thus, the industry profiles' offsets are substantially higher than the households' ones due to their increased base load. The industry loads' mean absolute deviations vary between 0.8 and 23 percentage points.

As a consequence, the industry load profiles are clustered into three different groups while the household load profiles remain in one group. The number of three is chosen because three is the best compromise between differentiation and effort.

Cluster 1 and 3 have an average load of 70% to 80% during the day and a base load of 20 to 30% at night but are shifted by a few hours. During the weekend, Cluster 1 exhibits the typical nightly base load while the load of Cluster 3 only sees the base load on Saturdays. In comparison, Cluster 2 does not have a typical day vs. night load profile. During working days the load varies between 50% and 100% and on weekends between 35% and 70%.

3. Simulation framework for stationary energy storage systems

To generate battery profiles and SPs from the IPs in Section 2 the software SimSES was used. SimSES is a modular object-oriented simulation tool, which was initiated by Naumann and Truong [38] and is now being further developed by the authors. The software allows the flexible usage of components, such as the power electronic or battery cell, of a BESS. The software code is programmed in MATLAB®, but will be converted to Python in the future and made available completely open-source. The current open-source version, including the simulation scripts for this publication and a link to the code of SimSES can be found online[3]. In this chapter the structure of SimSES (Section 3.1), the developed operation strategies (Sections 3.2–3.4) as well as the components used (Section 3.5) will be described.

3.1. Simulation structure

In SimSES the battery is implemented as a single-cell Equivalent Circuit Model (ECM). The terminal voltage U_T of each cell is calculated from the Open Circuit Voltage (OCV) and the voltage drop (overvoltage) ΔU across the series resistance R_i, due to the current I (Eq. 1). The OCV is a function of the SOC. The series resistance R_i is dependent on the current direction sign sgn(I), the temperature T and the SOC.

$$U_T = U_{OCV} - \Delta U = U_{OCV} - I \cdot R_i(SOC, \mathrm{sgn}(I), T) \quad (1)$$

The Power Electronics (PE) efficiency is modeled as a function which relies on the absolute output power $|P_{Storage}|$, the rated power P_{Rated} and the current direction sgn(I) (Eq. 2). Fixed PE efficiency values or other functions, for example based on own investigations, can be modeled in SimSES as well. Beside the Direct Current (DC)/Alternating Current (AC) link, the PE can also include a transformer model.

$$\eta_{PE} = f(|P_{Storage}|, P_{Rated}, \mathrm{sgn}(I)) \quad (2)$$

The core of SimSES is the EMS, which allows to simulate various tasks for a stationary BESS. As described in Section 1, the focus of this work is on the single-use applications FCR, SCI and PS.

3.2. Frequency containment reserve

The EMS for providing FCR in SimSES was developed according to the German regulatory framework [39,40]. The requested charging and discharging power $P_{Storage,set}$ is proportional to the frequency deviation Δf and is dependent on the prequalified power P_{PQ}, which has a minimum of 1 MW (Eq. 3). Below 49.8 Hz or above 50.2 Hz $P_{Storage,set}$ is set to $\pm P_{PQ}$.

$$\begin{aligned} P_{Storage,set}(t) &= P_{PQ} \cdot \frac{\Delta f(t)}{0.2\,Hz} && \text{for} \quad |\Delta f| \le 0.2\,\mathrm{Hz} \\ P_{Storage,set}(t) &= P_{PQ} && \text{for} \quad \Delta f > +0.2\,\mathrm{Hz} \\ P_{Storage,set}(t) &= -P_{PQ} && \text{for} \quad \Delta f < -0.2\,\mathrm{Hz} \end{aligned} \quad (3)$$

If the SOC falls below a predefined lower limit (SOC_{low}) or it exceeds an upper limit (SOC_{high}) the BESS in these simulations charges or discharges by trading energy on the electricity market, in particular the Intra-Day Market (IDM) [14]. Due to the current legal interpretation (May 9, 2019) [41], a BESS in the FCR market has to ensure that at all times the full prequalified power P_{PQ} can be provided for 15 min as long as the frequency f is in normal progression. The normal progression means that the frequency deviation Δf is continuously less than 50 mHz or none of the following criteria is met:

- $|\Delta f| > 200$ mHz
- $|\Delta f| > 100$ mHz for more than 5 min
- $|\Delta f| > 50$ mHz for more than 15 min

The SOC limits also depend on the prequalified power P_{PQ} and the storage capacity E_{BESS}, and are calculated according to Eq. 4.

$$SOC_{high} = \frac{E_{BESS} - 0.25\,\mathrm{h} \cdot P_{PQ}}{E_{BESS}} \quad SOC_{low} = \frac{0.25\,\mathrm{h} \cdot P_{PQ}}{E_{BESS}} \quad (4)$$

To reach these limits as infrequently as possible, the efficiency must be taken into account and therefore the SOC setpoint is above 50% (Eq. 5). The mean efficiency η_{mean} is calculated at the beginning of the simulations and is dependent on the efficiency of the battery and PE.

$$SOC_{Offset} = 0.5 \cdot \frac{(1 - \eta_{mean}^2)}{(1 + \eta_{mean}^2)} \quad SOC_{Set} = 50\% + SOC_{Offset} \quad (5)$$

Additionally to the SOC setpoint shift, the regulatory framework in Germany allows three different DOFs:

- *Frequency dead band:* In the frequency range between 49.99 Hz and 50.01 Hz, the output power of the BESS can be set to 0 MW and must not follow the frequency derivation according to Eq. 3.
- *Overfulfillment:* It is allowed to overfulfill the requested power

[3] http://www.ees.ei.tum.de/simses/

(Eq. 3) by 20 %.

- *Slope*: The requested FCR power (Eq. 3) must be provided within 30 s or earlier. Therefore, the slope of the provided FCR power can be adjusted within the time interval of 30 s allowing to control the charging or discharging rate.

In SimSES all DOF are only used, if the requested power either brings the SOC closer to optimum again or at least not further away. All degrees of freedom as well as the SOC limits, depending on the prequalified power P_{PQ}, are shown schematically in Fig. 2.

3.3. Residential photovoltaic battery storage system

In SimSES two different operation strategies for the SCI of BESS are implemented: *Greedy* and an extension of *feed-in damping* based on Zeh and Witzmann [29].

Greedy

The EMS for the greedy algorithm works with a simple comparison between the generation of the PV power system P_{PV} and the consumption by the household P_{load} at each timestep. Whenever a solar surplus occurs ($P_{PV} > P_{load}$), the BESS is charged and vice versa (Eq. 6). This conventional strategy is shown in Fig. 3 (top). These summer days show that the BESS is fully charged at around 9AM, which causes a rapid rise of the power fed into the grid. Another disadvantage of this strategy is the high charging power, which may lead to a faster decrease of the LIB capacity due to an increase of lithium plating as described in [30].

$$P_{Storage} = P_{PV} - P_{load} \tag{6}$$

Feed-in damping

In order to reduce the maximum power fed into the grid, a nearly constant BESS charging power $P_{Storage,\,Ch}$ during the whole daytime is calculated by the EMS. Reducing the maximum feed-in power allows for a higher self-consumption rate, if the maximum feed-in power is limited by the distribution grid operator as described in [19]. If a surplus ($P_{PV} > P_{load}$) occurs, the charging power $P_{Storage,Ch}$ is calculated by dividing the remaining battery capacity $E_{BESS,re}$ by the predicted remaining time t_{re}, until the load is higher than the PV generation, and the mean efficiency η_{mean} of the BESS (Eq. 7).

In this work, a perfect foresight for the duration of PV generation is assumed. If there is a higher consumption by the household than generation by the PV power system, the BESS is discharged. Fig. 3 (bottom) displays this operation strategy. In contrast to the *greedy* algorithm, the charging power is constant during the whole first day. The second day shows a more cloudy day. The remaining time t_{re} at this day is smaller than in day 1, so according to Eq. 7 the charging power $P_{Storage,ch}$ is higher. In addition, the second day also shows that after the PV generation surpasses load again ($P_{PV} - P_{load} > 0$), the remaining time t_{re} is recalculated. In this case, the storage can be charged with the full power, due to the short remaining time t_{re}.

$$P_{Storage,ch} = \frac{E_{BESS,re}}{t_{re} \cdot \eta_{mean}} \quad \text{for} \quad P_{PV} > P_{load} \tag{7}$$

3.4. Peak shaving storage system

Motivated by a tariff system consisting of an energy and a power related component, the storage application PS has the goal to minimize the maximum power peak value within a defined accounting period. Particularly large electricity consumers (annual demand > 100 MWh (in Germany)) can reduce the peak power provided by the power grid, which directly results in reduced operating expenses in form of reduced grid charges [42].

In order to reduce the power at the point of common coupling, the excess demand has to be covered by another power providing unit, such as a BESS. The BESS is used to decouple the supply and demand over a specified time. To maximize the benefit of the application, it is important that the dimensioning of the storage system is the best possible match for the power demand curve. Similar to other publications [43–45], a two-step approach of a linear programming algorithm and SimSES is applied.

First, a pre-processing linear optimization algorithm is used to minimize the power value for the peak shaving threshold $PS^{threshold}$, while it complies with the necessary constraints, such as meeting the power demand, and satisfying the energy and power specifications of the BESS. Depending on the shape of the load profile, the resulting value of the power threshold varies. Secondly, the resulting peak shaving threshold is used as an input parameter for the operation strategy within SimSES. This operation strategy works as follows: as soon as the power at the point of common coupling (from the grid) is above the specified threshold, the additionally required power is provided by the BESS, as illustrated in Fig. 4. In addition, the BESS will

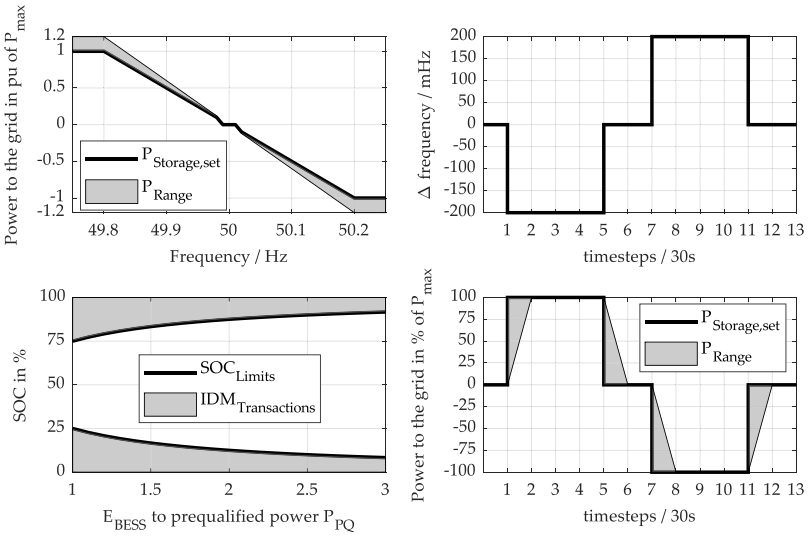

Fig. 2. Degrees of freedom and the SOC limits, depending on the prequalified power P_{PQ}. The top left subfigure shows the frequency dead band and the possible overfulfillment. The two subplots on the right show the slope and the bottom left subfigure shows the SOC limits.

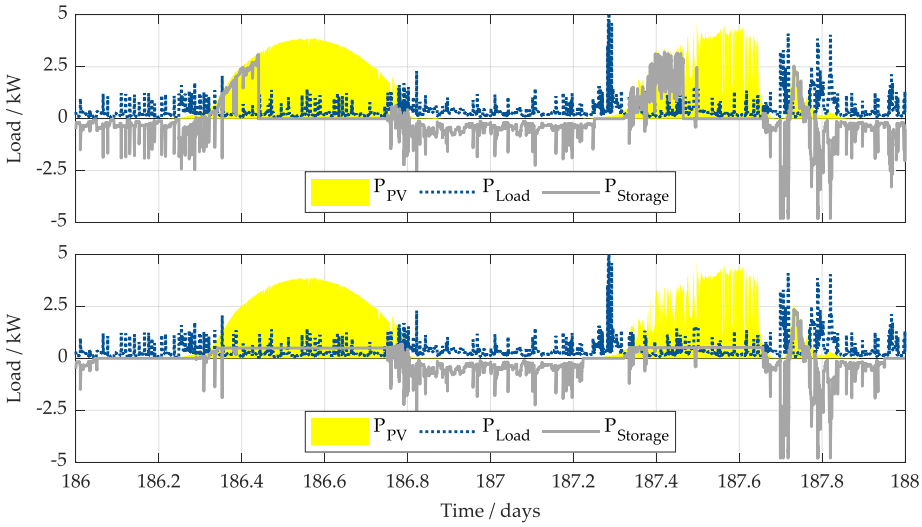

Fig. 3. Operation Strategies (top = *greedy*, bottom = *feed-in damping*) for the Residential Photovoltaic Battery Storage System. The shaded yellow area shows the generation of the PV power system, the blue line shows the load of the household and the gray line shows the storage power (positve = charging). (For interpretation of the references to color in this figure legend, the reader is referred to the web version of this article.)

recharge if the power value is below the previously determined optimal peak shaving threshold. This ensures that the charging of the storage system does not cause the exceedance of the threshold.

Through a close coordination of the two simulation tools in the chosen two-stage approach, both a near optimal PS threshold is found and simultaneously, the detailed technical specifications of the BESS are simulated via SimSES.

3.5. Simulation parameters

The battery cell used in all simulations was a LIB with a Lithium-Iron-Phosphate (LFP) cathode and a Carbon-Graphite(C) anode [46]. It is worth to mention, that other LIB types are also implemented in the simulation tool but the LFP:C cell is a promising battery chemistry for stationary applications, because of its characteristics such as high thermal stability, long cycle as well as calendar lifetime [3,47,48]. The parameterization of the ECM for the simulated LFP:C cell was carried out by Naumann [49].

To analyze the effects of cell selection, another cell with a Nickel-Manganese-Cobalt-Oxide (NMC) cathode and a C anode [50] was also simulated in the FCR application. The characterization of this cell is based on the work of Schuster [51]. The self-discharge and the temperature dependency of the cell is neglected in this work. Table 2 summarizes the parameters of these battery cells.

The PE is implemented as a function, which shows a high efficiency above 10% of the rated power P_{Rated} (Eq. 8). Exemplary values used for a high efficiency PE are k = 0.0345; p_0 = 0.0072, according to Notton et al. [52]. Here η_{PE} is independent of the direction of the power flow and no hysteresis is implemented. The maximum efficiency is observed at 0.46 · P_{Rated} with an efficiency η_{PE} = 96.9%.

Table 2
Parameters of the simulated Lithium-ion cells. Celltype 1 is a Lithium-ion battery with a Lithium-Iron-Phosphate (LFP) cathode and a Carbon-Graphite (C) anode. Celltype 2 is a Lithium-ion battery with a Nickel-Manganese-Cobalt (NMC) and a Carbon-Graphite (C) anode.

Parameter	Unit	Cell 1 [46]	Cell 2 [50]
Cell Identification	-	US26650FTC1	IHR18650A
Manufacturer	-	Murata	E-ONE Moli Energy Corp.
Chemistry	-	LFP:C	NMC:C
Capacity	mAh	2850	1950
Max. Charge Current	A	2.85	2
Max. Discharge Current	A	20	4
Nominal Voltage	V	3.2	3.7
Voltage Range	V	2 - 3.6	3 - 4.2

$$\eta_{PE} = \frac{\frac{|P_{Storage}|}{P_{Rated}}}{\frac{|P_{Storage}|}{P_{Rated}} + p_0 + k \cdot \left(\frac{|P_{Storage}|}{P_{Rated}}\right)^2} \quad (8)$$

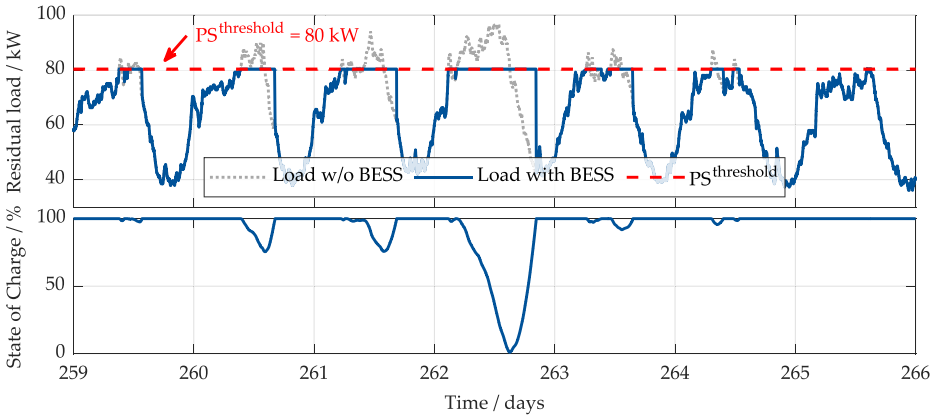

Fig. 4. Exemplary week of an industry load profile and its optimized PS threshold $PS^{threshold}$ following the PS operating strategy. The power above the threshold is provided by a stationary BESS. The solid blue line shows the industry load profile with the PS BESS. The associated SOC is illustrated at the subplot at the bottom. (For interpretation of the references to color in this figure legend, the reader is referred to the web version of this article.)

Frequency Containment Reserve

As already shown by others [3,13,14], a BESS in the FCR market is mostly in part-load operation. In order to achieve a high part-load efficiency, we minimized the inverter losses by modularization of the PE-unit into three identical smaller units based on the work of Schimpe et al. [53]. At 80% power of the rated power of PE unit 1, PE unit 2 starts to work. At 80% power of the rated power of PE unit 1 and PE unit 2, PE unit 3 starts to work. There is no hysteresis included in the simulations, which means that the switch-off values are equal to the switch-on values. According to the modeled PE efficiency, the average efficiency of this PE combination is 96%. This PE combination, together with the simulated LIB (η_{LIB} = 96%), results in an SOC shift, according to Eq. 5, of 54%.

In this work the BESS capacity E_{BESS} is set to 1.6 MWh with a maximum power of 1.6 MW. The prequalified power P_{PQ} is 1.12 MW, which results in a Power to Energy Ratio (PER) of 0.7. Thus, the available IDM power is 30% of the total BESS power. The losses of a transformer model for a potential integration to higher grid voltage levels, which would be necessary having a 1.6 MW / 1.6 MWh storage, are neglected.

Residential Photovoltaic Battery Energy Storage System

To ensure comparability, the simulations are carried out with a fixed annual household load $E_{load,a}$ of 5,000 kWh, which rounded corresponds to the mean of the IP. According to the work of Weniger et al. [21] and Hoppmann et al. [54], the PV system and the BESS can be operated economically in the ratio 1:1:1. An annual household load $E_{load,a}$ of 5,000 kWh leads to a PV peak power of 5 kWp and a BESS capacity E_{BESS} of 5 kWh.

Peak Shaving Storage System

For the PS application, 36 anonymized annual load profiles from commercial electricity consumers are utilized. In order to generate comprehensive standardized profiles, all normalized load curves are scaled to a peak power of 100 kW (see Section 2.3). The BESS is characterized by a nominal energy content of 100 kWh. We assume that 100% of the nominal storage energy and a rated power of 40 kW for the system's PE unit (consisting of a single inverter) can be used to operate the application.

Table 3 summarizes the parameter set for each simulation in SimSES. Other components, such as

- a transformer model for a potential integration to higher grid voltage levels,
- a cell-to-cell connection resistance,
- a battery management system,
- a thermal model for each cell as well as a thermal model for the whole storage system,
- an aging model of the battery cell as well as all other subcomponets,

were neglected in this paper, but can be modeled in principle in SimSES.

4. Storage profile analyzer tool

One goal of this work is finding reference SPs for the different storage applications. Therefore, groups of SPs were created using the software SimSES. In this chapter, a storage profile analyzer tool is presented which aims to extract the reference SP for each of the groups. The idea and the reasons for the analyzer tool are described in Section 4.1. Afterwards, the different characteristics are explained in Section 4.2. Finally, the determination of reference profiles from the characteristics is described in Section 4.3. Moreover, Appendix B provides some further analysis of the SPs including the distribution of the energy rate (E-rate). The E-rate at each timestep i is defined according to Eq. 9.

$$E_{rate,i} = \frac{P_{Storage,i}}{E_{BESS}} \quad (9)$$

4.1. Reasons for the storage profile analyzer tool

The extraction of a reference SP can be done in different kind of ways. Taking the mean SP by calculating the mean of all the SPs for the different applications is one option. This would lead to a smoothing of the profiles. Distinctive peaks would be neglected and the profiles would not be representative anymore. A more viable approach is the selection of one SP as reference SP for each application. Here, a median profile has to be found which represents the group of profiles. This selection is done using the storage profile analyzer tool. The tool takes the load of the storage and SOC data as input variables and outputs the characteristics described in the following subsection.

4.2. Extracted characteristics from profiles

To better analyze and compare the storage load profiles, six characteristics were defined which are distinctive for the profiles of the different applications. Those six characteristics aim to represent the differences within the storage applications.

1. Number of full equivalent cycles (FEC)

The total number of cycles FEC_{year} within the year is calculated by dividing the positive energy throughput E^{pos}_{year} by the storage capacity E_{BESS} (Eq. 10). The FEC_{year} varies between the applications and affects the aging of the battery [30].

$$FEC_{year} = \frac{E^{pos}_{year}}{E_{BESS}} \quad (10)$$

2. Efficiency (η_{BEES})

The efficiency of the analyzed storage η_{BEES} is calculated by counting the yearly energy that is extracted from the storage system E^{neg}_{year} divided by the energy that is stored in the storage system E^{pos}_{year}. The SOC at the beginning of the year and at the end of the year is taken into account as well (Eq. 11). This characteristic displays the losses in the storage system while operating in the specific application. For the calculation of the efficiency the surrounding temperature and the thermal management are not taken into account.

$$\eta_{BEES} = \frac{|E^{neg}_{year}|}{E^{pos}_{year} - [SOC_{end} - SOC_{start}] \cdot E_{BESS}} \quad (11)$$

3. Cycle depth in discharge direction (DOC_{dis})

The average DOC in discharge direction is calculated by using the SOC data of the current profile. This characteristic describes how deep the battery is discharged before recharging it. A higher DOC may lead to a higher cyclic aging of the battery [55]. To enable a comparison between the applications (different capacities) the DOC is measured in percentage of the total battery capacity. In SimSES a half-cycle detector

Table 3
Summary of the parameters for the simulation of the three applications with SimSES.

Application:	FCR	SCI	PS
Battery	LFP:CNMC:C	LFP:C	LFP:C
Storage Capacity	1.6 MWh	5 kWh	100 kWh
Max. Power	1.6 MW	5 kW	40 kW
PE mode	modular single unit	single unit	single unit
PV Power	-	5 kWp	-
Operation Strategy	15 min criteria	greedy feed-in damp	simple
PER	0.7	-	-
IDM Power	0.48 MW	-	-
PS-Limit	-	-	variable 62 - 92%

is implemented. The beginning of the half-cycle is a change from charging respectively resting to discharging. Analogously the end is at every change from discharging to charging or if the BESS reaches an SOC of 0%. Then the DOC is calculated by subtracting the SOC at the beginning and the SOC at the end of the half-cycle (see Eq. 12). Taking only the change from discharging to charging leads to a dependency of the DOC on the resolution. Many small changes of load might outweigh larger trends.

$$DOC_{dis} = SOC_{cycle,start} - SOC_{cycle,end} \quad (12)$$

4. Number of changes of sign ($n_{swapsign}$)

Depending on the storage application, the SP might change from charging to discharging and vice versa very often or just a few times per day. Those changes of signs activate the power electronics. When analyzing experimental SPs the user of the storage profile analyzer tool would have to define a threshold value to prevent faults of noise when the SP is close to zero. As the simulated SPs do not show the noise, a threshold value is not necessary.

5. Length of resting periods (t_{rest})

As the BESS is not used continuously over time, the length of resting periods represent another characteristic. During those times, the BESS is neither charged nor discharged. Here, the average value of resting period length in minutes is calculated. Depending on the application the length of those resting periods may vary significantly. This characteristic is chosen because auxiliary users can be turned off and other applications can be performed during long resting periods.

6. Energy between changes of sign ($E_{swapsign}$)

Another chosen characteristic is the energy that is charged or discharged between changes of signs, respectively. The amount of the energy is normalized to the battery's capacity and thus comparable between the different applications with different capacities. Here charged and discharged energy are calculated separately.

4.3. Determination of reference profiles

The storage profile analyzer tool extracts the different characteristics from each of the profiles of the specific group of SPs. For each application the characteristics can then be displayed in boxplots to visualize the spread and show the median values.

To determine each reference profile the percentage error δ of each profile's characteristic to the median characteristic is calculated (Eq. 13). This is done by subtracting the median of the characteristic $\tilde{K}_j$ from the profile's characteristic K_j, dividing the difference by the median of the characteristic and multiply the result with 100. Here, i is the number of the profile and j the number of the characteristic.

Afterwards, the root mean square percentage error (RMSPE) is identified for each profile (Eq. 14). This is done by taking the sum of the absolute percentage errors, dividing it by six (six characteristics), squaring it and extracting the root. This way all characteristics are weighted equally.

$$\delta_{i,j} = \frac{K_{i,j} - \tilde{K}_j}{\tilde{K}_j} \cdot 100 \quad (13)$$

$$RMSPE_i = \sqrt{\left(\frac{\sum_{j=1}^{6} |\delta_{i,j}|}{6}\right)^2} \quad (14)$$

The reference profile is then chosen as the profile which has the minimum root mean squared percentage error. Thus, this profile represents the group of profiles, while maintaining its variations and peculiarities.

5. Results and discussion

The storage profile analyzer tool outputs characteristics and reference SPs which will be compared and discussed in this section. First, the characteristics of the different applications (FCR, SCI, PS) are displayed in Section 5.1. Here, a comparison is done within each

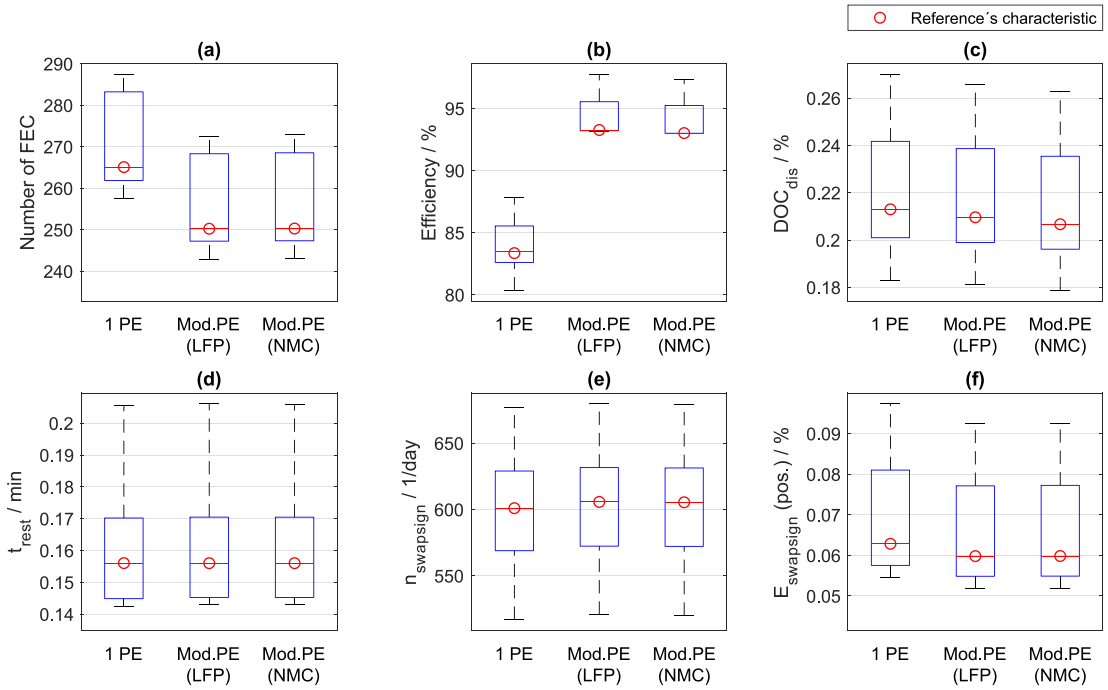

Fig. 5. Characteristics of a BESS providing FCR. The left box in each plot shows a BESS with one PE unit and a LFP:C cell. The center one in each plot shows a BESS with three modular PE units and a LFP:C cell and the right box in each plot shows a BESS with three modular PE units and a NMC:C cell.

application between power electronics and battery technology (FCR), operation strategies (SCI) and the three PS clusters. Afterwards, the characteristics of the reference SPs for different applications are compared to each other and thus differences in usage and load are explained (Section 5.2). Finally, exemplary days and weeks of the reference SP are shown and discussed (Section 5.3).

5.1. Characteristics of storage profiles of different applications

As described in Section 3, the simulated storage applications are FCR, SCI and PS. For each group of SPs performing one application, the different characteristics can be displayed in boxplots. These boxplots show the spread of the characteristics of a storage system performing the specific application. Each boxplot is created by using the characteristics of all the SPs. That means that for FCR five SPs, for SCI 74 SPs and for PS 36 SPs were used. Each profile contributes to each boxplot with one value. Those are the yearly number of FEC, the efficiency (η_{EES}) over the year, the average DOC in discharge direction, the average length of resting periods (t_{rest}), the average changes of sign per day ($n_{swapsign}$) and the average energy between changes of signs ($E_{swapsign}$). Each boxplot contains a red line which represents the median value. Moreover, the blue boxes display the 25th and the 75th percentiles, while the black whiskers correspond to a maximal absolute value of 2.7 times the standard deviation. The red crosses which are displayed above and underneath the boxplots show outlier outside of the box and whiskers. In addition, the red dot in each boxplot shows the value of the reference profile's characteristic (see Section 4.3). The average distance between the median value and the reference value is 2 %. The distributions of SOC, DOC in discharge direction and E-rate for all profiles and for the reference profiles of each application can be found in the appendix (Figs. B.21–B.28).

Fig. 5 displays the SPs characteristics of a BESS providing FCR. The PE units were varied as one differentiation while using the same battery technology (LFP:C). First of all, one PE unit was used (each left boxplot). Then a modular PE device was applied (each center boxplot). In addition to that, as a third boxplot, the LIB technology was varied as described in Section 3.5. Here also a modular PE device was used with a NMC:C LIB.

The first characteristic (Fig. 5 (a)) is the number of FEC within the year. Using only one PE unit leads to an increased number of FEC within the year compared to modular PE units. The high number of yearly cycles (> 240 FEC in all simulations), in combination with a small DOC (Fig. 5 (c)) requires a BESS, which has a high cycle stability in the middle SOC range (see also Appendix B.21–B.23).

The efficiency (Fig. 5 (b)) can be significantly increased when using modular PE units or at least having a PE with a high part-load efficiency. Furthermore, there are almost no long resting periods (Fig. 5 (d)) and the number of sign changes (Fig. 5 (e)) is higher compared to the other applications under test. Therefore, the PE must have a high control speed to meet these requirements. The positive energy of changes of sign (Fig. 5 (f)) is a little smaller when having modular PE compared to only one device. The variation of the cell shows hardly any influence - underlining, that choosing a suitable PE design is key for improving the system's efficiency. It is worth to mention here, that battery aging was not modeled.

Fig. 6 displays the SP characteristics of a SCI BESS. The order of the six boxplot-types is the same as described before. Only the ranges of the y-axes are different as a comparison within the SCI BESS is done at this point. Here, each diagram contains one boxplot for the *greedy* operation strategy and one for the *feed-in damping* strategy (see Section 3.3). The smoothing of the load at *feed-in damping* strategy leads to a smaller number of FEC (Fig. 6 (a)), a smaller DOC (Fig. 6 (c)), a higher length of resting periods (Fig. 6 (d)) and a smaller amount of charged energy between sign changes (Fig. 6 (f)) compared to the *greedy* algorithm. The efficiency of the SCI BESS with *feed-in damping* algorithm is lower than with *greedy* algorithm (Fig. 6 (b)). This is due to the fact that the *feed-in damping* storage system is more often in the partial-load range where the PE has a lower efficiency.

While the lower efficiency is a disadvantage, the *feed-in damping* algorithm also leads to smaller Es-rate and lower rest times of high SOC compared to *greedy* algorithm (Appendix B.24 and B.25). Those two properties are advantages of the *feed-in damping* algorithm as longer

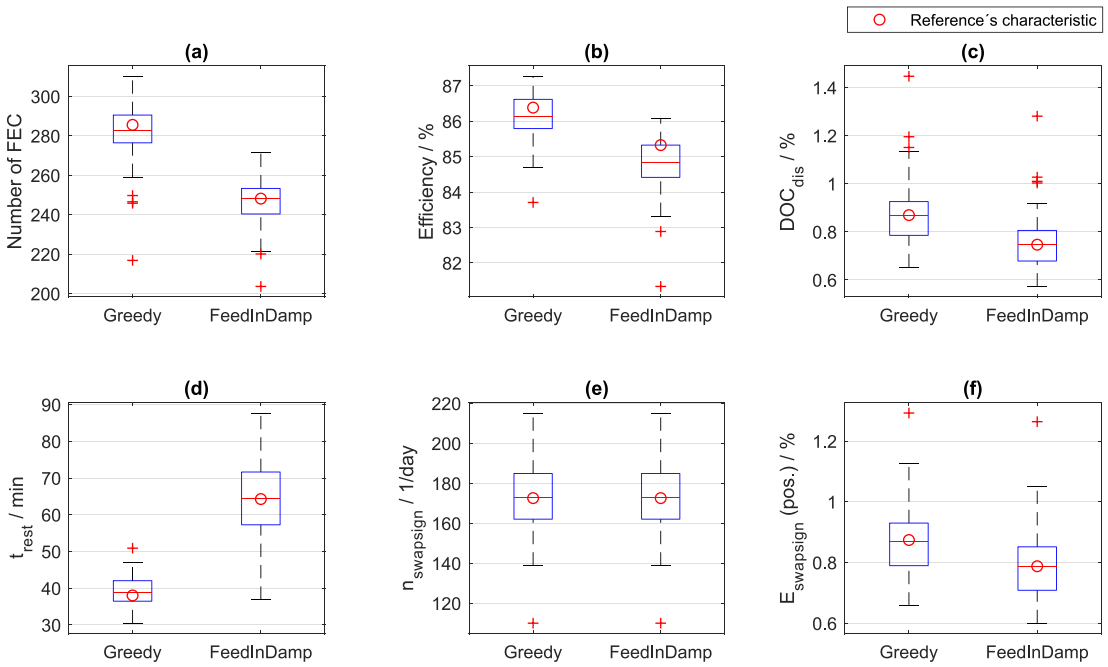

Fig. 6. Characteristics of an SCI performing BESS. The left box in each plot shows a SCI with *greedy* algorithm. The right box in each plot shows a SCI with the *feed-in damping* algorithm.

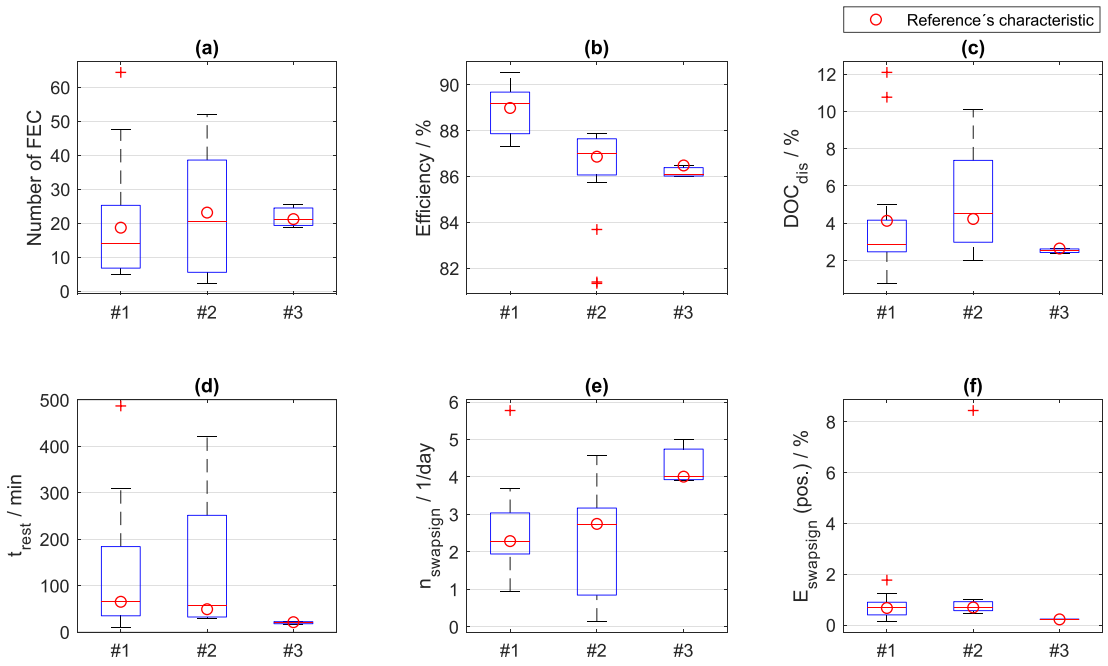

Fig. 7. Characteristics of a BESS in a PS application. The left box in each plot shows the characteristics for IP cluster 1. The box in the center for IP cluster 2 and the right one for IP cluster 3.

periods of high SOC may lead to an increased calendar aging [56]. Home storage system manufacturers should take these findings into consideration and try to avoid simple rule based strategies (*greedy*). Moreover, both algorithms lead to the same number of changes of signs per day (Fig. 6 (e)), as only the time of changes vary.

The SP characteristics of a BESS in the PS application are displayed in Fig. 7. The order of the diagrams is the same but the range of y-axes is different. The three box plots in each diagram contain the SP characteristics of the three clusters of IP (see 2.4). In contrast to the other two applications (FCR and SCI) the spread of the characteristics within each group is higher. The DOC, for example, varies between 2% and 10% for cluster 2. Thus, the storage's load varies significantly depending on the industry IP. Only cluster 3 shows relatively consistent characteristics in all diagrams.

5.2. Comparison of characteristics of reference storage profiles

After the analysis of the characteristics of each application's SPs, a comparison between application SPs is done in this subsection. Therefore, the six characteristics of each reference profile are displayed in spider diagrams with the same ranges to enhance comparability (Fig. 8). For the application of FCR the reference profiles' characteristics of one PE unit and a modular PE device are displayed (top). The modular PE with an NMC:C cell is not displayed as its characteristics are almost similar to the LFP:C ones (see Fig. 5). For SCI the reference characteristics of the two algorithms are shown (middle) and the PS characteristics are displayed for the three clusters (bottom).

FCR leads to a relatively high number of cycles ($>$ 240 FEC) and small average DOCs of 0.2%. Moreover, the average resting period length is small ($<$ 10 s) and the average number of changes of sign is relatively high (600 per day). This is due to the fact, that the grid frequency fluctuates around 50 Hz and the storage system reacts quickly on frequency changes by charging or discharging the battery (see Fig. A.12). The efficiency of the storage system performing FCR with modular PE is relatively high (93%). Using only one PE device leads to a reduced efficiency of 83%. This is because of the low converter efficiency in part-load operation.

Operating the storage system for SCI leads to similar number of cycles within the year as the application of FCR. Compared to the modular PE FCR application, the efficiency is lower (approx. 85%). The average DOC is higher when performing SCI than when performing FCR (0.9% to 0.75%). The average length of resting periods is much higher when operating as a SCI BESS than when performing FCR (38 to 65 min). During winter nights, for example, the storage rests for several hours, which increases the average resting period length. Moreover, the changes of signs per day are much lower than the characteristic of FCR. 170 changes of signs per day on average still appear to be high for a SCI BESS. This is due to the fact, that during charging of the storage system by photovoltaic energy, a short increase of load or a decrease of generation (e.g. clouds) can lead to a change of sign.

Performing PS as an application leads to a much smaller number of cycles (FEC $<$ 30) and changes of sign ($n_{swapsign}$ $<$ 4 per day) compared to FCR or SCI. In contrast to that, the average DOC is higher than the other applications reference characteristics (2% to 5%). The average length of resting periods is in the same range as the SCI characteristics (20 to 65 min). Thus, it is in resting mode for a longer period of time, it does not switch between charging and discharging very often and it is discharged relatively deep, when a discharge cycle is initiated. The storage's efficiency when performing PS is between 86% and 89%. The small number of FEC, in addition to the long average length of resting periods suggests potential benefits of application stacking (multi-use) for this application. However, this requires a sufficient power load forecast.

5.3. Reference storage profiles of different applications

After the analysis of the SP characteristics and the comparison between the different storage applications, exemplary weeks of the reference profiles are shown in this Section. As described in Section 2, the FCR reference profile and the SCI reference profile exist for a whole year. The PS reference profile is for 51 weeks starting with a Monday. Appendix A shows all complete reference profiles. All reference SPs as

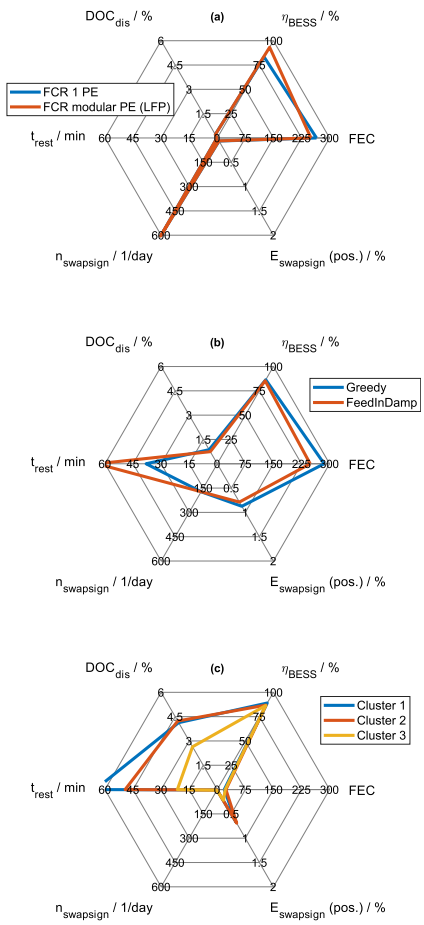

Fig. 8. Spider diagrams of the six characteristics of each reference profile (a: FCR, b: SCI and c: PS).

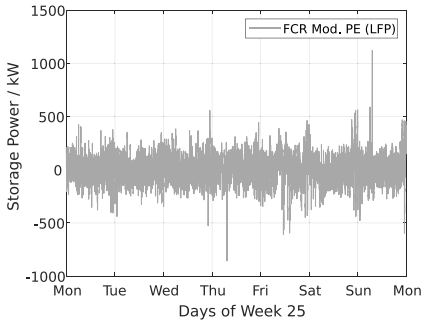

Fig. 9. Reference Storage Profile of a BESS providing FCR. Exemplary week in June.

well as the SOC at each timestep are available online free of charge, and are hosted on the servers of *TU Munich* [57].

As an example, the 25th week of the reference profile of the FCR application with modular PE and LFP:C battery technology is displayed in Fig. 9. The diagram's y-axis shows that the maximum power in this week is around 1.1 MW. IP for this resulting reference profile was the second year frequency profile [27] (year 2014, see Section 2.1). The profile shows a high fluctuation, which results in small DOCs, a lot of changes of sign and very short resting periods (see Section 5.2). To

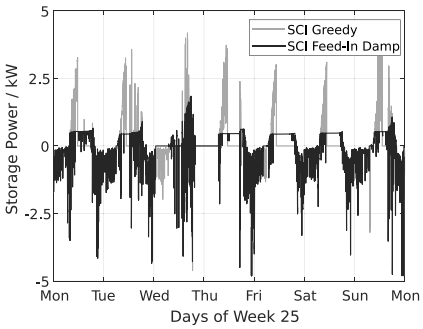

Fig. 10. Reference Storage Profile of a BESS performing SCI. Exemplary week in June.

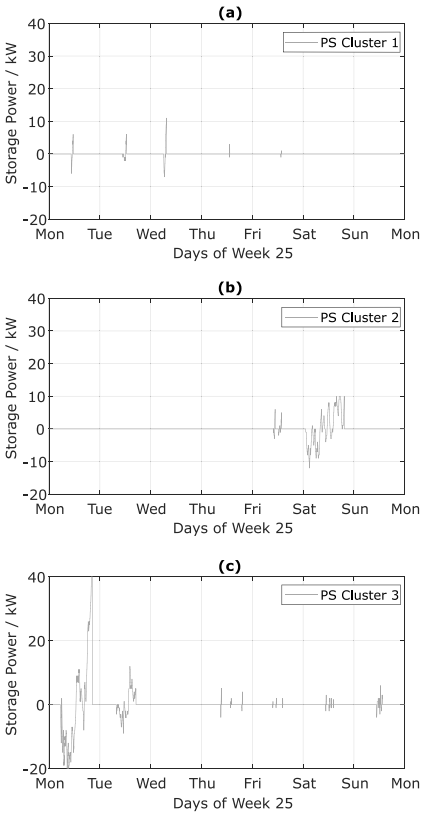

Fig. 11. Reference Storage Profile of a BESS in a PS application. Exemplary week in June. (a: Cluster 1, b: Cluster 2 and c: Cluster 3).

enable a greater degree of clarity, the profiles of FCR with one PE module and with NMC:C cell (modular PE) are not displayed within the diagram. These two show a similar course with high fluctuation.

Fig. 10 depicts the 25th week of the reference profiles of the two SCI BESS with *greedy* and *feed-in damping* algorithm. Input profile for those two resulting reference profiles was the 28th household load profile from the 74 *HTW-Berlin* load profiles [28] (see Section 2.1). As this week falls in June, the storage system gets charged by the PV generation during the day. In the evening and during the night it gets discharged until the battery is empty (e.g. Thursday night). The differences in the two operating strategies were explained in Section 3.3. The *feed-in damping* profile shows the typical limitation of the energy feed into the grid, which leads to lower Es-rate for the BESS.

The reference profiles (exemplary week 25) of the three clusters of PS application are shown in Fig. 11 (a: Cluster 1, b: Cluster 2, c: Cluster 3). Here, the maximal storage power was chosen as 40 kW (see Section 3.5). As described in the previous section, the PS BESS has the fewest number of cycles and changes of signs per day. The reference SPs confirm these numbers. Moreover, the relatively long resting periods and the differences between the three clusters are visible as well. The PS threshold values for the three clusters are set to 66 kW, 83 kW and 80 kW according to the pre-processing optimization in Section 3.4.

6. Conclusion and outlook

In this paper we presented a method to create standard profiles for stationary battery energy storage systems, the results of which are available as *open data* for download. Input profiles including frequency data, industry load profiles and household load profiles are pre-processed using a normalization and clustering method. These input profiles are then transformed into storage profiles including the storage power and the state of charge using a holistic simulation framework (SimSES). This modular object-oriented tool was used to analyze three standard applications for stationary battery energy storage systems in detail and an energy management system was programmed for the different applications: (i) The energy management system for providing frequency containment reserve in SimSES was developed according to the German regulatory framework and various degrees of freedom; the efficiency was taken into account to minimize the intra-day market transactions. Moreover, a modular power electronics topology was used. (ii) In addition to a simple *greedy* algorithm, a *feed-in damping* algorithm has been implemented for a residential battery energy storage system, which charges the storage system at a low E-rate over the whole day. (iii) A two-step approach with a linear programming algorithm and SimSES was applied for an industrial peak shaving battery energy storage systems to minimize the maximum power peak value.

The results have been post-processed using a storage profile analyzer tool in order to figure out six key characteristics of the different applications. These characteristics are essential for the design of a stationary battery energy storage system. For example, for a battery energy storage system providing frequency containment reserve, the number of full equivalent cycles varies from 4 to 310 and the efficiency from 81% to 97%. Additional simulations done with SimSES for one year showed a degradation from 4% (frequency containment reserve) to 7% (peak shaving).

The *open data* available results, including storage power as well as state of charge for all reference storage profiles, with a resolution of one second can be used for comparison with other self-developed energy management systems. Furthermore other system topologies or self-developed power electronic models can be simulated with SimSES and the simulation-outcome can be assessed against the numbers presented in this paper. Scientists are encouraged to conduct aging studies or battery management system tests using the platform SimSES and data provided herein.

In order to compare both different cell chemistries as well as storage technologies, future work could focus in more detail on battery degradation. Future applications for stationary battery energy storage systems could be: buffer-storage system to reduce the peak power at (fast-)charging stations, uninterruptible power supply or island grids. As soon as the first data sets are available, it might be worthwhile to analyze these use cases more precisely.

Authors Contribution

D.K. was the principle author tasked with coordinating and writing the paper and developing SimSES; B.T. programmed the profile analyzer tool and wrote contents within the data preparation, analysis and results; S.E. helped with programming and writing the peak-shaving algorithm; A.P. helped with gathering data and the selection of the characteristics. M.M. was co-responsible for the dynamization of the input data and helped with the selection of the characteristics. Both O.B. and A.J. contributed via fruitful scientific discussions. H.H. reviewed the manuscript and was giving valuable input throughout the manuscript preparation.

Declaration of Competing Interest

Done.

Acknowledgments

This work was financially supported by the Federal Ministry for Economic Affairs and Energy within the open_BEA project (Grant No. 03ET4072) and the EffSkalBatt project (Grant No. 03ET6148). Both projects are cared by Project Management Juelich. The responsibility for this publication rests with the authors.

Appendix A. Input and reference profiles

Fig. A.12 shows the frequency data (IP) of the whole year 2017 (top) and of one exemplary day (185) of year 2017 (bottom). The Figs. A.13–A.20 show the complete reference profiles. The FCR reference profile and the SCI reference profile are for a whole year. The PS reference profile are for 51 weeks starting with a Monday. All reference SP as well as the SOC at each timestep can be downloaded in a MATLAB R2019a® data format (*mat*) or hierarchical data format (*hdf5*) from the servers of TU Munich [57].

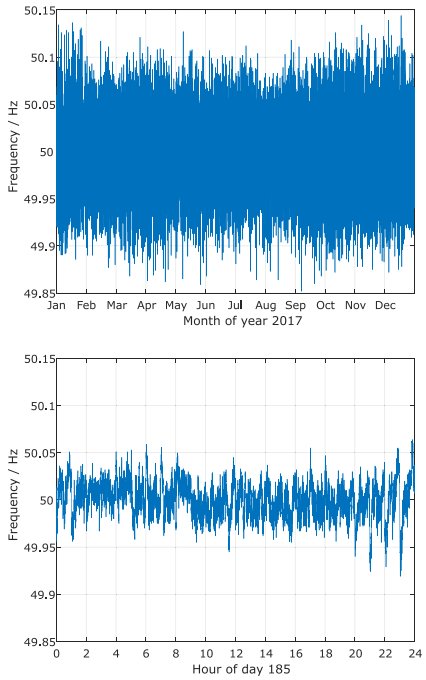

Fig. A.12. Sample sections of frequency data of the whole year 2017 (top) and of one exemplary day (185) of year 2017 (bottom).

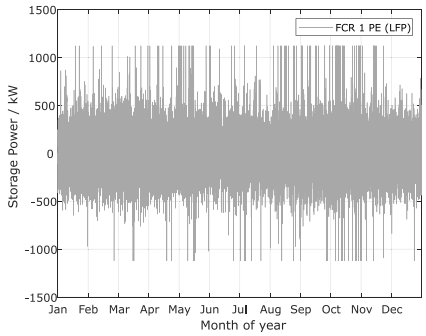

Fig. A.13. Yearly reference profile of a simulated BESS with one PE unit and a LFP:C cell providing FCR.

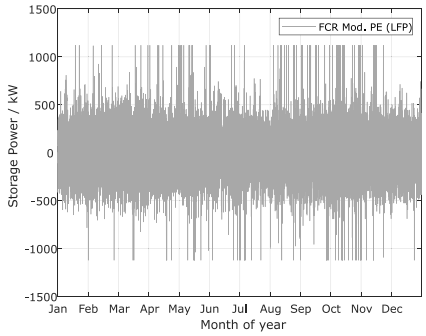

Fig. A.14. Yearly reference profile of a simulated BESS with three modular PE units and a LFP:C cell providing FCR.

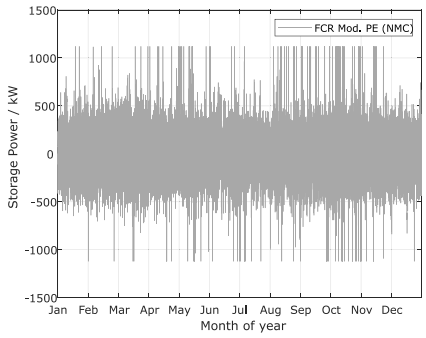

Fig. A.15. Yearly reference profile of a simulated BESS with three modular PE units and a NMC:C cell providing FCR.

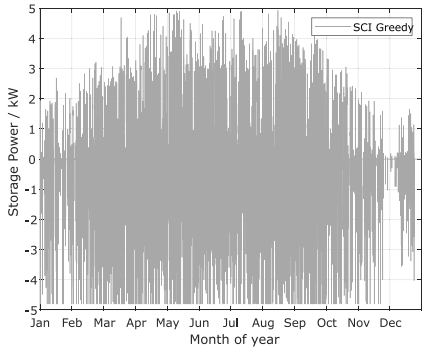

Fig. A.16. Yearly reference profile of a BESS for SCI with one PE unit and a LFP:C cell with the *greedy* algorithm.

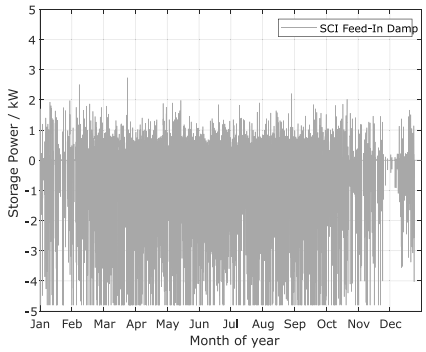

Fig. A.17. Yearly reference profile of a BESS for SCI with one PE unit and a LFP:C cell with the *feed-in damping* algorithm.

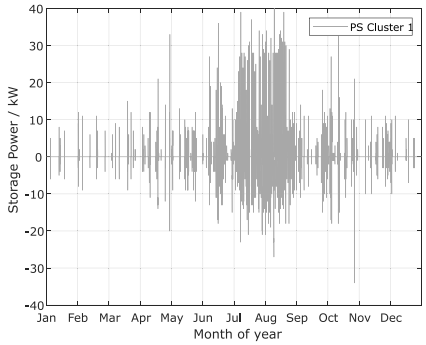

Fig. A.18. Yearly reference profile of a BESS in the application of PS with one PE unit and a LFP:C cell in cluster 1.

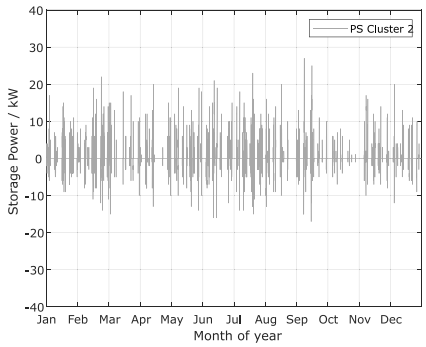

Fig. A.19. Yearly reference profile of a BESS in the application of PS with one PE unit and a LFP:C cell in cluster 2.

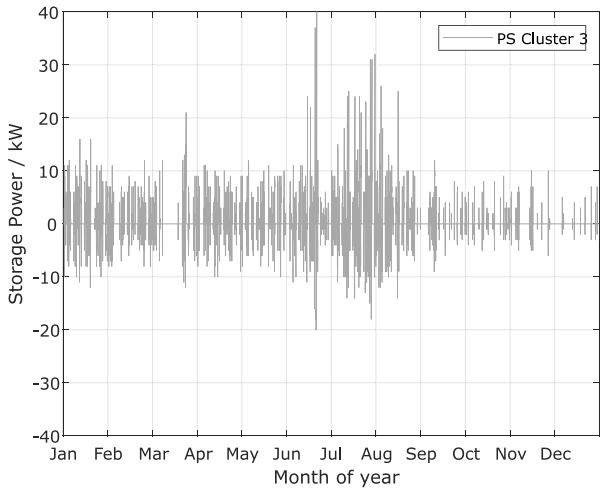

Fig. A.20. Yearly reference profile of a BESS in the application of PS with one PE unit and a LFP:C cell in cluster 3.

Appendix B. Further analysis with SimSES

B1. Frequency containment reserve

Figs. B.21, B.22 and B.23 shows additional analysis for the simulations of a BESS providing FCR. The left-hand plots (a, d) show the distribution of the SOC, the middle one (b, e) show the distribution of the DOC and the right-hand plots (c, f) show the distribution of the E-rate. The three plots at the top (a-c) at each figure show the mean results of all 5 simulations. The three plots at the bottom (d-f) show at each figure the result for the reference profile. All plots have a logarithmic y-axis.

B2. Residential photovoltaic battery storage system

Figs. B.24 and B.25 shows additional analysis for the simulations of a SCI BESS. The left-hand plots (a, d) show the distribution of the SOC, the middle one (b, e) show the distribution of the DOC and the right-hand plots (c, f) show the distribution of the E-rate. The three plots at the top (a-c) at each figure show the mean results of all 74 simulations. The three plots at the bottom (d-f) show at each figure the result for the reference profile. All plots have a logarithmic y-axis.

B3. Peak shaving storage system

Figs. B.26, B.27 and B.28 shows additional analysis for the simulations of a BESS in the application of PS. The left-hand plots show the distribution of the SOC, the middle one (b, e) show the distribution of the DOC and the right-hand plots (c, f) show the distribution of the E-rate. The three plots at the top (a-c) at each figure show the mean results of all simulations in the respective cluster. The three plots at the bottom (d-f) show at each figure the result for the reference profile in the respective cluster. All plots have a logarithmic y-axis.

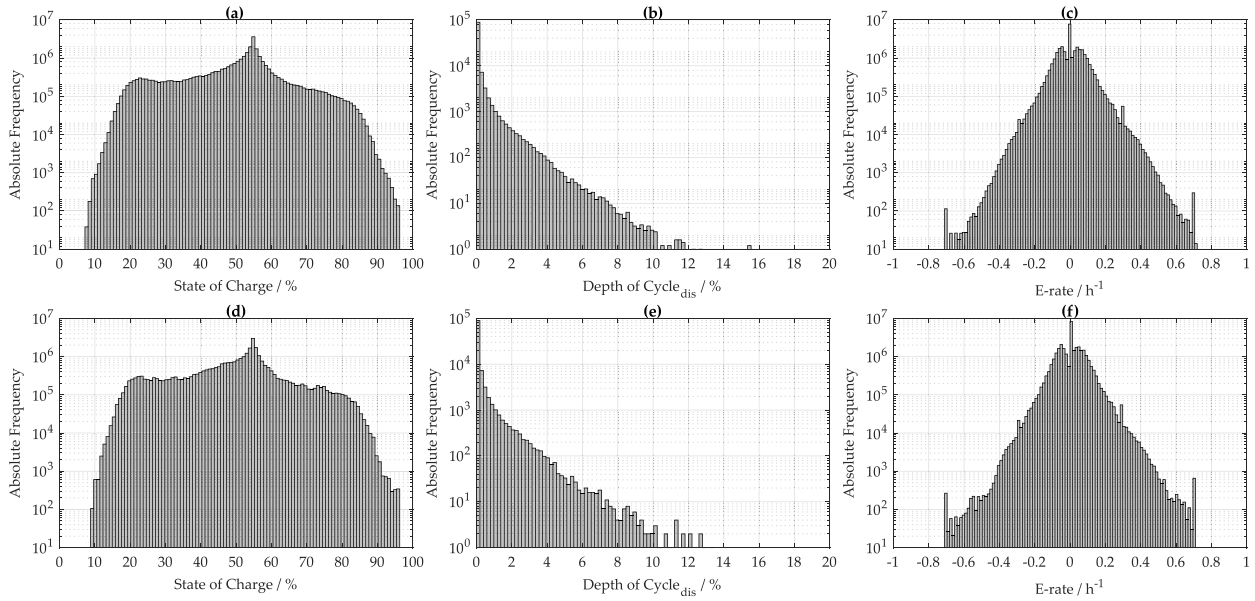

Fig. B.21. Additional analysis, SOC (a, d), DOC (b, e) and E-rate (c, f), of a simulated BESS with one PE unit and a LFP:C cell providing FCR. The three plots at the top (a-c) show the mean results of all 5 simulations. The three plots at the bottom (d-f) show the result for the reference profile.

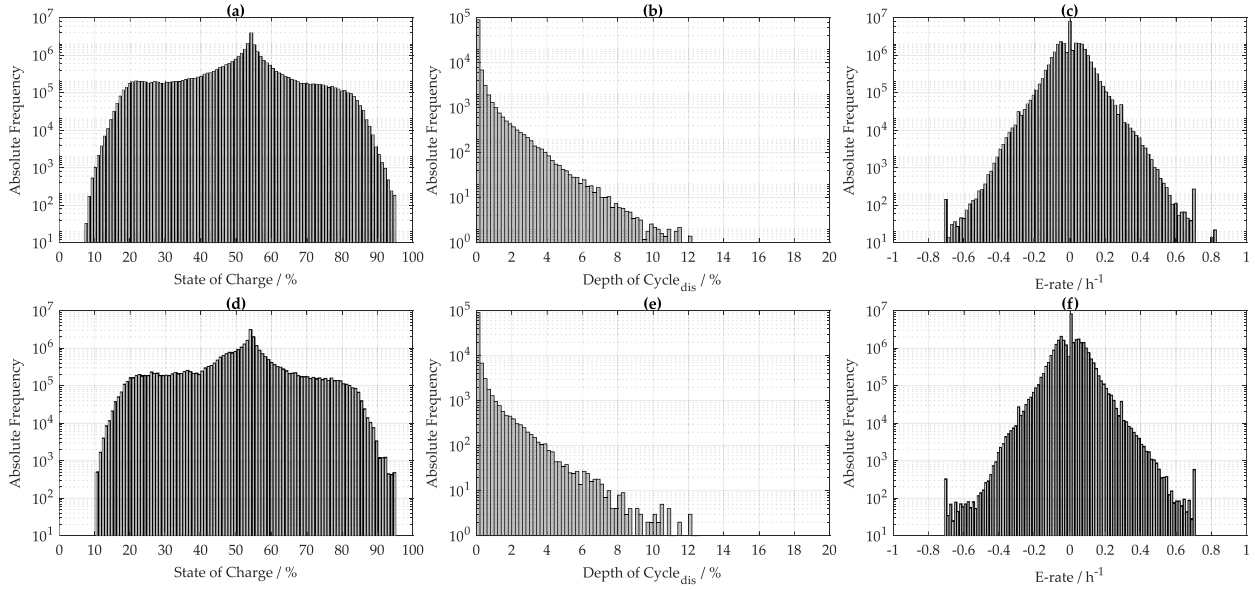

Fig. B.22. Additional analysis, SOC (a, d), DOC (b, e) and E-rate (c, f), of a simulated BESS with three modular PE units and a NMC:C cell providing FCR. The three plots at the top (a-c) show the mean results of all 5 simulations. The three plots at the bottom (d-f) show the result for the reference profile.

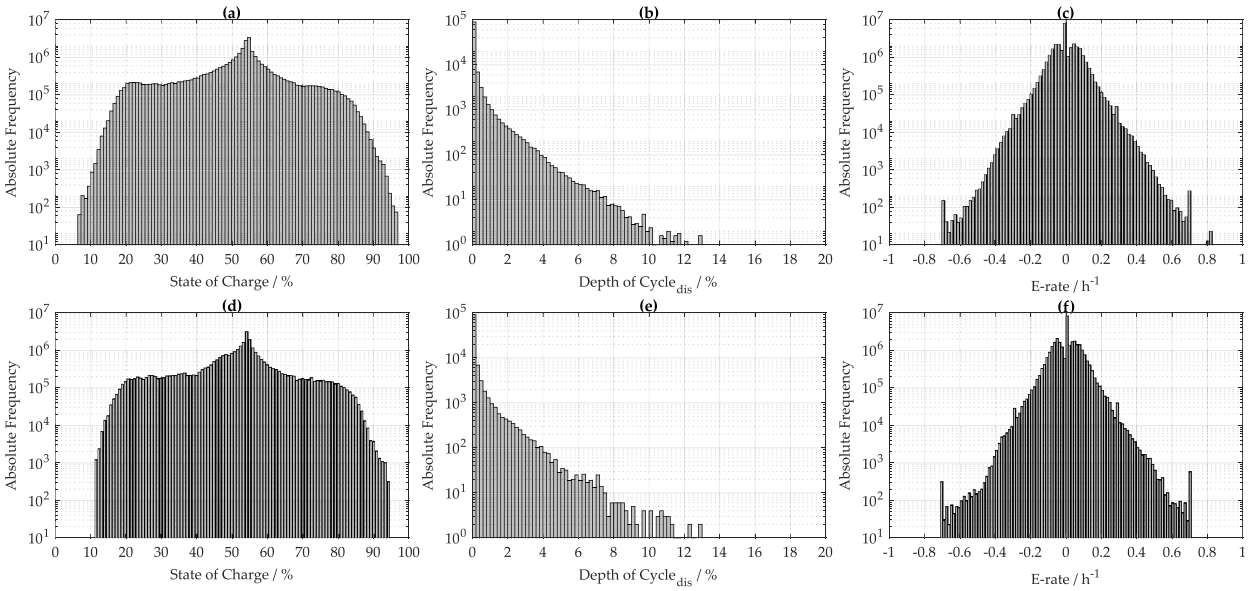

Fig. B.23. Additional analysis, SOC (a, d), DOC (b, e) and E-rate (c, f), of a simulated BESS with three modular PE units and a LFP:C cell providing FCR. The three plots at the top (a-c) show the mean results of all 5 simulations. The three plots at the bottom (d-f) show the result for the reference profile.

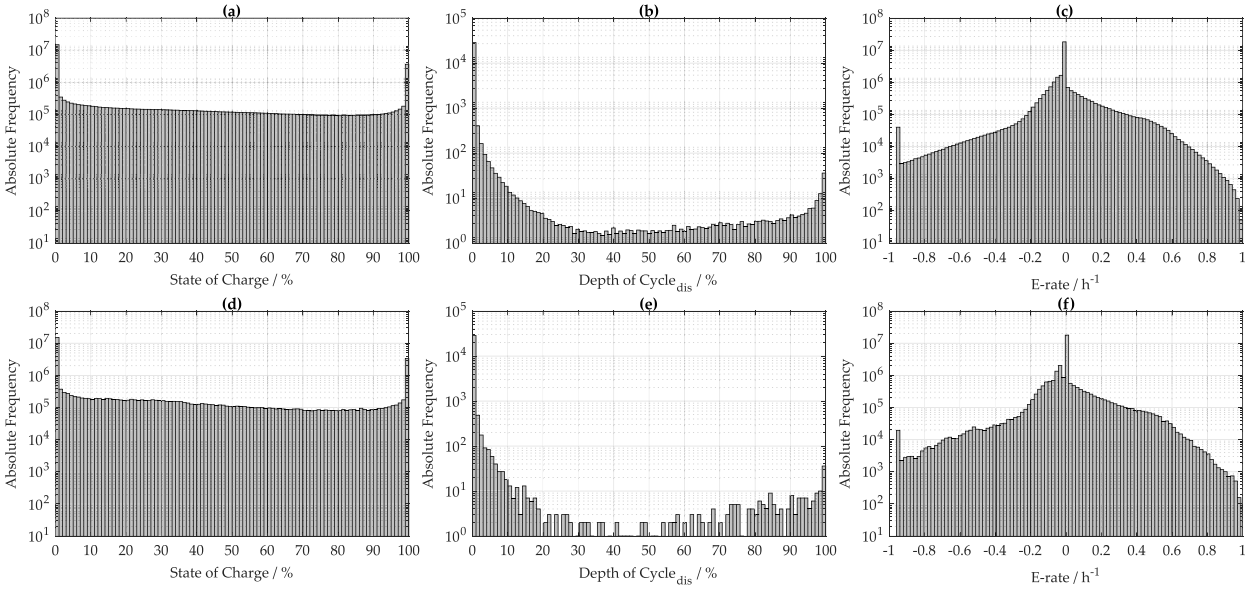

Fig. B.24. Additional analysis, SOC (a, d), DOC (b, e) and E-rate (c, f), of a SCI BESS with one PE unit and a LFP:C cell with the *greedy* algorithm. The three plots at the top (a-c) show the mean results of all 74 simulations. The three plots at the bottom (d-f) show the result for the reference profile.

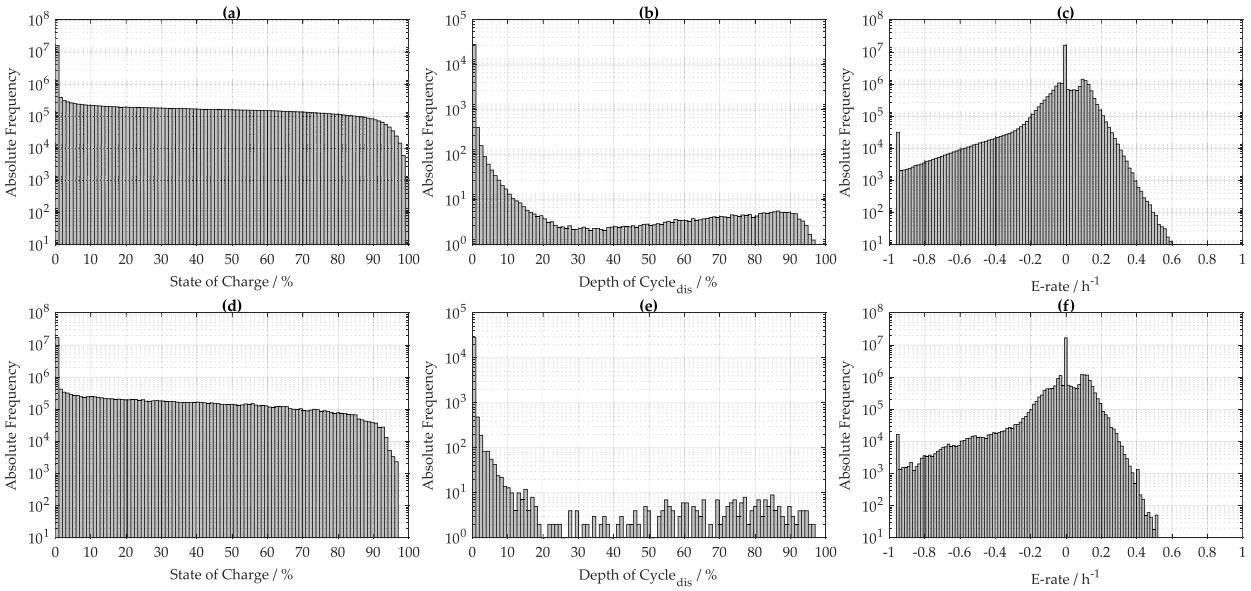

Fig. B.25. Additional analysis, SOC (a, d), DOC (b, e) and E-rate (c, f), of a SCI BESS with one PE unit and a LFP:C cell with the *feed-in damping* algorithm. The three plots at the top (a-c) show the mean results of all 74 simulations. The three plots at the bottom (d-f) show the result for the reference profile.

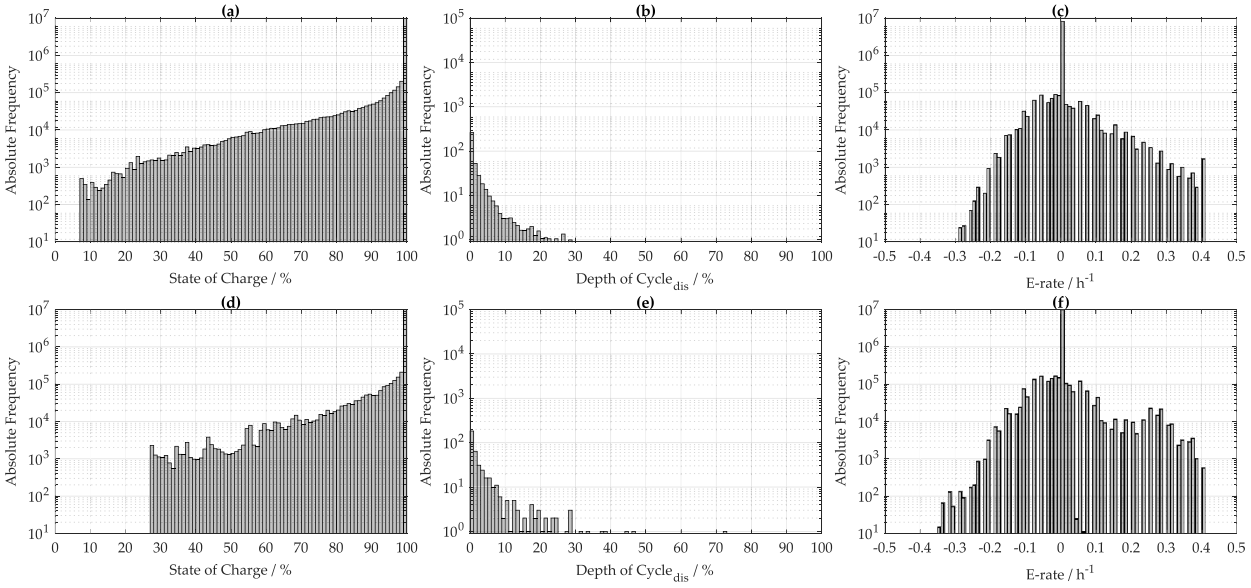

Fig. B.26. Additional analysis, SOC (a, d), DOC (b, e) and E-rate (c, f), of a BESS in the application of PS with one PE unit and a LFP:C cell in cluster 1. The three plots at the top (a-c) show the mean results of all simulations in cluster 1. The three plots at the bottom (d-f) show the result for the reference profile in cluster 1.

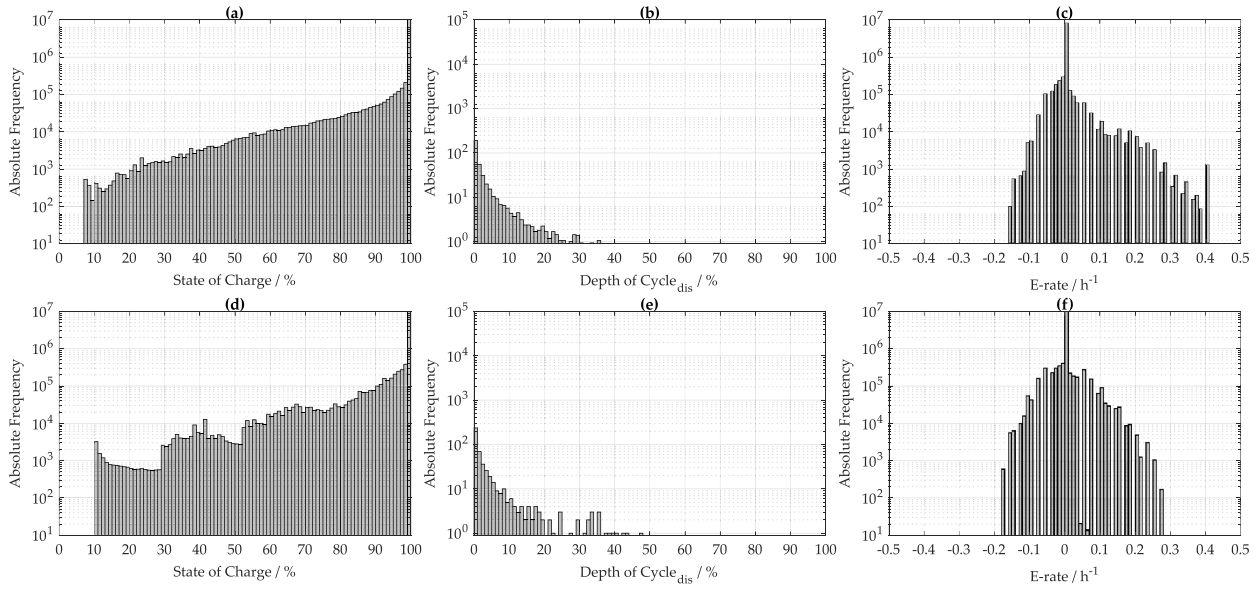

Fig. B.27. Additional analysis, SOC (a, d), DOC (b, e) and E-rate (c, f), of a BESS in the application of PS with one PE unit and a LFP:C cell in cluster 2. The three plots at the top (a-c) show the mean results of all simulations in cluster 2. The three plots at the bottom (d-f) show the result for the reference profile in cluster 2.

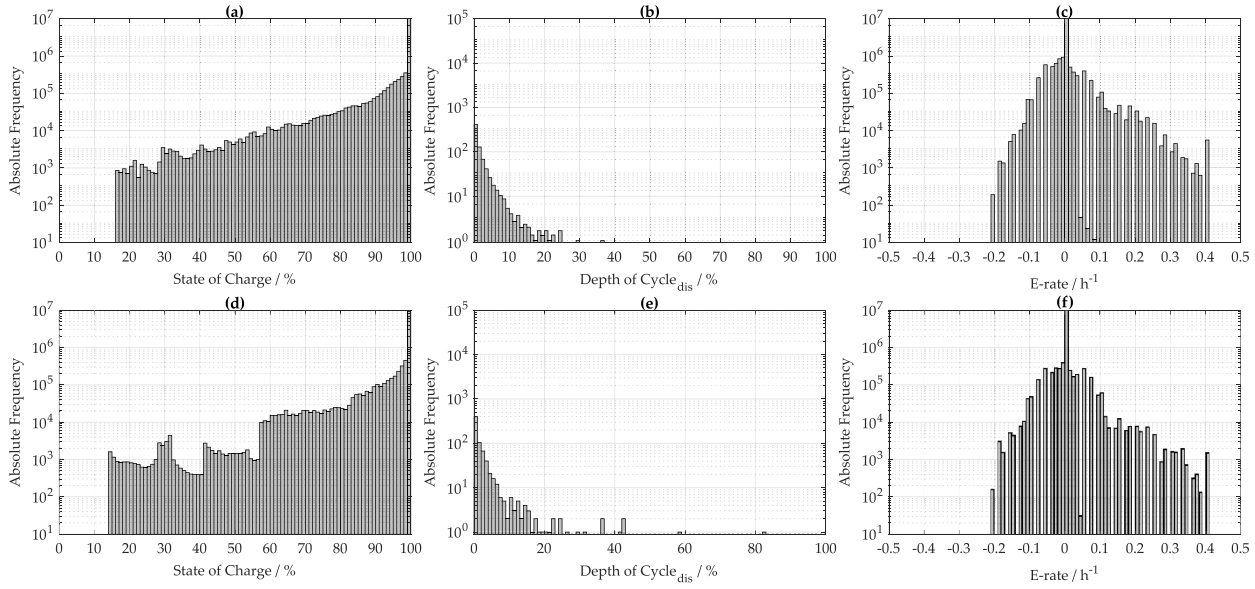

Fig. B.28. Additional analysis, SOC (a, d), DOC (b, e) and E-rate (c, f), of a BESS in the application of PS with one PE unit and a LFP:C cell in cluster 3. The three plots at the top (a-c) show the mean results of all simulations in cluster 3. The three plots at the bottom (d-f) show the result for the reference profile in cluster 3.

Supplementary material

Supplementary material associated with this article can be found, in the online version, at 10.1016/j.est.2019.101077

References

[1] TEAM CONSULT G.P.E. GmbH, Bedeutung der energiespeicherbranche für das energiesystem und die gesamtwirtschaft in deutschland (in german): pressekonferenz messe düsseldorf gmbh & bves bundesverband energiespeicher e.v. zur energy storage Europe 2018, 13.03.2018, https://www.bves.de/wp-content/uploads/2018/03/PK_ESE_Praesentation_2018.pdf.

[2] J. Eyer, G. Corey, Energy Storage for the Electricity Grid: benefits and Market Potential Assessment Guide: a Study for the Doe Energy Storage Systems Program.

[3] H. Hesse, M. Schimpe, D. Kucevic, A. Jossen, Lithium-ion battery storage for the grid—a review of stationary battery storage system design tailored for applications in modern power grids, Energies 10 (12) (2017) 2107, https://doi.org/10.3390/en10122107.

[4] M. Resch, J. Bühler, M. Klausen, A. Sumper, Impact of operation strategies of large scale battery systems on distribution grid planning in germany, Renew. Sustain.

Energy Rev. 74 (2017) 1042–1063, https://doi.org/10.1016/j.rser.2017.02.075.
[5] B. Diouf, R. Pode, Potential of lithium-ion batteries in renewable energy, Renew Energy 76 (2015) 375–380, https://doi.org/10.1016/j.renene.2014.11.058.
[6] O. Palizban, K. Kauhaniemi, Energy storage systems in modern grids—matrix of technologies and applications, J. Energy Storage 6 (2016) 248–259, https://doi.org/10.1016/j.est.2016.02.001.
[7] B. Dunn, H. Kamath, J.-M. Tarascon, Electrical energy storage for the grid: a battery of choices, Science 334 (6058) (2011) 928–935, https://doi.org/10.1126/science.1212741.
[8] T. Weitzel, C.H. Glock, Energy management for stationary electric energy storage systems: a systematic literature review, Eur. J. Oper. Res. (2017), https://doi.org/10.1016/j.ejor.2017.06.052.
[9] C.K. Das, O. Bass, G. Kothapalli, T.S. Mahmoud, D. Habibi, Overview of energy storage systems in distribution networks: placement, sizing, operation, and power quality, Renew. Sustain. Energy Rev. 91 (2018) 1205–1230, https://doi.org/10.1016/j.rser.2018.03.068.
[10] G. Carpinelli, F. Mottola, C. Noce, A. Russo, P. Varilone, A new hybrid approach using the simultaneous perturbation stochastic approximation method for the optimal allocation of electrical energy storage systems, Energies 11 (6) (2018) 1505, https://doi.org/10.3390/en11061505.
[11] A. Oudalov, D. Chartouni, C. Ohler, Optimizing a battery energy storage system for primary frequency control, IEEE Trans. Power Syst. 22 (3) (2007) 1259–1266, https://doi.org/10.1109/TPWRS.2007.901459.
[12] R. Hollinger, L.M. Diazgranados, F. Braam, T. Erge, G. Bopp, B. Engel, Distributed solar battery systems providing primary control reserve, IET Renew. Power Gener. 10 (1) (2016).
[13] J. Fleer, P. Stenzel, Impact analysis of different operation strategies for battery energy storage systems providing primary control reserve, J. Energy Storage 8 (2016) 320–338, https://doi.org/10.1016/j.est.2016.02.003.
[14] A. Zeh, M. Müller, M. Naumann, H. Hesse, A. Jossen, R. Witzmann, Fundamentals of using battery energy storage systems to provide primary control reserves in germany, Batteries 2 (3) (2016) 29, https://doi.org/10.3390/batteries2030029.
[15] Y.J.A. Zhang, C. Zhao, W. Tang, S.H. Low, Profit-maximizing planning and control of battery energy storage systems for primary frequency control, IEEE Trans Smart Grid 9 (2) (2018) 712–723, https://doi.org/10.1109/TSG.2016.2562672.
[16] J. Münderlein, M. Steinhoff, S. Zurmühlen, D.U. Sauer, Analysis and evaluation of operations strategies based on a large scale 5 mw and 5 mwh battery storage system, J. Energy Storage 24 (2019) 100778, https://doi.org/10.1016/j.est.2019.100778.
[17] M. Naumann, R.C. Karl, C.N. Truong, A. Jossen, H.C. Hesse, Lithium-ion battery cost analysis in pv-household application, 9th International Renewable Energy Storage Conference, IRES 2015, 73 (2015), pp. 37–47, https://doi.org/10.1016/j.egypro.2015.07.555.
[18] F. Cucchiella, I. D'Adamo, M. Gastaldi, Photovoltaic energy systems with battery storage for residential areas: an economic analysis, J. Clean. Prod. 131 (2016) 460–474, https://doi.org/10.1016/j.jclepro.2016.04.157.
[19] C.N. Truong, M. Naumann, R.C. Karl, M. Müller, A. Jossen, H.C. Hesse, Economics of residential photovoltaic battery systems in germany: the case of teslas powerwall, Batteries 2 (2) (2016) 14, https://doi.org/10.3390/batteries2020014.
[20] H. Hesse, R. Martins, P. Musilek, M. Naumann, C. Truong, A. Jossen, Economic optimization of component sizing for residential battery storage systems, Energies 10 (7) (2017) 835, https://doi.org/10.3390/en10070835.
[21] J. Weniger, T. Tjaden, V. Quaschning, Sizing of residential pv battery systems, 9th International Renewable Energy Storage Conference, IRES 2015, 46 (2014), pp. 78–87, https://doi.org/10.1016/j.egypro.2014.01.160.
[22] R. Tang, B. Yildiz, P.H. Leong, A. Vassallo, J. Dore, Residential battery sizing model using net meter energy data clustering, Appl. Energy 251 (2019) 113324, https://doi.org/10.1016/j.apenergy.2019.113324.
[23] F.M. Vieira, P.S. Moura, A.T. de Almeida, Energy storage system for self-consumption of photovoltaic energy in residential zero energy buildings, Renew Energy 103 (2017) 308–320, https://doi.org/10.1016/j.renene.2016.11.048.
[24] R. Martins, H. Hesse, J. Jungbauer, T. Vorbuchner, P. Musilek, Optimal component sizing for peak shaving in battery energy storage system for industrial applications, Energies 11 (8) (2018) 2048, https://doi.org/10.3390/en11082048.
[25] H. Dagdougui, N. Mary, A. Beraud-Sudreau, L. Dessaint, Power management strategy for sizing battery system for peak load limiting in a university campus, 2016 IEEE Smart Energy Grid Engineering (SEGE), IEEE, 21.08.2016 - 24.08.2016, pp. 308–312, https://doi.org/10.1109/SEGE.2016.7589542.
[26] E. Telaretti, L. Dusonchet, Battery storage systems for peak load shaving applications: Part 2: economic feasibility and sensitivity analysis, 2016 IEEE 16th International Conference on Environment and Electrical Engineering (EEEIC), IEEE, 07.06.2016 - 10.06.2016, pp. 1–6, https://doi.org/10.1109/EEEIC.2016.7555795.
[27] 50Hertz Transmission GmbH, Archiv netzfrequenz (in german): daten der entso-e netzfrequenz, 2019, https://www.50hertz.com/de/Transparenz/Kennzahlen/Regelenergie/ArchivRegelenergie/ArchivNetzfrequenz.
[28] T. Tjaden, J. Bergner, J. Weniger, V. Quaschning, Repräsentative elektrische lastprofile für wohngebäude in deutschland auf 1-sekündiger datenbasis (in German), https://pvspeicher.htw-berlin.de/daten/.
[29] A. Zeh, R. Witzmann, Operational strategies for battery storage systems in low-voltage distribution grids to limit the feed-in power of roof-mounted solar power systems, Energy Procedia 46 (2014) 114–123, https://doi.org/10.1016/j.egypro.2014.01.164.
[30] P. Keil, A. Jossen, Charging protocols for lithium-ion batteries and their impact on cycle life—an experimental study with different 18650 high-power cells, J. Energy Storage 6 (2016) 125–141, https://doi.org/10.1016/j.est.2016.02.005.
[31] G. Ning, B. Haran, B.N. Popov, Capacity fade study of lithium-ion batteries cycled at high discharge rates, J Power Source. 117 (1–2) (2003) 160–169, https://doi.org/10.1016/S0378-7753(03)00029-6.
[32] B. Everitt, Cluster analysis, 5th ed., Wiley series in probability and statistics, Wiley, Chichester West Sussex U.K., 2011.
[33] A. Al-Wakeel, J. Wu, K-Means based cluster analysis of residential smart meter measurements, 9th International Renewable Energy Storage Conference, IRES 2015 88 (2016) 754–760, https://doi.org/10.1016/j.egypro.2016.06.066.
[34] G. Le Ray, P. Pinson, Online adaptive clustering algorithm for load profiling, Sustain. Energy Grids Netw. 17 (2019) 100181, https://doi.org/10.1016/j.segan.2018.100181.
[35] G.J. Tsekouras, N.D. Hatziargyriou, E.N. Dialynas, Two-stage pattern recognition of load curves for classification of electricity customers, IEEE Trans. Power Syst. 22 (3) (2007) 1120–1128, https://doi.org/10.1109/TPWRS.2007.901287.
[36] F. McLoughlin, A. Duffy, M. Conlon, A clustering approach to domestic electricity load profile characterisation using smart metering data, Appl. Energy 141 (2015) 190–199, https://doi.org/10.1016/j.apenergy.2014.12.039.
[37] T. Räsänen, D. Voukantsis, H. Niska, K. Karatzas, M. Kolehmainen, Data-based method for creating electricity use load profiles using large amount of customer-specific hourly measured electricity use data, Appl. Energy 87 (11) (2010) 3538–3545, https://doi.org/10.1016/j.apenergy.2010.05.015.
[38] M. Naumann, C.N. Truong, M. Schimpe, D. Kucevic, A. Jossen, H.C. Hesse, Simses: Software for techno-economic simulation of stationary energy storage systems, International ETG Congress 2017, ETG-Fachbericht, VDE Verlag, Berlin and Offenbach, 2017, pp. 442–447.
[39] Deutsche Übertragungsnetzbetreiber, Eckpunkte und freiheitsgrade bei erbringung von primaerregelleistung (in German): Leitfaden für anbieter von primaerregelleistung, https://www.regelleistung.net/ext/static/prequalification?lang=en.
[40] Deutsche Übertragungsnetzbetreiber, Anforderungen an die speicherkapazitaet bei batterien für die primaerregelleistung (in German), https://www.bves.de/wp-content/uploads/2015/08/2015_08_26_Anforderungen_Speicherkapazitaet_Batterien_PRL.pdf.
[41] BVES, Beschränkung der ünb für speicher im regelenergiemarkt ist rechtswidrig (in German), 09.05., 2019, https://www.bves.de/uenb_rechtswidrige_blockade/.
[42] German Federal Office of Justice, Stromnetzentgeltverordnung (in German): Stromnev, 2005-07-25, https://www.gesetze-im-internet.de/stromnev/BJNR222500005.html.
[43] S. Englberger, H.C. Hesse, C.N. Truong, A. Jossen, Autonomous versus Coordinated Control of Residential Energy Storage Systems - Monitoring Profit, Battery Aging, and System Efficiency, in: D. Schulz (Ed.), NEIS 2018, VDE VERLAG GMBH, Berlin, 2019, pp. 1–7.
[44] S. Englberger, H. Hesse, D. Kucevic, A. Jossen, A techno-economic analysis of vehicle-to-building: battery degradation and efficiency analysis in the context of coordinated electric vehicle charging, Energies 12 (5) (2019) 955, https://doi.org/10.3390/en12050955.
[45] D. Kucevic, C.N. Truong, A. Jossen, H.C. Hesse, Lithium-ion Battery Storage Design for Buffering Fast Charging Stations for Battery Electric Vehicles and Electric Buses, in: D. Schulz (Ed.), NEIS 2018, VDE VERLAG GMBH, Berlin, 2019, pp. 1–6.
[46] Murata, Data sheet of Sony fortelion us26650ftc1 battery cell, 2017.
[47] A.-I. Stan, M. Swierczynski, D.-I. Stroe, R. Teodorescu, S.J. Andreasen, Lithium ion battery chemistries from renewable energy storage to automotive and back-up power applications — an overview, 2014 International Conference on Optimization of Electrical and Electronic Equipment (OPTIM), IEEE, 2014, pp. 713–720, https://doi.org/10.1109/OPTIM.2014.6850936.
[48] M. Müller, L. Viernstein, C.N. Truong, A. Eiting, H.C. Hesse, R. Witzmann, A. Jossen, Evaluation of grid-level adaptability for stationary battery energy storage system applications in europe, J. Energy Storage 9 (2017) 1–11, https://doi.org/10.1016/j.est.2016.11.005.
[49] M. Naumann, Techno-economic evaluation of stationary battery energy storage systems with special consideration of aging, Technical University of Munich, Munich, 2018 Phd thesis.
[50] Molicel, Product data sheet model ihr-18650a.
[51] S.F. Schuster, Reuse of Automotive Lithium-Ion Batteries: An Assessment from the Cell Aging Perspective, Universitätsbibliothek der TU München, München, 2016 Dissertation.
[52] G. Notton, V. Lazarov, L. Stoyanov, Optimal sizing of a grid-connected pv system for various pv module technologies and inclinations, inverter efficiency characteristics and locations, Renew Energy 35 (2) (2010) 541–554, https://doi.org/10.1016/j.renene.2009.07.013.

[53] M. Schimpe, M. Naumann, N. Truong, H.C. Hesse, S. Santhanagopalan, A. Saxon, A. Jossen, Energy efficiency evaluation of a stationary lithium-ion battery container storage system via electro-thermal modeling and detailed component analysis, Appl. Energy 210 (2018) 211–229, https://doi.org/10.1016/j.apenergy.2017.10.129.

[54] J. Hoppmann, J. Volland, T.S. Schmidt, V.H. Hoffmann, The economic viability of battery storage for residential solar photovoltaic systems – a review and a simulation model, Renew. Sustain. Energy Rev. 39 (2014) 1101–1118, https://doi.org/10.1016/j.rser.2014.07.068.

[55] S.F. Schuster, T. Bach, E. Fleder, J. Müller, M. Brand, G. Sextl, A. Jossen, Nonlinear aging characteristics of lithium-ion cells under different operational conditions, J. Energy Storage 1 (2015) 44–53, https://doi.org/10.1016/j.est.2015.05.003.

[56] M. Naumann, M. Schimpe, P. Keil, H.C. Hesse, A. Jossen, Analysis and modeling of calendar aging of a commercial lifepo4/graphite cell, J. Energy Storage 17 (2018) 153–169, https://doi.org/10.1016/j.est.2018.01.019.

[57] D. Kucevic, B. Tepe, S. Englberger, A. Parlikar, M. Muehlbauer, O. Bohlen, A. Jossen, H. Hesse, Standard battery energy storage system profiles: dataset, doi:10.14459/2019mp1510254.

5 Peak shaving with battery energy storage systems in distribution grids: A novel approach to reduce local and global peak loads

Main research question: *Can existing stationary BESSs reduce the need for grid reinforcement through central coordination?*

Motivated by a tariff system consisting of costs for the consumed energy and a demand charge for the highest peak power of an industrial consumer, the aim of state-of-the-art peak shaving is to minimize power peak value at one specific node b within a defined billing period. The expected benefit for the grid operator of this tariff scheme is to avoid cable overloading and lower peak loads on the transformer, which consequently would avoid cost intensive grid reinforcement [113]. With continuously falling costs for LIBs, storage systems are becoming more profitable for industrial consumers to reduce peak power charges. It is expected that the market for peak shaving storage system will grow dramatically in the future [111].

This publication shows a EMS for BESSs, targeted at industrial consumers to achieve both a load reduction at a central node in the distribution grid and electricity bill savings for the industrial consumer at a specific node b. The objective is to reduce the peak power at the transformer to the high-voltage grid or PCC in existing distribution grids by adapting the operation strategy of the BESS at individual industrial consumer sites.

The developed combined approach uses a scaling factor (σ_{b}) for the power profile at the PCC in order to combine this load profile with the load profile of an individual industrial consumer. This combined profile serves as the input for the peak shaving operation strategy, which is simulated with SimSES. The stress on the storage systems is compared to a state-of-the-art peak shaving strategy with regards to the six key characteristics described in Chapter 4. The effects on the distribution grid are determined using the functionality of the simulation tool eDisGo. This work can be summarized as follows:

- With accurate co-simulations of BESSs in SimSES and distribution grids in eDisGo, a comparative analysis for various operation strategies aiming to reduce both the local peak load and the global peak load is conducted.
- The storage systems are optimally sized regarding their economics using linear optimization.
- A novel combined operation strategy is developed that aims to reduce the peak power at the PCC in an example distribution grid while not significantly influencing the peak load reduction for the individual industrial consumer.

The results of this publication show that both the local peak load for the industrial consumer and the global peak load at the PCC can be reduced by adapting the state-of-the-art peak shaving strategy for BESSs. And although with this novel approach the BESSs reduce both peaks, the additional

stress for the six-month simulation period is on average only 1.2 FECs higher. The strategy in this publication only needs a communication from the PCC to the individual storage systems, but no communication between several BESSs in the distribution grid. This kind of communication is already used for photovoltaic generation units and can be adapted to storage systems as well [161].

Author contribution Daniel Kucevic was the principal author tasked with coordinating and writing the paper and developing the EMSs. Leo Semmelmann assisted with preparation and execution of the case studies. Nils Collath helped integrating the peak shaving algorithm. Andreas Jossen contributed via fruitful scientific discussions and reviewed the manuscript. Holger Hesse reviewed the manuscript and assisted with integrating the optimization of storage sizing. All authors discussed the data and commented on the results.

Peak Shaving with Battery Energy Storage Systems in Distribution Grids: A Novel Approach to Reduce Local and Global Peak Loads

Daniel Kucevic, Leo Semmelmann, Nils Collath, Andreas Jossen, Holger Hesse

Electricity, Volume 2, 2021

Permanent weblink:
https://doi.org/10.3390/electricity2040033

electricity

MDPI

Article

Peak Shaving with Battery Energy Storage Systems in Distribution Grids: A Novel Approach to Reduce Local and Global Peak Loads

Daniel Kucevic *, Leo Semmelmann, Nils Collath, Andreas Jossen and Holger Hesse

Institute for Electrical Energy Storage Technology, School of Engineering and Design, Technical University of Munich (TUM), 80333 Munich, Germany; leo.semmelmann@tum.de (L.S.); nils.collath@tum.de (N.C.); andreas.jossen@tum.de (A.J.); holger.hesse@tum.de (H.H.)

* Correspondence: daniel.kucevic@tum.de

Abstract: The growing global electricity demand and the upcoming integration of charging options for electric vehicles is creating challenges for power grids, such as line over loading. With continuously falling costs for lithium-ion batteries, storage systems represent an alternative to conventional grid reinforcement. This paper proposes an operation strategy for battery energy storage systems, targeted at industrial consumers to achieve both an improvement in the distribution grid and electricity bill savings for the industrial consumer. The objective is to reduce the peak power at the point of common coupling in existing distribution grids by adapting the control of the battery energy storage system at individual industrial consumer sites. An open-source simulation tool, which enables a realistic simulation of the effects of storage systems in different operating modes on the distribution grid, has been adapted as part of this work. Further information on the additional stress on the storage system is derived from a detailed analysis based on six key characteristics. The results show that, with the combined approach, both the local peak load and the global peak load can be reduced, while the stress on the energy storage is not significantly increased. The peak load at the point of common coupling is reduced by 5.6 kVA to 56.7 kVA and the additional stress for the storage system is, on average, for a six month simulation, period only 1.2 full equivalent cycles higher.

Keywords: battery energy storage system; lithium-ion; grid-integrated energy storage; peak shaving; distribution grid; peak load reduction

Citation: Kucevic, D.; Semmelmann, L.; Collath, N.; Jossen, A.; Hesse, H. Peak Shaving with Battery Energy Storage Systems in Distribution Grids: A Novel Approach to Reduce Local and Global Peak Loads. *Electricity* **2021**, 2, 573–589. https://doi.org/10.3390/electricity2040033

Academic Editor: Andreas Sumper

Received: 28 September 2021
Accepted: 4 November 2021
Published: 15 November 2021

1. Introduction

The steadily increasing demand for electrical energy is leading to new challenges for the power grid [1]. The grid infrastructure must be tailored to tolerate the peak load conditions and grid operators must ensure this [2]. Conventional grid reinforcement or transformer upgrading, as investigated by Brinkel et al., is one possible solution for covering the increasing demand or to enable the integration of more electric vehicles [3]. However, with falling costs of lithium-ion batteries (LIBs), stationary battery energy storage systems (BESSs) are becoming increasingly attractive as an alternative method to reduce peak loads [4,5].

The peak shaving field has seen an increasing interest in research during the last years. Oudalov et al. were among the first to introduce a BESS sizing methodology and operation strategy to reduce the peak load of an industrial customer, thereby reducing its total electricity bill. Since grid operators in many jurisdictions charge large-scale consumers for their highest power demand, it can be economically viable to install a BESS and discharge it when a certain power threshold is surpassed. The objective for optimal BESS operation is to maximize the profit of the peak shaving operations with respect to the shaved power, battery cycles per year, battery lifetime, and the power demand fee. The optimal trajectory of BESS charging and discharging events-resulting from the peak

shaving operating strategy-is retrieved through dynamic programming. In their work, electricity bill reduction to the amount of 8% was reached through a lead-acid based BESS. However, in this study the focus was on the optimization of the BESS and the economic effects and not on the possible grid relief achievements through the peak shaving strategy on the distribution grid. [6]

In the study of Mamun et al. the management of a lithium-ion based BESS was optimized in order to maximize peak shaving-induced electricity bill savings while minimizing battery degradation [7]. The focus here was on modeling the battery degradation mechanisms and the economic benefits and again not on the effects on the distribution grid. In the study of Tiemann et al. a large-scale peak shaving profitability analysis of more than 5300 industrial customer load profiles in Germany was conducted [8]. The authors also came to the conclusion that the peak shaving technology yields the highest profits, compared to other battery use cases. Furthermore, the authors state that in many cases minimal payback periods for peak shaving operations can be reached. This is supported by the work of Martins et al., who concluded that peak shaving is already profitable in many cases for industrial customers in Germany [9].

While most peak shaving related works are focused on industrial end-customer use cases, some recent works also highlight the possible benefits of the approach for the grid. For instance, in the work of Danish et al. a BESS located in a distribution grid was optimized in order to find the optimal size, location, and control strategy. The work was based on a 20 kV distribution grid in Kabul with 22 buses and the authors have concluded that an optimally placed BESS with a peak shaving operation strategy can significantly improve the system performance and power losses can be reduced up to 20.62% [10].

However, none of these studies investigated the effects of multiple BESSs located at various industrial consumers, including accurate co-simulations of both a BESS and a distribution grid. Furthermore, the potential of coupled energy management strategies has not yet been analyzed in order to achieve both an improvement in the distribution grid as well as electricity bill savings for industrial consumers.

1.1. Scope of the Study

This study shows different operation strategies for a number of stand-alone BESSs to reduce the local peak load (Strategy α) or the peak load at the point of common coupling (β) or both (γ). The BESSs located at various nodes in an example grid are economically optimal sized using a linear programming approach. First, these storage systems are operated with a state-of-the-art peak shaving strategy. In the second step, the identically sized BESSs are used and a centralized control approach is chosen to reduce the peak load at the point of common coupling (PCC). Finally, in a new approach introduced in this study, these two approaches are combined in order to achieve both a local and a global peak load reduction. This scope of the study is condensed as a graphical overview in Figure 1. The paper can be summarized as follows:

- With accurate co-simulations of BESSs and distribution grids, results for various operation strategies aiming to reduce both the local peak load and the global peak load are acquired.
- The storage systems are economical optimally sized using linear optimization.
- These storage systems are operated with a state-of-the-art peak shaving strategy as well as with a centralized approach and compared according to the peak load reduction at a specific node and the PCC.
- A newly combined approach is developed aimed to reduce the peak power at the PCC in an example distribution grid while not significantly influencing the peak load reduction for the individual industrial consumer.
- The stress on the storage system for the various operation strategies is derived from a detailed analysis based on six key characteristics.

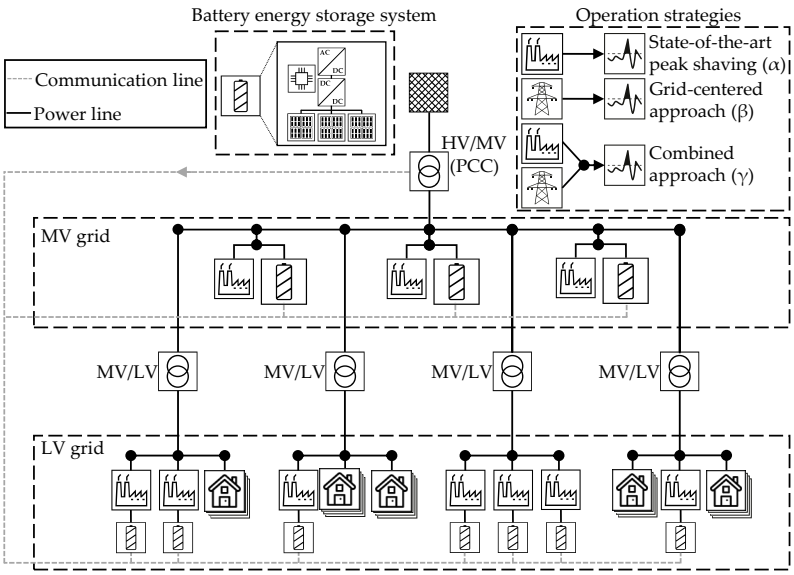

Figure 1. Graphical overview of the simulated grid and battery energy storage systems (BESSs), as well as the investigated operation strategies. The BESS, modeled in detail, located at various nodes in a test grid, is operated in three different operation strategies to reduce the local peak load (Strategy α) or the peak load at the point of common coupling (β) or both (γ).

1.2. Outline of the Paper

The remainder of this paper is structured as follows: Configuration of the grid and the BESS as well as the simulation settings are described in Section 2. Section 3 describes the methodology of this study, including a mathematical and graphical representation of all three energy management strategies used. The results of the simulations are presented and discussed in Section 4, while Section 5 concludes the paper with an outlook on potential directions of future work.

2. Simulation Settings and System Configurations

This section describes the simulation tools applied as well as the example grid used and the BESSs settings. To analyze the behavior and the effects on the distribution grid of storage systems, accurate simulations of BESSs and distribution grids are necessary. Figure 2 shows an overview of all simulation tools used in this work, which are all available open-source (open_BEA and SimSES: https://www.ei.tum.de/en/ees/research-teams/team-ses/system-analytics-and-integration/, accessed on 2 November 2021; eDisGo: https://github.com/openego/eDisGo, accessed on 2 November 2021). All settings, such as the selection of the grid, the simulation duration, and the operation strategy are defined within open_BEA. A further description of open_BEA can be found in [11]. In this work, open_BEA is used to analyze the effects of novel operation strategies for BESSs on the peak load at the PCC in a distribution grid.

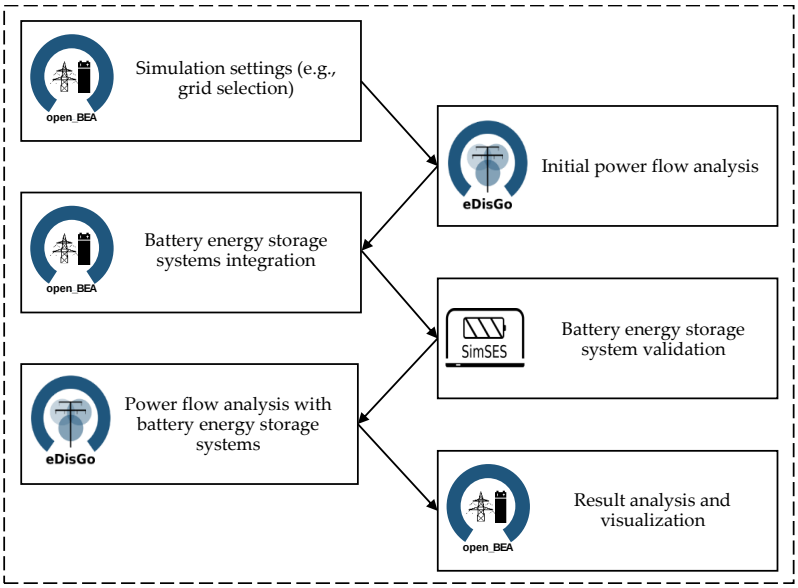

Figure 2. Overview of all open-source simulation tools, which have been adapted for use in this study. The open_BEA tool operates as both a central control unit and as a configuration unit. The eDisGo tool conducts the power flow analysis and SimSES operates as a validation unit for the battery energy storage systems' behavior.

In addition to the specification of the test grid and the operation strategies (ff − fl) of the BESSs, individual load demands are assigned to the various actors in the grid within open_BEA. Based on these load demands for residential or industrial consumers, the eDisGo software performs a power flow analysis for a selected period. In this step, the power flow analysis is conducted without storage systems. This allows determining the power flows at all specific nodes and lines for the entire simulation period. These power flow results as well as the power at the PCC are transferred back to open_BEA for the next simulation step. Based on the power flow results, the dis(-charging) strategy for each BESS is calculated according to the selected operation strategy (cf. Section 3).

The main task of SimSES is to validate the effects of the target power provided by the energy management system of the open_BEA tool regarding efficiency, temperature, and degradation of the BESS when applied to the storage system. Each implemented component, such as the power electronics unit or the battery type, is responsible for modeling its relevant principles [12]. SimSES can be split into a simulation part for modeling the physical behavior of the BESS and an evaluation part that provides technical results for this study. The validated BESS time series are now included in the grid and an additional power flow analysis is conducted with eDisGo and the results are fed back to open_BEA for further analysis and visualization.

2.1. Example Grid and Denotations

As our aim is to investigate the effects of various BESS strategies on the distribution grid, an example grid including an open loop medium voltage (MV)-grid with 146 underlying low voltage (LV)-grids is used. The exemplary grid is connected to the overlying grid level through a single substation (PCC). This grid was chosen because of its resemblance to the typical German grid structure [13]. A graphical representation is shown in Figure 3 in which the circuit breakers are marked in gray, the 146 MV/LV transformers in light blue, the PCC in red, and all branch tees in dark blue.

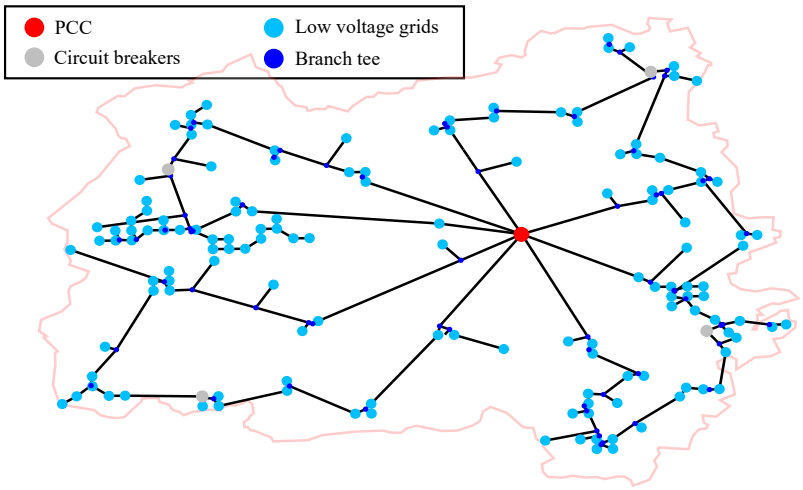

Figure 3. Graphical representation of the test distribution grid. The open circuit breakers are marked in gray, the MV/LV transformers are marked in light blue, the PCC in red, and all branch tees in dark blue.

The distribution grid includes 72 industrial consumers with an annual load above 100 MWh. Only these end-users can potentially benefit from applying peak shaving through a BESS as described in Section 3.1. Equation (1) defines the vector $\mathbf{N}$ for all industrial consumers b within the described distribution grid, with a total number of nodes B:

$$\mathbf{N} = [1, \cdots, \mathrm{b}, \cdots, \mathrm{B}]^{\mathrm{T}} \tag{1}$$

The current time step t within a defined time horizon T is defined by a vector H as shown in Equation (2):

$$\mathbf{H} = [1, \cdots, t, \cdots, \mathrm{T}] \tag{2}$$

Finally, the apparent power S_t^b at each node b for each time step t is defined by a matrix $\mathbf{S}$ (Equation (3)). The individual load profiles for these industrial consumers as well as all other consumers in the grid are according to a former publication [14].

$$\mathbf{S} = \begin{pmatrix} S_1^1 & \cdots & S_t^1 & \cdots & S_T^1 \\ \vdots & \ddots & \vdots & \ddots & \vdots \\ S_1^b & \cdots & S_t^b & \cdots & S_T^b \\ \vdots & \ddots & \vdots & \ddots & \vdots \\ S_1^B & \cdots & S_t^B & \cdots & S_T^B \end{pmatrix} \tag{3}$$

2.2. Battery Energy Storage System Setting

As described in the previous section, the SimSES simulation tool is used to validate the behavior of the BESS and to obtain detailed insights of the stress of the storage system. The parameters and settings shown in Table 1 are used in this paper to represent and simulate a realistic BESS. For the battery, a LIB with a lithium-iron-phosphate (LFP) cathode and a carbon/graphite (C) anode is selected [15]. This type of cell is particularly suitable for stationary applications due to its higher cycle durability [16]. The power electronics (AC/DC converter) is modeled by a constant load-independent part and a second part, including all load-dependent losses [17]. The maximum efficiency with this converter type is attained at 0.46· P^{rated} with an efficiency of η_{PE} = 96.9%. In accordance with the type of battery cell, the maximum e^{rate} is set to 1 h^{-1}.

Table 1. Parameters and settings of the simulated battery energy storage system (BESS) comprising battery cells, a power electronics unit, and a battery management system (BMS).

Parameter/Setting	Description/Value	Unit
Battery cell manufacturer	Murata	-
Battery cell type	US26650FTC1	-
Battery cell chemistry	LFP:C	-
Battery cell capacity	2850	mAh
Nominal cell voltage	3.2	V
Cell voltage range	2–3.6	V
Maximum efficiency of power electronics	96.9	%
Maximum e^{rate}	1	h^{-1}
Starting state of energy (SOE)	100	%

2.3. Simulation Setting

All results shown in this study are based on a simulation duration of six months, which represents a tradeoff between seasonal fluctuation and computation time, and a simulation step size of 15 min. The 15-minute time discretization is based on the fact that tariff calculations in Germany are calculated with maximum values in 15 min time step demand averages [18]. The simulation tools used in this work are implemented in Python. The linear optimization algorithm in Section 3.4 is implemented using MATLAB® programming language.

3. Problem Formulation and Applied Methods

3.1. Peak Shaving Operation Strategy: Strategy α

Motivated by a tariff system consisting of an energy demand charge and a peak power tariff, the aim of state-of-the-art peak shaving is to minimize the maximum power peak value at one specific node b within a defined billing period. The grid operator expects the use of this tariff scheme to avoid cable overloading and lower peak loads on the transformer [19].

In particular, large electricity consumers with an annual demand above a certain limit (in Germany 100 MWh [18]) can reduce the peak power provided by the power grid, which directly results in reduced operating expenses in the form of reduced grid charges. In order to reduce the peak power at a specific node b, the excess demand has to be either covered by another power providing unit, such as a diesel generator, or in our case, a BESS. The BESS is used to decouple the supply and demand over a specified time. Consequently, it is essential to find a peak shaving threshold $S^{thresh,b}$ above which the power is provided by the BESS.

In this work, we assume a straightforward charging approach as described in Equations (4) and (5): the BESS is charged whenever the apparent power S_t^b of the given load profile falls below a previously defined peak shaving threshold $S^{thresh,b}$ and discharged when the threshold is exceeded. With this strategy, the BESS is fully charged most of the time and is only used, if the local load is above the peak shaving threshold $S^{thresh,b}$. This operation mode is therefore independent of the load at the PCC and is therefore the most reliable strategy for a consumer with the only goal to reduce the local peak load. The methodology to find the peak shaving threshold $S^{thresh,b}$ is described in Section 3.4.

$$\text{Charging}: \quad S_t^b < S^{thresh,b} \quad \forall\, t \tag{4}$$

$$\text{Discharging}: \quad S_t^b > S^{thresh,b} \quad \forall\, t \tag{5}$$

3.2. Grid-Centered Peak Shaving: Strategy β

This subsection introduces an approach to use BESSs of distributed industrial customers to reduce power peaks at the grid operator's PCC. To achieve this, the vector of the

apparent power $\mathbf{S}^{\mathrm{PCC}}$ at the PCC is used to determine the operation strategy of BESSs of industrial customers instead of the local load profile vector.

$$\mathbf{S}^{\mathrm{PCC}} = \left[\mathrm{S}_1^{\mathrm{PCC}}, \cdots, \mathrm{S}_t^{\mathrm{PCC}}, \cdots, \mathrm{S}_{\mathrm{T}}^{\mathrm{PCC}}\right] \tag{6}$$

The optimization goal of grid-centered peak shaving is to minimize the peak power at the PCC instead of the power peak at a specific node b (Strategy α). Consecutively, the peak shaving thresholds of the industrial customers storage systems are recalculated in order to maximally reduce the peak power with a given BESS capacity by the previously introduced method, while $\mathbf{S}^{\mathrm{PCC}}$ serves as input for the peak shaving scheduling. The new threshold $\mathrm{S}^{\mathrm{thresh,PCC}}$ is calculated using an iterative approach [20].

3.3. Combined Peak Shaving Approach: Strategy γ

This subsection introduces an approach to use industrial customers' BESS to reduce both PCC and local peaks. First, a scaling factor $\mathrm{œ}_\mathrm{b}$ for every node b is calculated that sets the highest PCC power in relation to the highest power at a specific node b as showed in Equation (7).

$$\mathrm{œ}_\mathrm{b} = \frac{\max\left(\mathrm{S}_\mathrm{t}^\mathrm{b}\right)}{\max\left(\mathbf{S}^{\mathrm{PCC}}\right)} \tag{7}$$

In Equation (8), every load of the vector $\mathbf{S}^{\mathrm{PCC}}$ is multiplied by $\mathrm{œ}_\mathrm{b}$ to scale the PCC load profile down to the dimensions of the load profile at a specific node b. The scaled-down vector is denoted as $\mathbf{S}^{\mathrm{Scaled,b}}$.

$$\mathbf{S}^{\mathrm{Scaled,b}} = \mathbf{S}^{\mathrm{PCC}} \cdot \mathrm{œ}_\mathrm{b} \tag{8}$$

Based on $\mathbf{S}^{\mathrm{Scaled,b}}$ and the local load profile $\mathbf{S}_\mathrm{t}^\mathrm{b}$ at node b in Equation (9) a combined load profile $\mathrm{S}_t^{\mathrm{comb}}$ is created. For every point of time t in T, the maximum value of $\mathbf{S}^{\mathrm{Scaled,b}}$ and $\mathbf{S}^\mathrm{b}$ is used to obtain the combined load profile $\mathrm{S}_t^{\mathrm{comb}}$ that takes both the peaks at the PCC and the local peaks into account.

$$\mathbf{S}^{\mathrm{comb,b}} = \max(\mathbf{S}_\mathrm{t}^{\mathrm{Scaled,b}}, \mathbf{S}_\mathrm{t}^\mathrm{b}) \quad \forall t \tag{9}$$

Subsequently, $\mathrm{S}_t^{\mathrm{comb}}$ serves as the input for the peak shaving operation strategy. Again, the peak shaving thresholds of the industrial customers' storage systems are recalculated in order to maximally reduce the peak power with given capacities. The new threshold $\mathrm{S}^{\mathrm{thresh,comb}}$ is calculated using an iterative approach [20]. It must be noticed that this strategy is less reliable for the reduction of the local peak load than strategy α, since the BESS now also might be used to reduce the peak load at the PCC. However, this will be discussed in more detail in Section 4.

All three energy management strategies used in this work are depicted in Figure 4. All solid lines mark the results of the power flow analysis without BESS and the dashed lines marks the results of the power flow analysis including a BESS at a specific node b. The black solid line associated to the right y-axis shows the difference in power, covered by the BESS. In this example, a BESS with an energy content of 100 kWh is used to shave the peaks. The upper plot (a) shows the results for an exemplary industrial consumer if the BESS operates in a stand-alone peak shaving mode. While in this study the BESS works only in a real power operation, the apparent power is shown in the plot.

The solid line at subplot (b) shows the results for the power flow analysis at the PCC if the BESS at the same node b operates in a grid-centered peak shaving mode. The difference between with and without storage is very small due to the significantly higher load at the PCC compared to the load at a specific node b, so the dashed line follows the solid line almost exactly. The difference is displayed with the black solid line associated to the right y-axis. The maximum difference is with 100.2 kVA slightly higher than the maximum

power of the exemplary BESS. This is due to the fact that the BESS is placed at a specific node b and because of this, less energy has to be transmitted from the PCC to this node. This allows line losses to be reduced.

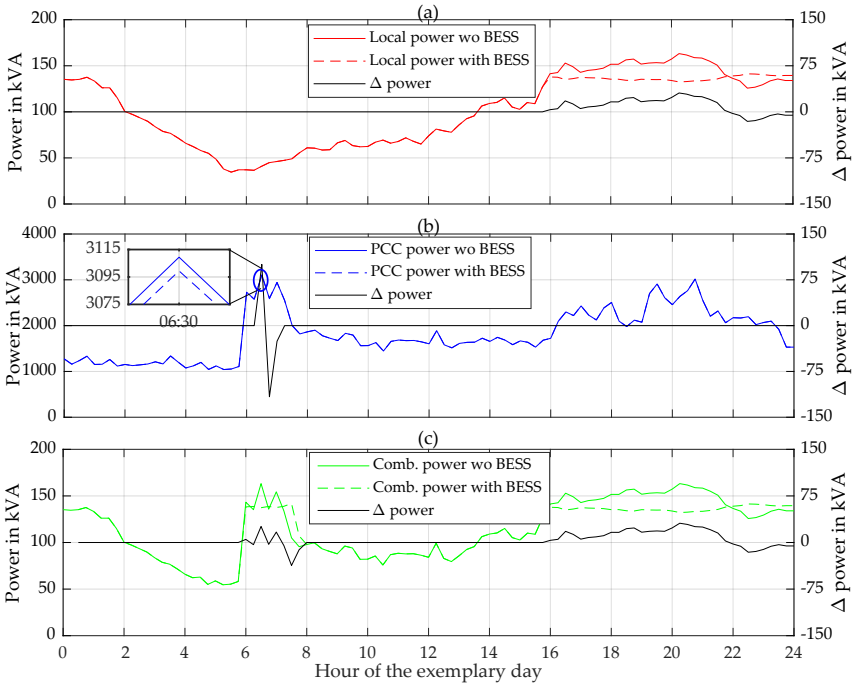

Figure 4. Graphical representation of all three energy management strategies used in this study. Subplot (**a**) shows an exemplary load profile for an industrial consumer at a specific node b. The related power at the point of common coupling is displayed in subplot (**b**) and subplot (**c**) shows the combined profile. The solid line marks the results of the power flow analysis without the battery energy storage system (BESS) at a specific node b and the dashed line marks the results of the power flow analysis including the BESS. The black solid line associated to the right y-axis shows the difference in power, covered by the BESS.

The lower plot (c) shows the combined load profile S_t^{comb} (solid line) for an exemplary industrial consumer, including the scaled load from the PCC. In the hours six to eight it can be seen that the scaled load profile from the PCC is responsible for the peak. Consequently the BESS shaves this peak and therefore ensures a lower peak load at the PCC. As with strategy α, the BESS also manages to shave the local peak between hours 16 and 22 with the combined strategy. Again the black solid line shows the difference in power, covered by the BESS. Compared to the other two strategies, the BESS is stressed twice on this exemplary day. The effects of this are discussed in the next chapter.

3.4. Battery Energy Storage System: Component Sizing

Sizing of the BESSs is conducted using an adopted version of a previously described linear programming optimization approach [9]: The cost function (Equation 10) allows finding a profit optimal compromise between electricity costs (tariff dominated by annual peak cost) as well as storage investment costs and a battery charge throughput penalty cost. Motivating low cycle counts and thus manageable cyclic aging within the project operation period, the throughput penalty cost (w_{tp}) are included and multiplied with the energy throughput ($BESS_{tp}$) of a BESS.

$$\mathrm{OBJ} = \mathrm{S}^{\mathrm{thresh,b}} \cdot \mathrm{p}_{\mathrm{peak}} \cdot \mathrm{t}_{\mathrm{proj}} + P_{max} \cdot \mathrm{e}^{\mathrm{rate}} \cdot \mathrm{p}_{\mathrm{BESS}}^{\mathrm{invest}} + BEES_{tp} \cdot w_{tp} \tag{10}$$

We choose a parameter set as follows: The storage investment costs p_{BESS}^{invest} are set to 350 $\frac{\$}{kWh}$ as motivated by [21]. A project operation/depreciation period of t_{proj}= 10 years well covered by BESS-assisted peak shaving analysis studies presented by Martins et al. [9] as well as degradation studies with the LFP:C battery cell is used herein [16,22].

In accordance with publicly available tariff tables provided by various distribution grids in Germany, a peak demand charge of $p_{peak} = 110 \frac{\$}{kVA \cdot a}$ was chosen. The e^{rate} has been set to $1\,h^{-1}$ as described in Section 2.2. For the lithium-ion based BESS investigated herein, we chose a value of unity for the this parameter yielding a well-balanced system layout and shaving of distinguished power peaks. Battery cycling and energy throughput is penalized using a weighting factor of w_{tp}= 0.001 $\frac{\$}{kWh}$ in order that the BESS is not dis(-charging) needlessly [23].

The boundary conditions of the BESS are described in the constraints Equations (11)–(15). The actual energy content for a specific time step t of a BESS, denoted as $E_t^{actual,b}$, must remain within the physical bounds of a storage system:

$$0 \cdot E^{nominal} \leq E_t^{actual,b} \leq 1 \cdot E^{nominal} \tag{11}$$

The charging and discharging powers ($P_t^{charge,b}$ and $P_t^{discharge,b}$) has to be lower than the rated power P^{rated} of the power electronics.

$$P_t^{charge,b} \leq P^{rated} \quad \forall\, b \tag{12}$$

$$P_t^{discharge,b} \geq -P^{rated} \quad \forall\, b \tag{13}$$

The charging and discharging power ($P_t^{charge,b}$ and $P_t^{discharge,b}$) for each step t and each BESS is also limited by the respective maximum energy rate (e^{rate}) of the storage system.

$$P_t^{charge,b} \leq e^{rate} \cdot E^{nominal} \quad \forall\, b \tag{14}$$

$$P_t^{discharge} \geq -e^{rate} \cdot E^{nominal} \quad \forall\, b \tag{15}$$

The actual energy content $E_t^{actual,b}$ of a BESS is calculated by adding the net charged energy $E_t^{charge,b}$ to the energy content of the previous time step and subtracting the discharged energy $E_t^{discharge,b}$. This energy conservation equation of a BESS is defined in Equation (16).

$$E_t^{actual,b} = E_{t-1}^{actual,b} + E_t^{charge,b} - E_t^{discharge,b} \tag{16}$$

In order to derive the best-suited BESS system sizing, we have applied this formulation (minimize (OBJ)) to the entire set of 72 scenarios. The linear optimization results in BESSs capacities of less than 10 kWh for 40 out of the 72 customers. These small storage sizes are neglected in this study, because the capacity is more in the range of home energy storage systems and no longer in the range of industrial storage systems [24]. The cost assumptions for the initial costs p_{BESS}^{invest} are therefore no longer valid. Furthermore, the peak load reduction and thus the cost savings would be minor in these cases and therefore are not considered further. Figure 5 visualizes relative peak shaving limits $S^{thresh,b}$ in % for all 32 BESS with a capacity above 10 kWh. The lower plot (b) shows the capacity for just these BESS.

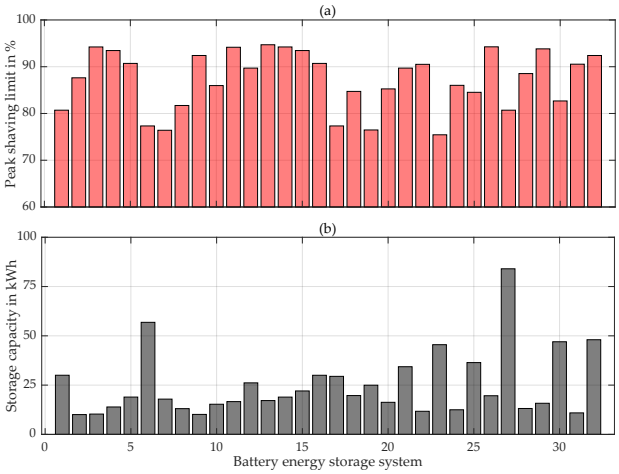

Figure 5. Results of the component sizing optimization. The upper plot (**a**) shows the peak shaving limits $S^{thresh,b}$ in % of the original peak power for all 32 battery energy storage system (BESS) with a capacity above 10 kWh. The lower plot (**b**) shows the capacity for just these BESS.

4. Case Studies and Discussion

This section discusses the impact of various strategies of storage systems on the test distribution grid for a six months simulation period. For this purpose, the load flows and potential reductions in peak load at the PCC are evaluated in detail and compared to the results obtained with a state-of-the-art peak shaving algorithm (Strategy α). The effects of these strategies as well as the resulting stress on the BESS are also investigated.

Figure 6 shows the relative peak load reduction for each of the 32 simulations with various operating strategies for the BESS. The reduction of the peak load at the local node b (= location of the BESS) is plotted on the abscissa and the reduction of the peak load at the PCC can be seen on the ordinate. The results are each related to the maximum power of the storage system. Based on an e^{rate} of 1 as defined in Section 2.2, the maximum power in kW is equal to the capacity of each BESS in kWh.

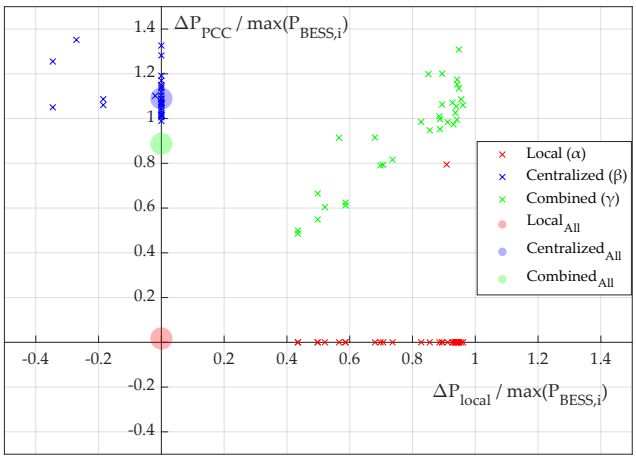

Figure 6. Relative peak load reduction for each simulation with various operating strategies for the battery energy storage system (BESS). The reduction of the peak load at the local node b (= location of the BESS) is plotted on the abscissa and the reduction of the peak load at the point of common coupling (PCC) can be seen on the ordinate. The red crosses show the reduction if the BESS is operated with strategy α. The blue crosses show the results for strategy β and the green ones for the combined approach (Strategy γ). The filled circles show the reduction of the peak load at the PCC if all 32 BESSs are integrated into the grid simultaneously.

The red crosses show the reduction if the BESS is operated with strategy α. It can be seen that the storage system reaches a reduction of the peak load at the associated node b in all 32 simulations. In most of the cases no peak load reduction at the PCC can be reached. The reason for this behavior is that in these cases the peaks in the load profile have a longer duration and thus the energy content is the limiting factor. As described in Section 3 and exemplary shown in Figure 4, the load profiles include reactive power, while the BESS in this study operates with active power only.

The initial motivation for a peak power tariff was to smooth out power peaks in the entire distribution grid. However, with this state-of-the-art peak shaving strategy only one case shows a reduction at the PCC. Even with all 32 storage systems integrated in the grid at the same time, only very small (13.63 kVA) improvements can be achieved with a conventional peak shaving algorithm.

The reduction for strategy β is marked with blue crosses. Since only one very high peak occurs at the PCC during the period under consideration, the change is almost identical with all 32 storage systems and corresponds to the maximum possible discharge power. Due to the fact that the BESS is located in different locations in the grid, line losses can be reduced during discharge. This results in relative reductions above one. However, for industrial customers themselves, the centralized algorithm never achieves a reduction in the peak load in this simulation setting.

The green crosses show the reduction if the BESS is operated in accordance to the newly developed combined approach (Strategy γ). In this case, both the local peak load and the global peak load will be reduced. It can be seen that the reduction at the location of the storage is nearly as high as with the state-of-the-art peak shaving strategy. However, a significant peak load reduction in the PCC is now also achieved. The filled circles in the figure show the reduction of the peak load at the PCC if all 32 BESSs are integrated into the grid simultaneously. Again, due to the fact that only one very high peak occurs at the PCC, the reduction with the centralized approach is almost the summed-up maximum possible discharge power of all BESSs. In contrast, with the combined approach with a reduction of 706.70 kVA, almost the same reduction is achieved as with the centralized approach (868.02 kVA).

Figure 7 supports the statements from the relative reduction plot by showing the absolute reduction for each simulation. The upper plot (a) shows the absolute peak load reduction for each simulation if the BESS is operated with strategy α. It can be seen that the peak reduction at the respective node b is minimum 5.05 kVA and maximum 53.3 kVA, which results with the numbers of Section 3.4 in an annual revenue of approximately $ 555.5 to $ 5,858.6. However, with this state-of-the-art peak shaving strategy only simulation 13 achieves a reduction at the PCC with 13.6 kVA. All others fail to reduce the peak load at the PCC. With the centralized approach (Strategy β), depicted in plot (b) the peak load at the PCC is reduced by 10.4 kVA to 83.1 kVA. The industrial consumers peak load is not reduced in any case, but is increased by up to 16.6 kVA in six cases.

The lower plot (c) shows the absolute peak load reduction for each simulation if the BESS is operated with strategy γ. The red bars show the difference in peak load at a local node b (=storage location), the blue bars show the peak load reduction at the PCC. The industrial consumers peak load reduction differs only in two cases above 1.0 kVA. The maximum occurs in simulation six with 2.8 kVA, which would result in a decreased annual revenue of $ 308.0. However, with this combined approach the peak load at the PCC is also reduced by 5.6 kVA to 56.7 kVA. Compared to the maximums before (53.3 kVA and 83.1 kVA), which both occurs at simulation six, the combined approach achieves a summed up reduction of 107.2 kVA. Integrating all 32 BESSs to the grid simultaneously, a reduction at the PCC of 706.7 kVA can be achieved.

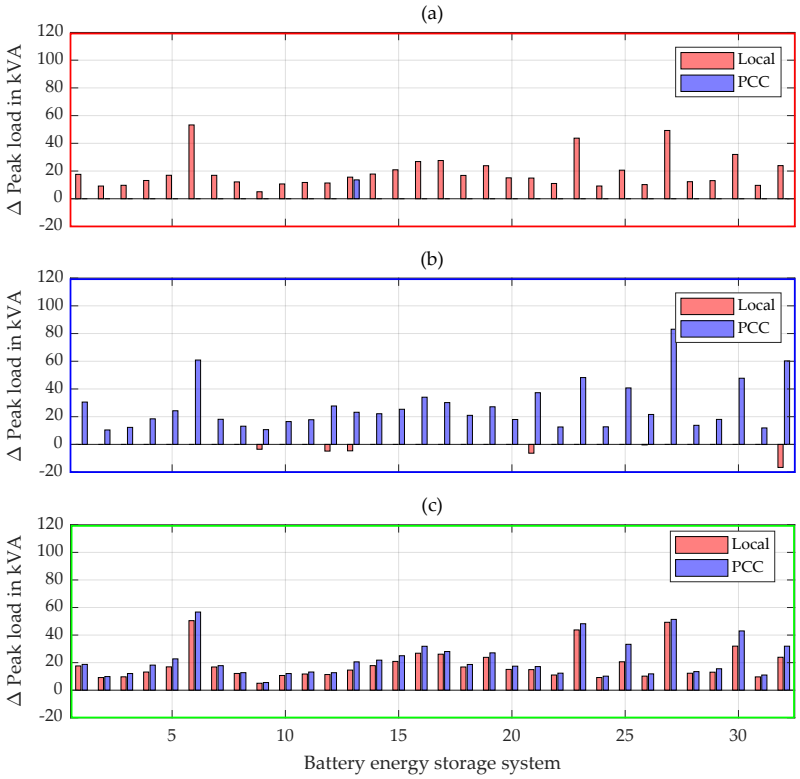

Figure 7. The upper plot (**a**) shows the absolute peak load reduction for each simulation if the battery energy storage system (BESS) is operated with strategy α. Plot (**b**) shows the results for the centralized approach (Strategy β). The lower plot (**c**) shows the absolute peak load reduction for each simulation if the BESS is operated with the newly developed combined approach (Strategy γ). The red bars show the difference in peak load at a local node b, the blue bars show the peak load reduction at the point of common coupling (PCC).

To evaluate the reduction in detail, the additional stress on the energy storage must also be considered. Figure 8 shows the results for all simulations using various key characteristics, which have been defined in a previous publication [14]. Subplot (a) shows the number of full equivalent cycles and the mean round-trip efficiency is displayed in subplot (b). The remaining characteristics describe the stress on the BESSs in greater detail. Subplot (c) shows the average cycle depth in discharge direction and the average resting time between two actions is illustrated in subplot (d). The number of alternations between charging and discharging (sign changes) per day is indicated in subplot (e), while subplot (f) shows the energy in relation to the BESS capacity that is charged or discharged between sign changes, respectively.

The highest peak at the PCC is 40.9 MVA and thus 1.4 MVA higher than the second highest peak. Consequently, all BESSs at the centralized approach (Strategy β) are only able to reduce this one maximum 15-minute peak and therefore only one sign change occurs. This also results in high resting times for the six month simulation period. Due to the losses in the storage system the total number of full equivalent cycles is 0.28 and consequently the cycle depth in discharge direction is 28% with a storage systems e^{rate} of one.

Comparing the results for strategy α and strategy γ, it can be seen that the BESSs have on average 1.2 full equivalent cycles more than the storage systems operating with a conventional peak shaving strategy. In the case of the LIB used, this results in a deviation in the remaining capacity of 0.01% (95.31 to 95.32) for the six month simulation period due to the high cycle stability. Resulting from very low additional stress on the storage system, there are hardly any differences for almost all other key characteristics. Only the duration

of the resting times between two actions falls significantly from 237.8 h to 131.3 h. However, this average resting time is still quite long and the storage systems remain underutilized with both strategies and it should be considered to use these to achieve additional revenues by using a multi-use approach [25]—a topic beyond the scope of this study.

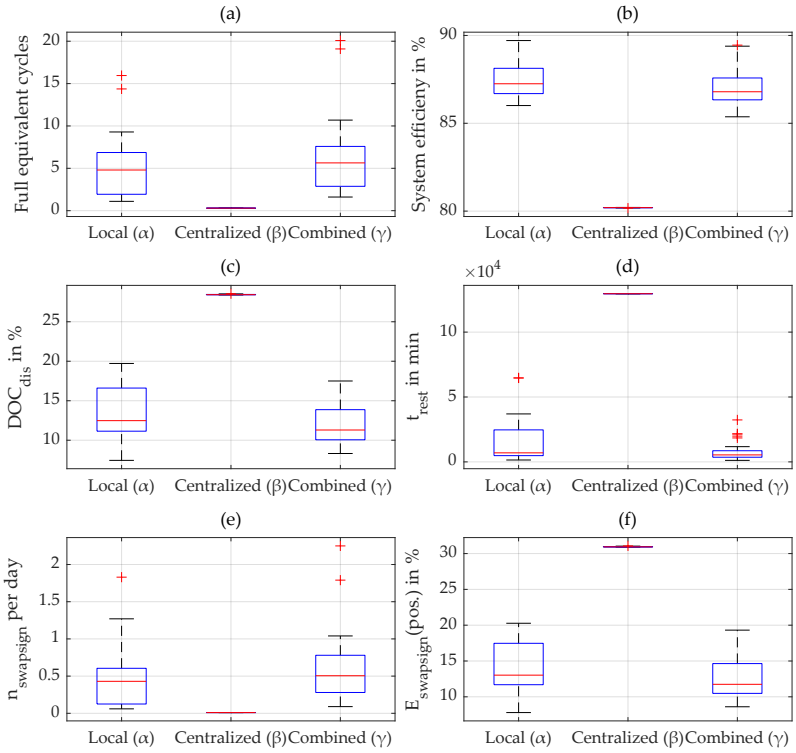

Figure 8. Detailed results about the additional stress on the battery energy storage systems (BESSs) for a six month simulation period. Subplot (**a**) shows the number of full equivalent cycles and the mean round-trip efficiency in % is displayed in subplot (**b**). Subplot (**c**) shows the average cycle depth in discharge direction in % and the average resting time in minutes between two actions is illustrated in subplot (**d**). The number of alternations between charging and discharging (sign changes) per day is indicated in subplot (**e**). Finally, subplot (**f**) shows the energy in relation to the BESS capacity that is charged between these sign changes.

5. Conclusions and Outlook

This paper presented a method to reduce the peak power at a specific node as well as at the transformer or PCC in distribution grids or microgrids by using BESSs. The storage systems are located at 32 various industrial consumers with individual load profiles in a MV-grid with 146 underlying LV-grids. A method of a combined operation strategy for BESSs located at industrial consumers has been developed to achieve both an improvement in the distribution grid as well as electricity bill savings for industrial consumers. By using and adapting the open_BEA framework, accurate co-simulations of BESSs and distribution grids are performed. The stress on the LIB-based stationary BESSs at the various strategies is evaluated by adapting the holistic energy storage simulation framework SimSES.

The newly developed combined approach (Strategy γ) uses a scaling factor for the power profile at the PCC in order to combine this load profile with the load profile of an individual industrial consumer. This combined profile serves as the input for the peak shaving operation strategy and the results are compared to a state-of-the-art peak shaving strategy (industrial consumer only; Strategy α) and a centralized approach (PCC only; Strategy β). The BESSs are economical optimally sized using a linear optimization approach.

Results show that with strategy γ both the local peak load and the global peak load can be reduced. The reduction at the location of the storage is nearly as high as with strategy α. With strategy γ the peak load at the PCC is reduced by 5.6 kVA to 56.7 kVA and the total reduction is always higher than with strategy α or strategy β. Although in this scenario the BESSs reduce both peaks, the additional stress for the six month simulation period is on average only 1.2 full equivalent cycles higher. This additional stress results in slightly higher aging (0.01%) with the used LIB.

Accelerated aging as well as adaptions in the energy management systems would have to be compensated financially by the grid operator to the storage owner or industrial consumer. However, it must be taken into account that the grid operator benefits economically by being able to avoid a possible grid reinforcement or transformer upgrade. The framework shown in this study requires communication (e.g., via the 5G communication standard [26,27] or the IEC 60870 standard [28]) between the grid operator and its current load at the PCC and the industrial consumer including the storage system. In addition, the algorithms introduced in this study require the creation of an economic and legal framework.

Future Work and Outlook

This study focuses on the technical potential of combined operation strategies for storage systems located at various industrial consumers in a distribution grid. The additional reduction in the peak load at the PCC may avoid the need of grid reinforcement or transformer exchange. Future work should focus on an economic analysis to compare the cost of installing a BESS with the costs of conventional grid reinforcement. From a grid perspective, future studies could also focus more on other grid-related applications as an additional service of the BESS, such as reactive power control.

Furthermore a highly discussed topic is the ecological assessment of storage systems. In addition to the economic assessment, it might also be worthwhile to perform an ecological analysis. This would allow a more precise comparison of the CO_2 impact of BESSs and the CO_2 impact caused by conventional grid reinforcement.

Author Contributions: D.K.: Conceptualization, Methodology, Software, Investigation, Writing—Original Draft L.S.: Methodology, Software, Formal analysis, Writing—Original Draft, Visualization N.C.: Methodology, Software, Writing—Review and Editing A.J.: Writing—Review and Editing, Supervision, Funding acquisition H.H.: Methodology, Writing—Review abd Editing, Supervision, Funding acquisition. All authors have read and agreed to the published version of the manuscript.

Funding: This publication was financially supported by the German Federal Ministry for Economic Affairs and Energy within the research project open_BEA (Grant No. 03ET4072), which is managed by Project Management Jülich. The responsibility for this study rests with the authors.

Institutional Review Board Statement: Not applicable.

Informed Consent Statement: Not applicable.

Data Availability Statement: Not applicable.

Conflicts of Interest: The authors declare no conflict of interest.

Parameters & variables

$E_t^{\text{actual,b}}$	actual energy content of a battery energy storage system at a specific node b for a specific time step t
$E_t^{\text{charge,b}}$	charged energy of a battery energy storage system at a specific node b for a specific time step t
$E_t^{\text{discharge,b}}$	discharged energy of a battery energy storage system at a specific node b for a specific time step t
$P_t^{\text{charge,b}}$	charging power of a battery energy storage system at a specific node b for a specific time step t
$P_t^{\text{discharge,b}}$	discharging power of a battery energy storage system at a specific node b for a specific time step t
P^{rated}	rated power of the power electronics
BESS_{tp}	energy throughput of a battery energy storage system
S_t^{b}	apparent power at a specific node b for a specific time step t
S_t^{comb}	combined apparent power including the power at a specific node b and the apparent power at the point of common coupling
$S^{\text{thresh,PCC}}$	peak shaving threshold power for a battery energy storage system operating with the grid-centered approach
$S^{\text{thresh,b}}$	peak shaving threshold power for a specific node b
$S^{\text{thresh,comb}}$	peak shaving threshold power for a battery energy storage system operating with the combined approach
œ_{b}	scaling factor: peak power at the point of common coupling in relation to the peak load at a specific node b
$\mathbf{S}^{\text{PCC}}$	vector of the apparent power at the point of common coupling for each time step t
$\mathbf{S}^{\text{Scaled,b}}$	scaled apparent power of the point of common coupling in relation to the peak load at a specific node b
$\mathbf{S}$	matrix for the apparent power at each node b for each time step t
e^{rate}	energy rate of the battery energy storage system
$\text{p}_{\text{BESS}}^{\text{invest}}$	storage investment costs per kWh
p_{peak}	annual peak demand charge per kVA
t_{proj}	project operation/depreciation period in years
w_{tp}	throughput penalty costs

Abbreviations

AC	alternating current
BESS	battery energy storage system

BMS	battery management system
C	carbon/graphite
DC	direct current
eDisGo	software for electric distribution grid optimization
LFP	lithium-iron-phosphate
LIB	lithium-ion battery
LV	low voltage
MV	medium voltage
open_BEA	open battery models for electrical grid applications
PCC	point of common coupling
SimSES	simulation of stationary energy storage systems
SOE	state of energy

Sets & indices

B	total number of nodes b in the distribution grid
H	time vector for the simulation period (time horizon)
T	time horizon
N	vector for all industrial consumers in the distribution grid
b	nodes with industrial consumers in the distribution grid
t	specific time step

References

1. Bollen, M.; Rönnberg, S. Hosting Capacity of the Power Grid for Renewable Electricity Production and New Large Consumption Equipment. *Energies* **2017**, *10*, 1325. [CrossRef]
2. Benetti, G.; Caprino, D.; Della Vedova, M.L.; Facchinetti, T. Electric load management approaches for peak load reduction: A systematic literature review and state of the art. *Sustain. Cities Soc.* **2016**, *20*, 124–141. [CrossRef]
3. Brinkel, N.; Schram, W.L.; AlSkaif, T.A.; Lampropoulos, I.; van Sark, W. Should we reinforce the grid? Cost and emission optimization of electric vehicle charging under different transformer limits. *Appl. Energy* **2020**, *276*, 115285. [CrossRef]
4. Nykvist, B.; Nilsson, M. Rapidly falling costs of battery packs for electric vehicles. *Nat. Clim. Chang.* **2015**, *5*, 329–332. [CrossRef]
5. Mehr, T.H.; Masoum, M.A.; Jabalameli, N. Grid-connected Lithium-ion battery energy storage system for load leveling and peak shaving. In Proceedings of the 2013 Australasian Universities Power Engineering Conference (AUPEC), Hobart, TAS, Australia, 29 September–October 2013; pp. 1–6. [CrossRef]
6. Oudalov, A.; Cherkaoui, R.; Beguin, A. Sizing and Optimal Operation of Battery Energy Storage System for Peak Shaving Application: 2007 IEEE Lausanne Power Tech. In Proceedings of the IEEE PowerTech, 2007 IEEE Lausanne, Lausanne, Switzerland, 1–5 July 2007; pp. 1–5. [CrossRef]
7. Mamun, A.; Narayanan, I.; Wang, D.; Sivasubramaniam, A.; Fathy, H.K. Multi-objective optimization of demand response in a datacenter with lithium-ion battery storage. *J. Energy Storage* **2016**, *7*, 258–269. [CrossRef]
8. Tiemann, P.H.; Bensmann, A.; Stuke, V.; Hanke-Rauschenbach, R. Electrical energy storage for industrial grid fee reduction—A large scale analysis. *Energy Convers. Manag.* **2020**, *208*, 112539. [CrossRef]
9. Martins, R.; Hesse, H.; Jungbauer, J.; Vorbuchner, T.; Musilek, P. Optimal Component Sizing for Peak Shaving in Battery Energy Storage System for Industrial Applications. *Energies* **2018**, *11*, 2048. [CrossRef]
10. Danish, S.M.S.; Ahmadi, M.; Danish, M.S.S.; Mandal, P.; Yona, A.; Senjyu, T. A coherent strategy for peak load shaving using energy storage systems. *J. Energy Storage* **2020**, *32*, 101823. [CrossRef]
11. Kucevic, D.; Englberger, S.; Sharma, A.; Trivedi, A.; Tepe, B.; Schachler, B.; Hesse, H.; Srinivasan, D.; Jossen, A. Reducing grid peak load through the coordinated control of battery energy storage systems located at electric vehicle charging parks. *Appl. Energy* **2021**, *295*, 116936. [CrossRef]
12. Naumann, M.; Truong, C.N.; Schimpe, M.; Kucevic, D.; Jossen, A.; Hesse, H.C. SimSES: Software for techno-economic Simulation of Stationary Energy Storage Systems. In *International ETG Congress 2017*; ETG-Fachbericht; VDE: Berlin/Offenbach, Germany, 2017; pp. 442–447.
13. Müller, U.P.; Schachler, B.; Scharf, M.; Bunke, W.D.; Günther, S.; Bartels, J.; Pleßmann, G. Integrated Techno-Economic Power System Planning of Transmission and Distribution Grids. *Energies* **2019**, *12*, 2091. [CrossRef]

14. Kucevic, D.; Tepe, B.; Englberger, S.; Parlikar, A.; Mühlbauer, M.; Bohlen, O.; Jossen, A.; Hesse, H. Standard battery energy storage system profiles: Analysis of various applications for stationary energy storage systems using a holistic simulation framework. *J. Energy Storage* **2020**, *28*, 101077. [CrossRef]
15. Murata. *Data Sheet of Sony Fortelion US26650FTC1 Battery Cell*; Murata: Kyoto, Japan, 2017.
16. Naumann, M.; Spingler, F.B.; Jossen, A. Analysis and modeling of cycle aging of a commercial $LiFePO_4$/graphite cell. *J. Power Sources* **2020**, *451*, 227666. [CrossRef]
17. Notton, G.; Lazarov, V.; Stoyanov, L. Optimal sizing of a grid-connected PV system for various PV module technologies and inclinations, inverter efficiency characteristics and locations. *Renew. Energy* **2010**, *35*, 541–554. [CrossRef]
18. German Federal Office of Justice. Stromnetzentgeltverordnung. (In German). Avaiable online: https://www.gesetze-im-internet.de/stromnev/BJNR222500005.html (accessed on 2 November 2021)
19. Tuunanen, J.; Honkapuro, S.; Partanen, J. Power-based distribution tariff structure: DSO's perspective. In Proceedings of the 2016 13th International Conference on the European Energy Market (EEM), Porto, Portuga, 6–9 June 2016; pp. 1–5. [CrossRef]
20. Collath, N.; Englberger, S.; Jossen, A.; Hesse, H. *Reduction of Battery Energy Storage Degradation in Peak Shaving Operation through Load Forecast Dependent Energy Management*; NEIS 2020, Ed.; VDE/ETG: Hamburg, Germany, 2020; pp. 1–6.
21. Mongird, K.; Viswanathan, V.; Balducci, P.; Alam, J.; Fotedar, V.; Koritarov, V.; Hadjerioua, B. An Evaluation of Energy Storage Cost and Performance Characteristics. *Energies* **2020**, *13*, 3307. [CrossRef]
22. Naumann, M.; Schimpe, M.; Keil, P.; Hesse, H.C.; Jossen, A. Analysis and modeling of calendar aging of a commercial LiFePO4/graphite cell. *J. Energy Storage* **2018**, *17*, 153–169. [CrossRef]
23. Vetter, J.; Novák, P.; Wagner, M.R.; Veit, C.; Möller, K.C.; Besenhard, J.O.; Winter, M.; Wohlfahrt-Mehrens, M.; Vogler, C.; Hammouche, A. Ageing mechanisms in lithium-ion batteries. *J. Power Sources* **2005**, *147*, 269–281. [CrossRef]
24. Figgener, J.; Stenzel, P.; Kairies, K.P.; Linßen, J.; Haberschusz, D.; Wessels, O.; Angenendt, G.; Robinius, M.; Stolten, D.; Sauer, D.U. The development of stationary battery storage systems in Germany—A market review. *J. Energy Storage* **2020**, *29*, 101153. [CrossRef]
25. Englberger, S.; Jossen, A.; Hesse, H. Unlocking the Potential of Battery Storage with the Dynamic Stacking of Multiple Applications. *Cell Rep. Phys. Sci.* **2020**, *1*. [CrossRef]
26. Gheisarnejad, M.; Khooban, M.H.; Dragicevic, T. The Future 5G Network-Based Secondary Load Frequency Control in Shipboard Microgrids. *IEEE J. Emerg. Sel. Top. Power Electron.* **2020**, *8*, 836–844. [CrossRef]
27. Garau, M.; Anedda, M.; Desogus, C.; Ghiani, E.; Murroni, M.; Celli, G. A 5G cellular technology for distributed monitoring and control in smart grid. In Proceedings of the 2017 IEEE International Symposium on Broadband Multimedia Systems and Broadcasting (BMSB), Cagliari, Italy, 7–9 June 2017; pp. 1–6. [CrossRef]
28. Hänsch, K.; Naumann, A.; Wenge, C.; Wolf, M. Communication for battery energy storage systems compliant with IEC 61850. *Int. J. Electr. Power Energy Syst.* **2018**, *103*, 577–586. [CrossRef]

6 Reducing grid peak load through the coordinated control of battery energy storage systems located at electric vehicle charging parks

Main research questions: *Is a multi-storage approach suitable for grid planning? And how should the battery control be coordinated?*

A predicted high EV penetration in urban distribution grids leads to challenges, such as line over loading for the grid operator. In particular introducing charging parks for shared cars or electric taxis in these urban areas may require grid reinforcement. In such a case installation of grid integrated storage systems represent a technical alternative. This paper proposes a method of coordinated control for multiple BESSs located at electrical vehicle charging parks in a distribution grid using linear optimization in conjunction with time series modelling.

As in Chapter 5, the objective is to reduce the peak power at the PCC in existing distribution grids with a high share of electric vehicles. The combination of the tools eDisGo and SimSES enables a more realistic simulation of the effects of storage systems with different EMSs on the distribution grid. The case study involves three charging parks with various sizes of coupled storage systems in a test grid in order to apply a novel approach to control all BESSs simultaneously.

A linear programming optimization tool for energy storage systems (lp_opt) is used to control the EMS of several storage system in a coordinated manner. Like SimSES, the lp_opt tool was developed at the Institute for Electrical Energy Storage Technology at the Technical University of Munich [8]. Aiming to reduce the peak power at the PCC, lp_opt calculates an operation strategy for each BESS, subject to linearized constraints of the distribution grid and the BESS. The tool was designed in the MATLAB optimization environment using a problem-based approach and besides the mathematical optimization solver of MATLAB, the tool is also compatible with the Gurobi solver [162]. In the following the highlights of this publication are summarized:

- An EMS for a multi-storage approach is developed to control and coordinate the charging and discharging of the BESSs. The method is applied to a test distribution grid and compared with a state-of-the-art peak shaving strategy.
- The impact of BESSs, located at charging parks, is evaluated on the basis of peak load reduction at the PCC with varying EV-share and BESS capacities.
- The coordinated control strategy can significantly reduce the peak load at the PCC. This allows grid operators to reduce or avoid grid reinforcement without influencing EV charging quality with reduced charging power or vehicle-to-grid approaches.

Analyzing the results of the BESSs using SimSES shows that the stress on the storage system is comparable with state-of-the-art peak shaving strategies. However, referring to Chapter 5 this multi-

storage approach now also needs communication between the storage systems. The method of this study is applied to an exemplary grid, but the open-source code available to the research community is easily adaptable to other individual parameter sets.

Author contribution Daniel Kucevic was the principal author tasked with coordinating and writing the paper and developing the software framework. Stefan Englberger assisted with integrating the optimization tool. Both Anurag Sharma and Anupam Trivedi reviewed the manuscript and gave valuable input throughout the developing of the methodology. Benedikt Tepe helped with gathering and preparation of the data. Birgit Schachler assisted with integrating the power flow analysis tool. Holger Hesse reviewed the manuscript and was giving valuable input throughout the manuscript preparation. Both Dipti Srinivasan and Andreas Jossen contributed via fruitful scientific discussions and reviewed the manuscript. All authors discussed the data and commented on the results.

Reducing grid peak load through the coordinated control of battery energy storage systems located at electric vehicle charging parks

Daniel Kucevic, Stefan Englberger, Anurag Sharma, Anupam Trivedi, Benedikt Tepe, Birgit Schachler, Holger Hesse, Dipti Srinivasan, Andreas Jossen

Applied Energy, Volume 295, 2021

Permanent weblink:
https://doi.org/10.1016/j.apenergy.2021.116936

Applied Energy 295 (2021) 116936

Contents lists available at ScienceDirect

Applied Energy

journal homepage: www.elsevier.com/locate/apenergy

Reducing grid peak load through the coordinated control of battery energy storage systems located at electric vehicle charging parks

Daniel Kucevic [a,*], Stefan Englberger [a], Anurag Sharma [b], Anupam Trivedi [c], Benedikt Tepe [a], Birgit Schachler [d], Holger Hesse [a], Dipti Srinivasan [c], Andreas Jossen [a]

[a] Institute for Electrical Energy Storage Technology, Technical University of Munich (TUM), Arcisstr. 21, 80333 Munich, Germany
[b] Newcastle University in Singapore (NU), 172A Ang Mo Kio Avenue 8, 567739, Singapore
[c] Department of Electrical and Computer Engineering, National University of Singapore (NUS), 4 Engineering Drive 3, 117583, Singapore
[d] Reiner Lemoine Institute gGmbH (RLI), Rudower Chaussee 12, 12489 Berlin, Germany

GRAPHICAL ABSTRACT

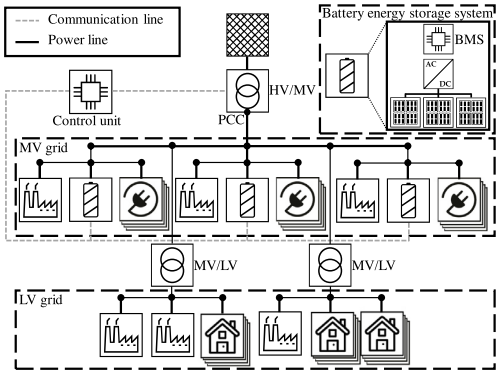

ARTICLE INFO

Keywords:
Battery energy storage system
Lithium-ion
Grid integrated energy storage
Electric vehicle charging
Linear optimization
Distribution grid
Peak load reduction

ABSTRACT

Both global climate change and the decreasing cost of lithium-ion batteries are enablers of electric vehicles as an alternative form of transportation in the private sector. However, a high electric vehicle penetration in urban distribution grids leads to challenges, such as line over loading for the grid operator. In such a case installation of grid integrated storage systems represent an alternative to conventional grid reinforcement. This paper proposes a method of coordinated control for multiple battery energy storage systems located at electrical vehicle charging parks in a distribution grid using linear optimization in conjunction with time series modeling. The objective is to reduce the peak power at the point of common coupling in existing distribution grids with a high share of electric vehicles. An open source simulation tool has been developed that aims to couple a stand alone power flow model with a model of a stand alone battery energy storage system. This combination of previously disjointed tools enables more realistic simulation of the effects of storage systems in different operating modes on the distribution grid. Further information is derived from a detailed analysis of the storage system based on six key characteristics. The case study involves three charging parks with various sizes of coupled storage systems in a test grid in order to apply the developed method. By operating these storage systems using the coordinated control strategy, the maximum peak load can be reduced by 44.9%. The rise in peak load reduction increases linearly with small storage capacities, whereas saturation behavior can be observed above 800 kWh.

* Corresponding author.
E-mail address: daniel.kucevic@tum.de (D. Kucevic).

https://doi.org/10.1016/j.apenergy.2021.116936
Received 27 January 2021; Received in revised form 12 March 2021; Accepted 4 April 2021
Available online 30 April 2021

Abbreviations

AC	Alternating current
BESS	Battery energy storage system
BMS	Battery management system
C	Carbon/graphite
DC	Direct current
eDisGo	Software for electric distribution grid optimization
EV	Electric vehicle
FEC	Full equivalent cycle
HV	High voltage
LFP	Lithium-iron-phosphate
LIB	Lithium-ion battery
lp_opt	Linear programming optimization tool for energy storage systems
LV	Low voltage
MV	Medium voltage
open_BEA	Open battery models for electrical grid applications
PCC	Point of common coupling
SimSES	Simulation of stationary energy storage systems
SOE	State of energy
V2G	Vehicle-to-grid

Sets & indices

B	Total number of nodes b in the distribution grid
b	Nodes in the distribution grid
b_j	Specific node b at location j in the distribution grid
b_k	Specific node b at location k in the distribution grid
H	Time vector for the simulation period (time horizon)
N	Vector for all nodes in the distribution grid
T	Time horizon
t	Specific time step

Parameters & variables

$\cos\varphi$	Power factor: ratio of real power to apparent power
η_b	Efficiency between the point of common coupling and a specific node b
η_{PE}	Efficiency of the power electronics
$E_t^{actual,b}$	Actual energy content of a battery energy storage system at a specific node b for a specific time step t
$E_t^{charge,b}$	Charged energy of a battery energy storage system at a specific node b for a specific time step t
$E_t^{discharge,b}$	Discharged energy of a battery energy storage system at a specific node b for a specific time step t
$E^{nominal}$	Nominal energy content of a battery energy storage system
e^{rate}	Energy rate of the battery energy storage system
$\mathbf{I}^{b_j \to b_k}$	Vector for the line current between two specific nodes b (b_j and b_k) for each time step t before integrating charging parks
$I_t^{b_j \to b_k}$	Line current between two specific nodes b (b_j and b_k) for a specific time step t before integrating charging parks
$\mathbf{I}^{*,b_j \to b_k}$	Vector for the line current between two specific nodes b (b_j and b_k) for each time step t after integrating charging parks
$I_{max}^{b_j \to b_k}$	Rated (maximum) line current between two specific nodes b (b_j and b_k)
$I_t^{*,b_j \to b_k}$	Line current between two specific nodes b (b_j and b_k) for a specific time step t after integrating charging parks
$P_t^{charge,b}$	Charging power of a battery energy storage system at a specific node b for a specific time step t
$P_t^{discharge,b}$	Discharging power of a battery energy storage system at a specific node b for a specific time step t
P^{rated}	Rated power of the power electronics
$\mathbf{S}$	Matrix for the apparent power at each node b for each time step t before integrating charging parks
$\mathbf{S}^{*,PCC}$	Vector of the apparent power at the point of common coupling for each time step t after integrating charging parks
$S_t^{*,PCC}$	Apparent power at the point of common coupling for a specific time step t after integrating charging parks
S_t^b	Apparent power at a specific node b for a specific time step t before integrating charging parks
$\mathbf{S}^{CP}$	Matrix for the charging park power at each node b for each time step t
$S_t^{CP,b}$	Charging park power at a specific node b for a specific time step t
$\mathbf{S}^{PCC}$	Vector of the apparent power at the point of common coupling for each time step t before integrating charging parks
S_t^{PCC}	Apparent power at the point of common coupling for a specific time step t before integrating charging parks
SOE^{max}	State of energy upper limit
SOE^{min}	State of energy lower limit
U	Single phase voltage

1. Introduction

Renewable energy sources and EVs are seen as future key drivers of a substantial decrease in carbon emissions in both the transportation and power generation sectors [1]. However, this transformation poses new challenges to the power grid [2]. While in rural areas, the increased share of renewable energies, resulting in over voltages is the main cause of grid reinforcement [3], in urban distribution grids, it is forecast by the European Federation for Transport and Environment, that the number of public chargers in the EU will increase from 185000 public chargers to 1.3 million in 2025 and 2.9 million in 2030 [4].

Furthermore, an increased demand for DC fast charging units is predicted in the report for urban areas in particular [4]. This is motivated by the increasing prioritization of shared cars or electric taxis in these urban areas. They recommend introducing charging parks at easily accessible locations, with dedicated parking spots for electric taxis and shared EVs, notably in cities. Nicholas and Wappelhorst estimate

in a report about regional charging infrastructure requirements that the number of DC fast charging stations in Germany will quadruple from about 2000 in 2018 to about 8000 in 2030 [5]. Both studies as well as recently published papers [6,7] identified that existing grid infrastructure is not capable to include the additional power of such charging parks. While this paper examines the possibility of reducing peak power at the PCC in distribution grids in urban areas using coordinated controlled BESSs located at these charging parks, different other approaches are currently being discussed in the literature, both with and without BESS, that aim to meet these challenges.

First, conventional grid reinforcement or transformer upgrading may enable the integration of more EVs, as investigated by Brinkel et al. [8]. It was shown with a multi-objective optimization that in most cases, the advantages of EV charging with a higher transformer capacity limit do not outweigh the disadvantages, such as the costs and emissions generated by reinforcing the transformer. In their analysis, Pudjianto et al. [9] forecast in their study related to Great Britain's distribution grid that massive grid reinforcement will be required, costing up to £36bn by 2050. They propose a number of various smart charging strategies to reduce the costs, but none of these are able to eliminate grid reinforcement completely.

Second, several vehicle-to-grid (V2G) approaches exist by which to reduce the peak power in distribution grids. V2G enables bidirectional power flow at a charging station. An overview of the V2G concept and possible V2G services is presented by both Tan et al. [10] and Kempton et al. [11]. Sovacool et al. [12] have published a review of the neglected social dimensions, such as user behavior and acceptance. They conclude that neither the political framework nor the interest of consumers is taken into account in the majority of V2G approaches. Another disadvantage is the impact of V2G applications on vehicle battery lifetime due to a higher cyclic aging, as proposed by Wang et al. [13] and Jafari et al. [14].

Third, a number of researchers, such as Hanemann et al. [15,16] are examining the effect of using different smart charging strategies. The authors describe the impact on the power grid of applying a number of different EV charging strategies and conclude that as a side effect the curtailment of renewable energy sources can be reduced by smart charging strategies. However, they focus on the effects on spot market and CO_2 prices rather than on the effect on the distribution grid. The studies by Mehta et al. focuses on how to achieve optimal integration of EVs in a distribution grid [17,18]. Their strategies achieve both economic benefits in terms of daily costs and technical benefits in terms of peak load reduction and optimized active and reactive power flow. As with the V2G strategies, however, it must also be assumed here that users will provide their EVs for those smart charging strategies and therefore expect longer charging times.

Finally, BESS can also be used as an alternative to conventional grid reinforcement. The various approaches and their advantages and disadvantages will be discussed in more detail in the following. A general overview of state-of-the-art stationary BESSs based on lithium-ion batteries (LIBs) is provided among others by Diouf et al. [19] and Hesse et al. [20].

In the context of state-of-the-art peak shaving, Gimelli et al. [21] and Martins et al. [22] have investigated on an optimal sizing and design of the BESS, but neither has examined the effects on the distribution grid.

Reihani et al. [23] conducted an analysis of peak shaving on an island in Hawaii with a high share of renewable energy sources. Here, however, the focus was more on forecasting than on operation of the BESS itself. The work by Schram et al. [24] and Nykamp et al. [25] focuses on the behavior of a single BESS operated in a peak shaving application. Chapaloglou et al. [26] and Prvins et al. [27] both introduced a novel approach to an optimized energy management algorithm for peak shaving applications in selected distribution grids.

Summarizing the literature, there seems to be a consensus that a high EV-share is coming along with an increased number of charging parks requires adaptations or new solutions in the power grid, especially in urban areas. None of the authors mentioned have considered the possibility of coupling multiple BESSs to reduce the peak power at the PCC in existing distribution grids and consequently to avoid or decelerate grid reinforcement requirements.

1.1. Scope of the study

This paper presents a method of reducing the peak power at the PCC in existing urban distribution grids in which a high share of EVs results in an increasing energy demand. A number of BESSs are located at various charging parks where the energy management systems are coordinated controlled with the aid of a linear optimization framework (lp_opt) which was adapted and expanded in the context of this study [28]. The stress on the stationary BESSs is evaluated by adapting a software framework for storage systems (SimSES) [29]. The impact on the distribution grid is analyzed by using a simulation tool for electric distribution grid optimization (eDisGo) [30].

This combination of previously disjointed tools within a newly developed interconnected simulation framework (open_BEA) leads to a more realistic simulation of the effects of BESSs over different locations on the distribution grid. The coordinated control method developed in this study is applied to an exemplary grid that comprises a MV grid with 146 underlying LV grids [30]. The charging parks are located by the MV grid, and the results are compared with a state-of-the-art peak shaving strategy for each BESS, initially developed by Oudalov et al. [31]. The MV grid is connected to the high voltage (HV) level via a transformer at a single substation (PCC). Both the peak load of the charging parks and the nominal energy of the BESSs are varied to analyze the effects in different cases. Fig. 1 illustrates the scope of the paper in detail.

The highlights of this paper can be summarized as follows:

- A new framework called open_BEA is developed to connect previously disjointed tools to enable accurate co-simulations of BESSs and distribution grids.
- The impact of BESSs, located at charging parks, is evaluated on the basis of peak load reduction at the PCC with varying EV-share and BESS capacities.
- A strategy is developed to control and coordinate the charging and discharging of the BESSs. The method is applied to a test distribution grid and compared with a state-of-the-art peak shaving strategy.
- Each BESS is evaluated using various key performance indicators along with its impact on the distribution grid.
- It is shown that the coordinated control strategy can significantly reduce the peak load on the PCC. This opens up new possibilities, allowing the grid operator to avoid grid reinforcement without influencing EV owners with reduced charging power or V2G strategies.
- The open-source code available to the research community is easily adaptable with individual parameter sets. Consequently, researchers or grid operators can use the method on their own storage systems or grid areas with individual charging park locations.

1.2. Outline of the paper

The remainder of this paper is structured as follows: Section 2 describes the open-source simulation tools eDisGo, SimSES and open_BEA. The problem formulation, objective function and constraints are presented in Section 3. Section 4 gives an overview of the test distribution grid, the origin of the input profiles and the settings applied in this study. The results of the simulations are presented and discussed in Section 5, while Section 6 concludes the paper with an outlook of future work.

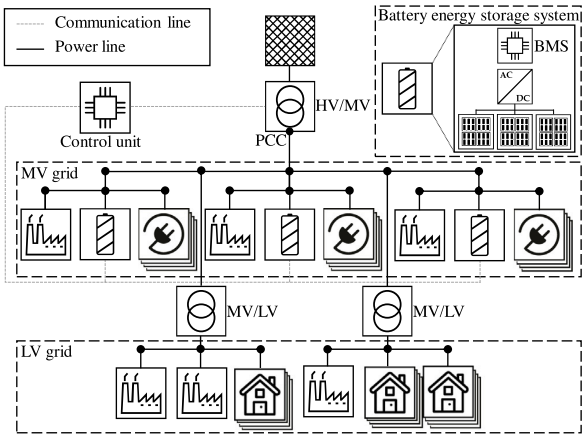

Fig. 1. Graphical overview of the paper. Several battery energy storage systems (BESSs), modeled in detail as shown in the blow-up, located at three different charging parks, are able to communicate with each other. They are coordinated and controlled by a central control unit to reduce the peak power at the point of common coupling (PCC).

2. Simulation framework and methodology

This section describes the newly developed interconnected simulation framework open_BEA, the expanded linear programming optimization tool lp_opt and the adaptation of the existing tools (eDisGo, SimSES), which are used in this study. Fig. 2 is a schematic representation of the functionalities and the information flows of the four different tools. All simulation tools used in this study are entirely open-source.[1,2] A description of further functionalities of all simulation tools can be found in Appendix A.

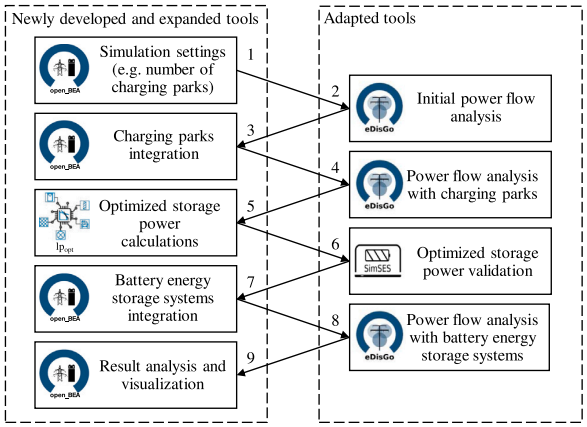

Fig. 2. Flowchart of all open-source simulation tools developed, expanded or adapted for use in this study. The newly developed tool open_BEA operates as both a central control unit and a configuration unit. The adapted tools eDisGo and SimSES are validation tools for both the distribution grid and the battery energy storage systems (BESSs). With the help of lp_opt the energy management of all BESSs is controlled coordinated.

The purpose of the individual simulation tools and the flow of information and data is described step by step below:

1. **Initial setting:** Within the newly developed open-source simulation tool open_BEA, the initial setting including the simulation duration, step size, and test grid is defined. Individual load demands are assigned to the various actors in the grid, such as domestic or industrial consumers.
2. **Initial power flow analysis:** Based on the load demands from the first step, the eDisGo software performs a power flow analysis for a selected period. In this step, the power flow analysis is conducted without charging parks and storage systems. The power flow results for all steps at all nodes and lines as well as the power at the PCC are transferred back to open_BEA for the next simulation step.
3. **Charging parks integration:** In addition to the first step, the number, locations, and load time series of charging parks are defined and integrated into the simulated grid.
4. **Power flow analysis including charging parks:** Here, the eDisGo software performs a power flow analysis with charging parks. The power flow results for all steps at all nodes and lines as well as the power at the PCC are again transferred back to open_BEA for the next simulation step.
5. **Optimized BESSs power calculations:** Within open_BEA, the linear optimization tool lp_opt is launched. The expanded tool calculates an operation strategy for each BESS, limited by linearized constraints due to the distribution grid and the BESS. Aiming to reduce the peak power at the PCC, a linearized power flow from the BESSs to the PCC is assumed within the tool. The (dis-)charging strategy is introduced in Section 3.
6. **BESSs validation:** The tool SimSES is used for validating BESS time series from the optimized BESSs power calculations. This enables both the losses and the degradation to be determined and allows the data (time series) to be fed back to open_BEA.
7. **BESSs integration:** In addition to step 3 BESSs including their dis(-charging) time series, located at charging parks, are integrated into the simulated grid.
8. **Power flow analysis including BESSs:** Here, the eDisGo software performs a power flow analysis with charging parks and BESSs. The power flow results for all steps at all nodes and lines as well as the power at the PCC are again transferred back to open_BEA for the analysis and visualization. This step is necessary to validate the linearized power flow from step 5.
9. **Result analysis and visualization:** Finally, the effects of the charging parks and the BESSs on the power flow at the PCC are analyzed. In addition, the stress on the BESSs are evaluated using a defined set of key performance indicators.

3. Problem formulation and coordinated control strategy

3.1. Problem definition

An increased number of charging stations can cause higher load peaks in distribution grids, which can subsequently lead to overloading of existing grids. BESSs are a possible solution in order to avoid grid reinforcement and avoid influencing EV owners with reduced charging power or V2G strategies. While at present BESSs usually work in stand alone mode in accordance with state-of-the-art peak shaving, this study shows the possibility of reducing peak power at the PCC in distribution grids in urban areas using coordinated controlled BESSs located at charging parks. The following sections describe the strategy used to reduce the peak power of the HV/MV transformer (PCC).

Fig. 3 shows an extended graphical representation of the study along with an overview of all denotations of the optimization framework developed in this section. A variable marked with an asterisk (∗) indicates that charging parks are included. Each charging park is equipped with a BESS. The BESSs are operated by a central control unit developed as part of this study, which can access the load at the PCC, the line loads and the demand of the charging parks. The central controller unit calculates a (dis-)charging strategy for each BESS, limited by a handful constraints due to the distribution grid and the BESS.

[1] open_BEA, SimSES and lp_opt: https://www.ei.tum.de/en/ees/research-teams/team-ses/system-analytics-and-integration/.

[2] eDisGo: https://github.com/openego/eDisGo.

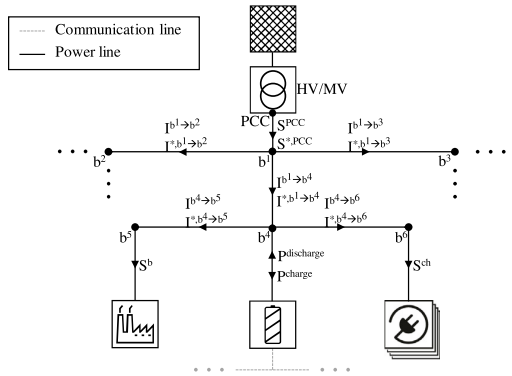

Fig. 3. Extended graphical representation of this study including all denotations from the optimization framework. A variable marked with an asterisk (∗) indicates that charging parks are included.

3.2. Problem formulation

Eq. (1) defines the vector **N** for all nodes b within the described distribution grid, with a total number of nodes B:

$$\mathbf{N} = [1, \dots, \mathrm{b}, \dots, \mathrm{B}]^{\mathrm{T}} \tag{1}$$

The time step t within a defined time horizon T is defined by a vector H as shown in Eq. (2):

$$\mathbf{H} = [1, \dots, t, \dots, \mathrm{T}] \tag{2}$$

The apparent power $\mathrm{S}_t^{\mathrm{b}}$ at each node b for each time step t before integrating charging parks is defined by a matrix **S** (Eq. (3)):

$$\mathbf{S} = \begin{pmatrix} \mathrm{S}^{1_1} & \cdots & \mathrm{S}_t^1 & \cdots & \mathrm{S}_{\mathrm{T}}^1 \\ \vdots & \ddots & \vdots & \ddots & \vdots \\ \mathrm{S}_1^{\mathrm{b}} & \cdots & \mathrm{S}_t^{\mathrm{b}} & \cdots & \mathrm{S}_{\mathrm{T}}^{\mathrm{b}} \\ \vdots & \ddots & \vdots & \ddots & \vdots \\ \mathrm{S}_1^{\mathrm{B}} & \cdots & \mathrm{S}_t^{\mathrm{B}} & \cdots & \mathrm{S}_{\mathrm{T}}^{\mathrm{B}} \end{pmatrix} \tag{3}$$

The current $\mathrm{I}_t^{\mathrm{b}_j \to \mathrm{b}_k}$ for a specific line between two specific nodes b_k and b_j at each time step t before integrating charging parks is defined by a vector $\mathbf{I}^{\mathrm{b}_j \to \mathrm{b}_k}$ as shown in Eq. (4). If two nodes are not linked to each other, this value in the matrix remains 0:

$$\mathbf{I}^{\mathrm{b}_j \to \mathrm{b}_k} = \left[\mathrm{I}_1^{\mathrm{b}_j \to \mathrm{b}_k}, \cdots, \mathrm{I}_t^{\mathrm{b}_j \to \mathrm{b}_k}, \cdots, \mathrm{I}_{\mathrm{T}}^{\mathrm{b}_j \to \mathrm{b}_k}\right] \quad \forall\, \mathrm{b}_j \in \mathbf{N},\ \mathrm{b}_k \in \mathbf{N},\ \mathrm{b}_j \neq \mathrm{b}_k \tag{4}$$

The apparent load $\mathrm{S}_t^{\mathrm{PCC}}$ at the PCC for each time step t before integrating charging parks is defined by a vector $\mathbf{S}^{PCC}$ (Eq. (5)):

$$\mathbf{S^{PCC}} = \left[\mathrm{S}_1^{\mathrm{PCC}}, \dots, \mathrm{S}_t^{\mathrm{PCC}}, \dots, \mathrm{S}_{\mathrm{T}}^{\mathrm{PCC}}\right] \tag{5}$$

The charging park power $\mathrm{S}_t^{\mathrm{CP,b}}$ for each time step t at each node b for each charging park with a coupled BESS results in a power matrix $\mathbf{S}^{CP}$ as shown in Eq. (6). If a node has no charging park, this value in the matrix remains 0:

$$\mathbf{S^{CP}} = \begin{pmatrix} \mathrm{S}_1^{\mathrm{CP},1} & \cdots & \mathrm{S}_t^{\mathrm{CP},1} & \cdots & \mathrm{S}_{\mathrm{T}}^{\mathrm{CP},1} \\ \vdots & \ddots & \vdots & \ddots & \vdots \\ \mathrm{S}_1^{\mathrm{CP,b}} & \cdots & \mathrm{S}_t^{\mathrm{CP,b}} & \cdots & \mathrm{S}_{\mathrm{T}}^{\mathrm{CP,b}} \\ \vdots & \ddots & \vdots & \ddots & \vdots \\ \mathrm{S}_1^{\mathrm{CP,B}} & \cdots & \mathrm{S}_t^{\mathrm{CP,B}} & \cdots & \mathrm{S}_{\mathrm{T}}^{\mathrm{CP,B}} \end{pmatrix} \tag{6}$$

The apparent load $\mathrm{S}_t^{*,\mathrm{PCC}}$ at the HV/MV transformer (PCC) for the time horizon T after integrating charging parks at various nodes b is defined by a vector $\mathbf{S}^{*,PCC}$ in Eq. (7):

$$\mathbf{S}^{*,PCC} = \left[\mathrm{S}_1^{*,\mathrm{PCC}}, \dots, \mathrm{S}_t^{*,\mathrm{PCC}}, \dots, \mathrm{S}_{\mathrm{T}}^{*,\mathrm{PCC}}\right] \tag{7}$$

The same applies to the matrix $\mathbf{I}^{*,\mathrm{b}_j \to \mathrm{b}_k}$, i.e. the current $\mathrm{I}_t^{*,\mathrm{b}_j \to \mathrm{b}_k}$ for each line after integrating charging parks at various nodes b (Eq. (8)):

$$\mathbf{I}^{*,\mathrm{b}_j \to \mathrm{b}_k} = \left[\mathrm{I}_1^{*,\mathrm{b}_j \to \mathrm{b}_k}, \cdots, \mathrm{I}_t^{*,\mathrm{b}_j \to \mathrm{b}_k}, \cdots, \mathrm{I}_{\mathrm{T}}^{*,\mathrm{b}_j \to \mathrm{b}_k}\right] \quad \forall\, \mathrm{b}_j \in \mathbf{N},\ \mathrm{b}_k \in \mathbf{N},\ \mathrm{b}_j \neq \mathrm{b}_k \tag{8}$$

3.3. Coordinated control strategy

The objective is to minimize the peak apparent load $\mathrm{S}_t^{*,\mathrm{PCC}}$ at the PCC for the time horizon T after integrating charging parks at various locations b. Therefore the objective function is defined in Eq. (9):

$$\text{minimize}: \left\{\max\left(\mathrm{S}_t^{*,\mathrm{PCC}}\right)\right\} \quad \forall\, t \tag{9}$$

The load at the PCC $\mathrm{S}_t^{*,\mathrm{PCC}}$ for all time steps t after integration of the charging parks with a coupled BESS is calculated in Eq. (10), while η_{b} is the efficiency between the PCC and a specific node b. The charging power $P_t^{\mathrm{charge,b}}$ and the discharging power $P_t^{\mathrm{discharge,b}}$ for a BESS at a specific node b are included in the coordinated control strategy together with a power factor $\cos\varphi$. The power factor $\cos\varphi$ and the efficiency η_{b} within the optimization framework (coordinated control strategy) is set to a constant factor (in this study to 1), which is necessary to perform a linear optimization:

$$\mathrm{S}_t^{*,\mathrm{PCC}} = \mathrm{S}_t^{\mathrm{PCC}} + \sum_{\mathrm{b} \in \mathbf{N}} \left(\frac{\mathrm{S}_t^{\mathrm{CP,b}}}{\eta_{\mathrm{b}}} + \frac{P_t^{\mathrm{charge,b}}}{\eta_{\mathrm{b}} \cdot \cos\varphi} - \frac{P_t^{\mathrm{discharge,b}}}{\cos\varphi} \cdot \eta_b \right) \quad \forall\, t \tag{10}$$

The power of each BESS is only subject to the following restrictions in Section 3.5 and thus is controlled coordinated by this objective function aiming to minimize the peak power at the PCC.

3.4. Optimization constraints: Distribution grid

In addition to the objective function (Eq. (9)), the grid is subject to distribution line loading constraints. First of all, the line loads $\mathrm{I}_t^{*,\mathrm{b}_j \to \mathrm{b}_k}$ have to be below their maximum rated current $\mathrm{I}_{\max}^{\mathrm{b}_j \to \mathrm{b}_k}$ as shown in Eq. (11).

$$\mathrm{I}_t^{*,\mathrm{b}_j \to \mathrm{b}_k} \leq \mathrm{I}_{\max}^{\mathrm{b}_j \to \mathrm{b}_k} \quad \forall\, \mathrm{b}_j \in \mathbf{N},\ \mathrm{b}_k \in \mathbf{N},\ \mathrm{b}_j \neq \mathrm{b}_k \tag{11}$$

The line loads $\mathrm{I}_t^{*,\mathrm{b}_j \to \mathrm{b}_k}$ after the charging park integration ($\mathrm{S}_t^{\mathrm{CP,b}}$) are calculated according to Eq. (12), where U is the single phase voltage.

$$\mathrm{I}_t^{*,\mathrm{b}_j \to \mathrm{b}_k} = \mathrm{I}_t^{\mathrm{b}_j \to \mathrm{b}_k} + \sum_{\mathrm{b} \in \mathbf{N}} \left(\frac{\mathrm{S}_t^{\mathrm{CP,b}}}{\mathrm{U}} + \frac{P_t^{\mathrm{charge,b}}}{\mathrm{U} \cdot \cos\varphi} - \frac{P_t^{\mathrm{discharge,b}}}{\mathrm{U} \cdot \cos\varphi} \right) \quad \forall\, t \tag{12}$$

3.5. Optimization constraints: Battery energy storage system

Furthermore, the BESS is also subject to a number of boundary conditions as described in the constraints Eqs. (13) – (17). The state of energy (SOE) must remain within the given bounds $\mathrm{SOE}^{\min}$ and $\mathrm{SOE}^{\max}$. The nominal energy content of a BESS is denoted as E^{nominal}, and the actual energy content for a specific time step t of a BESS is denoted as $E_t^{\mathrm{actual,b}}$.

$$\mathrm{SOE}^{\min} \cdot E^{\mathrm{nominal}} \leq E_t^{\mathrm{actual}} \leq \mathrm{SOE}^{\max} \cdot E^{\mathrm{nominal}} \tag{13}$$

The charging and discharging power ($P_t^{\mathrm{charge,b}}$ and $P_t^{\mathrm{discharge,b}}$) for each time step t and each BESS has to be lower than the respective maximum energy rate ($\mathrm{e}^{\mathrm{rate}}$) of the storage technology. In charging direction, the maximum $\mathrm{e}^{\mathrm{rate}}$ is denoted as $E_t^{\mathrm{charge,b}}$ and in discharging direction as $E_t^{\mathrm{discharge,b}}$.

$$P_t^{\mathrm{charge,b}} \leq \mathrm{e}_{rate}^{\mathrm{charge}} \cdot E^{\mathrm{nominal}} \quad \forall\, \mathrm{b} \tag{14}$$

$$P_t^{\mathrm{discharge}} \leq \mathrm{e}_{rate}^{\mathrm{discharge}} \cdot E^{\mathrm{nominal}} \quad \forall\, \mathrm{b} \tag{15}$$

The charging and discharging powers ($P_t^{\text{charge,b}}$ and $P_t^{\text{discharge,b}}$) are also limited by the rated power P^{rated} of the power electronics.

$$P_t^{\text{charge,b}} \leq P^{\text{rated}} \quad \forall\, \text{b} \tag{16}$$

$$P_t^{\text{discharge,b}} \leq P^{\text{rated}} \quad \forall\, \text{b} \tag{17}$$

The energy conservation of a BESS is defined in Eq. (18) and applies to any storage system at various nodes b. The actual energy content $E_t^{\text{actual,b}}$ of a BESS depends on the energy content of the previous time step, the charged energy $E_t^{\text{charge,b}}$ and the discharged energy $E_t^{\text{discharge,b}}$.

$$E_t^{\text{actual,b}} = E_{t-1}^{\text{actual,b}} + E_t^{\text{charge,b}} - E_t^{\text{discharge,b}} \tag{18}$$

3.6. Reference case: State-of-the-art peak shaving

Motivated by a tariff system consisting of an energy and a power related component, the aim of state-of-the-art peak shaving is to minimize the maximum power peak value at one specific node b within a defined billing period. Particularly large electricity consumers with an annual demand above a certain limit (in Germany 100 MWh [32]) can reduce the peak power provided by the power grid, which directly results in reduced operating expenses in the form of reduced grid charges.

In order to reduce the peak power at a specific node b, the excess demand has to be covered by another power providing unit, such as a diesel generator or in our case a BESS. The BESS is used to decouple the supply and demand over a specified time. Consequently, it is essential to find a peak shaving threshold above which the power is provided by the BESS. First, a pre-processing linear optimization algorithm similar to that described in other publications [33,34] is used to minimize the power value of the peak shaving threshold $\text{PS}^{\text{threshold}}$, while complying with the necessary constraints, such as meeting the power demand and satisfying the energy and power specifications of the BESS. Secondly, the resulting peak shaving threshold is used as an input parameter for the operation strategy within the open_BEA simulation tool.

In this study the state-of-the-art peak shaving strategy is used as follows: as long as the power of the consumer at a specific node b exceeds a specified threshold, the additionally required power is provided by the BESS. In addition, the BESS will recharge if the power value is below the previously determined optimal peak shaving threshold. This ensures that storage system charging does not cause the exceedance of the threshold. A more detailed description of the state-of-the-art peak shaving strategy is given by Martins et al. [22]. In Section 5, this state-of-the-art peak shaving strategy will be compared to the coordinated control strategy introduced in this study.

4. Test grid and applied settings

This section describes the test distribution grid and the applied settings used in the study. It also explains the main parameters of the example grid, the settings for the DC charging stations, and the load profiles used. Finally, it presents the settings and parameters relating to the BESS. However, the method presented in this paper is also applicable to other scenarios and grids.

4.1. Example grid

In order to apply and test the coordinated control strategy introduced in this paper, a synthetic test grid is selected consisting of a MV grid and 146 underlying LV grids [30]. This MV distribution grid is connected to the HV level via a transformer at a single substation (PCC), and the MV grid is operated as an open loop, which reflects the most common topology encountered in Germany [30]. The basic structure of the grid is presented in Table 1 and illustrated in Fig. 4.

Table 1
Parameters and settings of the synthetic distribution grid used in this study. The grid is connected to the high voltage level via a transformer at a single substation and is operated as an open loop.

Parameter/Setting	Number	Unit
Industrial consumers	82	–
Residential consumers	5787	–
Minimum annual consumption of a single consumer	1.3	MWh
Maximum annual consumption of a single consumer	7844.7	MWh
Total annual consumption excluding charging parks	31 953.0	MWh
Circuit breakers	4	–
LV lines	18 209	–
MV lines	225	–
Maximum load at the PCC	11.1	MW

4.2. Charging stations

The distribution of the charging stations is based on the work done by Luo et al. [35]. Accordingly, DC fast charging stations are mainly situated at locations with short parking times or those preferred by shared mobility users, such as shopping areas. We therefore allocated three charging parks in our test grid at different nodes that best fit these criteria. Fig. 4 shows the locations of the charging stations in the test grid.

A peak load of 350 kW is assumed for the DC fast charging units, which is in line with currently common fast chargers [36]. To evaluate different future scenarios, the DC fast charging stations at each of the charging parks were increased from two units to eight units. Accordingly, eight units are the equivalent of a peak load of 2.8 MW.

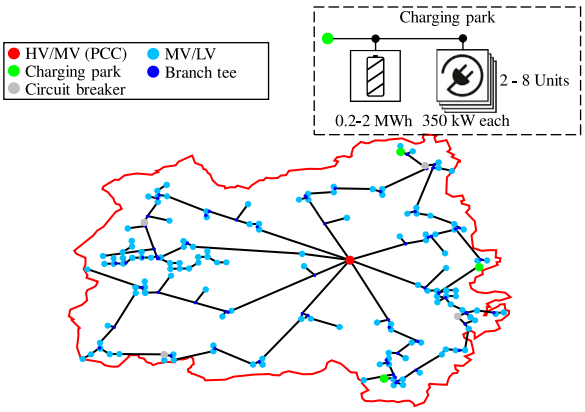

Fig. 4. Graphical representation of the test distribution grid showing the locations of the three charging parks with a battery energy storage system (BESS) connected (green). The circuit breakers are marked in gray, the MV/LV transformers are marked in light blue, the PCC in red and all branch tees in dark blue. As shown in the blow-up one BESS is connected to each charging park.

4.3. Load profiles

The simulation uses different load profiles for residential and industrial consumers. The 74 household loads used were created and published by *HTW Berlin* [37]. The industrial profiles are provided by industry partners of the Technical University of Munich. Of these, the three exemplary profiles that were determined as reference profiles in previous publications are used [38,39].

The load profiles of the EV charging stations have been examined by the Reiner Lemoine Institute. Based on the work of Nobis and Kuhnimhof [40], three different types of load profiles for charging parks have been defined. The profiles differ in time, frequency and peak load duration, depending on their position. Fig. 5 shows exemplary daily load profiles of the three charging parks used in this study.

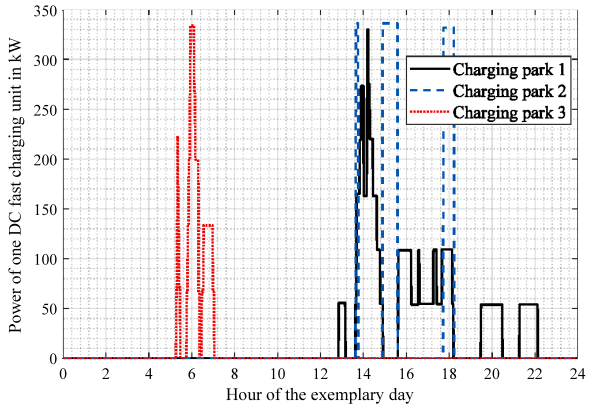

Fig. 5. Daily profile of the three different DC fast charging parks with an exemplary maximum power of 350 kW each.

The energy consumption of the charging parks is converted into a proportion of the total energy consumption (EV-share). For example, at each of the three charging park locations, the peak load is 700 kW, which corresponds to two DC fast charging units. This setting account for 4% (1.28 MWh) of the total energy consumption (31953 MWh as shown in Table 1) of the test distribution grid. With three DC fast charging units per charging location, the EV-share is 6%. The maximum EV-share considered in this study is 16%, which corresponds to eight DC fast charging units. Eight of these units are equivalent to a 2.8 MW peak load at each charging park, and this maximum was chosen so as not to exceed the maximum connection power to common MV nodes [41].

4.4. Battery energy storage system setting

The SimSES simulation tool, described in Appendix A.2 is used to validate the behavior of the BESS. The parameters and settings shown in Table 2 are used in this paper to represent and simulate a realistic BESS. A LIB with a lithium-iron-phosphate (LFP) cathode and a carbon/graphite (C) anode is selected [42]. This type of cell is particularly suitable for stationary applications due to its higher cycle durability [43,44]. The capacity of the BESS starts with 200 kWh increasing in increments of 200 kWh up to 2 MWh, again to ensure a connection to common MV nodes [41]

The power electronics (AC/DC converter) is modeled with a high efficiency above 10% of the rated power P^{rated} and the current charging power $P_t^{\text{charge,b}}$ or discharging power $P_t^{\text{discharge,b}}$ of a BESS, as shown in the example for charging case at a specific node b for a specific time step t in Eq. (19) [45]. In this study the following exemplary values are used: for the load dependent part $k = 0.0345$ and for the load independent part $p_0 = 0.0072$. The efficiency η_{PE} is independent of the direction of the power flow and there is no hysteresis. Maximum efficiency is attained at $0.46 \cdot P^{\text{rated}}$ with an efficiency of $\eta_{\text{PE}} = 96.9\%$. The maximum energy rate of the BESS (e^{rate}) in the discharging direction is set to a typical value of 2 h^{-1}. In accordance with the type of battery cell, the maximum e^{rate} in the charging direction is set to 1 h^{-1}. The battery management system (BMS) is configured such that the SOE remains within the range of 5-95%. The SOE at the beginning of the simulation is set to 50%.

$$\eta_{\text{PE}} = \frac{\frac{P_t^{\text{charge,b}}}{P^{\text{Rated}}}}{\frac{P_t^{\text{charge,b}}}{P^{\text{Rated}}} + p_{0+k} \cdot \left(\frac{P_t^{\text{charge,b}}}{P^{\text{Rated}}}\right)^2} \tag{19}$$

Table 2
Parameters and settings of the simulated battery energy storage system (BESS) comprising battery cells, a power electronics unit and a battery management system (BMS).

Parameter/Setting	Description/Value	Unit
Battery cell manufacturer	muRata	–
Battery cell type	US26650FTC1	–
Battery cell chemistry	LFP:C	–
Battery cell capacity	2850	mAh
Nominal cell voltage	3.2	V
Power electronics	*cf. Eq.* (19)	–
Maximum efficiency of power electronics	96.9	%
Maximum e^{rate} (discharge)	2	h^{-1}
Maximum e^{rate} (charge)	1	h^{-1}
Capacity per storage system	200–2000	kWh
SOE range	5–95	%
SOE start	50	%

4.5. Simulation settings

In order to take into account seasonal fluctuations, a simulation duration of six months from January to June is selected for the simulation. This enables reliable results (e.g. aging behavior) to be obtained for the BESS. The simulation step size chosen is 15 min. Hence, the profiles from Section 4.3, which have a higher time resolution, are averaged. The 15 min time steps represent a compromise between the duration of the simulation and the accuracy of the input profiles.

5. Results and discussion

This section discusses the impact of coordinated controlling the BESSs on the test distribution grid for a six months simulation period. For this purpose, the load flows and potential reductions in peak load at the PCC are evaluated in detail and compared to the results obtained with a state-of-the-art peak shaving algorithm. The effects of this and the resulting stress on the BESS are also investigated.

5.1. Reference case: State-of-the-art peak shaving

Fig. 6 shows the peak load change at the PCC in the form of a contour plot of a state-of-the-art peak shaving strategy, outlined in Section 3.6. Peak load reduction or increase in Fig. 6 refers to the scenario without charging parks (0% EV-share). The capacity of the BESS starts with 200 kWh increasing in increments of 200 kWh up to 2 MWh, while the EV-share increased in two percentage point steps from 4% to 16%. Positive values in the contour plot (dark blue areas) indicate the settings with a peak load reduction at the PCC, but since the BESSs are directly coupled to the charging parks and only shave the additional peaks occurring due to EVs, there are no significant peak reductions at the PCC.

Even if the BESSs are able to shave the entire peak, there are increases in the load at the PCC compared to the scenario without EVs, especially in an area with a high EV-share and large BESSs. These slight increases, indicated in yellow and red in Fig. 6, are due to the immediate recharging of the BESSs. This occurs especially when a charging park has already fallen below its peak shaving limit and the BESS is recharging, while the load at the PCC is still close to peak level. The additional power that the BESS at this point of time needs to recharge leads to an increase in the load at the PCC up to 7.5% compared to a scenario without EVs.

Hence, state-of-the-art peak shaving BESSs located at charging parks can help to avoid significant increases in the peak load at the PCC when the EV-share is rising, but it is these results, obtained for state-of-the-art peak shaving, which motivate the introduction of a coordinated and controlled strategy for the three BESSs.

Fig. 7 supports this statement, showing the power flow including the charging park load profiles at the PCC for one exemplary day for the

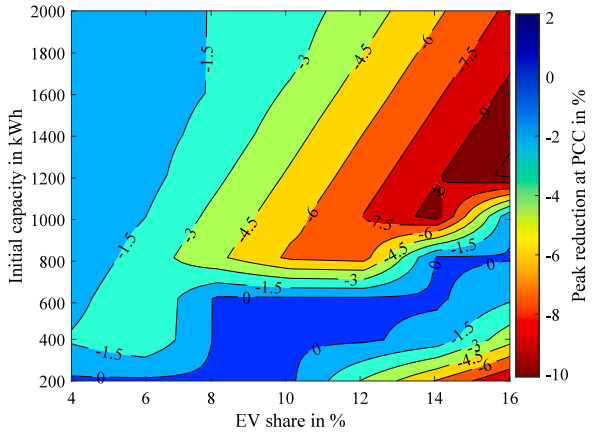

Fig. 6. Peak load reduction contour plot relating to a scenario without electric vehicles (EVs) at the point of common coupling (PCC) with increasing EV-share and battery energy storage systems (BESSs) of different sizes coupled to charging parks. The BESSs operate in stand alone mode in accordance with state-of-the-art peak shaving.

following scenario: 16% EV-share, and storage capacities of 800 kWh. The filled area ($Load_{PCC,PS}$) shows the power flow after including the charging parks and the BESSs are operating with a state-of-the-art peak shaving strategy. The charging parks are displayed in total ($Load_{CP,tot}$) and the load at the PCC is displayed both with ($Load_{PCC,with\,CP}$) and without ($Load_{PCC,wo\,CP}$) charging parks. The first peak of the charging station between 5:00 and 8:00 am is contrary to the peak at the PCC without EVs ($Load_{PCC,wo\,CP}$). Although this peak is shaved by the BESS unit using state-of-the-art peak shaving, there is no peak load reduction at the PCC, because the peak only occurs later that day. However, the peaks in the charging parks between 12 noon and 19:00 cause peaks in the distribution grid are not entirely shaved by the BESSs. By comparison with Fig. 5, it can be identified that only two out of three charging parks account for the additional peak, consequently only two BESSs are discharging in this time period and thus not the full available power of all three BESSs is used to reduce the peak load at the PCC.

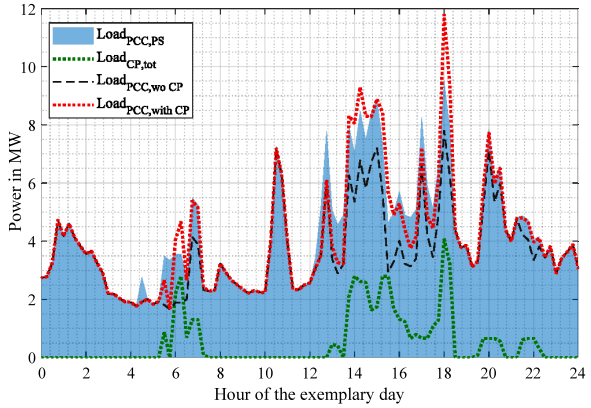

Fig. 7. Power flow including the charging park load profiles ($Load_{CP,tot}$) at the point of common coupling (PCC) for one exemplary day. The load at the PCC is displayed both with ($Load_{PCC,with\,CP}$) and without ($Load_{PCC,wo\,CP}$) charging parks. The battery energy storage systems (BESSs) operate in stand alone mode in accordance with state-of-the-art peak shaving and the resulting power flow is showed as a filled area ($Load_{PCC,PS}$).

5.2. Coordinated control strategy: Distribution grid results

The settings and case studies described in Section 4 are tested under application of the presented coordinated control strategy. Fig. 8 illustrates the peak load change at the PCC as a contour plot. Peak load reduction or increase in Fig. 8 refers to the scenario without charging parks (0% EV-share). The capacity of each BESS starts with 200 kWh increasing in increments of 200 kWh up to 2 MWh, while the EV-share increased in two percentage point steps from 4% to 16%. Positive values in the contour plot (dark blue areas) indicate the settings with a peak load reduction at the PCC.

A trend can be seen, in that the greater the storage capacity, the greater the peak reduction. As mentioned in Section 4, the peak load in the test distribution grid without EVs is 11.1 MW and the maximum peak load reduction of 44.9% (dark blue area in Fig. 8) at the PCC compared to a scenario without EVs occurs at the largest BESS capacity (2 MWh each) and the smallest EV-share (4%). Although each BESSs could theoretically discharge up to 4 MW (cf. Table 2), which would be 12 MW in total, no higher peak load reduction can be achieved. The reason for this behavior is that the power capability of the BESS is usually the limiting factor for the high peaks, while the peaks in the test distribution grid are wider with a low shaving limit and thus the energy content is limited.

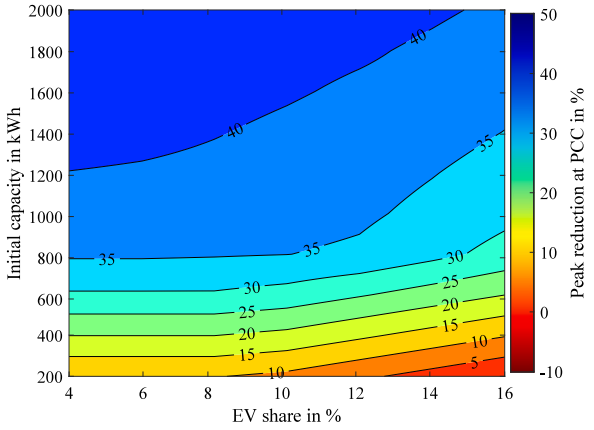

Fig. 8. Peak load reduction contour plot relating to a scenario without electric vehicles (EVs) at the point of common coupling (PCC) with an increasing EV-share and battery energy storage systems (BESSs) coupled to charging parks. The BESSs operate in accordance with the coordinated and coupled energy management system developed in this study.

However, the peak reduction only increases linearly up to a BESS capacity of 800 kWh, while saturation behavior sets in above 800 kWh BESS capacity. The trend lines for a given EV-share are shown in Fig. 9. Here, the abscissa shows the increasing BESS capacity, while the ordinate shows the peak load reduction relating to a scenario without EVs at the PCC. The reason for the saturation behavior is again that with higher BESS capacities and thus lower peak shaving limits the energy content is the limiting factor. With the physical link between energy and power not only the height of the power peak, but also the integral of the power needs to be covered by the BESSs. Up to an EV-share of 10%, charging parks are not responsible for peaks in the test distribution grid and for this reason, no differences can be seen in the trend lines in Fig. 9 for an EV-share of 4 to 8% up to a BESS capacity of 800 kWh.

This is supported by Table 3, where the peak load at the PCC is shown for all scenarios. However, from a storage size of 1 MWh onward, peaks that already include a power demand from the charging park can be shaved, resulting in slight differences in the trend lines. Only from 10% EV-share, the peak load at the PCC exceed the 11.1 MW of the initial scenario without EVs. In the test setting, the charging parks provide the highest peaks with 12.1 MW in the distribution grid with an EV-share of 16% as shown in Table 3. Nevertheless, even with a 16% EV-share, the three smallest simulated BESSs (200 kWh each) are able to ensure that the PCC is not subjected to greater peak loads than in a scenario without EVs.

Table 3
Peak load at the point of common coupling (PCC) in MW in the test distribution grid for a scenario without charging parks and for all case studies with and without battery energy storage systems (BESSs). The maximum load at the PCC is 11.1 MW without both charging parks and BESSs.

Initial capacity in kWh	EV-share in %													
	4		6		8		10		12		14		16	
	No BESS	With BESSs	No BESS	With BESSs	No BESS	With BESSs	No BESS	With BESSs	No BESS	With BESSs	No BESS	With BESSs	No BESS	With BESSs
200		10.0		10.0		10.0		10.2		10.5		10.8		11.1
400		8.9		8.9		8.9		9.0		9.4		9.9		10.0
600		7.9		7.9		7.9		8.0		8.3		8.6		8.9
800		7.2		7.2		7.2		7.2		7.3		7.6		8.0
1000	11.1	6.9	11.1	6.9	11.1	7.0	11.2	7.0	11.5	7.1	11.8	7.4	12.1	7.7
1200		6.7		6.7		6.8		6.9		7.0		7.2		7.5
1400		6.5		6.6		6.7		6.8		6.9		7.0		7.3
1600		6.4		6.5		6.6		6.6		6.7		6.8		7.1
1800		6.3		6.4		6.4		6.6		6.6		6.8		6.9
2000		6.1		6.2		6.3		6.4		6.5		6.6		6.8

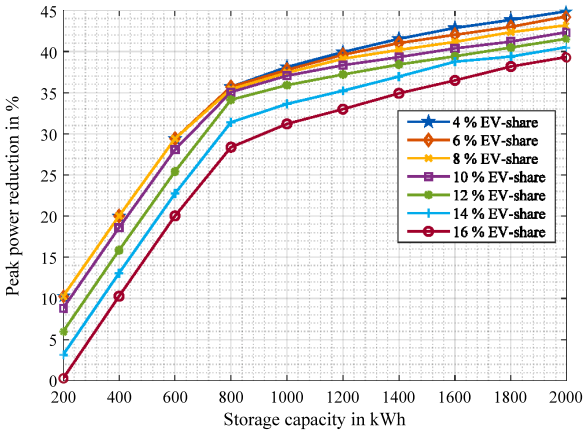

Fig. 9. Trend lines showing the reduction in peak load relating to a scenario without electric vehicles (EVs) at the point of common coupling (PCC) with an increasing EV-share and battery energy storage systems (BESSs) coupled to charging parks. The BESSs operate in accordance with the coordinated and coupled energy management system developed in this study.

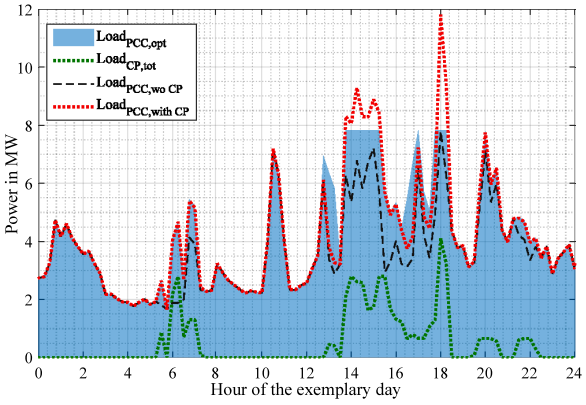

Fig. 10. Power flow including the charging park load profiles ($Load_{CP,tot}$) at the point of common coupling (PCC) for one exemplary day. is displayed both with ($Load_{PCC,with\,CP}$) and without ($Load_{PCC,wo\,CP}$) charging parks. The battery energy storage systems (BESSs) operate in accordance with the coordinated and coupled strategy developed in this study and the resulting power flow is showed as a filled area ($Load_{PCC,opt}$).

Fig. 10 shows the power flow including the charging park load profiles at the PCC for one exemplary day for the following scenario: 16% EV-share, and storage capacities of 800 kWh. The filled area ($Load_{PCC,opt}$) shows the power flow after including the charging parks and the BESSs are operating with coordinated control strategy. The charging parks are displayed in total ($Load_{CP,tot}$) and the load at the PCC is displayed both with ($Load_{PCC,with\,CP}$) and without ($Load_{PCC,wo\,CP}$) charging parks. The first peak of the charging station between 5:00 and 8:00 am is contrary to the peak at the transformer without EVs ($Load_{PCC,wo\,CP}$). While this peak is shaved by the BESS unit using state-of-the-art peak shaving (cf. Fig. 7), the BESSs do not discharge with the coordinated and coupled strategy, since there would be no load reduction on the PCC.

The peaks in the charging parks between 12 noon and 19:00 cause peaks in the distribution grid which are shaved by the BESSs. The peak load at the PCC here is 7.9 MW, which corresponds to the 28.4% peak reduction in the scenario without EVs, as shown in the contour plot Fig. 8. Although each BESSs in this scenario could theoretically discharge up to 1.6 MW (cf. Table 2), which would be a load reduction of 4.8 MW in total (43.2%), no higher peak load reduction can be achieved. Due to the base load, the BESSs can no longer be fully recharged below a certain peak load limit. As can be seen from Fig. 10, with a lower peak load limit, the energy (area between peak load limit ($max(Load_{PCC,opt})$) and $Load_{PCC,with\,CP}$) to be capped would increase and thus the energy content of the BESSs is limited.

5.3. Validation

All numbers in this study refer to results conducted with the non-linear power flow calculation tool eDisGo. However, as shown in Section 3.3, within the coordinated control strategy the power flow was linearized with the aim of performing a linear optimization. Fig. 11 shows the differences between the load flows calculated in the linear optimizer lp_opt and the load flows on the PCC validated with eDisGo. The differences are due to cable losses as well as to the non-linearity on the consumer side and the non-linearity at the power transmission. The maximum difference, however, is 0.23 MW, which corresponds to only 2.9% in relation to the maximum load on the PCC in the scenario without EVs.

When discussing about beneficial effects through coordinated BESS control, one should also consider the stress of a BESS. Fig. 12 shows the peak load reduction at the PCC per full equivalent cycle (FEC) for the six months simulation period. The FECs of all three BESSs are totaled. Two trends can be identified. First, the lower the BESS capacity, the greater the peak load reduction per FEC, and second, the lower the EV-share, the greater the peak load reduction per FEC. Consequently, small storage system with the only aim, reducing the peak power at the PCC are more efficient.

Analyzing the aforementioned trends in detail using a key characteristic of BESSs, it can be observed that BESSs with a capacity of less than 800 kWh are only subjected to a few FECs in the simulation period as shown in Fig. 13. This figure shows the mean number of FECs of

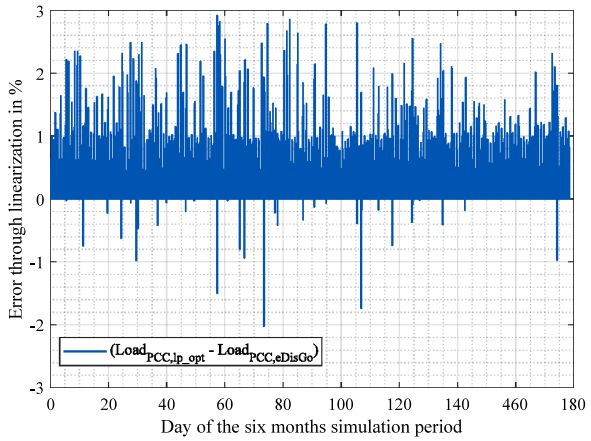

Fig. 11. Power flow comparison at the point of common coupling (PCC) between the power flow calculation used for the coordinate control strategy ($Load_{PCC,lp\_opt}$) and the non-linear power flow calculation with eDisGo ($Load_{PCC,eDisGo}$) for the six month simulation period.

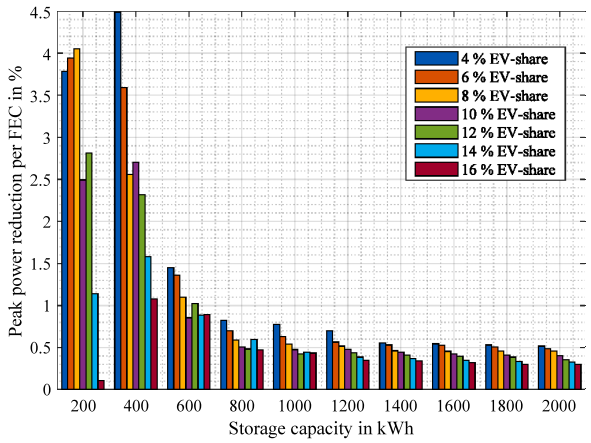

Fig. 12. Reduction in peak load relating to a scenario without electric vehicles (EVs) at the point of common coupling (PCC) per full equivalent cycle with increasing EV-share and battery energy storage systems (BESSs) coupled to charging parks. The BESSs operate in accordance with the coordinated and coupled energy management system developed in this study.

the three BESSs after a six month simulation period. Hence, due to the low stress, the BESSs remain most of the time in a high SOE range above 90%, which leads to an accelerated calendar degradation with the modeled battery cell [43].

However, as a result of the low stress, BESSs with an initial capacity below 800 kWh remain underutilized and it should be considered to use these for stacking multiple applications [46] - a topic beyond the scope of this study. Further analyses of storage behavior in different settings is presented in Appendix B, along with the six key characteristics from a previous publication [38].

6. Conclusion and outlook

This paper presents a method to reduce the power at the transformer or PCC in distribution grids with a high share of EVs. Charging parks are

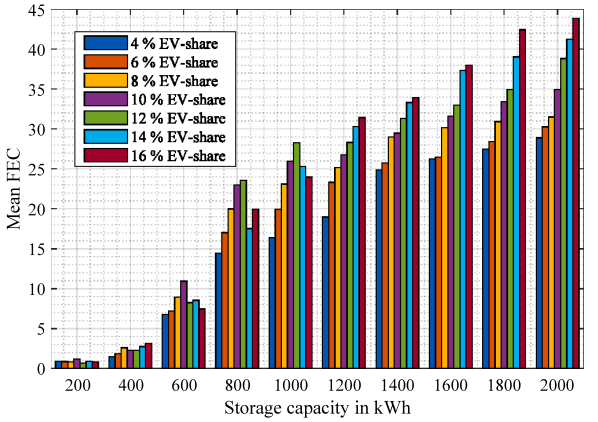

Fig. 13. Mean number of full equivalent cycles (FECs) of the three battery energy storage systems (BESSs) after a six month simulation period. The BESSs operate in accordance with the coordinated and coupled energy management system developed in this study.

located at three different nodes in a representative MV grid, and the EV-share varied in the course of a sensitivity analysis. At all three nodes, a BESS with various capacities is coupled and the attendant energy management system is controlled with the aid of a linear optimization framework, which was expanded as part of this study. The stress on the LIB based stationary BESSs is evaluated by adapting the holistic energy storage simulation framework SimSES, while the impact on the distribution grid is analyzed using the simulation tool eDisGo. The open_BEA framework developed as part of this study connects these previously disjointed tools to enable accurate co-simulations of BESSs and distribution grids.

The objective function, which has been developed to control and coordinate the charging and discharging of the BESSs is applied to a test distribution grid comprising 1 MV grid and 146 underlying LV grids. In total, there are 82 industrial consumers and 5787 residential consumers. The EV-share in this study starts with 4%, which corresponds to two DC fast charging units at each charging park, and ends with 16%.

The capacity of the coupled BESSs increases from an initial level of 200 kWh to 2000 kWh. The BESS is simulated in detail with a LFP:C cell model that comprises a degradation model, a power electronics model with a representative efficiency curve and a BMS that is responsible for monitoring the maximum cell currents and SOE limits.

There are no peak reductions at the PCC if the BESSs are operated in a stand alone mode with a state-of-the-art peak shaving algorithm. There are even slight increases up to 7.5% of the load at the PCC compared to a scenario without EVs. For most scenarios, however, no or only a very small increase in the peak load can be identified. Hence, state-of-the-art peak shaving BESSs located at charging parks can help to avoid significant increases in the peak load at the PCC when the EV-share is rising. Furthermore, individual overloaded or limiting lines can be relieved with this operation mode.

If the BESSs is operated using the coordinated control method developed in this study, the peak load at the PCC can be reduced in all scenarios by a maximum of 44.9%. While the rise in peak reduction increases linearly with small BESS capacities, a saturation behavior can be observed above 800 kWh.

The power flow was verified with the eDisGo simulation tool, showing that for the test grid, the linearization in lp_opt produces similar results as the validated model. The maximum difference of 0.184 MW corresponds to 1.7% in relation to the maximum load on the PCC in the scenario without EVs.

Analyzing the results of the simulation tool for the BESS (SimSES) shows a clear trend, in that the peak load reduction per FEC decreases with an EV-share and BESS capacity increase. For a storage capacity of 200 kWh and a 4% EV-share, a reduction of 3.5% at the PCC can be achieved, compared to the scenario without EVs. For the largest BESS of 2000 kWh and the highest EV-share of 16%, the reduction is only 0.3% per FEC. Further key indicators such as the total number of FECs show, that BESSs with a capacity of less than 800 kWh are only subjected to a low stress and remain underutilized within the simulation period.

The method presented in this study was applied to an exemplary grid. The numerical results therefore only apply to this test area. However, the open-source simulation tools allow operators to investigate their own distribution grids, and test the impact of various BESS capacities and locations. Both the effect of state-of-the-art peak shaving and coupled storage systems can be analyzed with the framework developed in this study.

6.1. Future work and outlook

This study focuses on the technical potential of coupled energy management systems for a number of BESSs in a distribution grid. The reduction in the peak load at the PCC can avoid the need to exchange a transformer or reinforce cables. Future work can therefore focus on an economic analysis. For example, the cost of installing a BESS can be compared with the costs of conventional grid reinforcement.

In addition to an economic analysis, it might also be worthwhile to perform an ecological assessment to enable more precise investigation of the differences between conventional grid reinforcement and BESSs installation. While some studies, such as the work done by Baumann et al. [47], already deal with the CO_2 impact of BESSs, there is a research gap concerning the impact of CO_2 caused by conventional grid reinforcement.

Smart charging strategies or the potential of V2G at residential charging locations can be used to reduce the stress on the distribution grid resulting from a high EV-share. Therefore, the simulation tools presented in this study can be used to investigate the effect of these strategies on the distribution grid.

Existing peak shaving BESSs can lead to a peak load reduction at the PCC if the grid operator exchanges his current grid status with the BESS operator. However, this will require the creation of an economic and legal framework.

CRediT authorship contribution statement

Daniel Kucevic: Conceptualization, Methodology, Software, Writing - original draft, Visualization. **Stefan Englberger:** Methodology, Software. **Anurag Sharma:** Methodology, Writing - review & editing. **Anupam Trivedi:** Methodology, Writing - review & editing. **Benedikt Tepe:** Data curation. **Birgit Schachler:** Software. **Holger Hesse:** Supervision, Conceptualization, Writing - review & editing. **Dipti Srinivasan:** Supervision, Writing - review & editing. **Andreas Jossen:** Supervision, Writing - review & editing.

Declaration of competing interest

The authors declare that they have no known competing financial interests or personal relationships that could have appeared to influence the work reported in this paper.

Acknowledgments

This publication was financially supported by the German Federal Ministry for Economic Affairs and Energy within the research project open_BEA (Grant No. 03ET4072), which is managed by Project Management Jülich. The responsibility for this study rests with the authors.

Appendix A. Simulation framework: Additional description of further functionalities

A.1. Open battery models for electrical grid applications

The holistic open-source simulation tool open_BEA developed in this study enables BESS to be integrated into MV grids as well as LV grids in order to analyze the effects of the various operating strategies. The source code is programmed in Python. The main characteristic is the ability to assign individual time series to the various actors in the grid, such as domestic or industrial consumers. Furthermore, EV charging parks are integrated at various nodes to investigate the effects of increasing the share of electric mobility. open_BEA connects the following previous disjoint tools to enable accurate co-simulations of BESSs and distribution grids.

A.2. Simulation of stationary energy storage systems

SimSES, initially developed in MATLAB® [29], was converted to Python in 2019 and underwent enhancement at the EES institute at the Technical University Munich. SimSES enables the detailed simulation and evaluation of stationary energy storage systems, with the main focus currently on LIBs. The tool has been used in several publications, mainly for stand alone [48,49] or coupled [28] home energy storage systems, but also for peak shaving storage systems [22] or frequency containment reserve applications [38].

The main characteristic of this modular and flexible software tool is its abstract approach to the energy storage model, which enables the variation and hybridization of storage technologies and technical subcomponents. In addition, stress characterization estimates the energy storage degradation. Various semi empirical aging models can be used for this purpose.

A.3. Software for electric distribution grid optimization

The purpose of the eDisGo software is to perform a power flow analysis for a certain time period. The processing of the input parameters (e.g. loads or line impedances) is done with eDisGo, while the single step non-linear power flow calculation is conducted using the open-source PyPSA software [50]. The eDisGo tool is implemented in Python and has been previously used in two studies [30,51].

Apart from this study, eDisGo enables to assess the potential of flexibility options as an economic alternative to conventional grid expansion. And thus to assess their potential in lower grid expansion needs that arise from an increase in both renewable capacities and new consumers in medium and low voltage grids. Hence, it is necessary in eDisGo to identify both the grid problems and the costs incurred.

A.4. Linear programming optimization tool for energy storage systems

Like SimSES, the lp_opt tool was developed at the Institute for Electrical Energy Storage Technology at the Technical University of Munich. With its flexible structure, it serves as a co-optimization framework for both stationery and mobile energy storage systems and their underlying operation strategies. The tool was designed in the MATLAB® optimization environment using a problem-based approach. Besides the mathematical optimization solver of MATLAB®, the tool is also compatible with the Gurobi solver [52]. Both have been presented in previous literature [28,33].

The operation strategy of either an individual BESS or a multi-storage system with multiple BESSs can be optimized using lp_opt. Depending on the defined technical components of the observed energy

system, there are several entities that can be optimized and simulated, taking into consideration generating units, demand curves, EVs, their charging stations, and stationary BESSs.

Appendix B. Coordinated control strategy: Additional battery energy storage system results

Six characteristics defined in a previous publication are used to analyze the storage behavior in different settings [38]. The following figures all show the mean value (characteristic) of the three BESSs after a six months simulation period based on the setting defined in Section 4.

Fig. B.14 shows the remaining capacity in %, which is linked to the mean SOE (Fig. B.15) and the number of FEC (Fig. 13). The mean round-trip efficiency is displayed in Fig. B.16. The remaining characteristics describe the stress on the BESSs.

Fig. B.17 shows the average cycle depth in discharge direction. The number of alternations between charging and discharging (sign changes) per day is indicated in Fig. B.18, while Fig. B.19 shows the energy that is charged or discharged between sign changes, respectively. Finally, Fig. B.20 shows the average resting times.

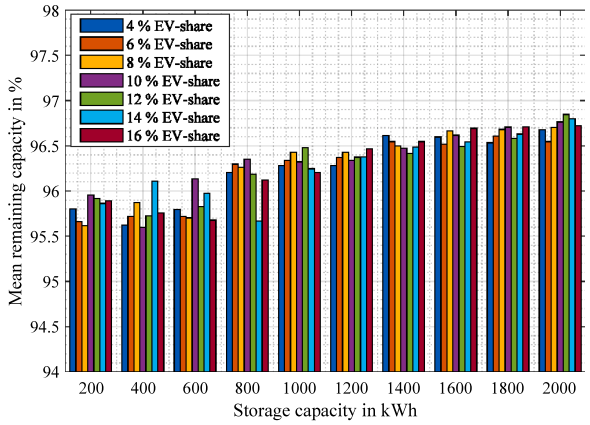

Fig. B.14. Mean remaining capacity of the three battery energy storage systems (BESSs) after a six month simulation period. The BESSs operate in accordance with the coordinated and coupled energy management system developed in this study.

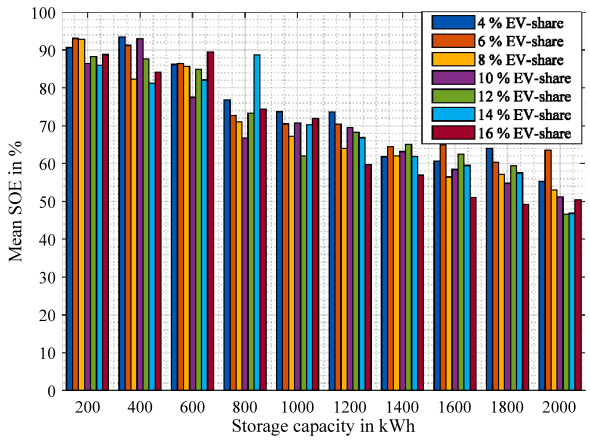

Fig. B.15. Mean state of energy of the three battery energy storage systems (BESSs) after a six month simulation period. The BESSs operate in accordance with the coordinated and coupled energy management system developed in this study.

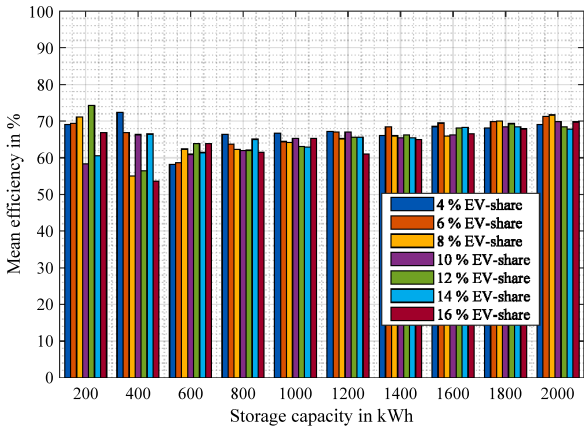

Fig. B.16. Mean efficiency of the three battery energy storage systems (BESSs) after a six month simulation period. The BESSs operate in accordance with the coordinated and coupled energy management system developed in this study.

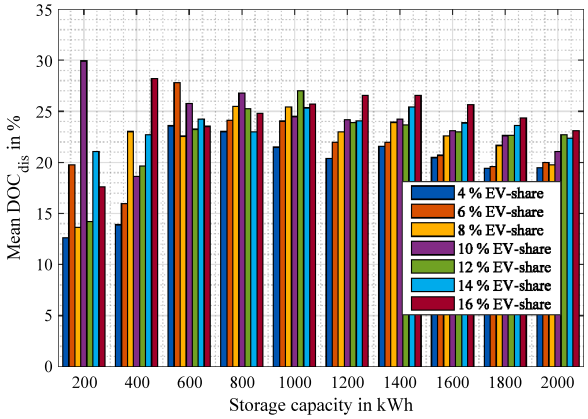

Fig. B.17. Mean depth of cycle in discharge direction of the three battery energy storage systems (BESSs) after a six month simulation period. The BESSs operate in accordance with the coordinated and coupled energy management system developed in this study.

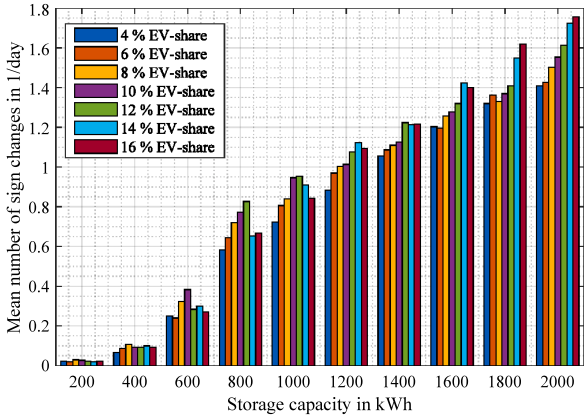

Fig. B.18. Average number of sign changes per day of the three battery energy storage systems (BESSs) after a six month simulation period. The BESSs operate in accordance with the coordinated and coupled energy management system developed in this study.

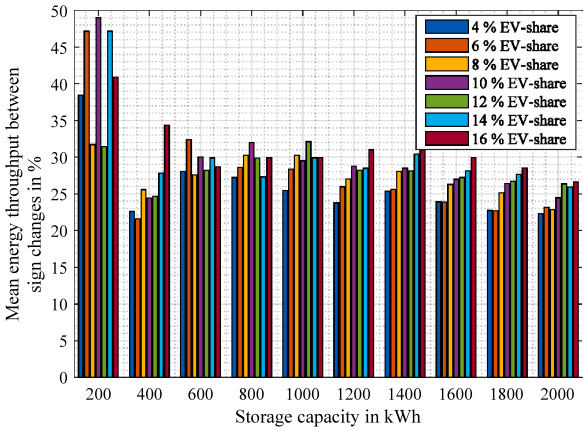

Fig. B.19. Average energy throughput between sign changes of the three battery energy storage systems (BESSs) after a six month simulation period. The BESSs operate in accordance with the coordinated and coupled energy management system developed in this study.

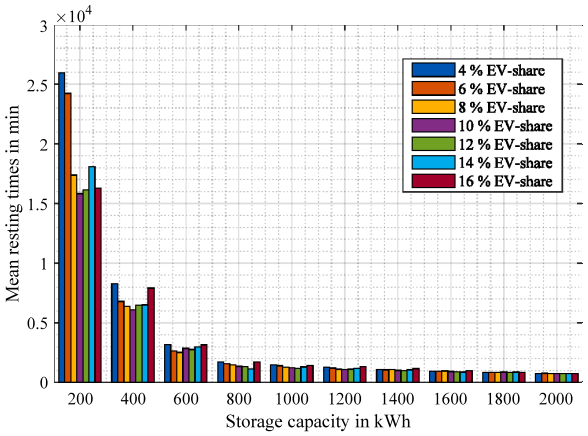

Fig. B.20. Average resting times of the three battery energy storage systems (BESSs) after a six month simulation period. The BESSs operate in accordance with the coordinated and coupled energy management system developed in this study.

References

[1] Richardson DB. Electric vehicles and the electric grid: A review of modeling approaches, impacts, and renewable energy integration. Renew Sustain Energy Rev 2013;19:247–54. http://dx.doi.org/10.1016/j.rser.2012.11.042.

[2] Crabtree G. The coming electric vehicle transformation. Science 2019;366(6464):422–4. http://dx.doi.org/10.1126/science.aax0704.

[3] Resch M, Bühler J, Klausen M, Sumper A. Impact of operation strategies of large scale battery systems on distribution grid planning in Germany. Renew Sustain Energy Rev 2017;74:1042–63. http://dx.doi.org/10.1016/j.rser.2017.02.075.

[4] Todts W, Mathieu L, Poliscanova J, Ambel CC, Muzi N, Alexandridou S. Recharge EU: How many charge points will Europe and its Member States need in the 2020s. URL https://www.transportenvironment.org/sites/te/files/publications/01%202020%20Draft%20TE%20Infrastructure%20Report%20Final.pdf.

[5] Nicholas M, Wappelhorst S. Regional charging infrastucture requirements in Germany through 2030. URL https://theicct.org/sites/default/files/publications/germany-charging-infrastructure-20201021.pdf.

[6] Galus MD, Vayá MG, Krause T, Andersson G. The role of electric vehicles in smart grids. Wiley Interdiscip Rev: Energy Environ 2013;2(4):384–400. http://dx.doi.org/10.1002/wene.56.

[7] Arias MB, Kim M, Bae S. Prediction of electric vehicle charging-power demand in realistic urban traffic networks. Appl Energy 2017;195:738–53. http://dx.doi.org/10.1016/j.apenergy.2017.02.021.

[8] Brinkel N, Schram WL, AlSkaif TA, Lampropoulos I, van Sark W. Should we reinforce the grid? Cost and emission optimization of electric vehicle charging under different transformer limits. Appl Energy 2020;276:115285. http://dx.doi.org/10.1016/j.apenergy.2020.115285.

[9] Pudjianto D, Djapic P, Aunedi M, Gan CK, Strbac G, Huang S, Infield D. Smart control for minimizing distribution network reinforcement cost due to electrification. Energy Policy 2013;52:76–84. http://dx.doi.org/10.1016/j.enpol.2012.05.021.

[10] Tan KM, Ramachandaramurthy VK, Yong JY. Integration of electric vehicles in smart grid: A review on vehicle to grid technologies and optimization techniques. Renew Sustain Energy Rev 2016;53(Supplement C):720–32. http://dx.doi.org/10.1016/j.rser.2015.09.012.

[11] Kempton W, Tomić J. Vehicle-to-grid power implementation: From stabilizing the grid to supporting large-scale renewable energy. J Power Sources 2005;144(1):280–94. http://dx.doi.org/10.1016/j.jpowsour.2004.12.022.

[12] Sovacool BK, Noel L, Axsen J, Kempton W. The neglected social dimensions to a vehicle-to-grid (V2G) transition: a critical and systematic review. Environ Res Lett 2017;13(1):013001. http://dx.doi.org/10.1088/1748-9326/aa9c6d.

[13] Wang D, Coignard J, Zeng T, Zhang C, Saxena S. Quantifying electric vehicle battery degradation from driving vs. vehicle-to-grid services. J Power Sources 2016;332:193–203. http://dx.doi.org/10.1016/j.jpowsour.2016.09.116.

[14] Jafari M, Gauchia A, Zhao S, Zhang K, Gauchia L. Electric vehicle battery cycle aging evaluation in real-world daily driving and vehicle-to-grid services. IEEE Trans Transp Electrif 2018;4(1):122–34. http://dx.doi.org/10.1109/TTE.2017.2764320.

[15] Hanemann P, Behnert M, Bruckner T. Effects of electric vehicle charging strategies on the German power system. Appl Energy 2017;203:608–22. http://dx.doi.org/10.1016/j.apenergy.2017.06.039.

[16] Hanemann P, Bruckner T. Effects of electric vehicles on the spot market price. Energy 2018;162:255–66. http://dx.doi.org/10.1016/j.energy.2018.07.180.

[17] Mehta R, Srinivasan D, Khambadkone AM, Yang J, Trivedi A. Smart charging strategies for optimal integration of plug-in electric vehicles within existing distribution system infrastructure. IEEE Trans Smart Grid 2018;9(1):299–312. http://dx.doi.org/10.1109/TSG.2016.2550559.

[18] Mehta R, Verma P, Srinivasan D, Yang J. Double-layered intelligent energy management for optimal integration of plug-in electric vehicles into distribution systems. Appl Energy 2019;233–234:146–55. http://dx.doi.org/10.1016/j.apenergy.2018.10.008.

[19] Diouf B, Pode R. Potential of lithium-ion batteries in renewable energy. Renew Energy 2015;76:375–80. http://dx.doi.org/10.1016/j.renene.2014.11.058.

[20] Hesse H, Martins R, Musilek P, Naumann M, Truong C, Jossen A. Economic optimization of component sizing for residential battery storage systems. Energies 2017;10(7):835. http://dx.doi.org/10.3390/en10070835.

[21] Gimelli A, Mottola F, Muccillo M, Proto D, Amoresano A, Andreotti A, Langella G. Optimal configuration of modular cogeneration plants integrated by a battery energy storage system providing peak shaving service. Appl Energy 2019;242:974–93. http://dx.doi.org/10.1016/j.apenergy.2019.03.084.

[22] Martins R, Hesse H, Jungbauer J, Vorbuchner T, Musilek P. Optimal component sizing for peak shaving in battery energy storage system for industrial applications. Energies 2018;11(8):2048. http://dx.doi.org/10.3390/en11082048.

[23] Reihani E, Motalleb M, Ghorbani R, Saad Saoud L. Load peak shaving and power smoothing of a distribution grid with high renewable energy penetration. Renew Energy 2016;86:1372–9. http://dx.doi.org/10.1016/j.renene.2015.09.050.

[24] Schram WL, Lampropoulos I, van Sark WG. Photovoltaic systems coupled with batteries that are optimally sized for household self-consumption: Assessment of peak shaving potential. Appl Energy 2018;223:69–81. http://dx.doi.org/10.1016/j.apenergy.2018.04.023.

[25] Nykamp S, Molderink A, Hurink JL, Smit GJM. Storage operation for peak shaving of distributed PV and wind generation. In: 2013 IEEE PES innovative smart grid technologies conference (ISGT). IEEE; 2013, p. 1–6. http://dx.doi.org/10.1109/ISGT.2013.6497786.

[26] Chapaloglou S, Nesiadis A, Iliadis P, Atsonios K, Nikolopoulos N, Grammelis P, Yiakopoulos C, Antoniadis I, Kakaras E. Smart energy management algorithm for load smoothing and peak shaving based on load forecasting of an island's power system. Appl Energy 2019;238:627–42. http://dx.doi.org/10.1016/j.apenergy.2019.01.102.

[27] Purvins A, Sumner M. Optimal management of stationary lithium-ion battery system in electricity distribution grids. J Power Sources 2013;242:742–55. http://dx.doi.org/10.1016/j.jpowsour.2013.05.097.

[28] Englberger S, Hesse H, Kucevic D, Jossen A. A techno-economic analysis of vehicle-to-building: Battery degradation and efficiency analysis in the context of coordinated electric vehicle charging. Energies 2019;12(5):955. http://dx.doi.org/10.3390/en12050955.

[29] Naumann M, Truong CN, Schimpe M, Kucevic D, Jossen A, Hesse HC. SimSES: Software for techno-economic simulation of stationary energy storage systems. In: International ETG congress 2017. ETG-Fachbericht, Berlin and Offenbach: VDE Verlag; 2017, p. 442–7.

[30] Müller UP, Schachler B, Scharf M, Bunke W-D, Günther S, Bartels J, Pleßmann G. Integrated techno-economic power system planning of transmission and distribution grids. Energies 2019;12(11):2091. http://dx.doi.org/10.3390/en12112091.

[31] Oudalov A, Cherkaoui R, Beguin A. Sizing and optimal operation of battery energy storage system for peak shaving application: 2007 IEEE lausanne power tech. In: IEEE PowerTech, 2007 IEEE Lausanne. 2007, p. 1–5. http://dx.doi.org/10.1109/PCT.2007.4538388.

[32] German Federal Office of Justice. Stromnetzentgeltverordnung (in German): StromNEV. 2005, URL https://www.gesetze-im-internet.de/stromnev/BJNR222500005.html.

[33] Englberger S, Hesse HC, Truong CN, Jossen A. Autonomous versus coordinated control of residential energy storage systems - monitoring profit, battery aging, and system efficiency. In: Schulz D, editor. NEIS 2018. Berlin: VDE VERLAG GMBH; 2019, p. 1–7, URL http://ieeexplore.ieee.org/stamp/stamp.jsp?tp=&arnumber=8669465&isnumber=8669446.

[34] Kucevic D, Truong CN, Jossen A, Hesse HC. Lithium-ion battery storage design for buffering fast charging stations for battery electric vehicles and electric buses. In: Schulz D, editor. NEIS 2018. Berlin: VDE VERLAG GMBH; 2019, p. 1–6, URL http://ieeexplore.ieee.org/stamp/stamp.jsp?tp=&arnumber=8669466&isnumber=8669446.

[35] Luo L, Gu W, Zhou S, Huang H, Gao S, Han J, Wu Z, Dou X. Optimal planning of electric vehicle charging stations comprising multi-types of charging facilities. Appl Energy 2018;226:1087–99. http://dx.doi.org/10.1016/j.apenergy.2018.06.014.

[36] ABB. High power charging: Fast charging just got faster. High power for next generation electric vehicles.. 2020, URL https://new.abb.com/ev-charging/products/car-charging/high-power-charging.

[37] Tjaden T, Bergner J, Weniger J, Quaschning V. Repräsentative elektrische Lastprofile für Wohngebäude in Deutschland auf 1-sekündiger Datenbasis (in German). URL https://pvspeicher.htw-berlin.de/daten/.

[38] Kucevic D, Tepe B, Englberger S, Parlikar A, Mühlbauer M, Bohlen O, Jossen A, Hesse H. Standard battery energy storage system profiles: Analysis of various applications for stationary energy storage systems using a holistic simulation framework. J Energy Storage 2020;28:101077. http://dx.doi.org/10.1016/j.est.2019.101077.

[39] Kucevic D, Tepe B, Englberger S, Parlikar A, Muehlbauer M, Bohlen O, Jossen A, Hesse H. Standard battery energy storage system profiles: Dataset. URL https://dataserv.ub.tum.de/s/m1510254/.

[40] Nobis C. Mobilität in Deutschland – MiD: Ergebnisbericht. URL https://elib.dlr.de/125879/.

[41] Stadtwerke Kiel AG. Richtlinie zum netzanschluss für neu- und bestandsanschlüsse: Netzebene 5 – mittelspannung (MS). 2016, URL https://www.swkiel-netz.de/swkn/media/dokumente/netzanschluss/netzanschluss_strom/tabs/archiv/2016-03-03_RL_SWK_Netzanschluss.pdf.

[42] Murata. Data sheet of sony fortelion US26650FTC1 battery cell. 2017, URL www.murata.com.

[43] Naumann M, Schimpe M, Keil P, Hesse HC, Jossen A. Analysis and modeling of calendar aging of a commercial LiFePO4/graphite cell. J Energy Storage 2018;17:153–69. http://dx.doi.org/10.1016/j.est.2018.01.019.

[44] Naumann M, Spingler FB, Jossen A. Analysis and modeling of cycle aging of a commercial LiFePO4/graphite cell. J Power Sources 2020;451:227666. http://dx.doi.org/10.1016/j.jpowsour.2019.227666.

[45] Notton G, Lazarov V, Stoyanov L. Optimal sizing of a grid-connected PV system for various PV module technologies and inclinations, inverter efficiency characteristics and locations. Renew Energy 2010;35(2):541–54. http://dx.doi.org/10.1016/j.renene.2009.07.013.

[46] Englberger S, Jossen A, Hesse H. Unlocking the potential of battery storage with the dynamic stacking of multiple applications. Cell Rep Phys Sci 2020;1. http://dx.doi.org/10.1016/j.xcrp.2020.100238.

[47] Baumann M, Peters JF, Weil M, Grunwald A. CO 2 footprint and life-cycle costs of electrochemical energy storage for stationary grid applications. Energy Technol 2017;5(7):1071–83. http://dx.doi.org/10.1002/ente.201600622.

[48] Naumann M, Karl RC, Truong CN, Jossen A, Hesse HC. Lithium-ion battery cost analysis in PV-household application. In: 9th International renewable energy storage conference, IRES 2015 73 (Supplement C). 2015, p. 37–47. http://dx.doi.org/10.1016/j.egypro.2015.07.555.

[49] Truong CN, Naumann M, Karl RC, Müller M, Jossen A, Hesse HC. Economics of residential photovoltaic battery systems in Germany: The case of teslas powerwall. Batteries 2016;2(2):14. http://dx.doi.org/10.3390/batteries2020014.

[50] Brown T, Hörsch J, Schlachtberger D. PyPSA: Python for power system analysis. J Open Res Softw 2018;6. http://dx.doi.org/10.5334/jors.188.

[51] Müller UP, Schachler B, Bunke W-D, Bartels J, Glauer M, Büttner C, Günther Stephan, Kötter Editha, Cussmann I, Hülk L, Scharf M, Mossakowski T, Wendiggensen J. Netzebenenübergreifendes Planungsinstrument zur Bestimmung des optimalen Netz- und Speicherausbaus in Deutschland integriert in einer OpenEnergyPlatform: open_ego - Projektabschlussbericht. URL https://www.uni-flensburg.de/fileadmin/content/abteilungen/industrial/dokumente/downloads/veroeffentlichungen/forschungsergebnisse/20190426endbericht-openego-fkz0325881-final.pdf.

[52] Gurobi Optimization LLC. Gurobi optimization. 2020, URL http://www.gurobi.com/.

7 Battery energy storage systems as an alternative to conventional grid reinforcement

Main research question: *Are BESSs an economical alternative to conventional grid reinforcement?*

While in the previous chapter the focus was on the technical analysis of the effects of established and developed operation strategies for BESSs on a distribution grid, this publication shows an economic analysis to determine the possibility of stationary storage systems as an alternative to conventional grid reinforcement. Costs for BESSs are compared with the costs for cable replacement in the MV grid and correlations are derived. To analyze future scenarios, predicted costs for both storage systems and grid reinforcement are included in this study.

Accurate co-simulations with the simulation tools SimSES and eDisGo, which have already been used several times, allow to apply the cost scenarios to use cases in a test grid. To avoid grid reinforcement, a BESS is integrated for each potential cable extension in the simulated MV grid. At these positions, a state-of-the-art peak shaving strategy is deployed by the BESS to reduce the grid load based on the former publication. For sizing the storage systems at the various positions, an iterative procedure is used in this publication. This work can be summarized as follows:

- An economic analysis of BESSs is conducted for storage capacities in a range between a few 100 kWh up to some MWh. Three scenarios are derived from the available data.
- The theoretical economic correlation of BESSs and grid reinforcement is applied to a use-case, by using the simulation tools SimSES and eDisGo.
- In particular, if small storage capacities are necessary to avoid grid reinforcement, grid operators should consider the possibility of a BESS integration.

The results show, that mainly in urban areas, BESSs can be competitive with conventional grid reinforcement. This ability to compete will be enhanced in the future. A detailed analysis for the BESS allows an estimation of additional revenue potential. These insights can be used in future studies to assign ancillary services, such as FCR, to the BESS with the aim of making it more competitive.

Author contribution Daniel Kucevic was the principal author tasked with coordinating and writing the paper and developing the simulation framework. Rebecca Meißner assisted with gathering and preparation of the data as well with the execution and writing of the case studies. Andreas Jossen contributed via fruitful scientific discussions and reviewed the manuscript. Holger Hesse reviewed the manuscript and gave valuable input throughout the manuscript preparation. All authors discussed the data and commented on the results.

Battery Energy Storage Systems as an Alternative to Conventional Grid Reinforcement

Daniel Kucevic, Rebecca Meißner, Andreas Jossen, Holger Hesse

International Conference on Applied Energy 2021, Bangkok (virtual), 2021

Permanent weblink:
https://doi.org/10.1016/energy-proceedings-9834

This manuscript was accepted on November 16th, 2021 by the scientific committee of the 13th International Conference on Applied Energy (ICEA) 2021. The paper is published in the conference proceedings of ICAE 2021 with open access.

International Conference on Applied Energy 2021
Nov. 29 - Dec. 2, 2021, in Bangkok, Thailand
Paper ID: 0048

Battery Energy Storage Systems as an Alternative to Conventional Grid Reinforcement

Daniel Kucevic[1*], Rebecca Meißner[1], Andreas Jossen[1], Holger Hesse[1]

[1]Institute for Electrical Energy Storage Technology, Technical University of Munich (TUM), Arcisstr. 21, 80333 Munich, Germany

[*]Corresponding Author

ABSTRACT

The upcoming transformation from internal combustion vehicles to electric vehicles in the private transport sector, together with the increasing demand for electricity, leads to challenges such as over-loading for the power grid. This study shows an economic analysis to what extent storage systems can be an alternative to conventional grid reinforcement. Current and predicted costs for storage systems are compared with the costs for cable replacement in the medium-voltage grid and correlations are derived. Accurate co-simulations of storage systems and the distribution grid allow these cost scenarios to be applied to use cases. In order to make the storage system competitive, multi-use scenarios can be considered. The detailed simulation allow insights about the stress of the storage system operating to avoid grid reinforcement.

Keywords: battery energy storage, grid reinforcement, grid integrated energy storage, energy management system, lithium-ion battery, economic analysis

NONMENCLATURE

Abbreviations	
BESS	battery energy storage system
e^{rate}	energy rate of the battery energy storage system
LIB	lithium-ion battery
LV	low voltage
MV	medium voltage
open_BEA	open battery models for electrical grid applications
SimSES	simulation of stationary energy storage systems

Parameters & symbols	
c_{BEES}	specific energy costs in $/kWh
c_{Grid}	specific grid reinforcement costs in $/km
Cap	maximum economic capacity in kWh
cap	length-specific capacity in kWh/km
d	discount factor
fit_1, fit_2	fitting parameters
l	length of grid reinforcement in km
r	discount rate
t_{BESS}	depreciation period of the BESS
t_{inv}	year of the investment
$t_{inv,c}$	year of the investment, corrected
t_{Grid}	depreciation period of the cables

1. INTRODUCTION

Increased electricity demand, mainly caused by electric vehicles and heat pumps, together with new generator units such as wind and solar power plants poses new challenges for the distribution grid [1]. While in rural areas, the increased share of renewable energies, resulting in over voltages is the main cause of grid reinforcement, in urban distribution grids, it is forecasted that over-loading will be the main driver therefore [2].

In the literature, various approaches exist to avoid grid reinforcement. Especially in the field of electric vehicles, a number of researches deal with controlled charging strategies or Vehicle-to-Grid approaches [3,4]. Battery energy storage systems (BESSs) are seen as an alternative without influencing owners of electric

Selection and peer-review under responsibility of the scientific committee of the 13th Int. Conf. on Applied Energy (ICAE2021).

vehicles [5]. Due to the decreasing costs of lithium-ion batteries (LIBs), this opportunity might be even more interesting in the future [6].

However, in the past stationary BESSs have been often used in behind-the-meter use cases to avoid overloading, such as buffer storage for electric vehicle charging stations [7]. This study evaluates the possibility of integration BESSs as an active part of distribution grid planning, which allows the grid owner to manage the energy flow of the storage system.

The use of energy storage is compared economically with conventional grid reinforcement. First, a cost model for current and future BESS prices is developed and compared with the costs for cable replacement in the medium-voltage (MV) grid. Second, these cost scenarios are applied to use cases in a test grid together with a detailed analysis of the BESS. This detailed analysis allows an estimation of additional revenues for the BESS. A graphical representation can be found in Fig. 1.

1.1 Outline of this study

The remainder of this paper is structured as follows: Configuration of the grid modeling tool as well as the simulation settings for the BESS are described in Section 2. Section 3 describes the methodology of this study including a data and graphical representation of the economics. Section 4 gives an outlook to the expected results of the use cases, where the cost scenarios are applied, and concludes the paper.

2. SIMULATION FRAMEWORK

2.1 Grid modeling

The holistic open-source simulation tool open_BEA expanded as part of this study enables BESSs to be integrated into MV grids as well as low-voltage (LV) grids in order to analyze the effects of the various operating strategies. The source code is programmed in Python and the framework has been used in a former publication [8]. The main characteristic is the ability to assign individual time series to the various actors in the grid, such as residential or industrial consumers.

Furthermore, electric vehicles charging parks can be integrated at various nodes to investigate the effects of increasing the share of electric mobility. One of these effects is the need of grid reinforcement. With open_BEA, conventional grid reinforcement can be compared with the usage of BESSs.

2.2 Simulation of stationary energy storage systems

To analyze the behavior of the BESS in various operation modes a detailed simulation is necessary [9]. In this study, the storage system is used to avoid conventional grid reinforcement. For the analysis of the BESS, a simulation tool of stationary energy storage systems (SimSES) is used.

SimSES is a holistic simulation framework specialized in evaluating energy storage technologies technically and economically [10]. With a modular approach, SimSES covers various topologies, system components such as power electronic units, and storage technologies

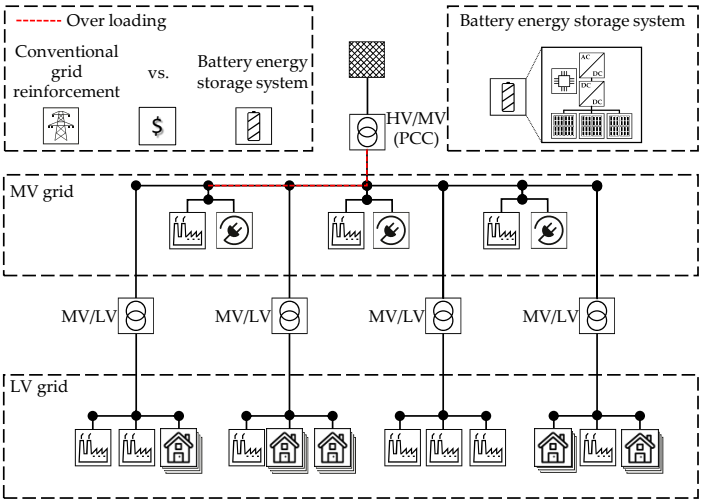

Fig. 1. Graphical overview of the test scenario where the cost model for battery energy storage system and grid reinforcement is applied. The test grid includes a medium voltage grid with several underlying low voltage grids. The storage system is modeled in detail as shown in the blow-up.

embedded in an energy storage application. SimSES is used in this contribution to gain insights about the stress of the storage system operating to reduce the peak load and consequently avoid grid reinforcement. As a result, lifetime forecasts for the storage system in this operation mode can be obtained, for example.

3. ECONOMIC COMPARISON OF BATTERY ENERGY STORAGE SYSTEMS AND GRID REINFORCEMENT

In this section, the economic correlation of BEESs and conventional grid reinforcement is investigated. After defining the cost components, a data research gives an overview of the current and future costs. To consider different assumptions and cost prognosis, the data is organized in cost scenarios by functional expressions.

3.1 Battery energy storage systems

With the focus to an economic comparison of the BESS and conventional grid reinforcement, the data research only includes investment costs. Issuances for operation and maintenance are neglected.

In case of the BESS, the specific energy costs are declared on system level, containing all costs for the storage section, power electronics and additional equipment for grid coupling and system balance [11]. Due to an impact of the BESS design and dimensioning on the specific costs, requirements on the data quality are needed [12]. With an integration in the MV-grid, the storage capacity ranges between an industrial- and large-scale system with a few 100 kWh up to some MWh [13].

In addition to the BESS specifications, each publication gives a cost development with at least three data points between 2016 and 2040. Linearly interpolated, the data set split up in three scenarios. While scenario *base* with a moderate cost development is defined by the mean values, the scenarios *low* and *high* represent optimistic and conservative prognosis in the 95 % confidence interval. To describe each scenario by a cost function, curve-fittings are performed. As a result, the hyperbola in Eq. (1) returns the specific energy costs c_{BESS} depending on the year of the investment t_{inv}. The fitting parameters fit_1 (\$/kWh) and fit_2 are dependent on the cost scenarios.

$$c_{BESS} = \frac{fit_1}{t_{inv} + fit_2} \quad (1)$$

Fig. 2 depicts the cost functions with the data points of the publications. Between 2020 and 2030 the specific energy costs decrease about 38.5 % from 468 \$/kWh to 288 \$/kWh in the scenario *base*.

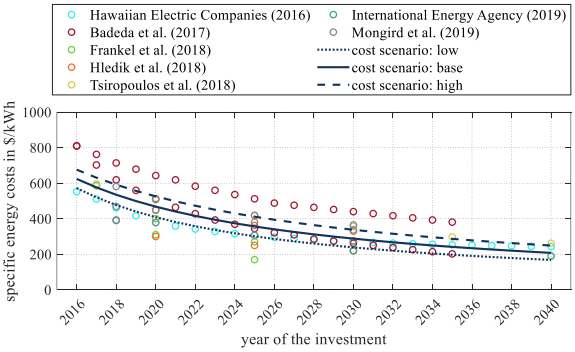

Fig. 2. Specific energy costs of the battery energy storage system depending on the year of the investment. Data points and resulting cost functions for the scenarios base, low and high are based on [12,14–20].

3.2 Grid reinforcement

The approach of conventional grid reinforcement is to avoid grid congestions by extending or replacing the equipment. In this economic comparison, the parallel installation of MV-cables is used to reinforce the grid. Therefore, the cable from type NA2XS2Y, 3x1x185 mm², which is common in German distribution grid, is set as standard equipment for the following data research. In this, the material as well as the installation costs are considered [21].

Moreover, because of the higher installation costs for compressed surface, the specific costs are classified by rural and urban areas. Due to the limited data situation, the resulting costs do not show a development trend and include no information concerning the future. This is why, the costs for the scenarios *base*, *low* and *high* are determined with the current data. Table 1 shows the specific grid reinforcement costs for these scenarios.

Table 1. Specific grid reinforcement costs in medium voltage-grids for cable extension in rural as well as urban areas. The data for the various scenarios are based on [21–29].

	specific costs in \$/km		
scenario	low	base	high
rural	116 000	133 000	150 000
urban	151 000	177 000	203 000

3.3 Economic correlation of battery energy storage systems and grid reinforcement

In the following, an economic correlation between the BESS capacity and the length of the grid reinforcement is defined, with the purpose to determine the maximum capacity that allows an economic use case for the BESS at a specific cable length. Under consideration of the cost functions, it is the point at which the discounted costs of the BESS equal to those of the grid reinforcement. In Eq. (2), the maximum economic storage capacity Cap is described by the discount factor d, the length-specific capacity cap, the correction on the year of the investment $t_{inv,c}$ and the length l.

$$\mathrm{Cap} = \mathrm{cap} \cdot \mathrm{t_{inv,c}} \cdot \mathrm{d} \cdot \mathrm{l} \tag{2}$$

With:

$$\mathrm{cap} = \frac{\mathrm{c_{Grid}}}{\mathrm{fit_1}}$$

$$\mathrm{t_{inv,c}} = \mathrm{t_{inv}} + \mathrm{fit_2}$$

$$\mathrm{d} = (1 + \mathrm{r})^{(\mathrm{t_{BESS}} - \mathrm{t_{Grid}})}$$

For extension lengths of 40 km in rural areas and 20 km in urban regions, the capacities, for which the discounted costs of the BESS are lower than for a conventional grid reinforcement, are displayed in Fig. 3. In addition, the capacities are compared for a year of the investment in 2020 and 2030. For this, the discount rate is assumed with 6 % and the depreciation periods for the BESS and the MV-cable are set with 10 years and 40 years [21,30].

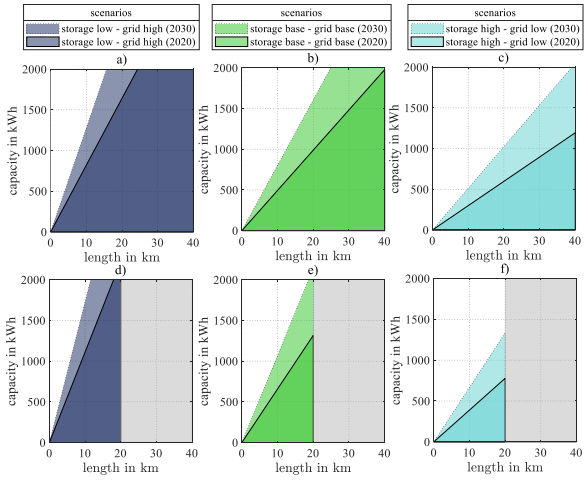

Fig. 3. Economic capacity of the battery energy storage system depending on the length of grid reinforcement in a) to c) for rural areas and d) to f) for urban areas.

4. CONCLUSION AND OUTLOOK

This study shows an economic analysis to what extent storage systems can be an alternative to conventional grid reinforcement. Current and predicted costs for storage systems are compared with the costs for cable replacement in the MV grid and correlations are derived. Accurate co-simulations of storage systems and the distribution grids allow these cost scenarios to be applied to use cases.

An economic analysis of storage systems is conducted for BESSs capacities in a range between a few 100 kWh up to some MWh. Three scenarios are derived from the available data. The results shows that between 2020 and 2030 the specific energy costs decrease about 38.5 % from 468 $/kWh to 288 $/kWh in a base scenario. To describe each scenario by a cost function, curve-fittings are performed.

The specific costs in $/km for conventional grid reinforcement are classified by rural and urban areas and again three scenarios are derived from the available data. The maximum economic storage capacity for a specific grid reinforcement length, a discount factor, and the year of investment is described through a linear equation.

The results show that even in urban areas, BESSs with a capacity above 1 MWh are not competitive with conventional grid reinforcement. Only if small storage capacities are necessary to avoid grid reinforcement, a BESS can currently be installed economically.

4.1 Outlook

The full paper will include simulations of a MV-grid with a high share of electric vehicles where grid reinforcement would be required. Ancillary services, such as frequency containment reserve, are assigned to the BESS with the aim of making it more competitive.

ACKNOWLEDGEMENT

This publication was financially supported by the German Federal Ministry for Economic Affairs and Energy within the research project open_BEA (Grant No. 03ET4072), managed by Project Management Jülich. The responsibility for this study rests with the authors.

AUTHOR CONTRIBUTIONS

Daniel Kucevic: Conceptualization, Methodology, Software, Investigation, Writing - Original Draft **Rebecca Meißner:** Methodology, Software, Formal analysis, Writing – Original Draft, Visualization **Andreas Jossen:** Writing - Review & Editing, Supervision **Holger Hesse:** Methodology, Writing - Review & Editing, Supervision

REFERENCES

[1] Stecca M, Ramirez Elizondo L, Batista Soeiro T, Bauer P, Palensky P. A Comprehensive Review of the Integration of Battery Energy Storage Systems into Distribution Networks. IEEE Open J. Ind. Electron. Soc. 2020:1.

[2] Resch M, Bühler J, Klausen M, Sumper A. Impact of operation strategies of large scale battery systems on distribution grid planning in Germany. Renewable and Sustainable Energy Reviews 2017;74:1042–63.

[3] Crozier C, Morstyn T, McCulloch M. The opportunity for smart charging to mitigate the impact of electric vehicles on transmission and distribution systems. Applied Energy 2020;268:114973.

[4] Brinkel N, Schram WL, AlSkaif TA, Lampropoulos I, van Sark W. Should we reinforce the grid? Cost and emission optimization of electric vehicle charging under different transformer limits. Applied Energy 2020;276:115285.

[5] Das CK, Bass O, Kothapalli G, Mahmoud TS, Habibi D. Overview of energy storage systems in distribution networks: Placement, sizing, operation, and power quality. Renewable and Sustainable Energy Reviews 2018;91:1205–30.

[6] Schmidt O, Hawkes A, Gambhir A, Staffell I. The future cost of electrical energy storage based on experience rates. Nat. Energy 2017;6:17110.

[7] Rubino L, Capasso C, Veneri O. Review on plug-in electric vehicle charging architectures integrated with distributed energy sources for sustainable mobility. Applied Energy 2017;207:438–64.

[8] Kucevic D, Englberger S, Sharma A, Trivedi A, Tepe B, Schachler B et al. Reducing grid peak load through the coordinated control of battery energy storage systems located at electric vehicle charging parks. Applied Energy 2021;295:116936.

[9] Kucevic D, Tepe B, Englberger S, Parlikar A, Mühlbauer M, Bohlen O et al. Standard battery energy storage system profiles: Analysis of various applications for stationary energy storage systems using a holistic simulation framework. Journal of Energy Storage 2020;28:101077.

[10] Naumann M, Truong CN, Schimpe M, Kucevic D, Jossen A, Hesse HC. SimSES: Software for techno-economic Simulation of Stationary Energy Storage Systems. In: International ETG Congress 2017: Die Energiewende blueprints for the new energy age proceedings November 28-29, 2017, World Conference Center, Bonn. Berlin, Offenbach: VDE Verlag; 2017, p. 442–447.

[11] Zakeri B, Syri S. Electrical energy storage systems: A comparative life cycle cost analysis. Renewable and Sustainable Energy Reviews 2015;42:569–96.

[12] Frankel D, Kane S, Tryggestad C. The new rules of competition in energy storage. [August 19, 2021]; Available from: https://www.mckinsey.com/industries/electric-power-and-natural-gas/our-insights/the-new-rules-of-competition-in-energy-storage.

[13] Figgener J, Stenzel P, Kairies K-P, Linßen J, Haberschusz D, Wessels O et al. The development of stationary battery storage systems in Germany – A market review. Journal of Energy Storage 2020;29:101153.

[14] Hawaiian Electric Companies. Book 3 of 4. In: The Honorable Chair and Members of the Hawaii Puvlic Utilities Commision, editor. PSIPs Update Report. Honolulu; 2016.

[15] Badeda J, Meyer J, Sauer DU. Modeling the influence of installed battery energy storage systems on the German frequency containment reserve market. In: Schulz D, editor. NEIS 2017: Conference on Sustainable Energy Supply and Energy Storage Systems Hamburg, 21-22 September 2017. Berlin: VDE VERLAG GMBH; 2018, p. 315–321.

[16] Hledik R, Chang J, Pfeifenberger J, Lueken R, Pedtke JI, Vollen J. The Economic Potential for Energy Storage in Nevada. [August 26, 2021]; Available from: https://www.brattle.com/news-and-knowledge/publications/the-economic-potential-for-energy-storage-in-nevada.

[17] Tsiropoulos I, Tarvydas D, Lebedeva N. Li-ion batteries for mobility and stationary storage applications: Scenarios for costs and market growth. Luxembourg; 2018.

[18] International Energy Agency. World Energy Outlook 2019. [August 26, 2021]; Available from: https://www.iea.org/reports/world-energy-outlook-2019.

[19] Mongird K, Viswanathan V, Alam J, Vartanian C, Sprenkle V, Baxter R. 2020 Grid Energy Storage Technology Cost and Performance Assessment. [August 26, 2021]; Available from: https://www.pnnl.gov/ESGC-cost-performance.

[20] Mongird K, Viswanathan VV, Balducci PJ, Alam MJE, Fotedar V, Koritarov VS et al. Energy Storage Technology and Cost Characterization Report.

[August 26, 2021]; Available from: https://www.energy.gov/eere/water/downloads/energy-storage-technology-and-cost-characterization-report.

[21] Deutsche Energie-Agentur GmbH (dena). dena-Verteilnetzstudie: Ausbau und Innovationsbedarf der Stromverteilnetze in Deutschland bis 2030. [August 19, 2021]; Available from: https://www.dena.de/themen-projekte/projekte/energiesysteme/dena-verteilnetzstudie/.

[22] Rehtanz C, Greve M, Häger U, Hagemann Z, Kippelt S, Kittl C et al. Verteilnetzstudie für das Land Baden-Württemberg. [August 19, 2021]; Available from: https://www.baden-wuerttemberg.de/de/service/presse/pressemitteilung/pid/verteilnetzstudie-fuer-baden-wuerttemberg-veroeffentlicht-1/.

[23] Pieltain Fernandez L, Gomez San Roman T, Cossent R, Mateo Domingo C, Frias P. Assessment of the Impact of Plug-in Electric Vehicles on Distribution Networks. IEEE Trans. Power Syst. 2011;26(1):206–13.

[24] Energynautics GmbH, Öko-Institut e.V., Bird & Bird LLP. Verteilnetzstudie Rheinland-Pfalz. [August 26, 2021]; Available from: https://energynautics.com/de/referenzen/verteilnetzstudie-rheinland-pfalz/.

[25] Braun M, Krybus I, Becker H, Bolgaryn R, Dasenbrock J, Gauglitz P et al. Verteilnetzstudie Hessen 2024 - 2034. [August 26, 2021]; Available from: https://www.energieland.hessen.de/verteilnetzstudie_hessen.

[26] Kneiske T, Czajkowski C, Lohmier D, Spalthoff C, Thurner L, Kupka J. ANaPlan - Automatisierte Netzausbauplanung im Verteilnetz. [August 26, 2021]; Available from: https://www.iee.fraunhofer.de/de/projekte/suche/2018/ANaPlan-automatisierte-netzausbauplanung-im-verteilnetz.html.

[27] E-Bridge Consulting GmbH. Moderne Verteilernetze für Deutschland: (Verteilernetzstudie). [August 26, 2021]; Available from: https://www.bmwi.de/Redaktion/DE/Publikationen/Studien/verteilernetzstudie.html.

[28] Harnisch S, Steffens P, Thies HH, Monscheidt J, Münch L, Böse C et al. Planungs- und Betriebsgrundsätze für ländliche Verteilungsnetze: Leitfaden zur Ausrichtung der Netze an ihren zukünftigen Anforderungen. [August 26, 2021]; Available from: http://elpub.bib.uni-wuppertal.de/servlets/DocumentServlet?id=5890.

[29] Tretschock M, Greve M, Probst F, Kippelt S, Wagner C, Rehtanz C et al. Gutachten zur Weiterentwicklung der Strom-Verteilnetze in Nordrhein-Westfalen auf Grund einer fortschreitenden Sektorenkopplung und neuer Verbraucher. [August 26, 2021]; Available from: https://www.wirtschaft.nrw/pressemitteilung/verteilnetzstudie-nrw.

[30] Battke B, Schmidt TS. Cost-efficient demand-pull policies for multi-purpose technologies – The case of stationary electricity storage. Applied Energy 2015;155:334–48.

8 Conclusion and outlook

This thesis proposed possible solutions to meet the future challenges of grid overloading in urban areas caused by an increasing number of charging opportunities for electric vehicles (EVs). Various energy management strategies for battery energy storage systems (BESSs) were developed to achieve an improvement in the distribution grid. The objective was to reduce the peak power at the point of common coupling by adapting the control of stand-alone as well as coupled BESS located at various nodes in the distribution grid. Open-source simulation tools, which enables a realistic simulation of the effects of storage systems in different operating modes on the distribution grid, were developed and adapted as part of this work. Consequently, an economic analysis was conducted to evaluate storage systems as an alternative to conventional grid reinforcement. The following section concludes this thesis with a focus on the several papers. Finally, section 8.2 gives an outlook to possible future research tasks.

8.1 Thesis conclusion

The development and adaptation of various simulation tools is the base of this thesis. In Chapter 3 a tool for the simulation of stationary energy storage systems (SimSES) was described in detail. SimSES provides several state-of-the-art energy storage models as well as associated periphery of a storage system. Within the paper, storage technology models based on current research for lithium-ion batteries (LIBs), redox flow batteries, as well as hydrogen storage-based electrolysis and fuel cell were described in detail. Standard stand alone operation strategies for energy storage systems like peak shaving, residential storage, and the provision of frequency containment reserve (FCR) were presented as part of this work.

To demonstrate the base functionalities of SimSES in greater detail, two case studies were discussed in the publication. The case studies were mapped to the applications of FCR and peak shaving. For these use-cases it was demonstrated how different energy storage system topologies can be investigated and analyzed with SimSES. Simulation results showed that special BESS topologies like a cascaded approach for the power electronic units lead to a substantial increase in system efficiency. SimSES provides an analysis with technical and economic evaluations illustrated by key performance indicators.

Some technical key performance indicators of SimSES were used to analyze various stand alone operation strategies in detail in Chapter 4. In this paper we presented a method to create standard profiles for stationary BESS and we made the results as open data available for download. Input profiles including frequency data, industry load profiles and residential load profiles were pre-processed using a normalization and clustering method. These input profiles were then transformed into storage profiles including the storage power and the state of energy (SOE) using the in Chapter 3 described holistic simulation framework SimSES.

SimSES was used to analyze stand alone applications for stationary BESS in detail and an energy

management system (EMS) was programmed for three different applications: an algorithm for providing FCR, two algorithms (greedy and feed-in damping) for a residential BESS, and an EMS for an industrial peak shaving BESS. The results were post-processed using a developed analyzer tool in order to figure out six key characteristics for BESS. For example, for a peak shaving BESS, the number of full equivalent cycle (FEC) varies from 4 to 63 and the average resting time from a few minutes up to eight hours. These characteristics are essential for the design of a storage system and they were used in this thesis for evaluating the impacts of different operation strategies on the BESS.

While in Chapter 3 and Chapter 4 the focus was on the development of SimSES and the analysis of established use-cases, in Chapter 5 a method to reduce the peak power at a specific node as well as at the transformer or point of common coupling (PCC) in distribution grids using BESSs was presented. The storage systems were located at 32 various industrial consumers with individual load profiles (cf. Chapter 4) in a medium voltage (MV) grid with 146 underlying low voltage (LV) grids. To improve a state-of-the-art peak shaving strategy, a method of a combined operation strategy for BESSs located at industrial consumers was developed to achieve both an improvement in the distribution grid as well as electricity bill savings for industrial consumers. By using and adapting a simulation framework (open_BEA), accurate co-simulations of BESSs and distribution grids were performed and the stress on the BESSs was evaluated using the key characteristics described in Chapter 4.

In this publication the BESSs were economical optimally sized using a linear optimization approach. The newly developed combined approach used a scaling factor for the power profile in order to combine the load profile at the PCC with the load profile of an individual industrial consumer. This combined profile served as the input for the operation strategy and the results were compared to a state-of-the-art peak shaving strategy. Results showed that with the developed approach both the local peak load and the global peak load can be reduced. Although in this scenario the BESSs reduced both peaks, the additional stress for the six month simulation period was on average only 1.2 full equivalent cycles higher than with a state-of-the-art peak shaving strategy.

To enhance the method from Chapter 5, in Chapter 6 a method to coordinate and couple multiple BESSs was introduced. The goal is again to reduce the power at the PCC in distribution grids with a high share of EVs. Charging parks located at three different nodes in a representative MV grid, and the EV-share was varied during a sensitivity analysis. At all three nodes, a BESS with increasing capacities of 200 kWh to 2000 kWh was coupled and the attendant EMS was controlled with the aid of a linear optimization framework, which was expanded as part of this study. The results are again compared to a state-of-the-art peak shaving strategy.

It was shown, that in a stand-alone mode there are no significant peak reductions at the PCC. This also matches with the results in Chapter 5. For most scenarios, however, no or only a very small increase in the peak load was identified. Hence, state-of-the-art peak shaving BESSs located at charging parks can help to avoid significant increases in the peak load at the PCC. But if the BESSs was operated using the coordinated control method, the peak load at the PCC was reduced in all scenarios by a maximum of 44.9 %. Analyzing the results in detail using the simulation tool SimSES a clear trend was identifiable: The peak load reduction per FEC decreased with an EV-share and BESS capacity increase. For example, the largest BESS of 2000 kWh and the highest EV-share of 16 %, the reduction was only 0.3 % per FEC.

While in Chapter 5 and Chapter 6 the focus was on the technical analysis of the effects of established and developed operation strategies for BESSs on a distribution grid, in Chapter 7 an economic anal-

ysis was conducted. Current and predicted costs for BESSs were compared with the costs for cable replacement in the MV-grid and correlations are derived. Using the various simulations tools allowed to apply these cost scenarios to use cases. The economic analysis of storage systems was conducted for BESSs capacities in a range between a few 100 kWh up to some MWh.

The results showed that between 2020 and 2030 the specific energy costs decrease about 38.5 % from 468 $/kWh to 288 $/kWh in a base scenario. The four investigated cases of cables extensions were avoided by integrating BESSs with a centralized peak shaving approach (cf. Chapter 5). The storage capacity was determined with an iterative procedure considering the loads at the positions with required grid reinforcement. The results showed, that mainly in urban areas, BESSs can be competitive with conventional grid reinforcement now and even more in 2030.

Finally, it can be summarized that grid operators should consider the possibility of a integration of an storage system with enhanced operation strategies as an alternative to grid reinforcement. Accelerated aging as well as adaptions in the energy management systems would have to be compensated financially by the grid operator to the storage owner or industrial consumer. However, it must be taken into account that the grid operator benefits economically by being able to avoid a possible grid reinforcement or transformer upgrade. The frameworks shown in this thesis requires communication (e.g., via the 5G communication standard [163, 164] or the IEC 60870 standard [161]) between the grid operator and its current load at the PCC and various stakeholders, as for example industrial consumer or storage operators. In addition, the algorithms introduced require the creation of an economic and legal framework.

8.2 Possible future research tasks

This thesis focused on the technical and economic potential of installing storage systems in distribution grids. The additional reduction in the peak load at the PCC may avoid the need of grid reinforcement or transformer exchange. From a grid perspective, future studies could also focus more on other grid-related applications as an additional service of the BESS, such as reactive power control. To improve the economic results, ancillary services, such as FCR, can be assigned to the BESS with the aim of making it more competitive to conventional grid reinforcement. There are already initial approaches to this in the literature, but without the aim of reducing the peak grid load [137, 165].

Furthermore, smart charging strategies or the potential of vehicle-to-grid at residential as well as public charging locations can be used to reduce the stress on the distribution grid resulting from a high EV-share. Research is already carried out in the context of vehicle-to-grid or smart charging, but mostly with the aim of reducing the owner's costs [166, 167]. The simulation tools presented in this thesis might be used to investigate the effect of these approaches on the distribution grid.

Another highly discussed topic is the ecological assessment of storage systems. It might also be worthwhile to perform an ecological assessment to enable more precise investigation of the differences between conventional grid reinforcement and BESSs installation. While some studies, such as the work done by Baumann et al. [168] and Parlikar et al. [169], already deal with the CO_2 impact of BESSs, there is a research gap concerning the impact of CO_2 caused by conventional grid reinforcement.

Bibliography

[1] Kucevic, D.; Tepe, B.; Englberger, S.; Parlikar, A.; Mühlbauer, M.; Bohlen, O.; Jossen, A.; Hesse, H.: *Standard battery energy storage system profiles: Analysis of various applications for stationary energy storage systems using a holistic simulation framework*, in: *Journal of Energy Storage 28*, p. 101077, 2020

[2] Kucevic, D.; Meißner, R.; Jossen, A.; Hesse, H.: *Battery Energy Storage Systems as an Alternative to Conventional Grid Reinforcement (accepted; unpublished work)*, in: Energy Proceedings (ed.): *13th International Conference on Applied Energy*, 2021

[3] Kucevic, D.; Göschl, S.; Röpcke, T.; Hesse, H.; Jossen, A.: *Reducing grid peak load through smart charging strategies and battery energy storage systems*, in: Energynautics GmbH (ed.): *5th E-Mobility Integration Symposium*, 2021

[4] Kucevic, D.; Truong, C.N.; Jossen, A.; Hesse, H.C.: *Lithium-Ion Battery Storage Design for Buffering Fast Charging Stations for Battery Electric Vehicles and Electric Buses*, in: Schulz, D. (ed.): *NEIS 2018*, VDE VERLAG GMBH, Berlin, 2019

[5] Kucevic, D.; Semmelmann, L.; Collath, N.; Jossen, A.; Hesse, H.: *Peak Shaving with Battery Energy Storage Systems in Distribution Grids: A Novel Approach to Reduce Local and Global Peak Loads*, in: *Electricity 2 (4)*, pp. 573–589, 2021

[6] Kucevic, D.; Englberger, S.; Sharma, A.; Trivedi, A.; Tepe, B.; Schachler, B.; Hesse, H.; Srinivasan, D.; Jossen, A.: *Reducing grid peak load through the coordinated control of battery energy storage systems located at electric vehicle charging parks*, in: *Applied Energy 295*, p. 116936, 2021

[7] Hesse, H.; Schimpe, M.; Kucevic, D.; Jossen, A.: *Lithium-Ion Battery Storage for the Grid—A Review of Stationary Battery Storage System Design Tailored for Applications in Modern Power Grids*, in: *Energies 10 (12)*, p. 2107, 2017

[8] Englberger, S.; Hesse, H.; Kucevic, D.; Jossen, A.: *A Techno-Economic Analysis of Vehicle-to-Building: Battery Degradation and Efficiency Analysis in the Context of Coordinated Electric Vehicle Charging*, in: *Energies 12 (5)*, p. 955, 2019

[9] Möller, M.; Kucevic, D.; Collath, N.; Parlikar, A.; Dotzauer, P.; Tepe, B.; Englberger, S.; Jossen, A.; Hesse, H.: *SimSES: A holistic simulation framework for modeling and analyzing stationary energy storage systems*, in: *Journal of Energy Storage 49*, p. 103743, 2022

[10] Naumann, M.; Truong, C.N.; Schimpe, M.; Kucevic, D.; Jossen, A.; Hesse, H.C.: *SimSES: Software for techno-economic Simulation of Stationary Energy Storage Systems*, in: VDE / ETG (ed.): *International ETG Congress 2017*, VDE Verlag, Berlin and Offenbach, 2017

[11] Richardson, D.B.: *Electric vehicles and the electric grid: A review of modeling approaches, Impacts, and renewable energy integration*, in: *Renewable and Sustainable Energy Reviews 19*, pp. 247–254, 2013

[12] Crabtree, G.: *The coming electric vehicle transformation*, in: *Science 366 (6464)*, pp. 422–424, 2019

[13] Resch, M.; Bühler, J.; Klausen, M.; Sumper, A.: *Impact of operation strategies of large scale battery systems on distribution grid planning in Germany*, in: *Renewable and Sustainable Energy Reviews 74*, pp. 1042–1063, 2017

[14] Todts, W.; Mathieu, L.; Poliscanova, J.; Ambel, C.C.; Muzi, N.; Alexandridou, S.: *Recharge EU: How many charge points will Europe and its Member States need in the 2020s*, ed. by Transport & Environment, Brussels, 2020, URL: `https://www.transportenvironment.org/sites/te/files/publications/01%202020%20Draft%20TE%20Infrastructure%20Report%20Final.pdf`, log-date:

[15] Nicholas, M.; Wappelhorst, S.: *Regional charging infrastucture requirements in Germany through 2030*, ed. by International Council on Clean Transportation, Washington, 2020, URL: `https://theicct.org/sites/default/files/publications/germany-charging-infrastructure-20201021.pdf`, log-date:

[16] Galus, M.D.; Vayá, M.G.; Krause, T.; Andersson, G.: *The role of electric vehicles in smart grids*, in: *Wiley Interdisciplinary Reviews: Energy and Environment 2 (4)*, pp. 384–400, 2013

[17] Arias, M.B.; Kim, M.; Bae, S.: *Prediction of electric vehicle charging-power demand in realistic urban traffic networks*, in: *Applied Energy 195*, pp. 738–753, 2017

[18] Shah, R.; Mithulananthan, N.; Bansal, R.C.; Ramachandaramurthy, V.K.: *A review of key power system stability challenges for large-scale PV integration*, in: *Renewable and Sustainable Energy Reviews 41*, pp. 1423–1436, 2015

[19] Hammons, T.J.: *Integrating renewable energy sources into European grids*, in: *International Journal of Electrical Power & Energy Systems 30 (8)*, pp. 462–475, 2008

[20] Braun, M. et al.: *Is the distribution grid ready to accept large-scale photovoltaic deployment? State of the art, progress, and future prospects*, in: *Progress in Photovoltaics: Research and Applications 20 (6)*, pp. 681–697, 2012

[21] Sinsel, S.R.; Riemke, R.L.; Hoffmann, V.H.: *Challenges and solution technologies for the integration of variable renewable energy sources—a review*, in: *Renewable Energy 145*, pp. 2271–2285, 2020

[22] Müller, M.: "Stationary Lithium-Ion Battery Energy Storage Systems A Multi-Purpose Technology", PhD Thesis, Munich: Technical University of Munich, 2017

[23] Müller, M.; Viernstein, L.; Truong, C.N.; Eiting, A.; Hesse, H.C.; Witzmann, R.; Jossen, A.: *Evaluation of grid-level adaptability for stationary battery energy storage system applications in Europe*, in: *Journal of Energy Storage 9*, pp. 1–11, 2017

[24] Resch, M.: "Large Scale Battery Systems in Distribution Grids", PhD Thesis, Barcelona: Universitat Politècnica de Catalunya, 2018

[25] Brinkel, N.; Schram, W.L.; AlSkaif, T.A.; Lampropoulos, I.; van Sark, W.: *Should we reinforce the grid? Cost and emission optimization of electric vehicle charging under different transformer limits*, in: *Applied Energy 276*, p. 115285, 2020

[26] Nykvist, B.; Nilsson, M.: *Rapidly falling costs of battery packs for electric vehicles*, in: *Nature Climate Change 5 (4)*, pp. 329–332, 2015

[27] Mehr, T.H.; Masoum, M.A.; Jabalameli, N.: *Grid-connected Lithium-ion battery energy storage system for load leveling and peak shaving*, in: IEEE (ed.): *2013 Australasian Universities Power Engineering Conference (AUPEC)*, IEEE, 2013

[28] Kempton, W.; Tomić, J.: *Vehicle-to-grid power implementation: From stabilizing the grid to supporting large-scale renewable energy*, in: *Journal of Power Sources 144 (1)*, pp. 280–294, 2005

[29] Tan, K.M.; Ramachandaramurthy, V.K.; Yong, J.Y.: *Integration of electric vehicles in smart grid: A review on vehicle to grid technologies and optimization techniques*, in: *Renewable and Sustainable Energy Reviews 53 (Supplement C)*, pp. 720–732, 2016

[30] Wang, D.; Coignard, J.; Zeng, T.; Zhang, C.; Saxena, S.: *Quantifying electric vehicle battery degradation from driving vs. vehicle-to-grid services*, in: *Journal of Power Sources 332*, pp. 193–203, 2016

[31] Jafari, M.; Gauchia, A.; Zhao, S.; Zhang, K.; Gauchia, L.: *Electric Vehicle Battery Cycle Aging Evaluation in Real-World Daily Driving and Vehicle-to-Grid Services*, in: *IEEE Transactions on Transportation Electrification 4 (1)*, pp. 122–134, 2018

[32] Hanemann, P.; Behnert, M.; Bruckner, T.: *Effects of electric vehicle charging strategies on the German power system*, in: *Applied Energy 203*, pp. 608–622, 2017

[33] Hanemann, P.; Bruckner, T.: *Effects of electric vehicles on the spot market price*, in: *Energy 162*, pp. 255–266, 2018

[34] Mehta, R.; Srinivasan, D.; Khambadkone, A.M.; Yang, J.; Trivedi, A.: *Smart Charging Strategies for Optimal Integration of Plug-In Electric Vehicles Within Existing Distribution System Infrastructure*, in: *IEEE Transactions on Smart Grid 9 (1)*, pp. 299–312, 2018

[35] Mehta, R.; Verma, P.; Srinivasan, D.; Yang, J.: *Double-layered intelligent energy management for optimal integration of plug-in electric vehicles into distribution systems*, in: *Applied Energy 233-234*, pp. 146–155, 2019

[36] Danish, S.M.S.; Ahmadi, M.; Danish, M.S.S.; Mandal, P.; Yona, A.; Senjyu, T.: *A coherent strategy for peak load shaving using energy storage systems*, in: *Journal of Energy Storage 32*, p. 101823, 2020

[37] Wilkening, L.: "Netzorientierter Betrieb von Batteriespeichersystemen in Verteilnetzen", PhD thesis, TUHH Universitätsbibliothek, 2021

[38] Naumann, M.: "Techno-economic evaluation of stationary battery energy storage systems with special consideration of aging", PhD Thesis, Munich: Technical University of Munich, 2018, URL: `http://mediatum.ub.tum.de/?id=1434981`, log-date:

[39] Zeh, A.: "Integration von Batteriespeichern in das deutsche Nieder- und Mittelspannungsnetz", PhD Thesis, Munich: Technical University of Munich, 2017, URL: `http://mediatum.ub.tum.de/?id=1351963`

[40] Zeh, A.; Witzmann, R.: *Operational Strategies for Battery Storage Systems in Low-voltage Distribution Grids to Limit the Feed-in Power of Roof-mounted Solar Power Systems*, in: *Energy Procedia 46*, pp. 114–123, 2014

[41] Zeh, A.; Müller, M.; Naumann, M.; Hesse, H.; Jossen, A.; Witzmann, R.: *Fundamentals of Using Battery Energy Storage Systems to Provide Primary Control Reserves in Germany*, in: *Batteries 2 (3)*, p. 29, 2016

[42] Schimpe, M.; Becker, N.; Lahlou, T.; Hesse, H.C.; Herzog, H.-G.; Jossen, A.: *Energy efficiency evaluation of grid connection scenarios for stationary battery energy storage systems*, in: *9th International Renewable Energy Storage Conference, IRES 2015 155*, pp. 77–101, 2018

[43] Zhang, J.; Ci, S.; Sharif, H.; Alahmad, M.: *Modeling Discharge Behavior of Multicell Battery*, in: *IEEE Transactions on Energy Conversion 25 (4)*, pp. 1133–1141, 2010

[44] Wang, Y.; Tian, J.; Sun, Z.; Wang, L.; Xu, R.; Li, M.; Chen, Z.: *A comprehensive review of battery modeling and state estimation approaches for advanced battery management systems*, in: *Renewable and Sustainable Energy Reviews 131*, p. 110015, 2020

[45] Pires, V.F.; Romero-Cadaval, E.; Vinnikov, D.; Roasto, I.; Martins, J.F.: *Power converter interfaces for electrochemical energy storage systems–A review*, in: *Energy conversion and management 86*, pp. 453–475, 2014

[46] Schimpe, M.; Naumann, M.; Truong, N.; Hesse, H.C.; Santhanagopalan, S.; Saxon, A.; Jossen, A.: *Energy efficiency evaluation of a stationary lithium-ion battery container storage system via electro-thermal modeling and detailed component analysis*, in: *Applied Energy 210*, pp. 211–229, 2018

[47] Liu, M.; Li, W.; Wang, C.; Polis, M.P.; Le Wang, Y.; Li, J.: *Reliability Evaluation of Large Scale Battery Energy Storage Systems*, in: *IEEE Transactions on Smart Grid 8 (6)*, pp. 2733–2743, 2017

[48] Li, X.; Wang, S.: *A review on energy management, operation control and application methods for grid battery energy storage systems*, in: *CSEE Journal of Power and Energy Systems*, 2019

[49] Li, X.; YAO, L.; Hui, D.: *Optimal control and management of a large-scale battery energy storage system to mitigate fluctuation and intermittence of renewable generations*, in: *Journal of Modern Power Systems and Clean Energy 4 (4)*, pp. 593–603, 2016

[50] Schimpe, M.: "System Simulation of Utility-Scale Lithium-Ion Battery Energy Storage Systems: An Assessment of the Energy Efficiency, the Battery Degradation, and the Economics of System Operation", PhD thesis, Munich: Technical University of Munich, 2019

[51] Bucciarelli, M.; Paoletti, S.; Vicino, A.: *Optimal sizing of energy storage systems under uncertain demand and generation*, in: *Applied Energy 225*, pp. 611–621, 2018

[52] Martins, R.; Hesse, H.; Jungbauer, J.; Vorbuchner, T.; Musilek, P.: *Optimal Component Sizing for Peak Shaving in Battery Energy Storage System for Industrial Applications*, in: *Energies 11 (8)*, p. 2048, 2018

[53] Wong, L.A.; Ramachandaramurthy, V.K.; Taylor, P.; Ekanayake, J.B.; Walker, S.L.; Padmanaban, S.: *Review on the optimal placement, sizing and control of an energy storage system in the distribution network*, in: *Journal of Energy Storage 21*, pp. 489–504, 2019

[54] Wakihara, M.: *Recent developments in lithium ion batteries*, in: *Materials Science and Engineering: R: Reports 33 (4)*, pp. 109–134, 2001

[55] Linden, D.; Reddy, T.B., eds.: *Linden's handbook of batteries*, McGraw-Hill, New York, 2011, URL: `https://www.accessengineeringlibrary.com/content/book/9780071624213`

[56] Mishra, A.; Mehta, A.; Basu, S.; Malode, S.J.; Shetti, N.P.; Shukla, S.S.; Nadagouda, M.N.; Aminabhavi, T.M.: *Electrode materials for lithium-ion batteries*, in: *Materials Science for Energy Technologies 1 (2)*, pp. 182–187, 2018

[57] Nitta, N.; Wu, F.; Lee, J.T.; Yushin, G.: *Li-ion battery materials: Present and future*, in: *Materials Today 18 (5)*, pp. 252–264, 2015

[58] Yoshio, M.; Brodd, R.J.; Kozawa, A.: *Lithium-ion batteries: Science and technologies*, Springer, New York, 2010

[59] Tian, H.; Qin, P.; Li, K.; Zhao, Z.: *A review of the state of health for lithium-ion batteries: Research status and suggestions*, in: *Journal of Cleaner Production 261*, p. 120813, 2020

[60] Barré, A.; Deguilhem, B.; Grolleau, S.; Gérard, M.; Suard, F.; Riu, D.: *A review on lithium-ion battery ageing mechanisms and estimations for automotive applications*, in: *Journal of Power Sources 241*, pp. 680–689, 2013

[61] Wang, J. et al.: *Degradation of lithium ion batteries employing graphite negatives and nickel–cobalt–manganese oxide + spinel manganese oxide positives: Part 1, aging mechanisms and life estimation*, in: *Journal of Power Sources 269*, pp. 937–948, 2014

[62] Smith, K.; Saxon, A.; Keyser, M.; Lundstrom, B.; Cao, Z.; Roc, A.: *Life prediction model for grid-connected Li-ion battery energy storage system*, in: American Automatic Control Council (ed.): *2017 American Control Conference (ACC)*, IEEE, 2017

[63] Vetter, J. et al.: *Ageing mechanisms in lithium-ion batteries*, in: *Journal of Power Sources 147 (1-2)*, pp. 269–281, 2005

[64] Notton, G.; Lazarov, V.; Stoyanov, L.: *Optimal sizing of a grid-connected PV system for various PV module technologies and inclinations, inverter efficiency characteristics and locations*, in: *Renewable Energy 35 (2)*, pp. 541–554, 2010

[65] Zhang, C.; Allafi, W.; Dinh, Q.; Ascencio, P.; Marco, J.: *Online estimation of battery equivalent circuit model parameters and state of charge using decoupled least squares technique*, in: *Energy 142*, pp. 678–688, 2018

[66] He, H.; Xiong, R.; Fan, J.: *Evaluation of Lithium-Ion Battery Equivalent Circuit Models for State of Charge Estimation by an Experimental Approach*, in: *Energies 4 (4)*, pp. 582–598, 2011

[67] Yang, X.-G.; Leng, Y.; Zhang, G.; Ge, S.; Wang, C.-Y.: *Modeling of lithium plating induced aging of lithium-ion batteries: Transition from linear to nonlinear aging*, in: *Journal of Power Sources 360*, pp. 28–40, 2017

[68] Kindermann, F.M.; Keil, J.; Frank, A.; Jossen, A.: *A SEI Modeling Approach Distinguishing between Capacity and Power Fade*, in: *Journal of The Electrochemical Society 164 (12)*, E287–E294, 2017

[69] Sturm, J.; Ludwig, S.; Zwirner, J.; Ramirez-Garcia, C.; Heinrich, B.; Horsche, M.F.; Jossen, A.: *Suitability of physicochemical models for embedded systems regarding a nickel-rich, silicon-graphite lithium-ion battery*, in: *Journal of Power Sources 436*, p. 226834, 2019

[70] Patsios, C.; Wu, B.; Chatzinikolaou, E.; Rogers, D.J.; Wade, N.; Brandon, N.P.; Taylor, P.: *An integrated approach for the analysis and control of grid connected energy storage systems*, in: *Journal of Energy Storage 5*, pp. 48–61, 2016

[71] Namor, E.; Torregrossa, D.; Cherkaoui, R.; Paolone, M.: *Parameter identification of a lithium-ion cell single-particle model through non-invasive testing*, in: *Journal of Energy Storage 12 (Supplement C)*, pp. 138–148, 2017

[72] Murata: *Data Sheet of Sony Fortelion US26650FTC1 battery cell*, 2017, URL: `www.murata.com`

[73] Naumann, M.; Spingler, F.B.; Jossen, A.: *Analysis and modeling of cycle aging of a commercial LiFePO4/graphite cell*, in: *Journal of Power Sources 451*, p. 227666, 2020

[74] Petit, M.; Prada, E.; Sauvant-Moynot, V.: *Development of an empirical aging model for Li-ion batteries and application to assess the impact of Vehicle-to-Grid strategies on battery lifetime*, in: *Applied Energy 172*, pp. 398–407, 2016

[75] Parthasarathy, C.; Hafezi, H.; Laaksonen, H.: *Lithium-ion BESS Integration for Smart Grid Applications - ECM Modelling Approach*, in: IEEE Power & Energy Society Innovative Smart Grid Technologies (ed.): *2020 IEEE Power & Energy Society Innovative Smart Grid Technologies Conference (ISGT)*, IEEE, 2020

[76] Schmalstieg, J.; Käbitz, S.; Ecker, M.; Sauer, D.U.: *A holistic aging model for Li(NiMnCo)O2 based 18650 lithium-ion batteries*, in: *Journal of Power Sources 257*, pp. 325–334, 2014

[77] Schuster, S.F.; Bach, T.; Fleder, E.; Müller, J.; Brand, M.; Sextl, G.; Jossen, A.: *Nonlinear aging characteristics of lithium-ion cells under different operational conditions*, in: *Journal of Energy Storage 1*, pp. 44–53, 2015

[78] Malhotra, A.; Battke, B.; Beuse, M.; Stephan, A.; Schmidt, T.: *Use cases for stationary battery technologies: A review of the literature and existing projects*, in: *Renewable and Sustainable Energy Reviews 56*, pp. 705–721, 2016

[79] Luo, X.; Wang, J.; Dooner, M.; Clarke, J.: *Overview of current development in electrical energy storage technologies and the application potential in power system operation*, in: *Applied Energy 137*, pp. 511–536, 2015

[80] Olabi, A.G.; Onumaegbu, C.; Wilberforce, T.; Ramadan, M.; Abdelkareem, M.A.; Al – Alami, A.H.: *Critical review of energy storage systems*, in: *Energy 214*, p. 118987, 2021

[81] Soto, E.A.; Bosman, L.B.; Wollega, E.; Leon-Salas, W.D.: *Peer-to-peer energy trading: A review of the literature*, in: *Applied Energy 283*, p. 116268, 2021

[82] Metz, D.; Saraiva, J.T.: *Use of battery storage systems for price arbitrage operations in the 15- and 60-min German intraday markets*, in: *Electric Power Systems Research 160*, pp. 27–36, 2018

[83] Brivio, C.; Mandelli, S.; Merlo, M.: *Battery energy storage system for primary control reserve and energy arbitrage*, in: *Sustainable Energy, Grids and Networks 6*, pp. 152–165, 2016

[84] Di Giorgio, A.; Giuseppi, A.; Liberati, F.; Pietrabissa, A.: *Controlled electricity distribution network black start with energy storage system support*, in: IEEE (ed.): *2017 25th Mediterranean Conference on Control and Automation (MED)*, IEEE, 2017

[85] Beil, I.; Allen, A.; Tokombayev, A.; Hack, M.: *Considerations when using utility-scale battery storage to black start a gas turbine generator*, in: IEEE (ed.): *2017 IEEE Power & Energy Society General Meeting (PESGM)*, IEEE, 2017

[86] Palizban, O.; Kauhaniemi, K.: *Energy storage systems in modern grids—Matrix of technologies and applications*, in: *Journal of Energy Storage 6*, pp. 248–259, 2016

[87] Ferreira, H.L.; Garde, R.; Fulli, G.; Kling, W.; Lopes, J.P.: *Characterisation of electrical energy storage technologies*, in: *Energy 53 (0)*, pp. 288–298, 2013, URL: `http://www.sciencedirect.com/science/article/pii/S0360544213001515`

[88] Xu, B.; Oudalov, A.; Poland, J.; Ulbig, A.; Andersson, G.: *BESS Control Strategies for Participating in Grid Frequency Regulation*, in: *IFAC Proceedings Volumes 47 (3)*, pp. 4024–4029, 2014

[89] Rebours, Y.G.; Kirschen, D.S.; Trotignon, M.; Rossignol, S.: *A Survey of Frequency and Voltage Control Ancillary Services—Part I: Technical Features*, in: *IEEE Transactions on Power Systems 22 (1)*, pp. 350–357, 2007

[90] Greenwood, D.M.; Lim, K.Y.; Patsios, C.; Lyons, P.F.; Lim, Y.S.; Taylor, P.C.: *Frequency response services designed for energy storage*, in: *Applied Energy 203*, pp. 115–127, 2017

[91] Thien, T.; Schweer, D.; vom Stein, D.; Moser, A.; Sauer, D.U.: *Real-world operating strategy and sensitivity analysis of frequency containment reserve provision with battery energy storage systems in the german market*, in: *Journal of Energy Storage 13*, pp. 143–163, 2017

[92] Deutsche Übertragungsnetzbetreiber: *Eckpunkte und Freiheitsgrade bei Erbringung von Primaerregelleistung (in German): Leitfaden für Anbieter von Primaerregelleistung*, ed. by 50Hertz Transmission GmbH; Amprion GmbH; TenneT TSO GmbH; TransnetBW GmbH, Berlin, Germany, 2014, URL: `https://www.regelleistung.net/ext/download/PQ_Bedingungen_FCR_aFRR_mFRR`, log-date:

[93] Deutsche Übertragungsnetzbetreiber: *Anforderungen an die Speicherkapazitaet bei Batterien für die Primaerregelleistung (in German)*, ed. by 50Hertz Transmission GmbH; Amprion GmbH; TenneT TSO GmbH; TransnetBW GmbH, Berlin, Germany, 2015, URL: `https://www.bves.de/wp-content/uploads/2015/08/2015_08_26_Anforderungen_Speicherkapazitaet_Batterien_PRL.pdf`, log-date:

[94] Schlachter, U.; Worschech, A.; Diekmann, T.; Hanke, B.; Maydell, K. von: *Optimised capacity and operating strategy for providing frequency containment reserve with batteries and power-to-heat*, in: *Journal of Energy Storage 32*, p. 101964, 2020

[95] Steber, D.; Bazan, P.; German, R.: *SWARM - strategies for providing frequency containment reserve power with a distributed battery storage system*, in: IEEE (ed.): *2016 IEEE International Energy Conference (ENERGYCON)*, IEEE, 2016

[96] Perroy, E.; Lucas, D.; Debusschere, V.: *Provision of Frequency Containment Reserve Through Large Industrial End-Users Pooling*, in: *IEEE Transactions on Smart Grid 11 (1)*, pp. 26–36, 2020

[97] Schlund, J.; Steinert, R.; Pruckner, M.: *Coordinating E-Mobility Charging for Frequency Containment Reserve Power Provision*, in: e-Energy (ed.): *Proceedings of the Ninth International Conference on Future Energy Systems*, ACM, New York, NY, USA, 2018

[98] Pavić, I.; Capuder, T.; Kuzle, I.: *Value of flexible electric vehicles in providing spinning reserve services*, in: *Applied Energy 157*, pp. 60–74, 2015

[99] Leadbetter, J.; Swan, L.: *Battery storage system for residential electricity peak demand shaving*, in: *Energy and Buildings 55*, pp. 685–692, 2012

[100] Vieira, F.M.; Moura, P.S.; Almeida, A.T. de: *Energy storage system for self-consumption of photovoltaic energy in residential zero energy buildings*, in: *Renewable Energy 103*, pp. 308–320, 2017

[101] Naumann, M.; Karl, R.C.; Truong, C.N.; Jossen, A.; Hesse, H.C.: *Lithium-ion Battery Cost Analysis in PV-household Application*, in: *9th International Renewable Energy Storage Conference, IRES 2015 73 (Supplement C)*, pp. 37–47, 2015

[102] Diouf, B.; Pode, R.: *Potential of lithium-ion batteries in renewable energy*, in: *Renewable Energy 76*, pp. 375–380, 2015

[103] Akinyele, D.; Belikov, J.; Levron, Y.: *Battery Storage Technologies for Electrical Applications: Impact in Stand-Alone Photovoltaic Systems*, in: *Energies 10 (11)*, p. 1760, 2017

[104] Moshövel, J.; Kairies, K.-P.; Magnor, D.; Leuthold, M.; Bost, M.; Gährs, S.; Szczechowicz, E.; Cramer, M.; Sauer, D.U.: *Analysis of the maximal possible grid relief from PV-peak-power impacts by using storage systems for increased self-consumption*, in: *Applied Energy 137*, pp. 567–575, 2015

[105] Göbel, C.; Cheng, V.; Jacobsen, H.-A.: *Profitability of Residential Battery Energy Storage Combined with Solar Photovoltaics*, in: *Energies 10 (7)*, p. 976, 2017

[106] Appen, J. von; Stetz, T.; Braun, M.; Schmiegel, A.: *Local Voltage Control Strategies for PV Storage Systems in Distribution Grids*, in: *IEEE Transactions on Smart Grid 5 (2)*, pp. 1002–1009, 2014

[107] Truong, C.N.; Naumann, M.; Karl, R.C.; Müller, M.; Jossen, A.; Hesse, H.C.: *Economics of Residential Photovoltaic Battery Systems in Germany: The Case of Teslas Powerwall*, in: *Batteries 2 (2)*, p. 14, 2016

[108] German Federal Office of Justice: *Stromnetzentgeltverordnung (in German): StromNEV*, 2005, URL: `https://www.gesetze-im-internet.de/stromnev/BJNR222500005.html`, log-date:

[109] Oudalov, A.; Cherkaoui, R.; Beguin, A.: *Sizing and Optimal Operation of Battery Energy Storage System for Peak Shaving Application: 2007 IEEE Lausanne Power Tech*, in: IEEE (ed.): *IEEE PowerTech, 2007 IEEE Lausanne*, 2007

[110] Shi, Y.; Xu, B.; Di Wang; Zhang, B.: *Using Battery Storage for Peak Shaving and Frequency Regulation: Joint Optimization for Superlinear Gains*, in: *IEEE Transactions on Power Systems 33 (3)*, pp. 2882–2894, 2018

[111] Figgener, J. et al.: *The development of stationary battery storage systems in Germany – A market review*, in: *Journal of Energy Storage 29*, p. 101153, 2020

[112] Collath, N.; Englberger, S.; Jossen, A.; Hesse, H.: *Reduction of Battery Energy Storage Degradation in Peak Shaving Operation through Load Forecast Dependent Energy Management*, in: VDE / ETG (ed.): *NEIS 2020*, 2020

[113] Tuunanen, J.; Honkapuro, S.; Partanen, J.: *Power-based distribution tariff structure: DSO's perspective*, in: IEEE (ed.): *13th International Conference on the European Energy Market (EEM)*, IEEE, 2016

[114] Papadopoulos, V.; Knockaert, J.; Develder, C.; Desmet, J.: *Peak Shaving through Battery Storage for Low-Voltage Enterprises with Peak Demand Pricing*, in: *Energies 13 (5)*, p. 1183, 2020

[115] Krata, J.; Saha, T.K.: *Real-Time Coordinated Voltage Support With Battery Energy Storage in a Distribution Grid Equipped With Medium-Scale PV Generation*, in: *IEEE Transactions on Smart Grid 10 (3)*, pp. 3486–3497, 2019

[116] Dixon, J.; Moran, L.; Rodriguez, J.; Domke, R.: *Reactive Power Compensation Technologies: State-of-the-Art Review*, in: *Proceedings of the IEEE 93 (12)*, pp. 2144–2164, 2005

[117] Sarkar, M.N.I.; Meegahapola, L.G.; Datta, M.: *Reactive Power Management in Renewable Rich Power Grids: A Review of Grid-Codes, Renewable Generators, Support Devices, Control Strategies and Optimization Algorithms*, in: *IEEE Access 6*, pp. 41458–41489, 2018

[118] Gayatri, M.; Parimi, A.; Pavan Kumar, A.V.: *A review of reactive power compensation techniques in microgrids*, in: *Renewable and Sustainable Energy Reviews 81*, pp. 1030–1036, 2018

[119] Shao, C.; Qian, T.; Wang, Y.; Wang, X.: *Coordinated Planning of Extreme Fast Charging Stations and Power Distribution Networks Considering On-Site Storage*, in: *IEEE Transactions on Intelligent Transportation Systems 22 (1)*, pp. 493–504, 2021

[120] Ciccarelli, F.; Del Pizzo, A.; Iannuzzi, D.: *An ultra-fast charging architecture based on modular multilevel converters integrated with energy storage buffers*, in: IEEE (ed.): *2013 Eighth International Conference and Exhibition on Ecological Vehicles and Renewable Energies (EVER)*, IEEE, 2013

[121] Zhao, D.; Thakur, N.; Chen, J.: *Optimal Design of Energy Storage System to Buffer Charging Infrastructure in Smart Cities*, in: *Journal of Management in Engineering 36 (2)*, p. 04019048, 2020

[122] Rahman, M.M.; Oni, A.O.; Gemechu, E.; Kumar, A.: *The development of techno-economic models for the assessment of utility-scale electro-chemical battery storage systems*, in: *Applied Energy 283*, p. 116343, 2021

[123] Yang, Y.; Bremner, S.; Menictas, C.; Kay, M.: *Battery energy storage system size determination in renewable energy systems: A review*, in: *Renewable and Sustainable Energy Reviews 91*, pp. 109–125, 2018

[124] Xu, X.; Bishop, M.; Donna G, O.; Chen, H.: *Application and modeling of battery energy storage in power systems*, in: *CSEE Journal of Power and Energy Systems 2 (3)*, pp. 82–90, 2016

[125] Bakhshi Yamchi, H.; Shahsavari, H.; Taghizadegan Kalantari, N.; Safari, A.; Farrokhifar, M.: *A cost-efficient application of different battery energy storage technologies in microgrids considering load uncertainty*, in: *Journal of Energy Storage 22*, pp. 17–26, 2019

[126] Zheng, Y.; Zhao, J.; Song, Y.; Luo, F.; Meng, K.; Qiu, J.; Hill, D.J.: *Optimal Operation of Battery Energy Storage System Considering Distribution System Uncertainty*, in: *IEEE Transactions on Sustainable Energy 9 (3)*, pp. 1051–1060, 2018

[127] BVES: *Beschränkung der ÜNB für Speicher im Regelenergiemarkt ist rechtswidrig (in German)*, Berlin, 2019, URL: `https://www.bves.de/uenb_rechtswidrige_blockade/`, log-date:

[128] Marchgraber, J.; Gawlik, W.; Wailzer, G.: *Reducing SoC-Management and losses of battery energy storage systems during provision of frequency containment reserve*, in: *Journal of Energy Storage 27*, p. 101107, 2020

[129] Zhao, X.; Callafon, R.A. de: *Modeling of battery dynamics and hysteresis for power delivery prediction and SOC estimation*, in: *Applied Energy 180*, pp. 823–833, 2016

[130] Stein, K.; Tun, M.; Matsuura, M.; Rocheleau, R.: *Characterization of a Fast Battery Energy Storage System for Primary Frequency Response*, in: *Energies 11 (12)*, p. 3358, 2018

[131] Keil, P.; Jossen, A.: *Charging protocols for lithium-ion batteries and their impact on cycle life—An experimental study with different 18650 high-power cells*, in: *Journal of Energy Storage 6*, pp. 125–141, 2016

[132] Bui, V.-H.; Hussain, A.; Im, Y.-H.; Kim, H.-M.: *An internal trading strategy for optimal energy management of combined cooling, heat and power in building microgrids*, in: *Applied Energy 239*, pp. 536–548, 2019

[133] He, G.; Chen, Q.; Kang, C.; Pinson, P.; Xia, Q.: *Optimal Bidding Strategy of Battery Storage in Power Markets Considering Performance-Based Regulation and Battery Cycle Life*, in: *IEEE Transactions on Smart Grid 7 (5)*, pp. 2359–2367, 2016

[134] Sbordone, D.A.; Di Pietra, B.; Bocci, E.: *Energy Analysis of a Real Grid Connected Lithium Battery Energy Storage System*, in: *9th International Renewable Energy Storage Conference, IRES 2015 75*, pp. 1881–1887, 2015

[135] Schimpe, M.; Piesch, C.; Hesse, H.; Paß, J.; Ritter, S.; Jossen, A.: *Power Flow Distribution Strategy for Improved Power Electronics Energy Efficiency in Battery Storage Systems: Development and Implementation in a Utility-Scale System*, in: *Energies 11 (3)*, p. 533, 2018

[136] Erickson, R.W.; Maksimović, D.: *Fundamentals of Power Electronics*, Springer International Publishing, Cham, 2020

[137] Englberger, S.; Jossen, A.; Hesse, H.: *Unlocking the Potential of Battery Storage with the Dynamic Stacking of Multiple Applications*, in: *Cell Reports Physical Science 1*, 2020

[138] Schmidt, O.; Melchior, S.; Hawkes, A.; Staffell, I.: *Projecting the Future Levelized Cost of Electricity Storage Technologies*, in: *Joule 3 (1)*, pp. 81–100, 2019

[139] Savulescu, S.C.: *Real-Time Stability in Power Systems*, Springer International Publishing, Cham, 2014

[140] Müller, U.P.; Schachler, B.; Scharf, M.; Bunke, W.-D.; Günther, S.; Bartels, J.; Pleßmann, G.: *Integrated Techno-Economic Power System Planning of Transmission and Distribution Grids*, in: *Energies 12 (11)*, p. 2091, 2019

[141] Tjaden, T.; Bergner, J.; Weniger, J.; Quaschning, V.: *Repräsentative elektrische Lastprofile für Wohngebäude in Deutschland auf 1-sekündiger Datenbasis (in German)*, ed. by Hochschule für Technik und Wirtschaft, 2015, URL: `https://pvspeicher.htw-berlin.de/daten/`.

[142] Röpcke, T.: *SimBEV: Simulation of battery electric vehicles*, ed. by Reiner Lemoine Institut, Berlin, 2021, URL: `https://github.com/rl-institut/simbev`, log-date:

[143] Oeding, D.; Oswald, B.R.: *Elektrische Kraftwerke und Netze*, Springer Berlin Heidelberg, Berlin, Heidelberg, 2016

[144] Schwab, A.J.: *Elektroenergiesysteme*, Springer Berlin Heidelberg, Berlin, Heidelberg, 2015

[145] Chatterjee, S.; Mandal, S.: *A novel comparison of gauss-seidel and newton-raphson methods for load flow analysis*, in: *2017 International Conference on Power and Embedded Drive Control (ICPEDC)*, IEEE, 2017

[146] Brown, T.; Hörsch, J.; Schlachtberger, D.: *PyPSA: Python for Power System Analysis*, in: *Journal of Open Research Software 6*, 2018

[147] Wienholt, L.; Müller, U.; Bartels, J.: *Optimal Sizing and Spatial Allocation of Storage Units in a High-Resolution Power System Model*, in: *Energies 11 (12)*, p. 3365, 2018

[148] Heilmann, C.; Wozabal, D.: *How much smart charging is smart?*, in: *Applied Energy 291*, p. 116813, 2021

[149] Amme, J.; Pleßmann, G.; Bühler, J.; Hülk, L.; Kötter, E.; Schwaegerl, P.: *The eGo grid model: An open-source and open-data based synthetic medium-voltage grid model for distribution power supply systems*, in: *Journal of Physics: Conference Series 977*, p. 012007, 2018

[150] Deutsche Energie-Agentur GmbH: *dena-Verteilnetzstudie: Ausbau und Innovationsbedarf der Stromverteilnetze in Deutschland bis 2030*, ed. by Deutsche Energie-Agentur GmbH, Berlin, 2012, URL: https://www.dena.de/themen-projekte/projekte/energiesysteme/dena-verteilnetzstudie/, log-date:

[151] Crastan, V.; Westermann, D.: *Elektrische Energieversorgung 3*, Springer Berlin Heidelberg, Berlin, Heidelberg, 2018

[152] Yang, P.; Tang, G.; Nehorai, A.: *A game-theoretic approach for optimal time-of-use electricity pricing*, in: *IEEE Transactions on Power Systems 28 (2)*, pp. 884–892, 2013

[153] Lu, R.; Hong, S.H.; Zhang, X.: *A Dynamic pricing demand response algorithm for smart grid: Reinforcement learning approach*, in: *Applied Energy 220*, pp. 220–230, 2018

[154] Appen, J. von; Braslavsky, J.H.; Ward, J.K.; Braun, M.: *Sizing and grid impact of PV battery systems - a comparative analysis for Australia and Germany*, in: IEEE (ed.): *2015 International Symposium on Smart Electric Distribution Systems and Technologies (EDST)*, IEEE, 2015

[155] Sundstrom, O.; Binding, C.: *Flexible Charging Optimization for Electric Vehicles Considering Distribution Grid Constraints*, in: *IEEE Transactions on Smart Grid 3 (1)*, pp. 26–37, 2012

[156] Hu, J.; You, S.; Lind, M.; Ostergaard, J.: *Coordinated Charging of Electric Vehicles for Congestion Prevention in the Distribution Grid*, in: *IEEE Transactions on Smart Grid 5 (2)*, pp. 703–711, 2014

[157] Komarnicki, P.; Lombardi, P.; Styczynski, Z.A.: *Elektrische Energiespeichersysteme*, Springer Berlin Heidelberg, Berlin, Heidelberg, 2021

[158] Klyapovskiy, S.; You, S.; Cai, H.; Bindner, H.W.: *Incorporate flexibility in distribution grid planning through a framework solution*, in: *International Journal of Electrical Power & Energy Systems 111*, pp. 66–78, 2019

[159] Sillaber, A.: *Leitfaden zur Verteilnetzplanung und Systemgestaltung*, Springer Fachmedien Wiesbaden, Wiesbaden, 2016

[160] Nykamp, S.; Molderink, A.; Hurink, J.L.; Smit, G.J.: *Statistics for PV, wind and biomass generators and their impact on distribution grid planning*, in: *Energy 45 (1)*, pp. 924–932, 2012

[161] Hänsch, K.; Naumann, A.; Wenge, C.; Wolf, M.: *Communication for battery energy storage systems compliant with IEC 61850*, in: *International Journal of Electrical Power & Energy Systems 103*, pp. 577–586, 2018

[162] Gurobi Optimization LLC: *Gurobi Optimization*, 2020, URL: http://www.gurobi.com/

[163] Gheisarnejad, M.; Khooban, M.-H.; Dragicevic, T.: *The Future 5G Network-Based Secondary Load Frequency Control in Shipboard Microgrids*, in: *IEEE Journal of Emerging and Selected Topics in Power Electronics 8 (1)*, pp. 836–844, 2020

[164] Garau, M.; Anedda, M.; Desogus, C.; Ghiani, E.; Murroni, M.; Celli, G.: *A 5G cellular technology for distributed monitoring and control in smart grid*, in: IEEE (ed.): *2017 IEEE International Symposium on Broadband Multimedia Systems and Broadcasting (BMSB)*, IEEE, 2017

[165] Stephan, A.; Battke, B.; Beuse, M.D.; Clausdeinken, J.H.; Schmidt, T.S.: *Limiting the public cost of stationary battery deployment by combining applications*, in: *Nature Energy 1 (7)*, 2016

[166] Fachrizal, R.; Shepero, M.; van der Meer, D.; Munkhammar, J.; Widén, J.: *Smart charging of electric vehicles considering photovoltaic power production and electricity consumption: A review*, in: *eTransportation 4*, p. 100056, 2020

[167] Sovacool, B.K.; Kester, J.; Noel, L.; Zarazua de Rubens, G.: *Actors, business models, and innovation activity systems for vehicle-to-grid (V2G) technology: A comprehensive review*, in: *Renewable and Sustainable Energy Reviews 131*, p. 109963, 2020

[168] Baumann, M.; Peters, J.F.; Weil, M.; Grunwald, A.: *CO 2 Footprint and Life-Cycle Costs of Electrochemical Energy Storage for Stationary Grid Applications*, in: *Energy Technology 5 (7)*, pp. 1071–1083, 2017

[169] Parlikar, A.; Truong, C.N.; Jossen, A.; Hesse, H.: *The carbon footprint of island grids with lithium-ion battery systems: An analysis based on levelized emissions of energy supply*, in: *Renewable and Sustainable Energy Reviews 149*, p. 111353, 2021

List of figures

List of tables